Mechanically Interlocked Superstructures in Aqueous Solution: Daisy Chains and Rotaxanes

Inauguraldissertation

zur

Erlangung der Würde eines Doktors der Philosophie

vorgelegt der

Philosophisch-Naturwissenschaftlichen Fakultät

der Universität Basel

von

Yves Aeschi

aus Himmelried (SO), Schweiz

Basel, 2020

Genehmigt von der Philosophisch-Naturwissenschaftlichen Fakultät auf Antrag von

Prof. Dr. Marcel Mayor

Prof. Dr. Eli Zysman-Colman

Basel, den 13.11.2018

Prof. Dr. Martin Spiess

Acknowledgments

I wish to express my gratitude to Prof. Dr. Marcel Mayor for accepting me as a part of his research group. It was exciting to pursue own ideas and drive research projects from cradle to publication. Many thanks go to Prof. Dr. Eli Zysman-Colman for co-referring this thesis and the examination. I would also like to thank Prof. Dr. Oliver Wenger for chairing the examination.

I thank Dr. Loïc Le Pleux, Dr.Tomáš Šolomek, Laurent Jucker and Dr. Henrik Peters for all the corrections and suggestions during proofreading of this thesis.

The teams of the Werkstatt (Markus Ast, Andres Koller, Andreas Sohler, Hisni Meha), Materialausgabe (Oliver Ilg, Markus Hauri, Roy Lips) and Analytics (Sylvie Mittelheisser, Dr. Heinz Nadig, Dr. Michael Pfeffer) deserve a lot of thanks for all the technical support and the benevolent atmosphere. I was happy to receive financial support from the Swiss Nanoscience Institute (SNI) PhD School, which was coordinated by Prof. Dr. Michel Calame.

I owe many thanks to Dr. Lukas Jundt (also known as the walking encyclopedia of music), whose contributions go beyond discussing chemical challenges. This certainly holds true not only for me but for a long list of people. It was a lot of fun to work with you ! (Yes, chemists do swear a lot! Da staunt der Laie und der Fachmann wundert sich…)

Many thanks go to Dr. Sylvie Drayss for jointly sorting out the initial ins and outs of the daisy chain project, which always kept taking unexpected turns. The rotaxane chemistry is now passed over into the capable hands of Laurent Jucker. I am very thankful for your motivation to conduct last-minute measurements and your honest opinions during proofreading and on chemical matters.

To the Lab 4-team (Dr. Lukas Jundt, Dr. Henrik Peters, Dr. Peter Ribar, Prof. Dr. Michal Juríček, Dr. Princekumar Ravat, Dr.Tomáš Šolomek, Dr. Sylvie Drayss, Laurent Jucker): it was a lot of fun with you and I enjoyed all the inspiring exchange we had. Special thanks go to Dr. Henrik Peters for the never-ending pun competitions, the loud music und discussions about almost everything imaginable. And also for all the kind little things during every-lablife and your honesty.

Without the uncomplicated access to excellent NMR facilities and the expertise of Prof. Dr. Daniel Häussinger and his team it would have been almost impossible to realize the projects in this thesis. Crucial ITC measurements were obtained thanks to the enthusiasm of Dr. Michal Valášek who invested considerable time to obtain good data. I am very happy about the committed collaboration with both of you.

For all the administrative work I would like to acknowledge Brigitte Howald and also Linda Bannwart, who organized all kinds of social events.

I would like to acknowledge all the Master- and Wahlpraktikum students who contributed to this work in some way. In particular I will never forget Sarahna Mishra (†), who is unfortunately not among us anymore.

Many thanks go to the “Gräsli-club” with Linda Bannwart, Henrik Peters and Lorenzo Bizzini for the cooking on Monday and sorry for my increasingly rare contributions during the final period of writing my thesis ;-) It was not only about the cooking, but I also enjoyed all the personal contacts and discussions about life

inside and outside of lab. This includes “Gräsli-outsiders” Kevin Weiland and Patrick Zwick! And not least of course also Dr. Sebastian “Sebu” Flückiger. I enjoyed a lot the ritual of having lunch together while chattering, discussing our brilliant, future business plans and complaining about failed experiments.

Thank you Meli, for the understanding and the mutual support we could always maintain under all circumstances. And thank you for the wonderful journey we began with Lauri and Minna.

Meli and I could count on unconditional support from our families (Marita & Francis, Hedi & Markus, Ariane & Lorenz) though the last years. It allowed us to found a family and still pursue our professions. We are deeply grateful for the benevolence we always receive from you.

Abstract

The hydrophobic effect is of fundamental importance for the self-assembly of functional units in biological systems. Eventually all life depends on the properties which are owed to the chemistry beyond covalently bound structures. Artificial supramolecular systems may be designed to mimic biological assemblies or to fulfill purposes unknown in the natural biological realm. This includes the template-directed self-assembly of rotaxanes, which can profit from the versatile applicability of the hydrophobic effect. In order to render organic compounds water-soluble and enable well-defined recognition modes, a particularly thoughtful molecular design is required. This work aims towards the synthesis of aqueous-based rotaxane-type structures, in particular rigid molecular daisy chains. *Diederich*-type cyclophanes were chosen as receptor components and suitable functionality for copper-catalyzed azide-alkyne cycloaddition (CuAAC) is introduced in all structures. The cyclophane part is ideally suited to accommodate rigid, π-conjugated structures. These key structural elements are thought to provide a suitable basis in the search towards building blocks for aqueous rotaxane synthesis. Three publications have resulted from these investigations, which are included in this thesis. After an introductory part, an overview of mechanically interlocked structures incorporating π-conjugated subunits is given. This is followed by *Assembly of [2]Rotaxanes in Water*, a publication in *European Journal of Organic Chemistry*, where the first investigations of aqueous-based rotaxane synthesis were published. Synthesis of molecular daisy chains is presented under *Aqueous Assembly of Zwitterionic Daisy Chains*. This article was published in *Chemistry – A European Journal*. As an invited contribution to the special issue of 50 Years of Rotaxanes in *European Journal of Organic Chemistry*, a manuscript prepared for submission was originally included under *Slow Formation of Pseudorotaxanes in Water: Large Influence of the Substitution Pattern*. The article was meanwhile published and is included in form of the peer-reviewed and edited final version. All chapters are followed by the corresponding supporting information, which contains the experimental data. To conclude, possible design considerations for aqueous-based, molecular daisy chains based on the preceding findings are given. The chapter *Outlook: Towards Kinetically Controlled Assembly of Molecular Daisy Chains* contains not only these design considerations but also the latest state of synthetic investigations towards a possible target structure.

Table of Contents

Introduction

From Supramolecular Chemistry to the Mechanical Bond

From the chemists' point of view, the concept of a chemical bond serves intuitively as a tool to link individual atoms. As a result, a virtually infinite structural diversity of chemical compounds exists, even if only chemically feasible structures in the organic realm are taken into account.[1] This implies an ever-lasting challenge for the design, synthesis and characterization of organic compounds according to one's wishes and needs. Within the vast chemical space, compounds that are able to specifically recognize other chemical entities can be identified. Such structures have indeed been synthesized and studied, which represents the birth of the field of supramolecular chemistry.[2,3] For the establishment of this field as a distinct chemical discipline by developing both chemistry and basic principles, the 1987 Nobel Prize was awarded to Cram, Lehn and Pedersen. A supramolecular complex in solution is always in equilibrium with its dissociated components. If the chemical exchange is interrupted by spatial entanglement of the individual components, a mechanically interlocked molecule (MIM) is obtained (Figure 1).[4] Such an interlocked species cannot be dissociated without breaking a covalent bond and has different physico-chemical properties than a stoichiometricallly equal mixture of its individual components. As a result, it must be considered as a discrete molecular entity, held together by a mechanical bond. If one returns to the notion of the limitless chemical space, the opportunity for compounds to exist either as individual or as interlocked species adds an additional degree of complexity to the universe of chemically feasible structures. This gives rise to topological isomerism.[5]

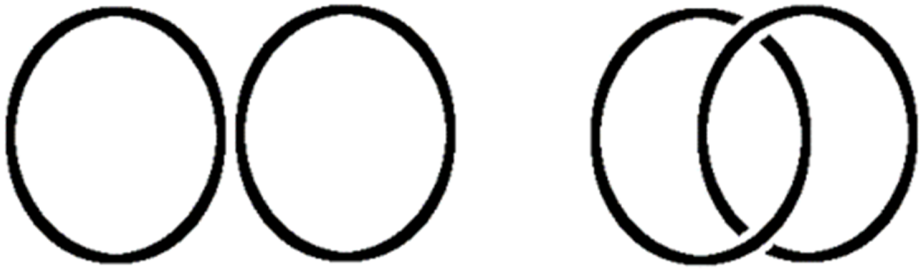

Figure 1. Topological isomerism between two rings and a mechanically interlocked chain link

One can illustrate the distinction of a MIM and the mixture of its individual components with a pair of rings in the macroscopic world. They can exist either discretely or as an interlocked chain, and it is natural to everyone that physical properties of separate rings and their chain are not equal. On a molecular scale two individual macrocyclic rings can exist as separate units or as a topologically isomeric, interlocked catenane (Figure **1**),[5] which represents one of the fundamental constructs in MIM chemistry.[4] Catenanes can in principle be oligomerized to yield [n]catenanes with the prefix [n] denoting the number of repeating units. From the first [2]catenane reported by Wassermann[6] obtained by an inefficient statistical synthesis followed by the first synthesis that relied on the covalent directed approach by Schill and Lüttringhaus,[7] catenane chemistry has evolved over more than five decades to the recently accomplished example of a linear polymeric [26]catenane.[8]

In addition to catenanes, the second fundamental construct in MIM chemistry are rotaxanes. They consist of a macrocycle encircling a molecular rod terminated with bulky end-groups, which are referred to as stoppers (Figure 2). Due to the bulkiness of the stoppers, the macrocycle cannot dissociate from the rotaxane structure and remains kinetically trapped. In contrast to catenanes, the nature of rotaxanes as mechanically interlocked molecules is not clearly defined.[9] This is a consequence of the topologically trivial nature of their subunits, i.e. components of a rotaxane still represent separate species according to the rules of topology.[10] A supramolecular complex of an axle and a host is termed a pseudorotaxane, which displays exchange kinetics. Under certain circumstances, a rotaxane can be considered to possess partial pseudorotaxane character because the exchange kinetics may be strongly influenced by the chemical environment.[9] Similar to catenanes, a prefix [n] denotes the total number of interlinked/interlocked components. Rotaxanes were historically obtained by statistical syntheses developed by Harrisson and Harrisson[11] and the covalent-directed approach developed by Schill[12] which was similar to the synthesis of the previously reported catenane. Both were, however, ineffective due to poor threading statistics or the laborious synthetic route.

Template-directed methods were therefore developed to simplify reaction protocols and to improve yields, which enabled a routine, preparative scale synthesis of rotaxanes.[4] Supramolecular templation is the most versatile and consequently the most frequently used method for MIM synthesis. Among the many methods available for interlocking,[4,13] threading of an axle into macrocyclic receptor

followed by stoppering (rotaxane) or macrocyclization (catenane) are most frequently applied (Figure 2).

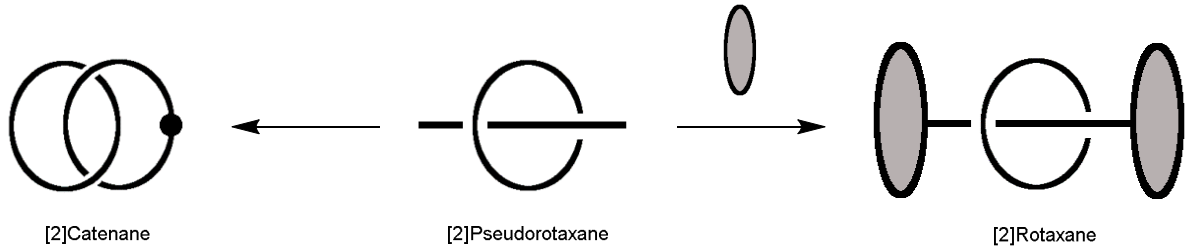

Figure 2. Assembly of a [2]catenane and a [2]rotaxane from a pseudorotaxane.

Rotaxanes and Molecular Daisy Chains

The receptor component of a rotaxane (Figure 3a) can be covalently attached to the axle to result in a hermaphroditic molecule, which can self-recognize intra- or intermolecularly depending on the molecular design (Figure 3b).[14] The intermolecular recognition can in principle result in cyclic [*c*n]- or acyclic [*a*n] supramolecular daisy chains, a nomenclature which was coined by Stoddart et al.[15] Upon introduction of stoppers, interlocked daisy chain-rotaxanes are obtained (Figure 3b).

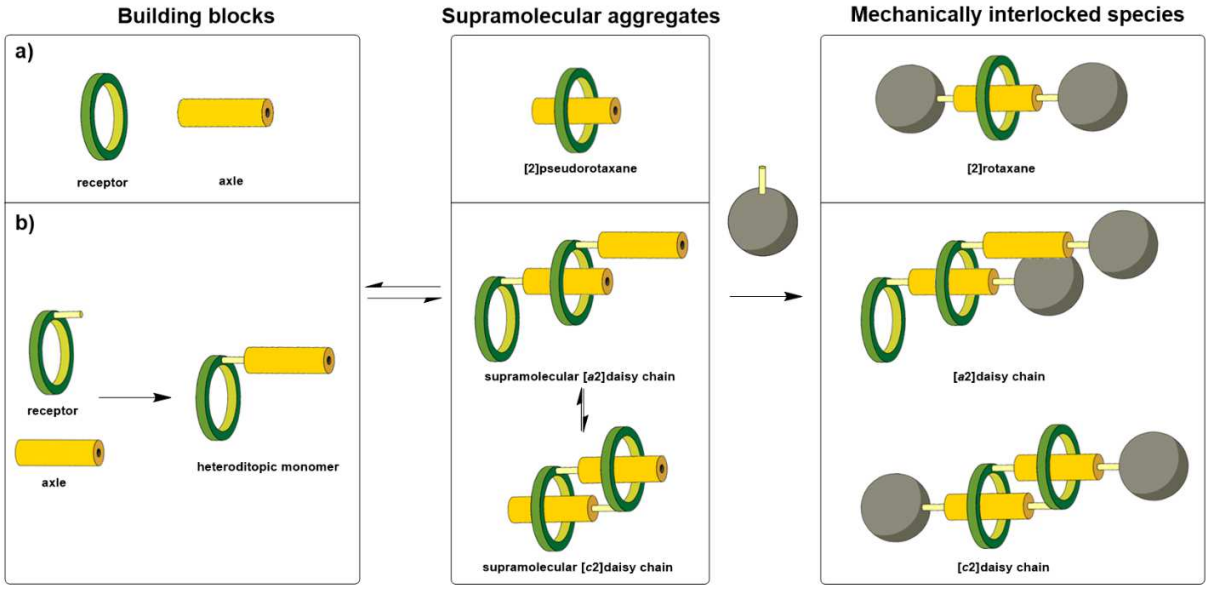

Figure 3a/b. Visualization of the analogy between formation of **a)** rotaxanes and **b)** molecular daisy chains. While the components are in equilibrium with their interlinked, supramolecular aggregates, the interlocked species are irreversibly trapped (=interlocked) after covalent attachment of the stopper.

Supramolecular daisy chains with pseudorotaxane character were initially developed by the groups of Stoddart[15] and Sauvage.[16] One of the first examples of mechanically interlocked daisy chains was synthesized by the Stoddart group, relying on the crown-ether-ammonium ion recognition motif. From a triphenylphosphonium-stoppered axle component encircled by an aldehyde-functionalized crown ether, the interlocked, heteroditopic structure was assembled *via* a *Wittig*-reaction (Figure 4).[17] Other early syntheses of interlocked daisy chains have been synthesized on the basis of cyclodextrin–aromatic guest[18,19]recognition motifs. A key contribution to the early development of molecular daisy chains was the introduction of switchable elements into the structure, realized by the Sauvage group (Figure 5).[20] This example relied on the Cu(I)-templation strategy which the group frequently applied in pioneering MIM syntheses.[21,22]

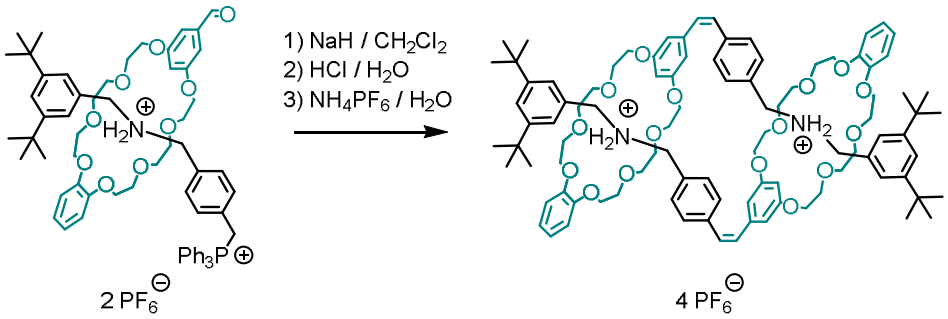

Figure 4. The first interlocked [*c*2]daisy chain.[17] A yield of 10 % for the cyclic dimer was reported.

By stoppering of a Cu(I)-templated, supramolecular [*c*2]daisy chain with a trityl-terminated terpyridine moiety, a switchable daisy chain was obtained, which can contract and extend by metal ion exchange between Cu(I) and Zn(II).[20] Switchable daisy chains that can respond towards addition/removal of zinc ions,[23] change of electrochemical potential,[24,25] pH-value,[26–30] light,[23] solvent[31] and temperature[24] have been developed thereafter by various groups. Integration of light- responsive daisy chains led to the formation of materials with macroscopically swichtable properties.[23,32] Such early examples are mostly based on [*c*2]daisy chains because the formation of dimeric structures is entropically favored over oligomerization to larger aggregates. By formation of cyclic structures both recognition sites are occupied, thus maximizing enthalpic contributions.[14] Nevertheless, larger [*c*3]- and [*c*4]daisy chains could be obtained in certain cases, sometimes by serendipity[18,33] but also by meticulous control of geometric arrangement of host/guest conjugates.[34,35]

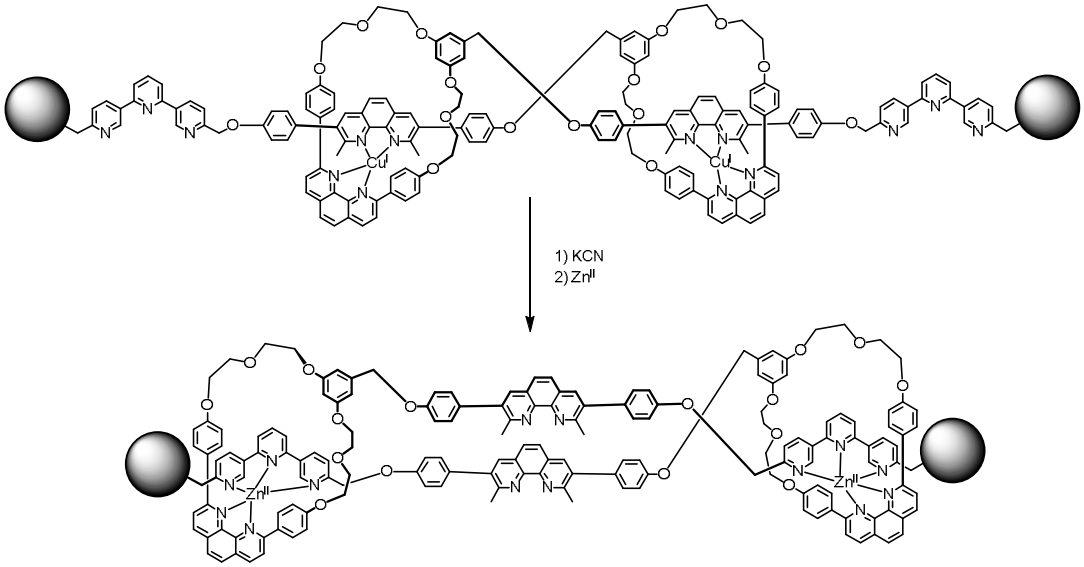

Figure 5. Sauvage's switchable [*c*2]daisy chain.

Hydrophobic, Template-Directed Assembly

For the template-directed synthesis of MIMs, implementation of supramolecular recognition sites into the molecular structure is indispensable.[4] The recognition site will finally constitute a part of the molecular structure and will remain as a rudiment. Recognition strategies based on cation–crown ether, π-donor–acceptor or hydrogen bonding interactions provide the driving force for binding. In contrast, solvophobic recognition essentially functions in reverse, i.e. by maximization of solvent interactions as the main contribution, although direct interactions of a host and a guest may also contribute significantly to the total free energy of binding. Entropic contributions can result from the decrease of partially ordered domains of the solvation network at the solute/solvent interface,[36] whereas enthalpic contributions arise from expulsion of high-energy solvent molecules located in a recognition site, resulting in increased interaction of liberated solvent molecules within the solvent bulk. The solvent enthalpic contributions are particularly pronounced in highly polar and protic solvents as a result of their strong cohesive forces.[37] In addition, binding strength in hydrophobic recognition is often enhanced by synergistic contributions from van-der-Waals-, π-donor/acceptor- and ion pairing interactions. Among the solvophobic effects, the hydrophobic effect[36] is the most commonly known and used driving force for supramolecular assembly as it is particularly strong due to the strong cohesive forces of water. A significant advantage of hydrophobic assembly is the potential for high association strength that many receptors such as cyclodextrins, cucurbiturils and cyclophanes demonstrate[4] in combination with the broad range of organic molecules, many of which by default have a hydrophobic surface. This is particularly advantageous if a traceless recognition motif is required, which does not strongly interfere with electronic properties of the target structure or if the installation of specialized recognition site needs to be avoided. In return it is required that host and guest or their complexes are soluble in an aqueous environment. If hydrophobic properties are not well balanced, then either phase segregation or undesired parasitic aggregation may occur. Similar considerations are of importance in the field of medicinal chemistry and represented by Lipinski's rule of 5,[38] which provides an empirical guideline for drug design with an emphasis on balancing hydrophilic and hydrophobic properties. Therefore, organic structures often require solubilizing groups such as ionic centers or decoration with hydrogen bond donor/acceptors. Such structural features must be thoughtfully integrated into water-compatible, supramolecular systems. In particular, the use of larger conjugated structures for MIM assembly brings along an inherent discrepancy between aqueous solubility and strong hydrophobicity, which must be accounted for in the molecular design.

Diederich-Type Cyclophanes

Aqueous-based MIMs are most frequently based on cyclodextrins, cucurbiturils and water-soluble cyclophanes.[4] For (supra)molecular daisy chain synthesis, cyclodextrin receptors combined with naphthalene-, azobenzene-, stilbene-, or cinnamic acid-derived guests are well represented in literature[14,23] while other receptors are scarcely used[39] for this purpose.

For the construction of daisy chains a receptor must be monofunctionalized with a connection point for a guest. The *Diederich*-type cyclophanes (Figure 6) are well suited for such a modification and much of their chemistry is well established in literature.[40] Strong, enthalpically driven complexation of various hydrophobic guests in water has been described, which is referred to as a "nonclassical hydrophobic effect".[41,37,40] A multitude of derived structures from those shown in Figure 6 have been synthesized by the Diederich group and almost every structural parameter was modified, including e.g. solubilizing groups,[50] larger aromatic spacer units[43] and topological changes to yield different macrotricyclic hosts.[44,45] Whereas the parent cyclophanes form complexes with benzene guests and naphthalenes,[42] their derivatives with modified cavity sizes allowed complexation of a number of larger guests such as paracyclophanes, steroids[43,44] or polycyclic aromatic hydrocarbons like pyrene, perylene and fluoranthrene.[45] Even enzyme models based on such cyclophanes were implemented, ranging from esterases[46] over cytochrome P-450 [47] to pyruvate oxidase mimics.[48]

The parent cyclophanes shown in Figure 6 are ideally suited for modifications which allow for the formation of daisy chains. Binding properties can be altered by changing the cavity diameter or the choice of decorating groups (R in Figure 6). Solubility in aqueous environment is provided by the presence of ionic ammonium centers and can further be tuned by groups R. A linker chain of four methylene units (n = 4) results in an ideal cavity size for the accommodation of 1,4-substituted benzenes and 2,6-substitued naphthalenes.[42] Installation of methoxy groups in place of R results in a higher critical aggregation concentration (CAC) of ~10 mM, a deeper cavity and a stronger affinity for guests compared to the unsubstituted analogue. The methyl equivalent shows a rather low solubility in water and a lower CAC of <0.02 mM but, in return, higher complexation strengths than the aforementioned cyclophanes.[42] Thus, the methoxy-decorated **CyOMe$_8$** is ideal for rotaxane synthesis and complexation studies in water. Although the affinity for a hydrophobic guest decreases by addition of organic solvents,[42] co-solvent such as MeOH, DMSO or CH_3CN may still be used to increase the solubility, resulting in a lower but sufficiently strong solvophobic effect. Therefore, supramolecular assemblies based on *Diederich*-type cyclophanes are not limited to pure water. A few reports of MIM syntheses incorporating **CyOMe$_8$** exist,[49] making it the only cyclophane of this type from which interlocked compounds have been synthesized to date.

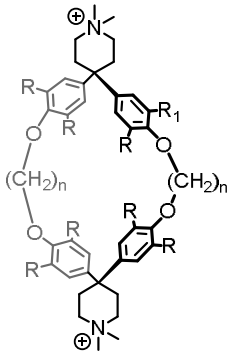

CyOMe$_8$: n = 4, R = OMe

Figure 6. Parent structure of *Diederich*-type cyclophanes with structural variations of the oligomethylene linker chains and decoration of the cavity. The counterion was omitted, generally the most water-soluble chloride form was used by our group or the groups of Diederich and Anderson.

In order to fulfill the requirements for the synthesis of rigid daisy chains, connection points for the coupling of aromatic guest moieties must be introduced. Copper(I)-catalyzed cycloaddition (CuAAC) click-chemistry[51] is ideal for MIM synthesis, although palladium-catalyzed cross-couplings may also fulfill the principles of click chemistry.[52] The two approaches towards daisy chains in this thesis rely on acetylene-functionalized *Diederich*-type cyclophanes, which can be coupled to a guest subunit by either CuAAC or Sonogashira cross-coupling. In approach a) (Figure 7) one aromatic subunit of **CyOMe$_8$** was replaced by an acetylene functionalized cresyl-unit, whereas in approach b) one spiropiperidine unit is replaced by propargylic methyl ether function. In another approach c) one of the side spacers is replaced with a N,N-bis(ethylene)-4-iodoaniline moiety, which can be employed for efficient Pd-catalyzed couplings owing to the iodo-subsituent. The slightly larger cavity size might be beneficial to compensate for possible unfavorable conformations of the flexible side-chains upon functionalization, whereas the methyl decoration is introduced to achieve high association constants in organic solution.

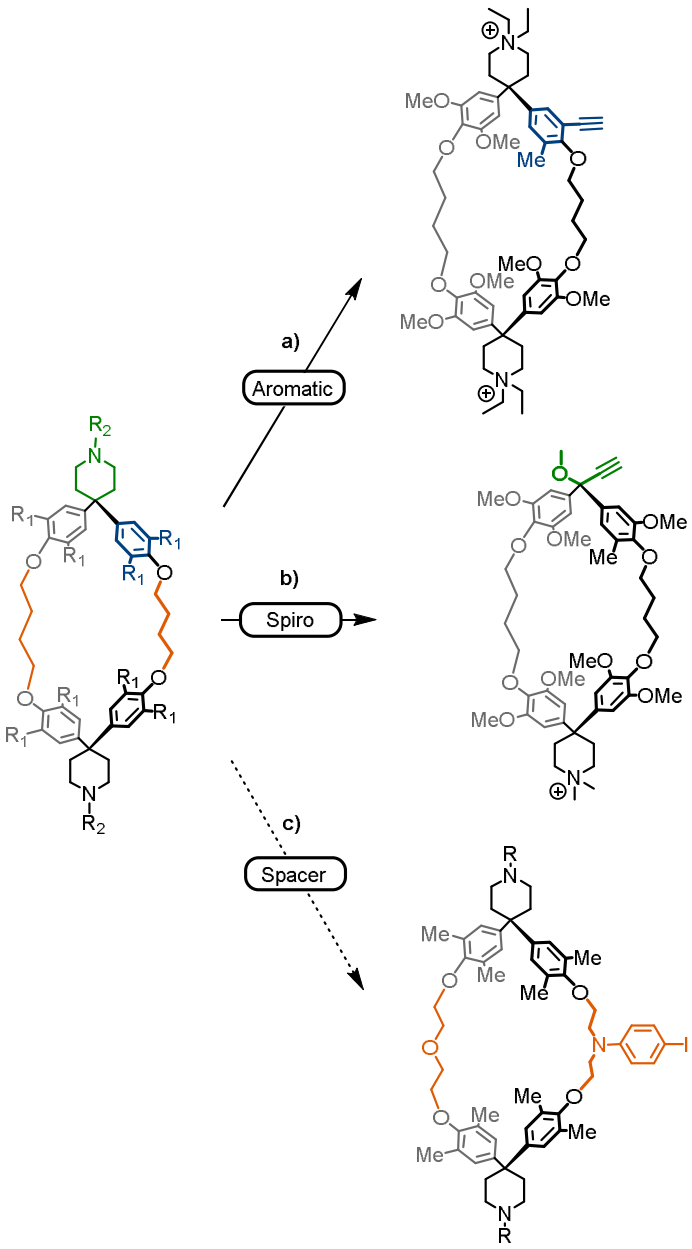

Figure 7. New, modified *Diederich*-type cyclophanes, which are either synthesized or discussed in this thesis.

Rigid, Water-Soluble Oligophenylenethynylene (OPE) Rods

Daisy chains are ideally synthesized from rigid monomers with low conformational flexibility in order to minimize the penalty in conformational entropy upon dimerization and avoid unimolecular self-threading. Moreover, a defined preorganization allows to control the aggregation mode of the monomeric daisy chains. OPE-type building blocks are ideal building blocks due to their high rigidity and their linear arrangement.[53–55] Although rigidity is in general favorable for template-directed assembly of MIMs, the combination with their intrinsic hydrophobicity results in a poor solubility particularly in water and lower alcohols. A number of OPEs or their diyne analogues were implemented into interlocked architectures, such as rotaxanes and insulated molecular wires of Tsuji [56–59], Anderson[49,60] or Bunz[61]. To increase solubility in aqueous-based media, strongly hydrophilic groups must be introduced. Neutral oligoethylene glycol chains and sugars or ionic groups such as carboxylates, sulfonates or quaternary ammonium ions have been used as solubilizers for poly(aryleneethynylene)s.[54] Out of these, most suitable for the purpose of rotaxane systems are compactly substituted, ionic arenes without any unnecessary side-chains to prevent the aryl moiety from acting as a stopper due to steric bulk. Synthetically well-accessible salicylic- or phthalic acid derivatives seem ideal building blocks for this purpose. Examples of OPE rods equipped with arylic carboxylate groups are often used as spacers in metal organic framework (MOF)-related chemistry,[62–65] conjugated polymers [66] and rotaxane syntheses.[49,60] The OPEs presented in this work are therefore based on salicylic-, terephthalic- or isophthalic acid derivatives. Preliminary complexation studies in collaboration with Dr. Sylvie Drayss-Orth[67] underpinned the suitability of carboxylate-OPE rods for host–guest systems in combination with *Diederich*-type cyclophanes. The remaining requirement for MIM synthesis by CuAAC are azide- substituents, by virtue of which modularly applicable building blocks are obtained. Throughout this thesis, all OPE rods are functionalized with aliphatic azides due to their lower photosensitivity compared to arylic azides. [68]

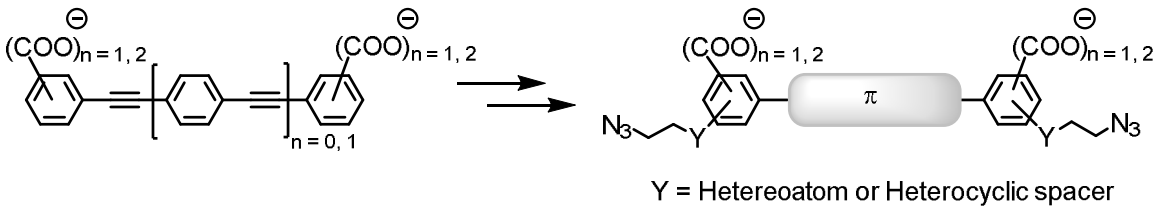

Figure 8. Left: General structure of the OPE rods studied in collaboration with Dr. Sylvie Drayss-Orth for their suitability of pseudorotaxane formation in combination with **CyOMe$_8$**. Right: General structure of azidoethyl-substituted OPE carboxylates which were targeted and synthesized in this work. Counterions are omitted.

Copper-Catalyzed Azide-Alkyne Cycloaddition

Ever since the original publications by Meldal,[69] Sharpless and Fokin[70] usage of copper catalyzed azide-alkyne cycloaddition (CuAAC) "click chemistry" has increased steadily. Numerous reaction protocols including the use of auxiliary ligands were published.[71,72] The term "click chemistry" applies to any kind of reaction which allows for a modular synthesis, is high-yielding, simple to perform and allows for simple isolation of products. It was originally branded by Sharpless[52] and is meanwhile often used synonymously with CuAAC, although it often does not fulfill all principles to which the definition of click chemistry was originally bound. Nevertheless, owing to its robustness, reliability, chemoselectivity and benign reaction conditions, CuAAC has emerged as an indispensable tool for constructing mechanically interlocked molecules.[51,73] By functionalization of building blocks with azide groups and terminal alkynes, a molecular construction kit is obtained which enables a modular construction of MIMs. Both functionalities are chemically well accessible and stable in spite of their potentially high reactivity. The explosion hazard of organic azides can be strongly reduced by designing precursors such that that the total number of carbon- and oxygen atoms exceeds the number of nitrogen atoms bound in azide groups by a factor of at least 3: $(N_C+N_O)/N_N \geq 3$. [74] The mechanism of this reaction was experimentally shown to proceed via a dinuclear copper complex,[75] confirming results from an earlier study.[76]

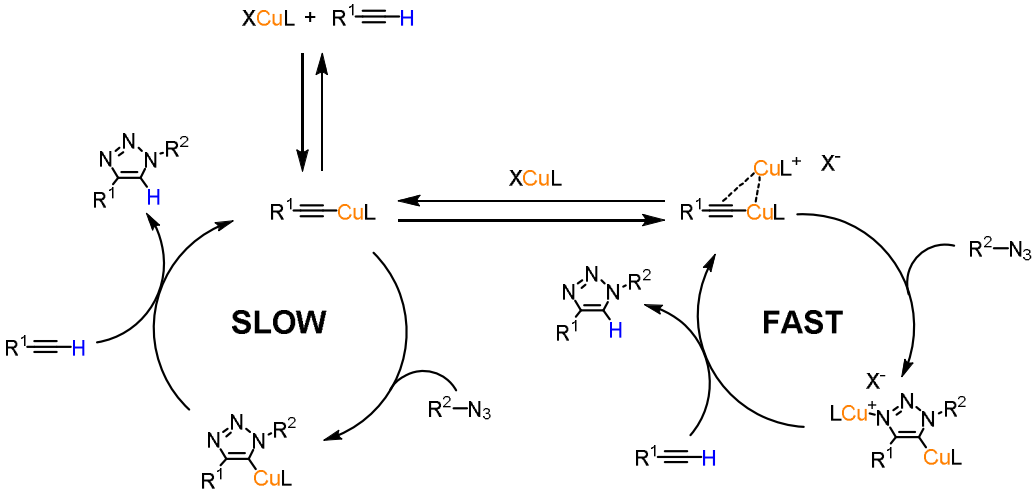

Figure 9. Mechanism of the CuAAC reaction, which can proceed via a two different catalytic cycles. It was shown that the main productive contribution stems from the cycle involving a dinuclear copper species.[75]

Chapters of this work

1. π-Conjugated, Interlocked Molecules: Opportunities, Challenges and Prospects

Among interlocked molecules, large π-conjugated structures are less commonly found than other types of structural motifs. Such structures offer a wide variety of unique properties owing to their rigidity and optical or electrochemical addressability. This allows to construct not only materials with sophisticated optoelectronic properties but also to synthesize rigid nanostructures with well-defined three dimensional structures. Moreover, a non-covalent linkage of molecular subunits can be employed for functionalization beyond the scope of covalent modification. Such modifications can be used for modulation of optoelectronic properties of a compound, for stabilization against physical or chemical stressors or for controlling aggregation and solubility. The intention of this chapter is to give an overview of conjugated structures in MIMs and point out remarkable properties in a few selected examples.

2. Assembly of [2]Rotaxanes in Water

To develop a model system for the construction of MIMs incorporating *Diederich*-type cyclophanes relying on a CuAAC-based assembly strategy, a series of naphthalenes equipped with propargyl-terminated oligoethyleneglycol chains in 2,6-positions was synthesized and analyzed for the suitability to prepare rotaxanes. Thermodynamics of pseudorotaxane formation was examined by fluorescence titration and isothermal titration calorimetry, revealing high binding constants of the naphthalene axles and **CyOMe$_8$**. Rotaxane formation was then examined by analytical HPLC after stoppering of the pseudorotaxane with a bulky, water-soluble azide-bearing stopper. It was found that tetraethylene glycol chains sufficiently solubilize the naphthalene cores and avoid precipitation of the guest from the aqueous cyclophane solution. The naphthalene guests proved to be suitable for MIM synthesis in combination with **CyOMe$_8$**. A rotaxane based on a naphthalene-2,6-dicarboxylate axle was synthesized in 59 % yield, however, the obtained samples contained impurities that could not be removed due to hydrolytic instability of the rotaxane. This was followed by the synthesis of a more robust, hydrolytically stable 2,6-dioxynaphthalene-based rotaxane . In this case, a yield of 19 % could be obtained after purification by HPLC. The synthetic work, physical measurements and preparation of the manuscript were carried out in close collaboration with Dr. Sylvie Drayss, and an early version of the manuscript is therefore included in her PhD thesis, the

TOC graphic was additionally designed by her. ^{1}H-NMR measurements and assignments were supported by Prof. Dr. Daniel Häussinger and his Wahlpraktikum student Felix Raps. Isothermal titration calorimetry (ITC) was performed by Dr. Michal Valášek. This work was published in *European Journal of Organic Chemistry*, **2017**, 4091–4103.

3. Aqueous assembly of Zwitterionic Daisy Chains

The synthesis of molecular daisy chains based on a positively charged *Diederich*-type cyclophane and a negatively charged salicylate-based OPE rod is presented. The synergistic combination of the hydrophobic effect and ion-pairing interaction leads to strong aggregation of the daisy chain monomer which was investigated by concentration-dependent ^{1}H-NMR in D_2O/MeOD (v/v, 4:1) mixtures. Due to the simultaneous presence of several aggregates, no quantitative assessment of the association strength could be made. The binding strength of a salicylate-based OPE and **CyOMe$_8$** as a model system was therefore examined, revealing a very large association constant (4 * 10^6 M^{-1}) confirming the beneficial effect of the additional electrostatic attraction. Mechanically interlocked daisy chains were then obtained from a *click*-stoppering reaction in H_2O/MeOH (v/v, 4:1), using a similar stopper as in chapter 2. From this reaction [*c*2]- and [*a*2]daisy chains were obtained after purification by preparative HPLC. Characterization of the final products by ^{1}H-NMR supported the interlocked nature of the daisy chains and, according to the expectations, the cyclic dimer consisted of a mixture of C_i- and C_2-symmetric diastereomers. Initial analytical separation attempts were supported by Dr. Sylvie Drayss and ^{1}H-NMR DOSY measurements were performed by PD Dr. Daniel Häussinger. Dr. Michal Valášek contributed ITC measurements to determine thermodynamic binding parameters and attempted to obtain calorimetric data for the dissociation of daisy chains. This work was originally included as an accepted manuscript in this work. Meanwhile it has been published in *Chemistry – A European Journal,* **2019**, 25, 285–295.

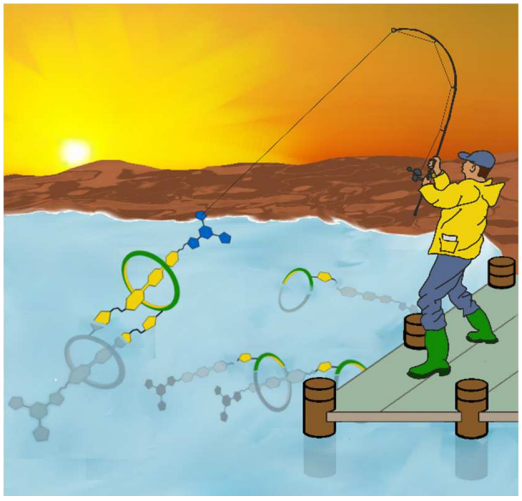

4. Slow Formation of Pseudorotaxanes in Water: Large Influence of the Substitution Pattern

As the zwitterionic daisy chains and their hermaphroditic precursor in chapter 3 were insoluble in pure water, OPE rods with additional charges could improve the solubilization. Compactly substituted terephthalate- and isophthalate solubilizers were synthesized to introduce additional carboxylate groups along with the required azide functionality. These OPE rods were intended as model compounds to probe the association behavior in combination with **CyOMe$_8$**. Slow pseudorotaxane formation kinetics in the order of hours to days for a complete reaction were observed. The binding constants of these OPE rods in MeOD/D_2O 19:1 were compared to the salicylate rod from chapter 3 and found to be of similar magnitude. VT-NMR indicated that the pseudorotaxanes are thermodynamically stable at elevated temperatures. The combination of a high thermodynamic stability and kinetic inertness in an aqueous-based system is unprecedented. Together with the peripheral azide substituent, these OPE-Rods represent promising building blocks for supramolecular systems with kinetically controlled association processes or co-conformational switching. This work was supported by Laurent Jucker, who proofread the manuscript and contributed analytical data for host/guest association and compound characterization. Prof. Dr. Daniel Häussinger conducted VT-NMR measurements for thermal stability determination of the pseudorotaxanes. This article was originally included as prepared for submission to *European Journal of Organic Chemistry* as an invited contribution to the Special Issue Dedicated to 50 Years of Rotaxanes. Meanwhile, the article has been published in *European Journal of Organic Chemistry*, **2019**, 3384–3390 and is included as its final version in this thesis.

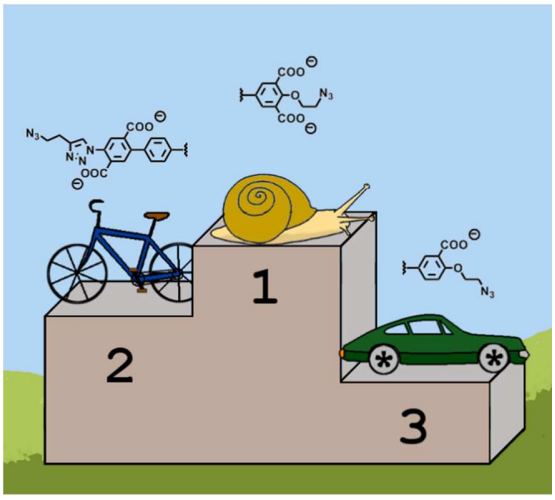

5. Outlook: Towards Kinetically Controlled Assembly of Molecular Daisy Chains

An approach towards the synthesis of a highly rigid daisy chain is presented, which relies on the isophthalate solubilizer and the spiro-functionalized cyclophane (Figure 7) presented in the previous chapter and the introduction. In this approach it was attempted combine several design considerations: (I) an exceptionally rigid linkage of OPE rod and cyclophane to promote to reduce the entropic penalty of daisy chain formation; (II) Improved solubility features due to non-zero net charge of the target structure (III) kinetic control over the association mode by a bulky isophthalate end-group. This work was supported by Yanik Weber during his Laboratory practical. As the synthesis of the target structure could not be completed, this chapter is presented as a possible outlook for highly rigid daisy chain structures.

References

[1] P. Kirkpatrick, C. Ellis, *Nature* **2004**, *432*, 823–823.
[2] J. M. Lehn, *Science* **1993**, *260*, 1762–1763.
[3] J.-M. Lehn, *Supramolecular Chemistry: Concepts and Perspectives*, Wiley-VCH Verlag GmbH & Co. KGaA, Weinheim, FRG, **1995**.
[4] C. J. Bruns, J. F. Stoddart, *The Nature of the Mechanical Bond: From Molecules to Machines*, John Wiley & Sons, Inc., Hoboken, NJ, USA, **2016**.
[5] H. L. Frisch, E. Wasserman, *J. Am. Chem. Soc.* **1961**, *83*, 3789–3795.
[6] E. Wasserman, *J. Am. Chem. Soc.* **1960**, *82*, 4433–4434.
[7] G. Schill, A. Lüttringhaus, *Angew. Chem. Int. Ed. Engl.* **1964**, *3*, 546–547.
[8] Q. Wu, P. M. Rauscher, X. Lang, R. J. Wojtecki, J. J. de Pablo, M. J. A. Hore, S. J. Rowan, *Science* **2017**, *358*, 1434–1439.
[9] P. R. Ashton, I. Baxter, M. C. T. Fyfe, F. M. Raymo, N. Spencer, J. F. Stoddart, A. J. P. White, D. J. Williams, *J. Am. Chem. Soc.* **1998**, *120*, 2297–2307.
[10] G. A. Breault, C. A. Hunter, P. C. Mayers, *Tetrahedron* **1999**, *55*, 5265–5293.
[11] I. T. Harrison, S. Harrison, *J. Am. Chem. Soc.* **1967**, *89*, 5723–5724.
[12] G. Schill, H. Zollenkopf, *Justus Liebigs Ann. Chem.* **1969**, *721*, 53–74.
[13] M. Xue, Y. Yang, X. Chi, X. Yan, F. Huang, *Chem. Rev.* **2015**, *115*, 7398–7501.
[14] J. Rotzler, M. Mayor, *Chem Soc Rev* **2013**, *42*, 44–62.
[15] P. R. Ashton, I. Baxter, S. J. Cantrill, M. C. T. Fyfe, P. T. Glink, J. F. Stoddart, A. J. P. White, D. J. Williams, *Angew. Chem. Int. Ed.* **1998**, *37*, 1294–1297.
[16] M. C. Jiménez, C. Dietrich-Buchecker, J.-P. Sauvage, A. De Cian, *Angew. Chem. Int. Ed.* **2000**, *39*, 1295–1298.
[17] S. J. Rowan, S. J. Cantrill, J. F. Stoddart, A. J. P. White, D. J. Williams, *Org. Lett.* **2000**, *2*, 759–762.
[18] T. Hoshino, M. Miyauchi, Y. Kawaguchi, H. Yamaguchi, A. Harada, *J. Am. Chem. Soc.* **2000**, *122*, 9876–9877.
[19] T. Fujimoto, Y. Sakata, T. Kaneda, *Chem. Commun.* **2000**, 2143–2144.
[20] M. C. Jiménez, C. Dietrich-Buchecker, J.-P. Sauvage, *Angew. Chem.* **2000**, *39*, 3284–3287.
[21] J. P. Sauvage, *Acc. Chem. Res.* **1990**, *23*, 319–327.

[22] R. S. Forgan, J.-P. Sauvage, J. F. Stoddart, *Chem. Rev.* **2011**, *111*, 5434–5464.
[23] K. Iwaso, Y. Takashima, A. Harada, *Nat. Chem.* **2016**, *8*, 625–632.
[24] C. J. Bruns, J. Li, M. Frasconi, S. T. Schneebeli, J. Iehl, H.-P. Jacquot de Rouville, S. I. Stupp, G. A. Voth, J. F. Stoddart, *Angew. Chem. Int. Ed.* **2014**, *53*, 1953–1958.
[25] C. J. Bruns, M. Frasconi, J. Iehl, K. J. Hartlieb, S. T. Schneebeli, C. Cheng, S. I. Stupp, J. F. Stoddart, *J. Am. Chem. Soc.* **2014**, *136*, 4714–4723.
[26] J. Wu, K. C.-F. Leung, D. Benítez, J.-Y. Han, S. J. Cantrill, L. Fang, J. F. Stoddart, *Angew. Chem.* **2008**, *120*, 7580–7584.
[27] F. Coutrot, C. Romuald, E. Busseron, *Org. Lett.* **2008**, *10*, 3741–3744.
[28] L. Fang, M. Hmadeh, J. Wu, M. A. Olson, J. M. Spruell, A. Trabolsi, Y.-W. Yang, M. Elhabiri, A.-M. Albrecht-Gary, J. F. Stoddart, *J. Am. Chem. Soc.* **2009**, *131*, 7126–7134.
[29] P. Waelès, B. Riss-Yaw, F. Coutrot, *Chem. Eur. J.* **2016**, *22*, 6837–6845.
[30] A. Goujon, G. Mariani, T. Lang, E. Moulin, M. Rawiso, E. Buhler, N. Giuseppone, *J. Am. Chem. Soc.* **2017**, *139*, 4923–4928.
[31] S. Tsukagoshi, A. Miyawaki, Y. Takashima, H. Yamaguchi, A. Harada, *Org. Lett.* **2007**, *9*, 1053–1055.
[32] A. Goujon, T. Lang, G. Mariani, E. Moulin, G. Fuks, J. Raya, E. Buhler, N. Giuseppone, *J. Am. Chem. Soc.* **2017**, *139*, 14825–14828.
[33] C. J. Bruns, M. Frasconi, J. Iehl, K. J. Hartlieb, S. T. Schneebeli, C. Cheng, S. I. Stupp, J. F. Stoddart, *J. Am. Chem. Soc.* **2014**, *136*, 4714–4723.
[34] J. Voignier, J. Frey, T. Kraus, M. Buděšínský, J. Cvačka, V. Heitz, J.-P. Sauvage, *Chem. - Eur. J.* **2011**, *17*, 5404–5414.
[35] J.-C. Chang, S.-H. Tseng, C.-C. Lai, Y.-H. Liu, S.-M. Peng, S.-H. Chiu, *Nat. Chem.* **2017**, 128-134
[36] D. Chandler, *Nature* **2005**, *437*, 640–647.
[37] E. A. Meyer, R. K. Castellano, F. Diederich, *Angew. Chem. Int. Ed.* **2003**, *42*, 1210–1250.
[38] C. A. Lipinski, F. Lombardo, B. W. Dominy, P. J. Feeney, *Adv. Drug Deliv. Rev.* **2001**, *46*, 3–26.
[39] L. Cao, L. Isaacs, *Org. Lett.* **2012**, *14*, 3072–3075.
[40] F. Diederich, in *Mod. Cyclophane Chem.*, Wiley-VCH Verlag GmbH & Co. KGaA, Weinheim, FRG, **2005**, pp. 519–546.
[41] F. Diederich, *Angew. Chem. Int. Ed. Engl.* **1988**, *27*, 362–386.
[42] S. B. Ferguson, E. M. Sanford, E. M. Seward, F. Diederich, *J. Am. Chem. Soc.* **1991**, *113*, 5410–5419.
[43] F. Diederich, D. R. Carcanague, *Angew. Chem. Int. Ed. Engl.* **1990**, *29*, 769–771.
[44] B. R. Peterson, F. Diederich, *Angew. Chem. Int. Ed. Engl.* **1994**, *33*, 1625–1628.
[45] F. Diederich, K. Dick, D. Griebel, *J. Am. Chem. Soc.* **1986**, *108*, 2273–2286.
[46] F. Diederich, G. Schuermann, I. Chao, *J. Org. Chem.* **1988**, *53*, 2744–2757.
[47] D. R. Benson, R. Valentekovich, F. Diederich, *Angew. Chem. Int. Ed. Engl.* **1990**, *29*, 191–193.
[48] P. Mattei, F. Diederich, *Angew. Chem. Int. Ed. Engl.* **1996**, *35*, 1341–1344.
[49] M. J. Frampton, H. L. Anderson, *Angew. Chem. Int. Ed.* **2007**, *46*, 1028–1064.
[50] B. Kenda, F. Diederich, *Angew. Chem. Int. Ed.* **1998**, *37*, 3154–3158.
[51] K. D. Hänni, D. A. Leigh, *Chem Soc Rev* **2010**, *39*, 1240–1251.
[52] H. C. Kolb, M. G. Finn, K. B. Sharpless, *Angew. Chem. Int. Ed.* **2001**, *40*, 2004–2021.
[53] U. H. F. Bunz, *Chem. Rev.* **2000**, *100*, 1605–1644.
[54] U. H. F. Bunz, *Macromol. Rapid Commun.* **2009**, *30*, 772–805.
[55] R. R. Tykwinski, *Angew. Chem. Int. Ed.* **2003**, *42*, 1566–1568.
[56] J. Terao, S. Tsuda, Y. Tanaka, K. Okoshi, T. Fujihara, Y. Tsuji, N. Kambe, *J. Am. Chem. Soc.* **2009**, *131*, 16004–16005.
[57] M. Kiguchi, S. Nakashima, T. Tada, S. Watanabe, S. Tsuda, Y. Tsuji, J. Terao, *Small* **2012**, *8*, 726–730.
[58] J. Terao, A. Wadahama, A. Matono, T. Tada, S. Watanabe, S. Seki, T. Fujihara, Y. Tsuji, *Nat. Commun.* **2013**, *4*, DOI 10.1038/ncomms2707.
[59] H. Masai, J. Terao, T. Fujihara, Y. Tsuji, *Chem. Eur. J.* **2016**, *22*, 6624–6630.

[60] H. W. Daniell, E. J. F. Klotz, B. Odell, T. D. W. Claridge, H. L. Anderson, *Angew. Chem. Int. Ed.* **2007**, *46*, 6845–6848.
[61] J. S. Park, J. N. Wilson, K. I. Hardcastle, U. H. F. Bunz, M. Srinivasarao, *J. Am. Chem. Soc.* **2006**, *128*, 7714–7715.
[62] T. M. Fasina, J. C. Collings, J. M. Burke, A. S. Batsanov, R. M. Ward, D. Albesa-Jové, L. Porrès, A. Beeby, J. A. K. Howard, A. J. Scott, et al., *J. Mater. Chem.* **2005**, *15*, 690–697.
[63] X. Song, X. Liu, M. Oh, M. S. Lah, *Cryst. Growth Des.* **2010**, *10*, 3222–3227.
[64] T. L. H. Doan, H. L. Nguyen, H. Q. Pham, N.-N. Pham-Tran, T. N. Le, K. E. Cordova, *Chem. Asian J.* **2015**, *10*, 2660–2668.
[65] R. J. Marshall, S. L. Griffin, C. Wilson, R. S. Forgan, *Chem.Eur. J.* **2016**, *22*, 4870–4877.
[66] H. Häger, W. Heitz, *Macromol. Chem. Phys.* **1998**, *199*, 1821–1826.
[67] S. C. Drayss-Orth, PhD Thesis, **2016**, DOI 10.5451/unibas-006672844.
[68] P. R. Serwinski, P. M. Lahti, *Org. Lett.* **2003**, *5*, 2099–2102.
[69] C. W. Tornøe, C. Christensen, M. Meldal, *J. Org. Chem.* **2002**, *67*, 3057–3064.
[70] V. V. Rostovtsev, L. G. Green, V. V. Fokin, K. B. Sharpless, *Angew. Chem. Int. Ed.* **2002**, *41*, 2596–2599.
[71] M. Meldal, C. W. Tornøe, *Chem. Rev.* **2008**, *108*, 2952–3015.
[72] J. E. Hein, V. V. Fokin, *Chem. Soc. Rev.* **2010**, *39*, 1302–1315
[73] M. Xue, Y. Yang, X. Chi, X. Yan, F. Huang, *Chem. Rev.* **2015**, *115*, 7398–7501.
[74] S. Bräse, C. Gil, K. Knepper, V. Zimmermann, *Angew. Chem. Int. Ed.* **2005**, *44*, 5188–5240.
[75] L. Jin, D. R. Tolentino, M. Melaimi, G. Bertrand, *Sci. Adv.* **2015**, *1*, e1500304–e1500304.
[76] B. T. Worrell, J. A. Malik, V. V. Fokin, *Science* **2013**, *340*, 457–460.

π-Conjugated, Interlocked Molecules: Opportunities, Challenges and Prospects

One is tempted to consider the synthesis of many classes of π-conjugated structures as a routine task. The repertory of synthetic methodology has expanded not least due to the development of palladium catalyzed cross-coupling,[1] which gives access to previously unknown or only tediously accessible conjugated structures. Such materials are of interest not only due to their electronic nature,[2] but also due to their often rigid and planar structure. These key properties make π-conjugated materials unique building blocks for supramolecular systems.[3] Despite the continuous development of new synthetic methods, chemistry still faces synthetic challenges when it comes to π-conjugated structures, such as carbon-rich materials,[4,5] conjugated macrocycles and cages,[5–7] or open-shell structures.[8] Moreover, design of materials for organic electronics[2] with tailored optoelectronic properties is an ongoing challenge. From a materials science perspective, it is required not only to control intramolecular properties, but also intermolecular behavior such as aggregation, solubility and the nature of a local chemical environment. For example, non-covalent functionalization can significantly contribute to the stability and solubility of substance classes which are otherwise unstable, hard to characterize or unprocessable. While covalent modification of π-conjugated systems represents a conservative approach to modify molecular properties, the possibility of introducing mechanical bonds[9] or for supramolecular modification[10] provides additional and sometimes complementary options to do so. In certain cases, covalent modification may not even be an option. For example, in carbon allotropes consisting almost exclusively of an sp^2- or sp-hybridized conjugated structure, this would lead to a disturbance of their pristine structure.[4,5] Whereas supramolecular complexes are kinetically labile and thermodynamic stability depends on the chemical and physical environment, mechanically interlocked molecules (MIMs) are kinetically inert. Dissociation of MIMs requires the breaking of covalent bonds or very harsh reaction conditions to induce dissociation,[9] thus their robustness is comparable to structures linked by covalently. Wholly new design considerations may arise from mechanically bonded π-systems. These are frequently neglected or overlooked as often this option is either considered to be too complex for practical implementation or simply not part of the organic chemist's thought pattern. The increasing

impact of MIM-based molecular machines on fundamental science has been paid tremendous attention after awarding the 2016 Nobel Prize for the development of molecular machinery. This topic has already been extensively reviewed.[9,11,12] While it remains fascinating that chemistry is able to implement large amplitude motions on a molecular scale, the impact that the mechanical bond has on static molecular properties is equally exciting. From the viewpoint of fundamental research, π-conjugated MIMs may add opportunities for the implementation of completely new optoelectronic functions and/or stabilization of unprecedented classes of conjugated materials. This includes for example conjugated superstructures with a high degree of rigidity or unprecedented topologies, the development of interlocked cages or scaffolds and stabilization of labile substances by mechanically bonded subunits. From a more applied viewpoint of chemistry, the potential impact of MIMs on materials chemistry becomes evident if one considers that the first organic electronic devices have entered the mass consumer market. Organic light emitting diodes (OLEDs) have become ubiquitous and the increasing commercialization of organic-/dye-sensitized solar cells is ongoing. Materials with optimizations relying on mechanical bonds may eventually find applications in the area of organic electronics. Dedicated attention to the latest developments of static MIMs involving extended π-systems should therefore be paid.

The synthesis and handling of π-conjugated structures often poses specific challenges beyond finding an expedient synthetic pathway. In the case of rigid and planar conjugated core structures, π- π-stacking often leads to poor solubility,[13] which results in the necessity of introducing solubilizing groups or deplanarizing substituents. Without adequate solubilizers, characterization by common spectroscopic techniques is sometimes difficult if not impossible and processability for a desired application may not be given. In addition, π-conjugated molecules may display insufficient stability towards light, temperature or chemically reactive species. The reactivity results from often narrow π-π* gaps in conjugated systems, especially for near infrared (NIR)-active compounds. A very common phenomenon resulting from excited state reactivity is the bleaching of dyes upon exposure to UV-radiation. This is known in everyday life when old, colored magazines lose their colors or in the laboratory where it is common that certain chromophores are photobleached during optical measurements. Some substance classes may therefore be inapplicable for a desired purpose due to their unstable nature under a given set of conditions. This is further aggravated by strong absorptivity of light, which leads to population of

more reactive excited states upon irradiation. Classically, thermodynamic stability issues of a chromophore would be resolved by adjustment of the electronic structure with electron-donating or withdrawing substituents, whereas kinetic stability can be increased by introducing steric protection in the form of bulky substituents. The introduction of a mechanically bonded unit can represent a more modular way of modifying the above properties. MIMs always have a three-dimensional structure which breaks planarity and thus improves solubility. Additionally, a π-system can be encapsulated to provide kinetic protection against physical and chemical stress. Compared to stabilization by modification of the electronic structure with substituent effects this holds the advantage that the parent electronic nature of a chromophore can be retained, which of course also depends on the extent of its interaction with the encapsulating component. In return, electronic modulation by strong interaction of the interlocked components can also be exploited to increase stability. These principles were implemented in the development of various insulated molecular wires and chromophores[14] which are perhaps among the most likely candidates for technical application. An exceptionally valuable opportunity in MIM chemistry is the potential for a modular assembly of multi-component systems of large molecular size, which could not be reasonably achieved by a covalent assembly strategy. Such interlocked assemblies may serve as tools for examination of photophysical or electronic properties of well-defined, non-covalently bound structures without the necessity to take into account association/dissociation dynamics an equilibria or stoichiometrical variations of the individual components. In addition, hierarchical structures and topologically interesting materials may serve to pioneer the three-dimensional, spatially precise arrangement of chromophores. Such materials could be used for mimicking biological processes or could lead to the emergence of unusual electrochemical and photophysical properties.

Naturally, these opportunities often bring along new synthetic challenges, which can be alleviated to some extent by application of modular assembly strategies. It is certainly not always required to rely on mechanically bonded subunits and a supramolecular complex may also fulfill a desired purpose. However, the robustness that MIMs provide qualify them as superior options in many cases because they are discrete chemical entities which can be characterized and handled as such. No solvent- or concentration-dependent dissociation occurs and the stoichiometry is always well defined. This work aims to give an overview of established concepts that organic-

based MIM chemistry can contribute to materials chemistry and point out remarkable examples with unusual topological features or physical properties. The challenges that π-conjugated structures pose and the opportunities they provide are quite specific. Therefore, the scope is limited to examples where the aforementioned properties arise from this structural feature. The following criteria were considered for this work: (i) chemical stabilization, (ii) control of solubility and aggregation, (iii) modulation of optoelectronic properties, (iv) topologically interesting, π-conjugated materials. Often a combination of these criteria is applicable. The given examples are roughly divided in two sections containing (i) – (iii) and (iv). In advance to these two sections, a brief overview over the most common assembly strategies for π-conjugated MIMs is given. A focus on organic and non-dynamic, covalently interlocked materials is laid, thus excluding MIMs assembled by metallosupramolecular chemistry and imine/boronic acid linkage.

Strategies for assembling conjugated MIMs

Receptors & Recognition: The introduction of mechanical bonds usually relies on directed supramolecular assembly strategies[11] to avoid the necessity of statistical assembling. Directed methods rely either on supramolecular-, covalent-, or metal-templation. As a hybrid between covalent and supramolecular templation, intramolecular recognition may also be an option for constructing MIMs. In recent years, the method of active metal templation[15] was additionally established. Once a supramolecular assembly is obtained, dissociation needs to be prevented by introducing insurmountable steric barriers in the form of bulky stoppers or catenation, depending on the desired topology. There are various methods available for interlocking supramolecular assemblies, of which the most frequently applied ones are shown in Figure 1.

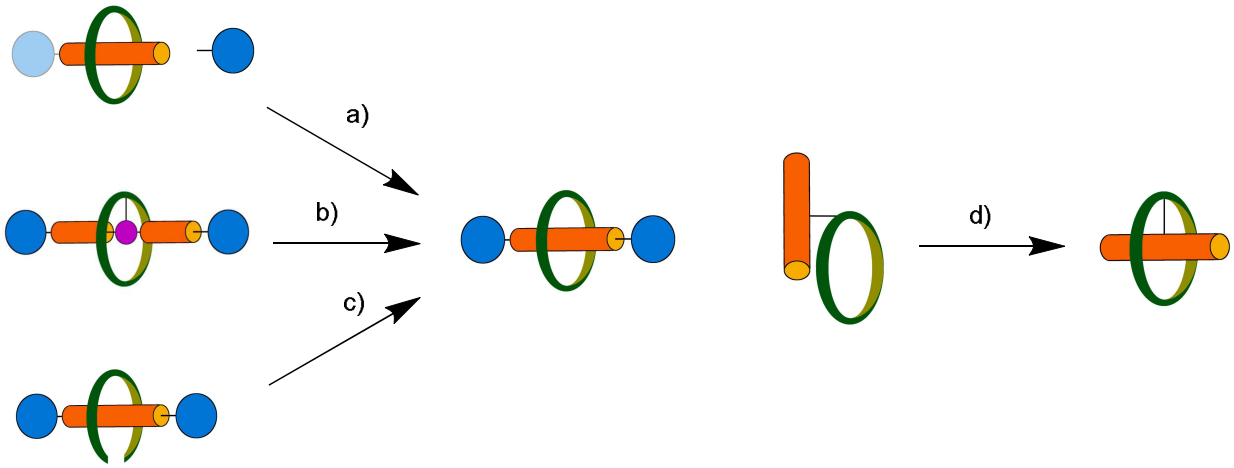

Figure 1. Methods for template-directed rotaxane syntheses presented in this work. a) Stoppering followed by threading, which can start from an unstoppered axle (capping) or from a monostoppered axle (snapping);[11] b) active metal templation, here shown as intermediate with all components bound to the catalytic metal template; c) clipping: in this approach, the macrocycle is either closed by intermolecular or intramolecular macrocyclization; d) intramolecular slipping approach. Catenane syntheses in this work all rely on clipping approaches which essentially is equivalent to the macrocyclization of a pseudorotaxane axle.

For template-directed assembly, a multitude of host-guest recognition motifs is available, among which a few are predominantly applied in the construction of π-conjugated MIMs. In functional materials the introduction of a dedicated recognition site, which has no other purpose than to promote supramolecular assembly, should ideally not be required. This results for example in a comparably rare occurrence of the classical crown-ether/cation recognition motif for the construction of conjugated MIMs. Still, derivatives of crown ethers occur frequently in form of electron-rich hydroquinone- and dioxynaphthalene ether-based cyclophanes, which are bridged by oligoethylene oxide units. These derivatives eventually rely on π-donor/acceptor recognition, which is among the most frequently used driving forces for conjugated MIM assembly. The predominantly used class of receptors capable of recognizing conjugated guests are the cationic, viologen-type receptors which have been synthesized in various sizes (Figure 2).[16,17]

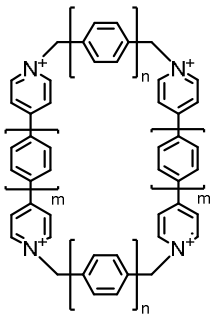

Figure 2. Generalization of the viologen-type receptors developed by Stoddart et. al. The parent receptor with n = 1 and m = 0 is widely used and well known under the nickname "blue box". Larger receptors such as ExBox (n = 1, m = 1) are capable of complexing polycyclic aromatic hydrocarbons (PAHs) and large chromophores such as porphyrins.

These electron-poor receptors are capable of recognizing electron-rich and/or extended conjugated units, spanning from relatively small hydroquinone ethers and tetrathiafulvalenes to polycyclic aromatic hydrocarbons and C_{60}-fullerenes. Charge-transfer interactions are only observed in combination with electron-rich guests, therefore resulting in distinctively different optoelectronic properties of a resulting MIM compared to the parent components. As electrochemical reduction is possible for these receptors, they convey additional functionality to a MIM which was extensively used for switchable structures based on the "blue box"-receptor (Figure 2). One-electron reduction of viologens generates radical cations, which tend to associate mutually and hence create a new type of radical-radical interaction based recognition system. By anion exchange, their solubility features can be tuned from organic-soluble (PF_6^-) to water-soluble (Cl^-) making them applicable in a wide range of chemical environments. Other types of donor-acceptor interactions have emerged on the basis of naphthalene- and perylenediimide (NDI and PDI) acceptors and the aforementioned electron-donating electron-rich aromatics. MIMs based on such a recognition motif are inherently neutral and thus eliminate the sometimes tedious struggle of dealing with counterions.

Most conjugated building blocks are of relatively unpolar nature and hence possess no specific driving force for recognition except for relatively weak Van der Waals interactions, though especially aromatics with large surface area may still possess a significant driving force for aggregation.[13] A driving force relying on the expulsion of solvent can therefore compensate for the lack of strong intermolecular interactions of host and guest. Exceptionally useful and perhaps the most important receptors for constructing insulated molecules are the cyclodextrins (CDs, Figure 3),[16,18] which are water-soluble and recognize hydrophobic guests with high specifity.

They are manufactured at large scale, widely commercially available and exist with various cavity sizes (α,β, or γ-CD). A wide range of hydrophobic guests can be incorporated into these CDs, ranging from simple alkyl chains to pyrene- and perylene derivatives.

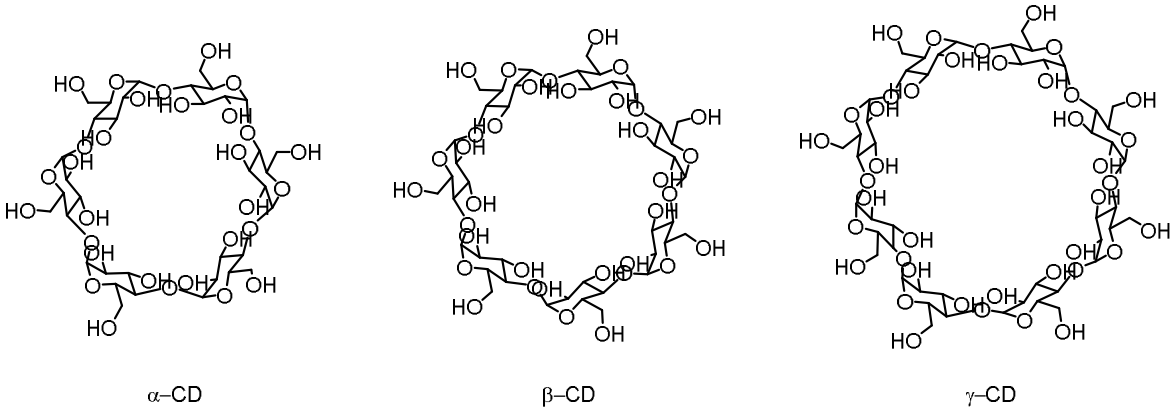

Figure 3. The three most common cyclodextrins in axial view consisting of 6 (α-CD), 7 (β-CD) or 8 (γ-CD) D-glucose units, linked by 1,4-glycosidic bonds. The hydroxyl groups which largely point outwards of the cavity can be further functionalized.

As an additional benefit, their hydroxyl groups can be further functionalized with a diversity of functional groups, even when already introduced into an interlocked assembly.[19,20] Thus, CDs may also serve as a hub for the post-assembly modification of MIMs. Cucurbiturils[16] (Figure 4) are also often encountered as hosts for aromatic units and are commercially available as well, but do not come close to the synthetic flexibility of cyclodextrins. Similar to cyclodextrins, they come with different cavity sizes, depending on the number of methylene-bridged glycoluril units.

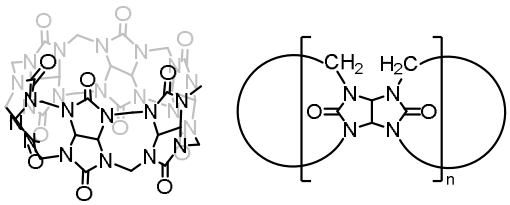

Figure 4. Cucurbit[6]uril (left) and generalized structure of cucurbit[n]urils (right).

A major disadvantage of a solvophobic recognition motif is the inherent lack of specific interaction. As a result, a desired complexation mode might be completely absent if the self-association of either host or guest is stronger than association to a binary complex. Furthermore, unspecific aggregate formation (e.g. micelles, bilayers) or even phase segregation due to insolubility can occur. The latter problem cannot always be compensated for by a different choice

of solvent as this may completely disrupt solvophobic forces. These limitations must be carefully taken into account when designing target structures, especially when dealing with larger, π- conjugated structures.

Assembly by transition metal templation is among the most powerful protocols for synthesizing MIMs, especially for structures with a high degree of complexity or strain. The Cu(I)-phenanthroline or bipyridine recognition motif[15,21,22] has been most frequently applied among these and gave rise to some of the most intriguing interlocked structures (Figure 5).

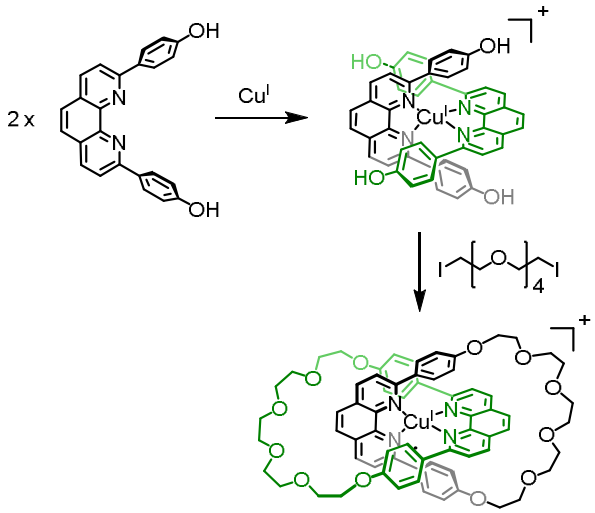

Figure 5. Sauvage's copper-phenanthroline-based catenane, which embodies the seminal work for a wider variety of MIMs.

It still remains one of the most successfully applied protocols today – more than 30 years after its first appearance. The reason for this success lies certainly in the stability and the predictable geometry of the templated complexes, resulting in well-preorganized structures for MIM synthesis. These complexes can be isolated and characterized prior to MIM formation as they exhibit no or only little exchange dynamics, which allows to exclude the presence of undesired aggregation modes. The catalytic activity of Cu(I) complexes can be harnessed for Glaser-Hay-Eglington, Cadiot-Chodkiewicz or copper-catalyzed alkyne azide cycloaddition (CuAAc) reactions. It is therefore of no surprise that this approach evolved to *active* metal templation[15] in which the catalytic activity of the transition metal template is exploited for mechanical bond formation. Unlike in the passive metal templated assembly, the catalytic metal may be added in substoichiometric amounts and no preassembled Cu(I)-complex is isolated in such protocols. Assembly strategies relying on transition metal-based methods are never traceless as they come at the price of vestigial ligands in the target structure, which may be undesirable when tailoring

of optoelectronic properties is intended. However this is of no concern if a MIM is merely synthesized for its interesting topology or unprecedented structural elements.

Stabilization and modulation of optoelectronic properties by encapsulation.

Rotaxanation of chromophores is a particularly successful example which has proven to enhance the ruggedness of various chromophores and to control their local chemical environment to modify their photophysical properties. Although this topic has been reviewed previously,[9,11,14,23] it is briefly presented herein for the sake of topical completeness. This was realized for small, insulated chromophores and also for oligo-/polymeric insulated molecular wires (IMWs).[14] Stability of otherwise rather fragile squaraine and cyanine NIR dyes was strongly enhanced by rotaxanation,[24,25] which are both known to be either attacked by nucleophiles or photooxidized in absence of an insulating macrocycle.

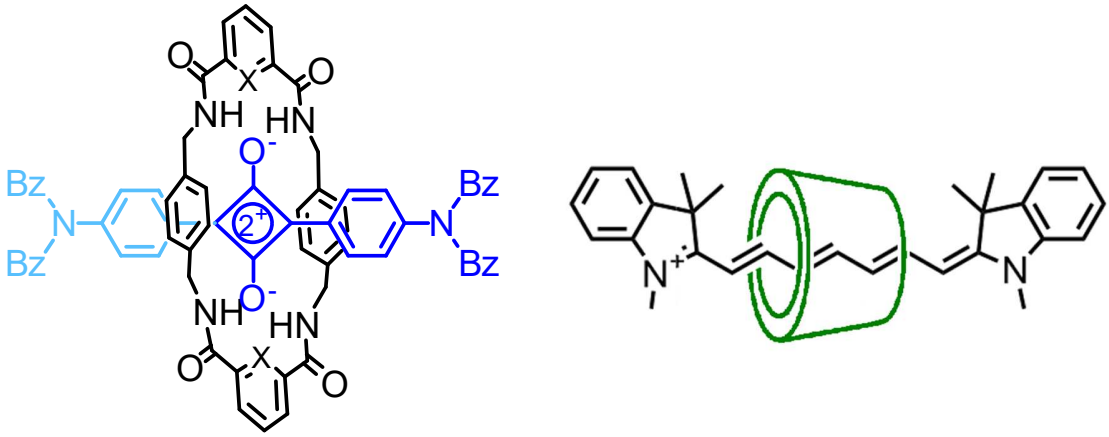

Figure 6. Left: A squaraine, which was protected by rotaxanaton (X = C or N).[24] Right: An α-CD-encapsulated cyanine dye.[26]

Polymeric and oligomeric IMWs[14,23,27] based on azo-dyes, anthracene-, phenylethynyl-, styryl-, phenylene-, and thiophene units[11,14,28] were encapsulated with α / β / γ-CDs or cyclophanes. Improved photostability, solubility, photo- and electroluminescence yields were observed. These improvements underpin the benefits that MIM-based materials may bring into future optoelectronic applications.[23] Usage of rotaxanated chromophores to control aggregation in photovoltaic devices[29,30] was attempted as well, yet no particular improvement of power conversion efficiency could be achieved. β-CD/Fluorene-based IMWs could be rendered organic-soluble (e.g. in cyclohexane, $CHCl_3$) by silylation, alkylation or esterification of the peripherial

hydroxyl groups while still retaining favorable optoelectronic properties.[19,20] Without this modification, these polymers were exclusively soluble in high-polarity solvents or water. Post-functionalization of these CD-based rotaxanes was achieved by introducing triarylamine donor chromophores (Figure 7).[31] Charge-separated states between triarylamine donor and conjugated axle were observed upon photoexcitation, demonstrating the potential of such assemblies for light harvesting systems.

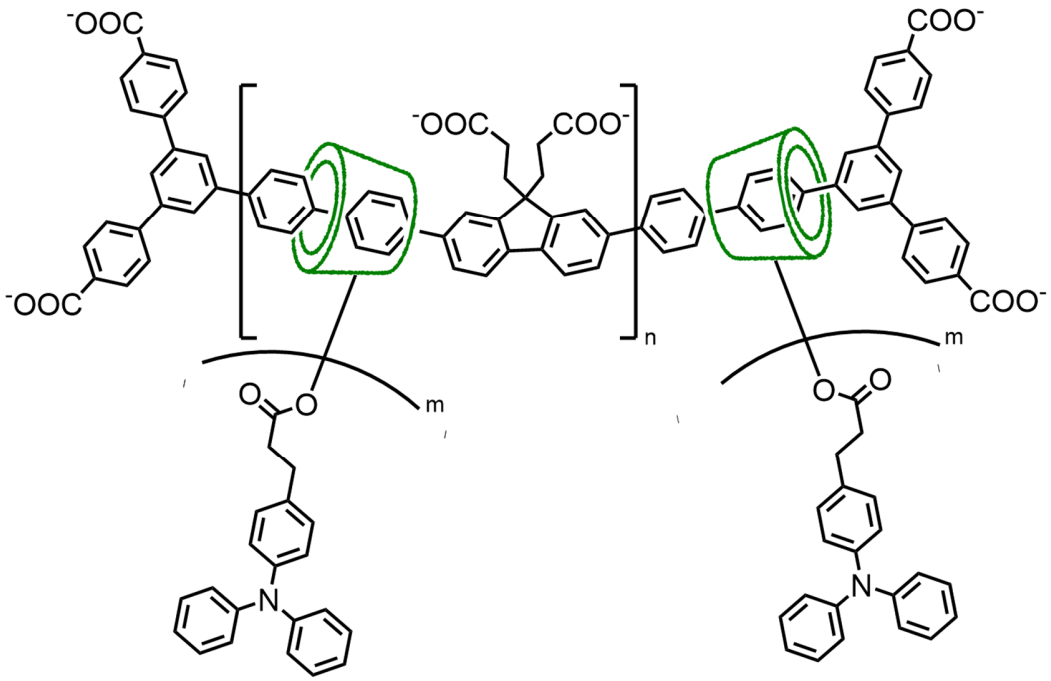

Figure 7. An IMW, which was functionalized with triphenylamine by esterification of the CD-hydroxyl groups after assembly.[31]

Terao et al. have synthesized molecular wires based on [1]rotaxanes[32] obtained by intramolecular "slipping" of oligophenylenethynylene (OPE) subunits (Figure 8) functionalized with permethylated cyclodextrins (pm-α-CD).[33] The [1]rotaxane precursors are highly modular, insulated, 1,4-functionalized phenylene building blocks and their copolymers with phenyleneethynylene units have displayed very high charge carrier mobilities.[34]

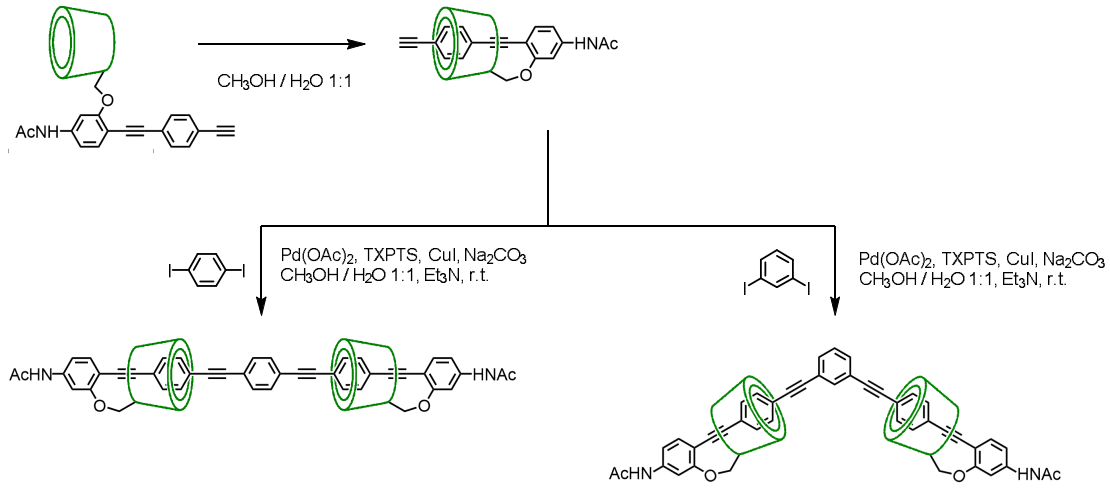

Figure 8. [1]rotaxanes developed by Terao: The shown linear and kinked precursors were further co-polymerized by *Sonogashira* cross-coupling to give insulated zigzag polymers.[34] For this purpose, the acetanilide functionality was further transformed to an aryl iodide by a saponification and diazotation/iodination-protocol.

This was achieved by rational control of conjugation length with meta-connected phenylene units. Combined with tight encapsulation of the conjugated structure with pm-α-CD, structural fluctuations of the polymer could be reduced, thus increasing electronic regularity of the individual orbital domains. As a result, intramolecular charge hopping processes are faster and finally result in a higher conductivity. It is noteworthy that these conjugated polymers are only solubilized due to the encircling pm-α-CD units, instead of commonly employed, covalently bound side-chains. By employing such an intramolecular rotaxanation approach, the synthetic complexity can be reduced due to the disappearing necessity of introducing a stopper unit.

[9]cumulenes could be stabilized by rotaxanation as shown by Anderson, Tykwinsky and co-workers.[35] Using an active-metal templation strategy with macrocyclic phenanthroline ligands, oligoyne rotaxane precursors were assembled by Cadiot-Chodkiewicz coupling and transformed to the [9]cumulenes by an acidic reductive elimination reaction (Figure 9). The obtained rotaxanes were stable for several weeks under argon atmosphere and in the absence of light, whereas the dumbbell counterparts decomposed within a few hours. Owing to the increased stability, these rotaxanes could survive short purification steps, which finally allowed for a detailed investigation of their properties. This includes thermal characterization by differential scanning calorimetry (DSC), which further confirmed thermal stability enhancement by rotaxanation.

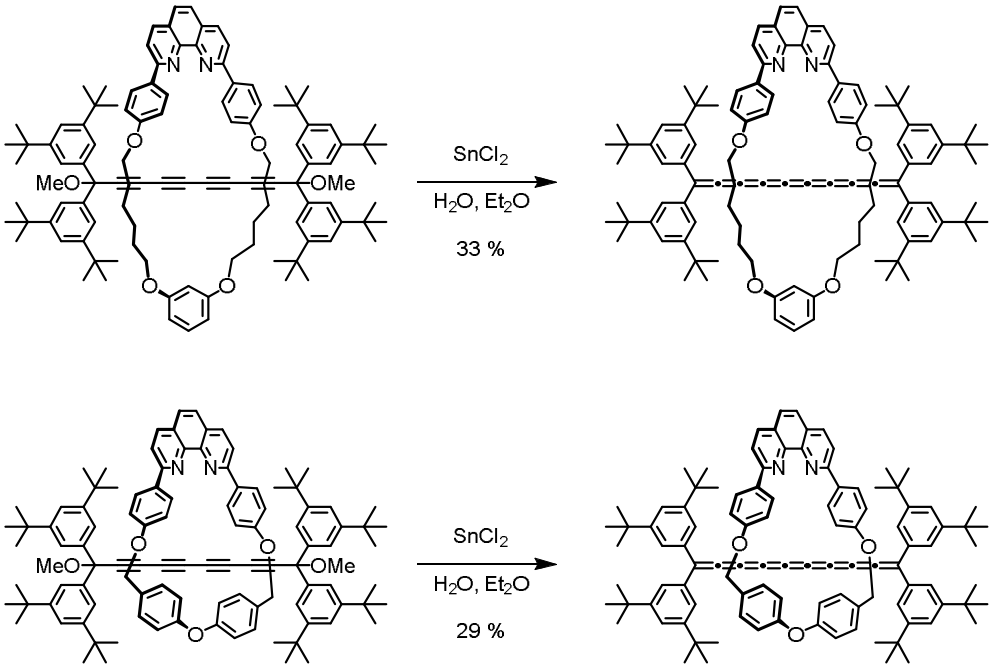

Figure 9. Synthesis of cumulene rotaxanes with two different protecting macrocycles. Reductive elimination of the oligoyne precursors gave the cumulenic systems. [35]

Improved thermal stability of oligoynes by rotaxanation was also observed, using the same active-template strategy for assembly.[36] When the phenanthroline moiety of such a hexayne rotaxane was complexed with $Re(CO)_3Cl$ to probe optical features of the complex,[37] unexpected quenching of the metal complex luminescence was observed. By combined spectroscopic and theoretical studies, an energy transfer from the ^{3}MLCT state to the low-lying T_1 state of the hexayne axle was identified, which finally undergoes nonradiative relaxation.

Electronic properties of conjugated rotaxanes can also be examined on a microscopic level by single-molecule conductance measurements. Such measurements rely on statistical formation of molecular junctions. The interpretation of results from single-molecular conductance measurements can be cumbersome as junction formation can result in different geometries and aggregation phenomena between analyte molecules may occur within the junction. When considering that an additional complex formation equilibrium must be taken in account it may be difficult to disentangle the effects due to poorly defined junction geometry and stoichiometry from those which specifically arise from the complex in the junction. Interlocked molecules eliminate the possibility of dissociation and disrupt interaction of π-conjugated chromophores, which is known to result in the formation of conductive aggregates.[38] Rotaxanation is therefore a promising tool for the development of well-defined single-molecular junctions, however only

very few reports of single-molecule conductance measurements incorporating conjugated MIMs exist.[39,40] This is certainly not least due to a considerable effort which has to be made to integrate the additional anchoring group functionality required for single molecule conductance experiments into rotaxanes. A CD-insulated rotaxane based on a conjugated rod obtained by Terao's slipping protocol (Figure 10) was examined by STM-BJ.[39]

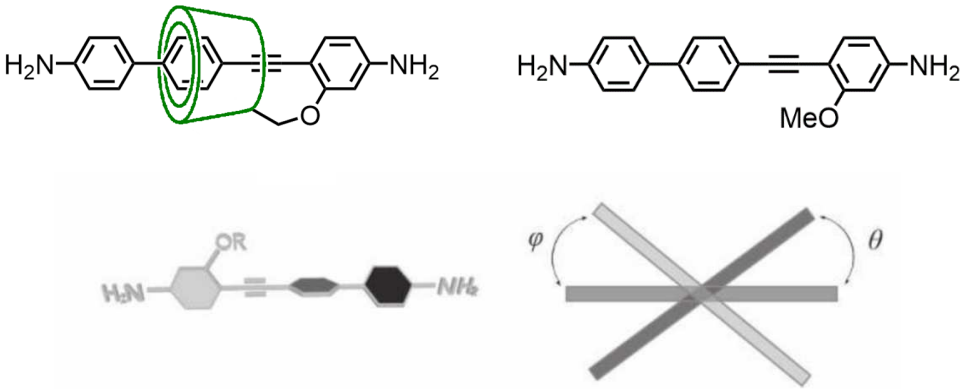

Figure 10. Top left: Terao's slipping rotaxane with amino anchoring groups. Top right: unrotaxanated molecular wire. Bottom: graphical representation of the rotational variation about the biphenyl axis. The picture at the bottom was adopted from reference [39] with permission of John Wiley and Sons.

Comparison with the equivalent, unrotaxanated compound revealed a lower conductance and less conductance fluctuations of the insulated structure. In combination with computational studies this was attributed to a higher rotational barrier of the biphenyl benzene rings und a higher dihedral angle, resulting in a lower, but more defined degree of π-overlap between the biphenyl benzene rings. In another example, conductance measurements of a hexayne rotaxane with 3,5-diphenylpyridine stoppers were performed (Figure 11).[41] The pyridine anchoring groups are integrated into the stopper functionality, serving additionally as steric protecting groups for the hexayne. A weakly enhanced conductance and a decreased probability of junction formation was observed when comparing the rotaxane to the dumbbell, thus it was concluded that the frontier orbitals involved in charge conduction are only slightly affected by the presence of the macrocycle.

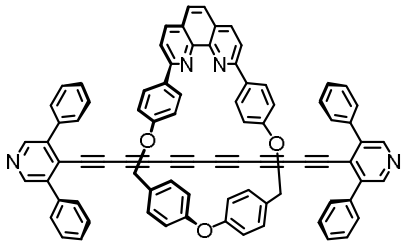

Figure 11. A 3,5-diphenylpyridine-stoppered hexayne rotaxane. [41]

The stabilization of open-shell organic structures was achieved by rotaxanation and catenation, resulting in persistent radicals, which otherwise exhibit very limited stability. An oligoaniline axle[42] encircled by cucurbit[7]uril (CB[7]) (Figure 12) showed markedly enhanced thermodynamic and kinetic stability in comparison with its uncomplexed dumbbell. The oxidation potential of the neutral form to the radical cation was found to be decreased by 570 mV in presence of the CB[7] host, such that even under aerobic conditons spontaneous oxidation occurs. This was attributed to the fact, that CB[7] binds more strongly to the aniline radical cation than to the neutral dumbbell, resulting in a stabilization of the oxidized state. The rotaxanated radical cation was shown to be more resistant towards oxidation to the quinoid form. As conductive polyaniline radical cations already find technical application, this example demonstrates how close to actual applications MIM-based modulation of electronic properties can already be realized.

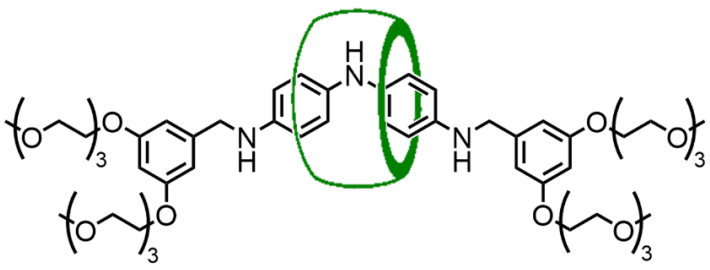

Figure 12. Andersons CB[7]-rotaxane. [42]

Radical stabilization in MIMs was also reported by the Stoddart group. The radical pairing interaction of viologen derivatives was employed for the synthesis of catenated viologen/diazapyrenium radicals.[43] These catenane monoradicals are persistent at ambient

conditions in air and display a series of discrete electrochemical reduction steps as determined by differential pulse voltammetry (DPV).

Conjugated Topological Structures

Due to their inherent rigidity, conjugated and aromatic subunits are of particular interest for constructing shape-persistent superstructures. Coupling chemistry of sp- and sp^2-centers has evolved tremendously to offer a broad substrate scope. Owing to the freedom of structural variation, this chemistry made it possible to construct rigid scaffolds relying on conjugated materials. By choosing shape-persistent building blocks with a high degree of preorganization, interlocked, three-dimensional molecules of large size and high complexity were realized. As the electrochemical and optical addressability of conjugated materials can be tuned, emergent properties arising from the electronic though-space coupling of the MIM subunits can be implemented. Early development in assembling large conjugated chromophores were pioneered by the Sauvage group.[44–46] Various syntheses of interlocked molecules incorporating large chromophores such as porphyrins and fullerenes were published, all profiting from the reliability of transition metal templation.

The first example of a fully conjugated catenane (Figure 13) is the oligothiophene-phenanthroline catenane synthesized by Bäuerle et al.[47,48] In their synthetic approach, Sauvage's Cu(I)-templation method was employed. The catenane showed only weak perturbation of the optical properties compared to its monomer, but markedly different electrochemical behavior. Thus it can be concluded, that electronic coupling through space indeed results from the intertwined nature of the two conjugated macrocycles.

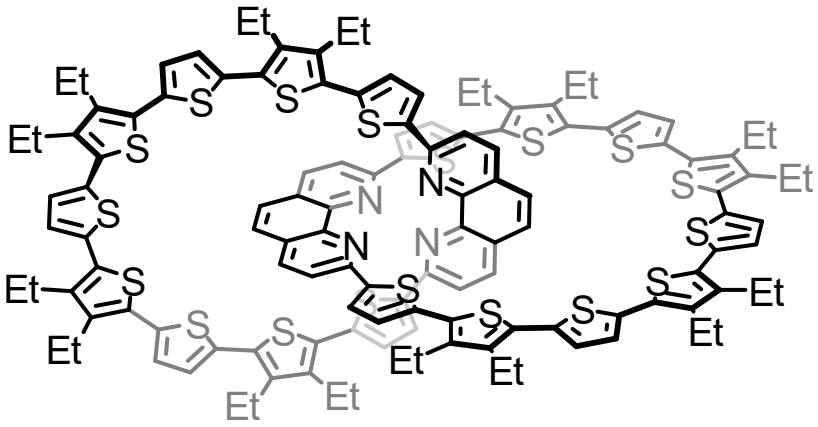

Figure 13. Structure of Bäuerle's oligothiophene catenane. [47]

More recently an interlocked catenane was synthesized by Cong and Zhu,[49] displaying a Möbius-conjugated π-system in the solid state. Most noteworthy these catenane syntheses still rely on Sauvage's copper templation, displaying both the robustness and usefulness of this method in particular when considering the high yield of these cyclization reactions. However, optoelectronic properties of this catenane did not show any remarkable features resulting from catenation. This was attributed to the absence of a Möbius twist in solution.

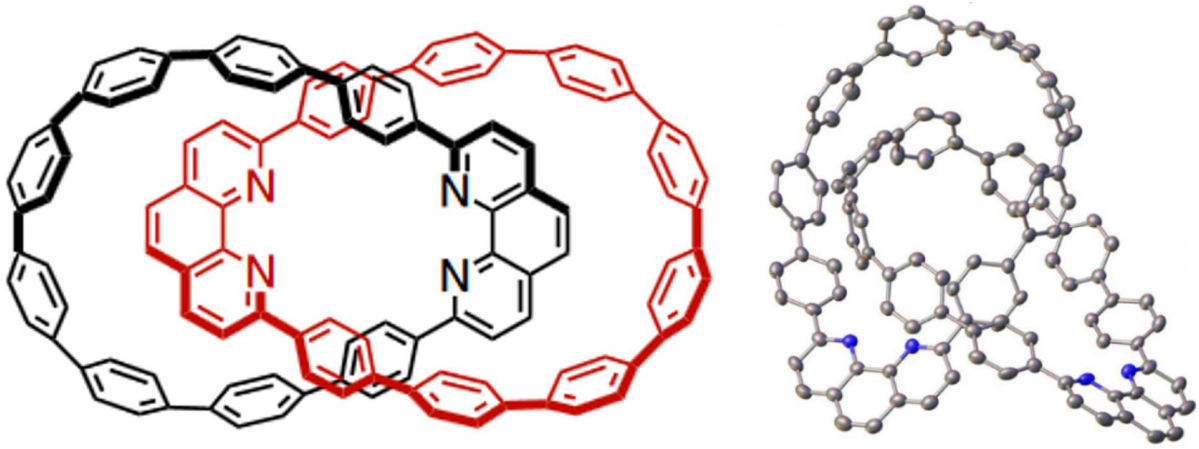

Figure 14. Left: Molecular structure of the catenane by Cong and Zhu. Right: ORTEP representation of the solid state structure in which the Möbius-twisted phenylene ring becomes apparent. Hydrogen atoms omitted for clarity. Both pictures were adopted from reference [49].

More complex catenane topologies were realized based on conjugated building blocks as presented by the Zhang group (Figure 15).[50] An interlocked, shape-persistent arylene-ethynylene cage was synthesized by a dynamic combinatorial approach relying on alkyne metathesis. The compound was found to be self-templating as no specific recognition feature was introduced into the structure. The extent to which formation of an intertwined structure occurs was in this case

strongly solvent dependent, 59 % yield were observed for the reaction in a mixture of $CCl_4/CHCl_3$, whereas a reaction in toluene preferentially yielded the monomeric cage. Interestingly, application of this chemistry for synthesizing catenated structures is not universal in this case, as it was shown that variation of size and symmetry of the building blocks does inhibit the formation of interlocked cages. [51]

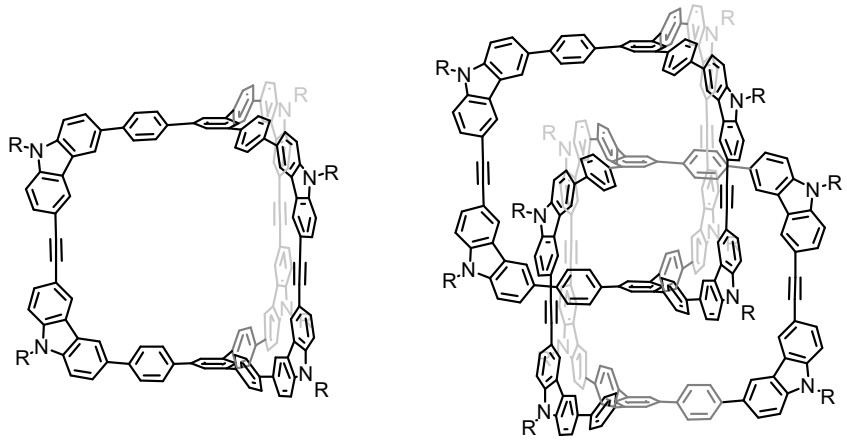

R = $C_{16}H_{33}$ or CO_2tBu

Figure 15. Zhang's Interlocked, conjugated cages and its monomer.[50] The Boc-protecting groups were of advantage for chromatographic purification due to their polarity. Complete separation of the alkyl-substituted cages could not be achieved.

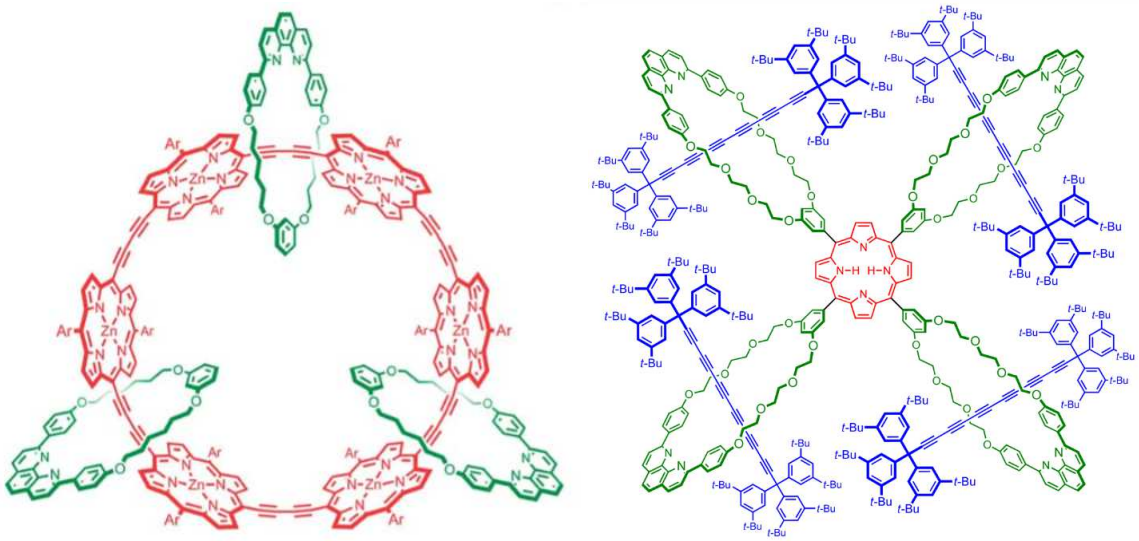

Figure 16. Porphyrin/Oligoyne [4]catenane (left) and [5]rotaxane assembled by the Anderson group. Pictures were adopted from references [52] and [53].

The oligoyne rotaxane assembly concept developed by Anderson et al. was extended to the syntheses of a catenated nanoring[52] and [3]- and [5]rotaxanes incorporating a central

porphyrinic hub, surrounded by hexayne rotaxanes (Figure 16).[53] In these rotaxanes, it was shown that the hexayne axles act as sinks for the excited singlet state of the phenanthroline-based macrocycles. It was hypothesized by Anderson at al.[53] that such hub-centered structures may serve as preorganized model structures for the synthesis of cyclic carbon allotropes.

Recognition of large π-conjugated surfaces by complementary shaped receptors or donor-acceptor interactions has been frequently applied in supramolecular chemistry.[13] However, MIMs based on these substance classes remain exotic. The noncovalent functionalization of single-walled carbon nanotubes (SWCNTs) to form interlocked rotaxane structures is one example which has been accomplished. The Pérez group, described SWCNT-templated rotaxanation relying on a linear, extended tetrathiafulvalene (exTTF) precursor which strongly aggregates with SWCNTs (Figure 17). [54] In a clipping approach, macrocyclization by a ring-closing metathesis reaction (RCM) was accomplished by templation with threaded SWCNTs. As there is no stopper unit in this system, the macrocycles could be expected to slip off, consequently qualifying this system as pseudorotaxane.[55] Intriguingly, the macrocycle could not be removed by sonication in CH_2Cl_2, refluxing in tetrachloroethane (b.p. 147 °C) or washing with CH_2Cl_2, but only by heating to 360 °C. This approach was followed by employing other types of aromatic units in the receptor components, such as porphyrin,[56] pyrene and anthraquinone.[57] In all these cases, similar thermal stability, resistance to sonication and washing with CH_2Cl_2 was maintained, confirming the rotaxane character under ordinary laboratory conditions. The presence of threaded macrocycles on the SWCNTs could be confirmed by TEM and AFM.[56] By Miki and Ohe[58] a threading approach of anthracene-based cycloparaphenyleneacetylene was presented. Complexation occurred in *o*-dichlorobenzene at room temperature, while only those complexes with a tight fit of receptor and SWCNT gave threaded complexes. The complexes could be dissociated by calcination, displaying similar stabilities as the SWCNT/ring complexes described by Pérez *et al.*

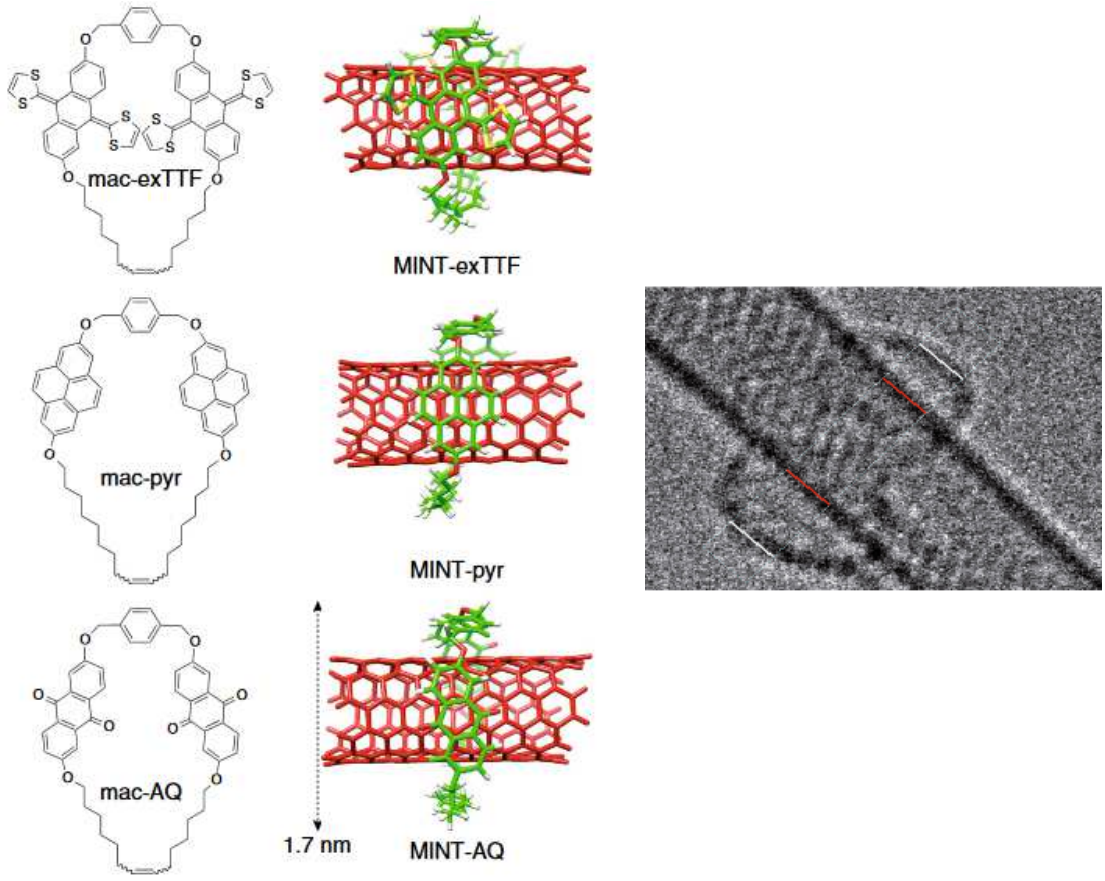

Figure 17. Left: Chemical structure of the macrocycles, which were used for regulation of the catalytic activity of SWCNTs, together with the molecular models of the threaded complexes. Right: HR-TEM image of the nanotube/mac-AQ complex. Both pictures were adopted from reference [57].

It was hypothesized that the kinetic stability of these complexes arises from the enormous aspect ratio of carbon nanotubes.[56] This is however contradictive to the possibility of threading a macrocycle onto the nanotubes as presented by Niki and Ohe, who reported that threading occurs within a few hours in *o*-dichlorobenzene at room temperature. No significant kinetic barrier was observed for threading, still dissociation required high temperatures. This points towards high binding strength, which makes harsh conditions the only option to achieve decomplexation. It would be of particular interest to clarify whether dissociation is indeed only prevented by exceptionally strong and association. If so, then this would in principle represent a new method of inducing rotaxane character. To probe the electronic influence of the non-covalently bound ring components on the properties of carbon nanotubes, (6,5)-enriched SWCNT functionalized with exTTF, pyrene or anthraquinone were examined for their catalytic activity in

the reduction of nitroaromatics by hydrazine.[59] A strong positive correlation between electron donating strength of the host and catalytic activity of the SWCNT rotaxanes was observed, demonstrating the strong influence of electronic coupling between the macrocycle and carbon nanotubes.

Conclusion

Assemblies of insulated, mechanically bonded, π-conjugated subunits show considerable potential to contribute to the fine-tuning of optoelectronic functionality. Mechanical encapsulation of chromophores can convey stability to otherwise fragile substance classes, as demonstrated with chromophores with low π-π* gaps and organic radicals. Additionally, non-covalently bound subunits can serve as a platform for post-assembly functionalization of MIMs. Especially CDs have proven to be powerful building blocks for such purposes, owing to their peripheral hydroxyl groups. Entirely new classes of conjugated superstructures can be assembled, employing chromophores as hubs for hierarchical assemblies or conjugated rods as struts. Such structures enable chemists to realize three-dimensionally extended superstructures and chromophore assemblies. Some approaches have displayed a high degree of modularity, in particular when considering cyclodextrin-based rotaxanes. They do not only allow chemists to choose among various host/guest combinations, but also to post-functionalize them. This is not only desirable regarding potential applications, but also for tailoring model systems for fundamental research. Especially characterization of single-mulecule conductance in insulated MIMs could be of particular interest to probe the influence of through space interaction of rotaxanes which still display co-conformational dynamics. Such examples are still underrepresented to date and may be more frequently encountered in the future. Towards more extended, conjugated structures, examples of interlocked systems grow increasingly rare. An inspiring example are the interlocked carbon nanotubes, which challenge the definition of an interlocked superstructure. The non-covalent modulation of the SWCNT structure was demonstrated by regulation of their catalytic activity in nitroaromatics reduction, giving a prospect of the potential functions which could be realized by such superstructures.

References

[1] C. C. C. Johansson Seechurn, M. O. Kitching, T. J. Colacot, V. Snieckus, *Angew. Chem. Int. Ed.* **2012**, *51*, 5062–5085.
[2] S. R. Forrest, M. E. Thompson, *Chem. Rev.* **2007**, *107*, 923–925.
[3] F. J. M. Hoeben, P. Jonkheijm, E. W. Meijer, A. P. H. J. Schenning, *Chem. Rev.* **2005**, *105*, 1491–1546.
[4] F. Diederich, *Nature* **1994**, *369*, 199–207.
[5] F. Diederich, M. Kivala, *Adv. Mater.* **2010**, *22*, 803–812.
[6] W. Zhang, J. S. Moore, *Angew. Chem. Int. Ed.* **2006**, *45*, 4416–4439.
[7] C. Yu, Y. Jin, W. Zhang, *Chem. Rec.* **2015**, *15*, 97–106.
[8] S. Kumar, Y. Kumar, S. Keshri, P. Mukhopadhyay, *Magnetochemistry* **2016**, *2*, 42.
[9] C. J. Bruns, J. F. Stoddart, *The Nature of the Mechanical Bond: From Molecules to Machines*, John Wiley & Sons, Hoboken, NJ, USA, **2016**.
[10] J.-M. Lehn, *Supramolecular Chemistry: Concepts and Perspectives*, Wiley-VCH Verlag GmbH & Co. KGaA, Weinheim, FRG, **1995**.
[11] M. Xue, Y. Yang, X. Chi, X. Yan, F. Huang, *Chem. Rev.* **2015**, *115*, 7398–7501.
[12] S. Erbas-Cakmak, D. A. Leigh, C. T. McTernan, A. L. Nussbaumer, *Chem. Rev.* **2015**, *115*, 10081–10206.
[13] C. R. Martinez, B. L. Iverson, *Chem. Sci.* **2012**, *3*, 2191.
[14] M. J. Frampton, H. L. Anderson, *Angew. Chem. Int. Ed.* **2007**, *46*, 1028–1064.
[15] J. D. Crowley, S. M. Goldup, A.-L. Lee, D. A. Leigh, R. T. McBurney, *Chem. Soc. Rev.* **2009**, *38*, 1530.
[16] Z. Liu, S. K. M. Nalluri, J. F. Stoddart, *Chem. Soc. Rev.* **2017**, *46*, 2459–2478.
[17] E. J. Dale, N. A. Vermeulen, M. Juríček, J. C. Barnes, R. M. Young, M. R. Wasielewski, J. F. Stoddart, *Acc. Chem. Res.* **2016**, *49*, 262–273.
[18] G. Crini, *Chem. Rev.* **2014**, *114*, 10940–10975.
[19] M. J. Frampton, G. Sforazzini, S. Brovelli, G. Latini, E. Townsend, C. C. Williams, A. Charas, L. Zalewski, N. S. Kaka, M. Sirish, et al., *Adv. Funct. Mater.* **2008**, *18*, 3367–3376.
[20] S. Brovelli, F. Meinardi, G. Winroth, O. Fenwick, G. Sforazzini, M. J. Frampton, L. Zalewski, J. A. Levitt, F. Marinello, P. Schiavuta, et al., *Adv. Funct. Mater.* **2010**, *20*, 272–280.
[21] J. P. Sauvage, *Acc. Chem. Res.* **1990**, *23*, 319–327.
[22] S. Durot, F. Reviriego, J.-P. Sauvage, *Dalton Trans.* **2010**, *39*, 10557–10570.
[23] S. Brovelli, F. Cacialli, *Small* **2010**, *6*, 2796–2820.
[24] J. J. Gassensmith, J. M. Baumes, B. D. Smith, *Chem. Commun.* **2009**, 6329–6338.
[25] L. D. Patsenker, A. L. Tatarets, O. P. Klochko, E. A. Terpetschnig, in *Adv. Fluoresc. Report. Chem. Biol*, Springer Berlin Heidelberg, Berlin, Heidelberg, **2010**, pp. 159–190.
[26] C. M. S. Yau, S. I. Pascu, S. A. Odom, J. E. Warren, E. J. F. Klotz, M. J. Frampton, C. C. Williams, V. Coropceanu, M. K. Kuimova, D. Phillips, et al., *Chem. Commun.* **2008**, 2897–2899.
[27] A. Harada, A. Hashidzume, H. Yamaguchi, Y. Takashima, *Chem. Rev.* **2009**, *109*, 5974–6023.
[28] L. Zalewski, J. M. Mativetsky, S. Brovelli, M. Bonini, N. Crivillers, T. Breiner, H. L. Anderson, F. Cacialli, P. Samorì, *Small* **2012**, *8*, 1835–1839.
[29] Y. Ou, G. Chen, J. Yin, G.-A. Yu, S. Hua Liu, *J. Coord. Chem.* **2011**, *64*, 3062–3067.
[30] T. Putnin, H. Le, T.-T. Bui, J. Jakmunee, K. Ounnunkad, S. Péralta, P.-H. Aubert, F. Goubard, A. Farcas, *Eur. Polym. J.* **2018**, *105*, 250–256.
[31] G. Sforazzini, A. Kahnt, M. Wykes, J. K. Sprafke, S. Brovelli, D. Montarnal, F. Meinardi, F. Cacialli, D. Beljonne, B. Albinsson, et al., *J. Phys. Chem. C* **2014**, *118*, 4553–4566.
[32] J. Terao, S. Tsuda, Y. Tanaka, K. Okoshi, T. Fujihara, Y. Tsuji, N. Kambe, *J. Am. Chem. Soc.* **2009**, *131*, 16004–16005.
[33] S. Tsuda, J. Terao, N. Kambe, *Chem. Lett.* **2009**, *38*, 76–77.
[34] J. Terao, A. Wadahama, A. Matono, T. Tada, S. Watanabe, S. Seki, T. Fujihara, Y. Tsuji, *Nat. Commun.* **2013**, *4*, DOI 10.1038/ncomms2707.

[35] M. Franz, J. A. Januszewski, D. Wendinger, C. Neiss, L. D. Movsisyan, F. Hampel, H. L. Anderson, A. Görling, R. R. Tykwinski, *Angew. Chem. Int. Ed.* **2015**, *54*, 6645–6649.
[36] L. D. Movsisyan, M. Franz, F. Hampel, A. L. Thompson, R. R. Tykwinski, H. L. Anderson, *J. Am. Chem. Soc.* **2016**, *138*, 1366–1376.
[37] L. D. Movsisyan, M. D. Peeks, G. M. Greetham, M. Towrie, A. L. Thompson, A. W. Parker, H. L. Anderson, *J. Am. Chem. Soc.* **2014**, *136*, 17996–18008.
[38] S. Wu, M. T. González, R. Huber, S. Grunder, M. Mayor, C. Schönenberger, M. Calame, *Nat. Nanotechnol.* **2008**, *3*, 569–574.
[39] M. Kiguchi, S. Nakashima, T. Tada, S. Watanabe, S. Tsuda, Y. Tsuji, J. Terao, *Small* **2012**, *8*, 726–730.
[40] D. C. Milan, M. Krempe, A. K. Ismael, L. D. Movsisyan, M. Franz, I. Grace, R. J. Brooke, W. Schwarzacher, S. J. Higgins, H. L. Anderson, et al., *Nanoscale* **2017**, *9*, 355–361.
[41] D. C. Milan, M. Krempe, A. K. Ismael, L. D. Movsisyan, M. Franz, I. Grace, R. J. Brooke, W. Schwarzacher, S. J. Higgins, H. L. Anderson, et al., *Nanoscale* **2017**, *9*, 355–361.
[42] R. Eelkema, K. Maeda, B. Odell, H. L. Anderson, *J. Am. Chem. Soc.* **2007**, *129*, 12384–12385.
[43] J. Sun, Z. Liu, W.-G. Liu, Y. Wu, Y. Wang, J. C. Barnes, K. R. Hermann, W. A. Goddard, M. R. Wasielewski, J. F. Stoddart, *J. Am. Chem. Soc.* **2017**, *139*, 12704–12709.
[44] J.-C. Chambron, V. Heitz, J.-P. Sauvage, *J. Chem. Soc. Chem. Commun.* **1992**, 1131–1133.
[45] F. Diederich, C. Dietrich-Buchecker, J.-F. Nierengarten, J.-P. Sauvage, *J. Chem. Soc. Chem. Commun.* **1995**, 781–782.
[46] M. Andersson, M. Linke, J.-C. Chambron, J. Davidsson, V. Heitz, L. Hammarström, J.-P. Sauvage, *J. Am. Chem. Soc.* **2002**, *124*, 4347–4362.
[47] P. Bäuerle, M. Ammann, M. Wilde, G. Götz, E. Mena-Osteritz, A. Rang, C. A. Schalley, *Angew. Chem. Int. Ed.* **2007**, *46*, 363–368.
[48] G. Götz, X. Zhu, A. Mishra, J.-L. Segura, E. Mena-Osteritz, P. Bäuerle, *Chem. - Eur. J.* **2015**, *21*, 7193–7210.
[49] Y.-Y. Fan, D. Chen, Z.-A. Huang, J. Zhu, C.-H. Tung, L.-Z. Wu, H. Cong, *Nat. Commun.* **2018**, *9*, DOI 10.1038/s41467-018-05498-6.
[50] Q. Wang, C. Yu, H. Long, Y. Du, Y. Jin, W. Zhang, *Angew. Chem. Int. Ed.* **2015**, *54*, 7550–7554.
[51] Q. Wang, C. Yu, C. Zhang, H. Long, S. Azarnoush, Y. Jin, W. Zhang, *Chem. Sci.* **2016**, *7*, 3370–3376.
[52] M. J. Langton, J. D. Matichak, A. L. Thompson, H. L. Anderson, *Chem. Sci.* **2011**, *2*, 1897–1901.
[53] D. R. Kohn, L. D. Movsisyan, A. L. Thompson, H. L. Anderson, *Org. Lett.* **2017**, *19*, 348–351.
[54] A. de Juan, Y. Pouillon, L. Ruiz-González, A. Torres-Pardo, S. Casado, N. Martín, Á. Rubio, E. M. Pérez, *Angew. Chem. Int. Ed.* **2014**, *53*, 5394–5400.
[55] P. R. Ashton, I. Baxter, M. C. T. Fyfe, F. M. Raymo, N. Spencer, J. F. Stoddart, A. J. P. White, D. J. Williams, *J. Am. Chem. Soc.* **1998**, *120*, 2297–2307.
[56] L. de Juan-Fernández, P. W. Münich, A. Puthiyedath, B. Nieto-Ortega, S. Casado, L. Ruiz-González, E. M. Pérez, D. M. Guldi, *Chem. Sci.* **2018**, *9*, 6779–6784.
[57] M. Blanco, B. Nieto-Ortega, A. de Juan, M. Vera-Hidalgo, A. López-Moreno, S. Casado, L. R. González, H. Sawada, J. M. González-Calbet, E. M. Pérez, *Nat. Commun.* **2018**, *9*, DOI 10.1038/s41467-018-05183-8.
[58] K. Miki, K. Saiki, T. Umeyama, J. Baek, T. Noda, H. Imahori, Y. Sato, K. Suenaga, K. Ohe, *Small* **2018**, *14*, 1800720.
[59] M. Blanco, B. Nieto-Ortega, A. de Juan, M. Vera-Hidalgo, A. López-Moreno, S. Casado, L. R. González, H. Sawada, J. M. González-Calbet, E. M. Pérez, *Nat. Commun.* **2018**, *9*, DOI 10.1038/s41467-018-05183-8.

Assembly of [2]Rotaxanes in Water

ChemPubSoc Europe

DOI: 10.1002/ejoc.201700640

EurJOC European Journal of Organic Chemistry

Full Paper

[2]Rotaxanes

Assembly of [2]Rotaxanes in Water

Yves Aeschi,[a,b] Sylvie Drayss-Orth,[a] Michal Valášek,[c] Felix Raps,[a] Daniel Häussinger,[a] and Marcel Mayor*[a,b,c,d]

Abstract: Two [2]rotaxanes have been assembled in water from modular subunits through Cu^{I}-catalyzed azide–alkyne "click" chemistry. For this purpose, 2,6-disubstituted naphthalene axles with solubilizing oligo(ethylene glycol) (OEG) chains (n = 1–5) and propargyl terminal groups were synthesized and examined for their propensity to form inclusion complexes with a dicationic Diederich-type cyclophane host. The dependence of pseudorotaxane formation on the linkers between the naphthalene core and OEG chains, and in the case of ester linkers on different spacer lengths, was analyzed by titration experiments. In addition, the inclusion complexes of two [2]rotaxanes were trapped by using a water-soluble azide-functionalized stopper. Repetitive chromatography finally enabled the isolation of both mechanically interlocked [2]rotaxanes.

Introduction

Over the last decades, numerous mechanically interlocked molecules (MIMs), such as rotaxanes and catenanes, with large structural diversity have been synthesized and investigated. This synthetic advancement has inspired chemists to design MIMs with physical- and chemical-responsive properties to obtain systems of increasing complexity that can function as switches,[1–9] molecular muscles,[10–17] and molecular machines.[18–27] The Nobel Prize in chemistry was awarded in 2016 for achievements in the field of molecular machinery, many examples of which rely on supramolecular structures. Rotaxane-based systems have been investigated extensively, but the vast majority of these compounds are assembled and functionalized only in organic solvents. Many of them are insoluble in water and/or their functional features are disrupted upon dissolution in an aqueous environment. This is striking as the most sophisticated molecular machines are biomolecules that function in water,[28] for example, ATP-synthase,[29–33] kinesin,[34–37] and myosin,[38–40] naming just a few. Acting as both a hydrogen-bond donor and acceptor, water preferentially interacts mutually, resulting in an infinite dynamic network of hydrogen bonds with localized and structured clustering.[41,42] Owing to its polar nature, water is able to include the polar moieties of other molecules in the hydrogen-bonding network. On the other hand, the absence of such polar functionalities in molecules gives rise to the hydrophobic effect, by which nonpolar molecules are segregated from the water bulk. Protein folding and assembly is a prominent example, as protein functional structures in an aqueous environment are largely dependent on hydrophobic interactions between nonpolar amino acid residues present in the amino acid chain. From a supramolecular chemistry perspective, the hydrophobic effect is an appealing driving force for host–guest association as it potentially leads to high association constants (K_a).[37] Although the classical hydrophobic effect is characterized by an entropy gain, the nonclassical effect is enthalpically driven. In the first case, molecules of water, which solvate the guest, are released from an ordered network into the solvent bulk. In the second case, high-energy insulated water molecules located in the host cavity are replaced by a hydrophobic guest. The released water molecules participate in the hydrogen-bonding network of the water bulk, which results in an enthalpy gain. Most known water-soluble rotaxane systems that rely on the hydrophobic effect comprise cyclodextrin,[43–46] pillar[n]arene,[47–49] or cucurbit[n]uril[50–52] as host molecules, and for some of these systems acidic media or organic co-solvents are required.[51,53–55] Prominent examples of synthetically modifiable water-soluble macrocycles are the quaternary ammonium-functionalized dicationic spiro-cyclophanes developed and extensively studied by Diederich and co-workers.[56,57] The dichloride of cyclophane **1**[56] (Scheme 1) forms 1:1 inclusion complexes with aromatic compounds, for example, 2,6-disubstituted naphthalene derivatives, in protic solvents due to a nonclassical hydrophobic effect.[57–59] Binding constants of up to 1.6×10^5 M^{-1} have been reported for complexes with neutral guests in water.[60] The 2,6-disubstituted naphthalenes generally prefer an axial-type inclusion geometry[59] and are arranged as an offset π stack as well as an edge-to-face stack (T stack) within the four electron-rich diphenylmethane cavity walls of **1**.[60] The eight methoxy groups oriented in the planes of the benzene rings provide additional depth to the apolar cavity and diminish the tendency of self-aggregation of

[a] *Department of Chemistry, University of Basel, St. Johanns-Ring 19, 4056 Basel, Switzerland*
E-mail: marcel.mayor@unibas.ch
[b] *Swiss Nanoscience Institute, University of Basel, Klingelbergstrasse 82, 4056 Basel, Switzerland*
[c] *Institute for Nanotechnology (INT), Karlsruhe Institute of Technology (KIT), P. O. Box 3640, 76021 Karlsruhe, Germany*
[d] *Lehn Institute of Functional Materials (LIFM), Sun Yat-Sen University, Guangzhou, China*
http://www.chemie.unibas.ch/~mayor/
Supporting information and ORCID(s) from the author(s) for this article are available on the WWW under https://doi.org/10.1002/ejoc.201700640.

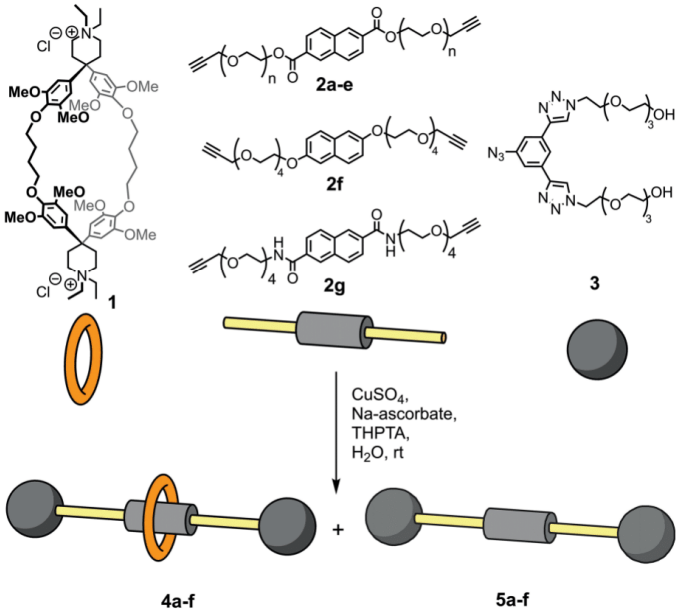

Scheme 1. Conceptual assembly of the [2]rotaxanes **4a**–**f** from cyclophane **1**, axles **2a**–**f**, and stopper **3** by trapping the supramolecular complex by CuAAC in water. Also, the formation of the dumbbells **5a**–**f** as expected byproducts is included (*n* = 1: **a**; *n* = 2: **b**; *n* = 3: **c**; *n* = 4: **d**; *n* = 5: **e**).

the cyclophane, thereby resulting in a rather high critical aggregation concentration (cac) in water (cac = 1×10^{-2} M) compared with similar cyclophanes without methoxy decoration.[57] Anderson and co-workers synthesized rotaxanes with the methoxy-decorated Diederich cyclophane **1** and azo dyes[43,61] or oligo(phenylene-ethynylenes) (OPEs) functionalized on one terminus with water-soluble charged stoppers[62–64] as axles in aqueous media. To enable rotaxane formation and trapping, the OPE-based rotaxane synthesis required a large excess of copper(I) salt and ammonium chloride (ca. 1000 equiv.), whereas the azo dye rotaxane formation required a strongly acidic medium. Our aim was the development of a molecular toolbox to access water-soluble, mechanically interlocked compounds in a modular fashion. The cyclophanes reported by Diederich and co-workers offer diverse possibilities for synthetic modification[56,65–67] on the one hand and high binding strength for hydrophobic guests on the other. Furthermore, we chose Cu^{I}-catalyzed alkyne–azide 1,3-cycloaddition (CuAAC) "click" chemistry coupling conditions for our systems as this reaction is most advantageous for its broad substrate scope, mild reaction conditions, and high reaction rates.[68–70] To optimize the molecular design for water-based MIM assembly of, for example, rotaxanes and daisy chains,[71] we are developing modular building blocks that can be coupled by "click" chemistry in a rapid and modular manner.

Here we present the synthesis and full characterization of a new type of rotaxane that are assembled in water without requiring organic co-solvents. In a threading-followed-by-stoppering method,[72] cyclophane **1** initially forms an inclusion complex with tetra(ethylene glycol) (TEG)-functionalized axles **2d/f**. In the rotaxanation step, the azide group of water-soluble stopper **3** subsequently reacts with the terminal propargyl groups of the axles in a "click" reaction. Only a few water-soluble stoppers bearing an azide group have been reported in the literature. Due to either their weakly hydrophilic character[73] or the presence of a cyclodextrin cavity,[55] which potentially competes as host with cyclophane **1**, these compounds were not ideally suited to our system. Therefore, we developed the hydrophilic and synthetically well-accessible stopper **3** that contains two TEG chains.

We additionally prepared and investigated a series of five increasingly hydrophilic guests bearing a naphthalene-2,6-dicarboxylate core (**2a**–**e**) with propargyl-terminated oligo(ethylene glycol) esters (*n* = 1–5). The naphthalene-2,6-dicarboxylate core motif displayed limited stability in the uncomplexed state and thus **2f** and 2**g** were prepared as hydrolytically stable alternatives to **2d**, incorporating 2,6-dioxynaphthalene and naphthalene-2,6-dicarboxamide cores, respectively. The binding strengths of axles **2c**–**g** towards cyclophane **1** were determined by fluorescence titration and isothermal titration calorimetry (ITC). For **2a**–**e** the tendency for rotaxane formation by stoppering with **3** was examined under different conditions to determine the length of the OEG chain necessary to obtain isolable yields of rotaxanes.

Results and Discussion

Synthesis of the Rotaxane Components

Axles **2a**,**b** were synthesized from the appropriate monopropargyl OEG ether **6a**,**b** (see the Supporting Information) by basic transesterification of naphthalene-2,6-dicarboxylic dimethyl ester (Scheme 2). High reaction temperatures (130 °C) were required to drive methanol out of the equilibrium while simultaneously distilling off the solvent. This method allowed for a quick synthesis of axles **2a**,**b**. However, this method required a considerable excess of the corresponding alcohol. It turned out that for the axles **2c**–**e**, which comprise longer ethylene glycol chains (n = 3–5), a Mitsunobu reaction starting from naphthalene-2,6-dicarboxylic acid (**7b**) and **6c**–**e** resulted in higher yields. Compound **2f** was obtained in a two-step procedure starting from 2,6-dihydroxynaphthalene, which was alkylated with tetra(ethylene glycol) monotosylate in the presence of caesium carbonate. Careful deoxygenation was required to avoid oxidation of the deprotonated dioxynaphthalene, which resulted in impurities with comparable chemical physical properties, making their separation from the target structure very challenging. This was followed by alkylation of the terminal hydroxy groups with propargyl bromide. Compound **2g** was synthesized from 2,6-naphthalenedicarbonyl chloride and 1-amino-TEG-propargyl ether in very good yield.

The TEG chains of stopper **3** were attached in the one-pot in situ desilylation/"click" reaction of 3,5-bis(trimethylsilylethynyl)aniline[74] and tetra(ethylene glycol) monoazide, simultaneously forming two triazole rings, which provide steric bulk, followed by the high-yielding transformation of the aromatic amine to the azide group (Scheme 3).

Cyclophane **1** was synthesized according to the established procedure described in the literature.[62]

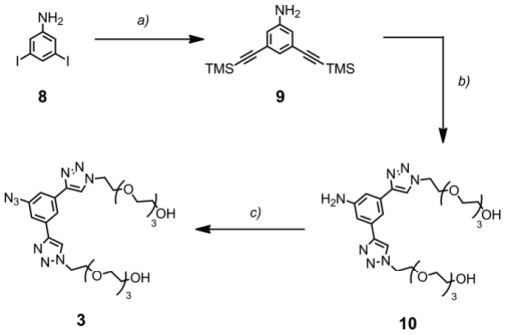

Scheme 3. Synthesis of stopper **3**. Reagents and conditions: a) TMS-acetylene, $[Pd(PPh_3)_2Cl_2]$, PPh_3, CuI, NEt_3, THF, 73 %; b) K_2CO_3, acetone, MeOH, then tetra(ethylene glycol) monoazide, $CuSO_4$, sodium ascorbate, 77 %; c) $NaNO_2$, HCl, NaN_3, H_2O, 85 %.

Binding Studies

We found that axles **2a**,**b** were practically insoluble in water, and the binding studies with cyclophane **1** were therefore only conducted for axles **2c**–**g**. Aliquots of a solution of host **1** were added to solutions of the respective naphthalene derivative **2c**–**g** and the changes in fluorescence intensity were recorded. For the carboxylates and carboxamides, strong fluorescence quenching was observed, whereas the dioxynaphthalene **2f** showed moderate fluorescence enhancement. As representative examples, the fluorescence titrations of naphthalene axles **2d** and **2f** are displayed in Figure 1. The association constants for **1**∩**2c**–**g** were obtained from nonlinear regression of the titration curves (see the Supporting Information). For the guests **2c**–**e**, values of (1.2–1.7) × 10^5 M^{-1} were obtained, whereas the

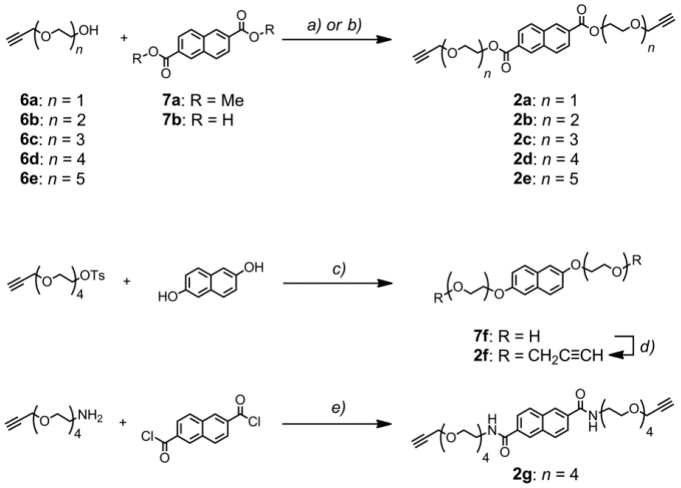

Scheme 2. Synthesis of axles **2a**–**e**. Reagents and conditions: a) **7a**, NaH, THF, 130 °C, 45 min, **2a** 42 %, **2b** 14 %; b) **7b**, PPh_3, DEAD, r.t., 16 h, **2c** 82 %, **2d** 64 %, **2e** 43 %; c) Cs_2CO_3, CH_3CN, reflux, 16 h, 44 % (**7f**); d) NaH, 1-bromo-2-propyne, THF, r.t., 3 h 54 % (**2f**); e) Et_3N, DCM, r.t., overnight, 84 %.

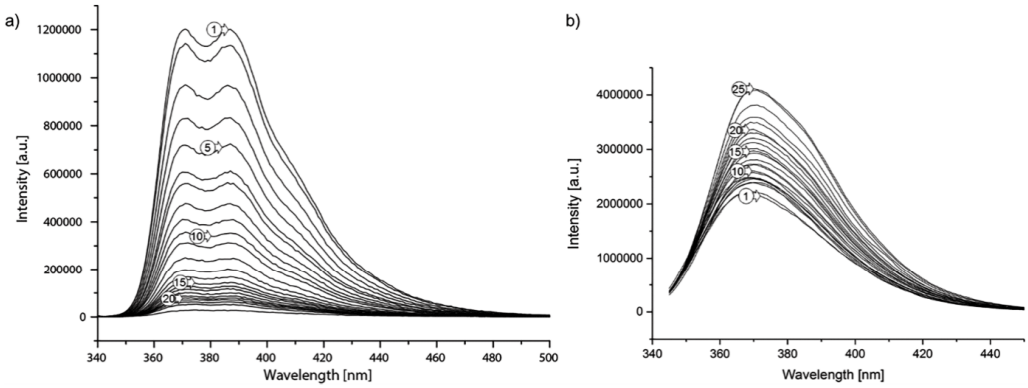

Figure 1. a) Titration of 20.0 μM **2d** with cyclophane: Curve 1) 0.0 equiv., 5) 0.7 equiv., 10) 1.6 equiv., 15) 3.4 equiv., 20) 6.0 equiv., 24) 20 equiv. (λ_{exc} = 333 nm). b) Titration of 20.0 μM **2f** with cyclophane **1**: 1) 0.0 equiv., 5) 0.7 equiv., 10) 1.6 equiv., 15) 3.4 equiv., 20) 6.0 equiv., 25) 80 equiv. (λ_{exc} = 340 nm). Both titrations were conducted in water at 22 °C.

titration of **2f** with **1** gave values ranging from 10^4 to 4×10^4 M^{-1} (Table 1). The lack of reproducibility of the fluorescence titration experiments of the host–guest complex **1**∩**2f** is probably due to both the tendency of **2f** to self-aggregate and precipitate in the absence of equimolar amounts of cyclophane and the relatively weak fluorescence enhancement response $I_{saturated}/I_0 \approx 2$, which make the measurements error-prone. In the case of **2g**, the fluorescence titration was found to be inapplicable for the determination of K_a, because the value of K_a is too low for the method. A preliminary test run revealed a K_a value of less than 2×10^3 M^{-1}.[75]

Table 1. Thermodynamic data for the binding of axles **2c**–**g** to cyclophane **1**.

Axle	n[a]	K_a[b] [M^{-1}]	K_a[c] [M^{-1}]	ΔH [kJ mol^{-1}]	ΔS [J K^{-1} mol^{-1}]
2c	3	1.7×10^5	1.41×10^5	–32.9	–98.7
2d	4	1.4×10^5	1.32×10^5	–45.5	–54.0
2e	5	1.2×10^5	1.04×10^5	–38.4	–32.7
2f	4	$(1–4) \times 10^4$[d]	5.08×10^4	n.d.[e]	n.d.[e]
2g	4	<2000[d]	2.51×10^3	n.d.[e]	n.d.[e]

[a] OEG spacer length. [b] Determined by fluorescence titration. [c] Determined by ITC. [d] Estimations due to inadequate data quality. [e] n.d. = not determined due to insufficient data quality to disentangle entropic and enthalpic contributions.

The results of the ITC measurements were consistent with the findings from the fluorescence titration (see pages S13–S19 in the Supporting Information). The measurements on **2c**–**e** revealed association constants between 1.04×10^5 and 1.41×10^5 M^{-1} with mainly enthalpic contributions (Table 1). The values of K_a for **2f** and **2g** with **1** were found to be 5.08×10^4 and 2.51×10^3 M^{-1}, respectively. In these last two cases, the binding isotherms lacked the necessary sigmoidal shape to distinguish between enthalpic and entropic contributions.

The trends and magnitudes of the binding strengths of naphthalenes **2c**–**g** correspond well with the data on binding in MeOH and H_2O found in the literature,[57,60] yet we were surprised by the extent to which the carboxamide functions of **2g** disrupt the strength of the binding to **1**.[57] This can be attributed to the strong hydrogen-bonding ability of the amide functions close to the recognition site, which results in a partial loss of the solvation shell of these groups, reducing the overall complexation strength.

Screening Reactions

Initially we prepared axles **2a**–**e** as we expected the highest binding constants for naphthalene-2,6-dicarboxylates with **1**.[57] Our prime interest was to investigate to what extent pseudorotaxanes could be trapped by Cu^I-catalyzed "click" reactions between the pseudo-rotaxane and the stopper. Of particular interest was whether the variation in the length of the ethylene glycol subunits significantly affects the yields. Three variations of reaction conditions for the Cu^I-catalyzed azide–alkyne cycloaddition (CuAAC) reaction were investigated for all five axles **2a**–**e**. Analysis was conducted by LC–ESI-MS, which revealed insufficient chromatographic separation of cyclophane, dumbbell, and rotaxane to allow for integration of the UV signals at high-injection concentrations. We therefore injected very dilute samples and integrated the extracted ion traces to obtain a parameter for a rough comparison between the screening experiments (see the Supporting Information).

The reactions performed under conditions 1 and 3 contained cyclophane in equimolar amount only, whereas 5 equivalents of **1** were employed under conditions 2. As common conditions for CuAAC reactions, the combination of copper(II) sulfate and sodium ascorbate[70] was used. As the precipitation of some reactants was observed at high salt concentration, only 1 equivalent of sodium ascorbate was deployed. Under conditions 3, tris(3-hydroxypropyltriazolylmethyl)amine (THPTA)[76] was also added as a ligand to stabilize the Cu^I ions; this has been reported to increase the reaction rate of Cu^I-catalyzed azide–alkyne cycloadditions.[77]

The reactions incorporating **2a** and **2b** did not reach full conversion, even after prolonged stirring, which appears to be due to the limited solubility of these two axles. Even the presence of the cyclophane did not lead to the complete dissolution of these axles, which has already been reported by Anderson and co-workers for lipophilic chromophores of comparable size.[62] An ethylene glycol chain with a minimum of three units seems to be necessary to ensure sufficient solubility in the presence of **1** (Table 2, conditions 1), however, no trend in yield for **2b**–**d** can be deduced from the data. An excess of cyclophane (conditions 2) significantly enhances the formation of rotaxane as the equilibrium is shifted more towards the pseudorotaxane. THPTA seems to have a marginal effect on the yield of rotaxane (conditions 3), although the copper catalyst is stabilized for a prolonged time, avoiding the appearance of a blue/green discoloration due to the formation of Cu^{II} species.

Table 2. Total concentrations and equivalents of reactants and reagents in the CuAAC screening reactions under conditions 1–3.[a]

Conditions	Cyclophane [mM]	Axle [mM]	Stopper [mM]	$CuSO_4$ [mM]	Na ascorb. [mM]	THPTA [mM]
1	0.5	0.5	1.0	0.5	0.5	
2	2.5	0.5	1.0	0.5	0.5	
3	0.5	0.5	1.0	0.5	0.5	0.5

[a] All reactions were performed at room temperature and under argon.

Of particular interest was the influence of the length of the oligo(ethylene glycol) chain of the axles **2a**–**e**. Thus, all three reaction conditions were applied to all five axles and the obtained reaction mixtures were analyzed after 2 hours by LC–ESI-MS (see pages S20–S27 in the Supporting Information). As an indicator of the amount of rotaxane and dumbbell formed, their ion counts in the LC–ESI-MS experiment were used. Even if these two species should display different ionization behavior in the experiment, the ratio between the ion counts of the rotaxane and the dumbbell (**4**/**5**) still allows the most favorable conditions for rotaxane formation to be identified (Table 3).

Table 3. Influence of the axle length on the association constant (K_a) and product distribution under different reaction conditions.

Axle (*n*)	K_a [10^5 M^{-1}]	**4/5** Cond. 1	Cond. 2	Cond. 3	Stopper **3** conversion[a]
2a (1)	–	0.02	0.15	0.13	incomplete
2b (2)	–	0.14	0.44	0.19	incomplete
2c (3)	1.7	0.35	2.04	0.31	complete
2d (4)	1.4	0.43	1.40	0.56	complete
2e (5)	1.2	0.33	2.63	0.47	complete

[a] As conversion could not be quantified in our case, the remarks are based on the absence of the *m*/*z* stopper signal in the total ion current chromatograms.

Synthesis, Isolation. and Characterization of Rotaxanes 4d and 4f

Tetra(ethylene glycol) axle **2d** was selected for the synthesis of **4d** as a compromise between hydrophilicity and synthetic accessibility. Although all the axles in the series **2c**–**e** were soluble in the presence of **1**, the availability of inexpensive TEG derivatives compared with the corresponding penta(ethylene glycol) counterparts favored the choice of **2d** over **2e**. To drive the equilibrium further towards pseudorotaxane formation, the total concentration was increased four-fold compared with the screening conditions, and THPTA was also employed, as in conditions 3. The success of rotaxane formation was monitored, as in the screening reactions, by LC–ESI-MS analysis and based on the intensities of the corresponding MS signals a very promising rotaxane/dumbbell ratio of 9.24 was observed. The reaction mixture was directly purified by Sephadex® LH-20 size-exclusion chromatography with MeOH as the mobile phase. After repetitive chromatography the desired rotaxane **4d** was obtained as an impure sample still containing small amounts of cyclophane **1** (22 mol-% based on ^{1}H NMR analysis, corresponding to about 7 wt.-%), which could neither be removed by normal- or reversed-phase chromatography due to hydrolytic cleavage of the naphthoic esters during evaporation of the eluent. The reason for this was most probably a catalytic effect of the buffer components, which are required for elution of quaternary ammonium salts from silica gel. Another consequence of the limited stability during purification was that dumbbell **5d** could also not be obtained in pure form, as it hydrolyzed even more rapidly during removal of the solvent.

The ^{1}H NMR spectra of the rotaxane **4d**, its axle **2d**, and the cyclophane **1** are displayed in Figure 2a–c, respectively, to document the successful rotaxane formation. Upfield shifts of protons of the naphthalene-2,6-dicarboxylic ester subunit and the 1,4-dioxybutyl subunit of the cyclophane corroborate rotaxane formation, whereas the downfield shift of the former propargylic CH_2 protons document the successful stoppering by triazole formation. The ^{1}H NMR spectrum of the isolated sample (Figure 2a) further allowed us to determine the isolated yield of the rotaxane **4d** to be 59 %.

To avoid hydrolytic instability, a rotaxane based on **2g** with 2,6-dicarboxamide linkers was envisaged, which was then not further pursued due to the very low association constant with **1**. As an alternative, **2f** seemed to be more promising due to its higher binding strength. The concentrations were increased to the maximal attainable, 5 mM **2f** in the presence of 5 equiv. of **1** and 1 equiv. of THPTA/Cu^I. LC–ESI-MS analysis of the crude mixture as above revealed an excellent rotaxane/dumbbell ratio of 17.29. A major part of the cyclophane excess could be removed by size-exclusion chromatography on Sephadex® LH-20 followed by normal-phase chromatography with NH_4HCO_3 as buffer in the mobile phase and subsequent chloride anion exchange on DOWEX® 1X8. The low isolated yield of 19 % does not represent the reaction yield but rather reflects the losses due to strong adsorption on the stationary phase during chromatographic purification.

The formation of rotaxane **4f** was confirmed by its ^{1}H NMR spectrum, in which the effect of the cyclophane on encapsulating the axle becomes clearly visible by comparison with the ^{1}H NMR spectrum of the dumbbell **5f** (Figure 3). A strong chemical upfield shift of the naphthalene protons induced by their direct orientation in the shielding regions of the cyclophane's aromatic rings is observed.[57] The resonances of the methylene

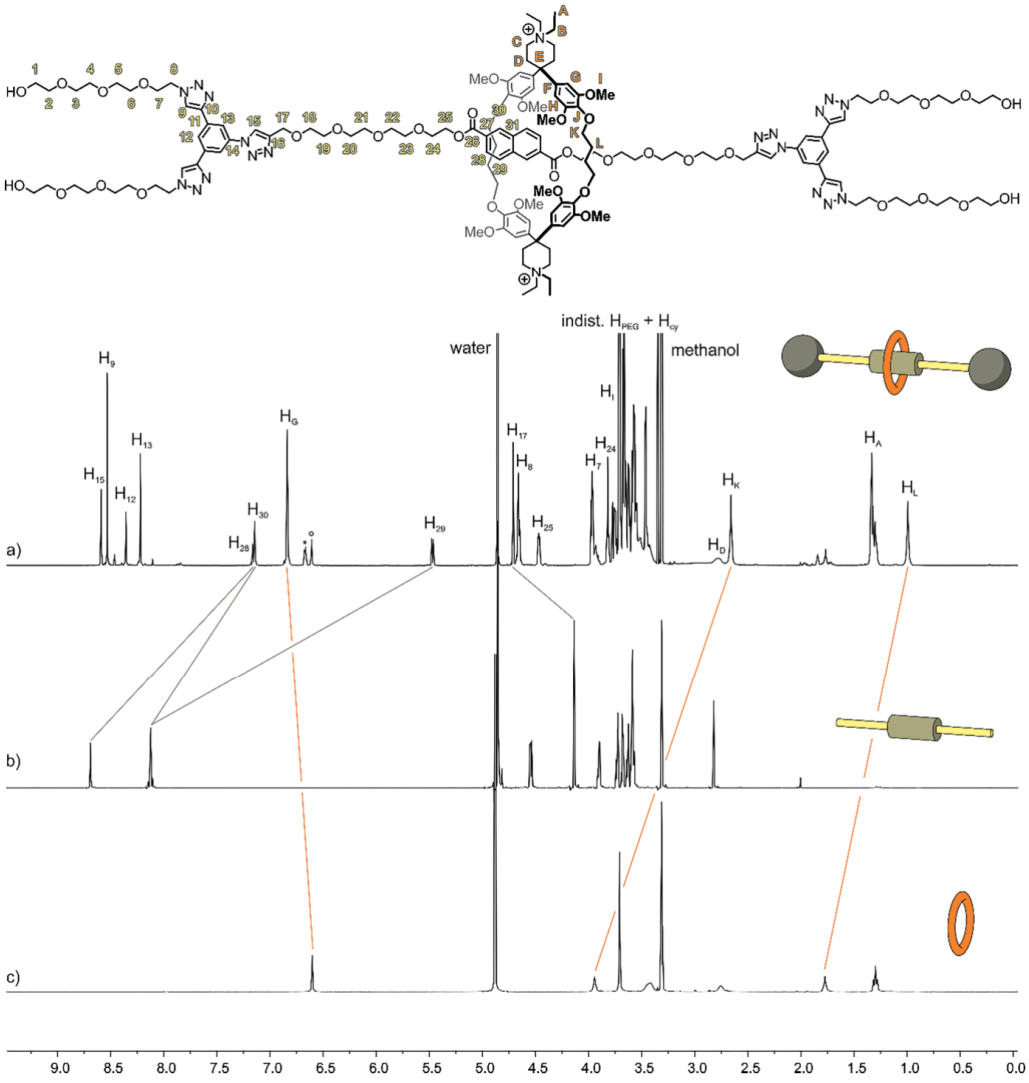

Figure 2. ^{1}H NMR spectra of a) rotaxane **4d** (600 MHz, 298 K, MeOD), b) axle **2d** (500 MHz, 298 K, MeOD), and c) the cyclophane **1** (500 MHz, 298 K, MeOD). Complexation-induced shifts of selected protons: 30-H 1.55 ppm; 29-H 2.65 ppm; 28-H 0.96 ppm, K-H 1.28 ppm; L-H 0.79 ppm. The peak of the free cyclophane is indicated by a small circle, the unknown impurity by an asterisk.

protons of the cyclophane also exhibit a significant upfield shift. Additional evidence for the interlocked structure is found in the distinct NOE cross-peaks (see the ^{1}H NOESY spectrum, Figure SI-1.2, in the Supporting Information) between the naphthalene protons and the methylene chains and methoxy protons of the cyclophane as well as the cross-peaks between the proton of the newly formed triazole and the benzene ring of the stopper.

To investigate the stopper quality, the stabilities of the rotaxanes **4d** and **4f** were monitored at elevated temperature and for elongated periods. The temperature of a 2 mM aqueous solution of rotaxane **4d** was successively increased in steps of 10 °C and the composition of the solution was analyzed by ESI-LC-MS. The temperature was kept for 1 hour at each temperature. Up to 70 °C, neither slippage nor decomposition of the rotaxane was observed. At 80 °C, a new signal of low intensity,

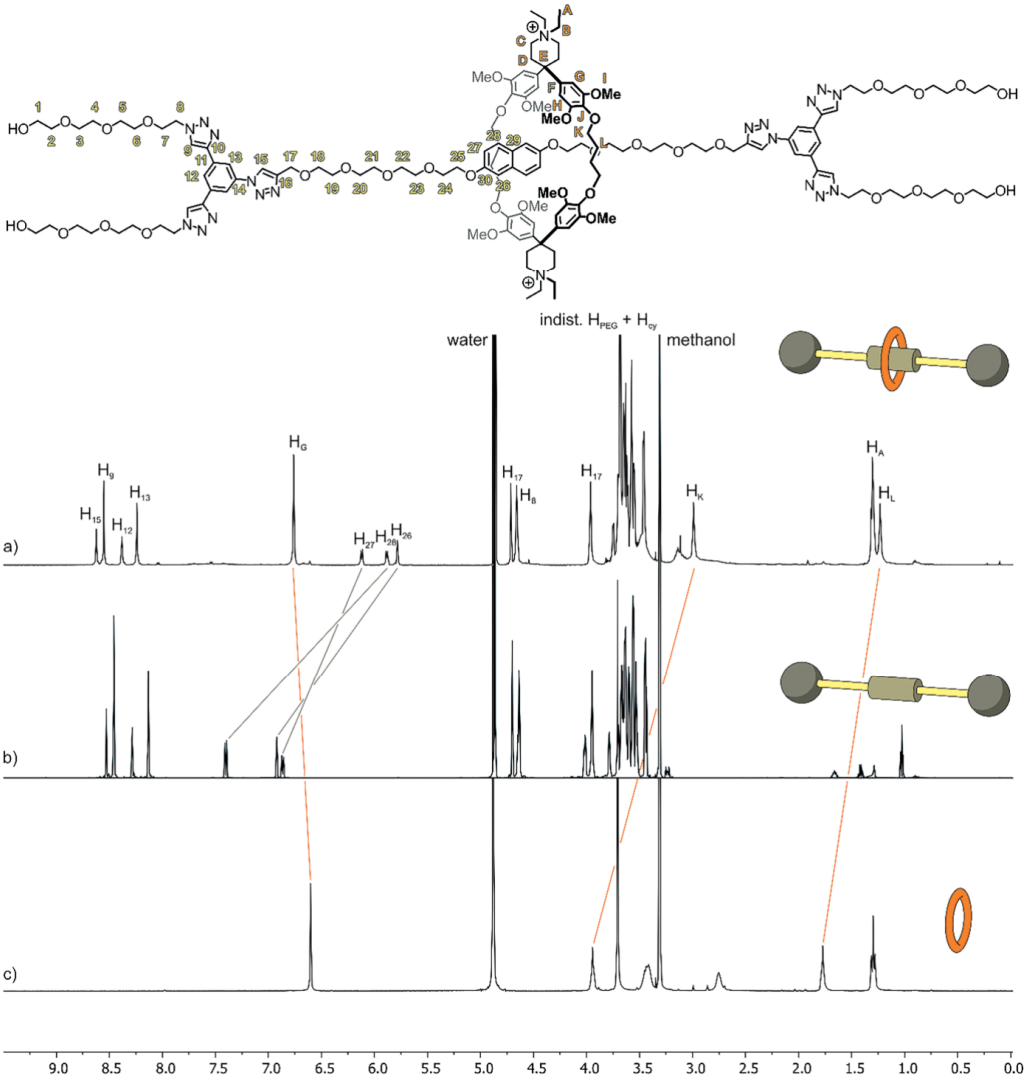

Figure 3. ^{1}H NMR spectra of a) rotaxane **4f** (600 MHz, 298 K, MeOD), b) dumbbell **5f** (600 MHz, 298 K, MeOD), and c) cyclophane **1** (500 MHz, 298 K, MeOD). Complexation-induced shifts of selected protons: 28-H 1.52 ppm; 27-H 0.75 ppm; 26-H 1.13 ppm, K-H 0.95 ppm; L-H 0.54 ppm.

corresponding to a single hydrolyzed ester, as well as a slight increase in the cyclophane signal indicated the decomposition of **4d** by ester hydrolysis. Exposed to the same experiment, **4f** displayed stability up to 100 °C, as neither peaks for **5f** nor for **1** were detected. In addition, an NMR sample of **4f** in CD_3OD (5 mM) remained unchanged after storage for 3 weeks. Also, heating at 60 °C for 20 hours did not alter the ^{1}H NMR spectrum. Altogether, the stability investigations corroborate the mechanical stability of rotaxanes stoppered through a "click" reaction with **3**.

In accordance with the fluorescence titrations, fluorescence spectroscopy revealed that rotaxane **4d** shows only weak fluorescence compared with axle **2d**. The small bathochromic shift of 4 nm in the UV absorption spectrum and the absence of a donor–acceptor absorption band are in accordance with the literature for complexes of **1** and naphthalene derivatives.[57]

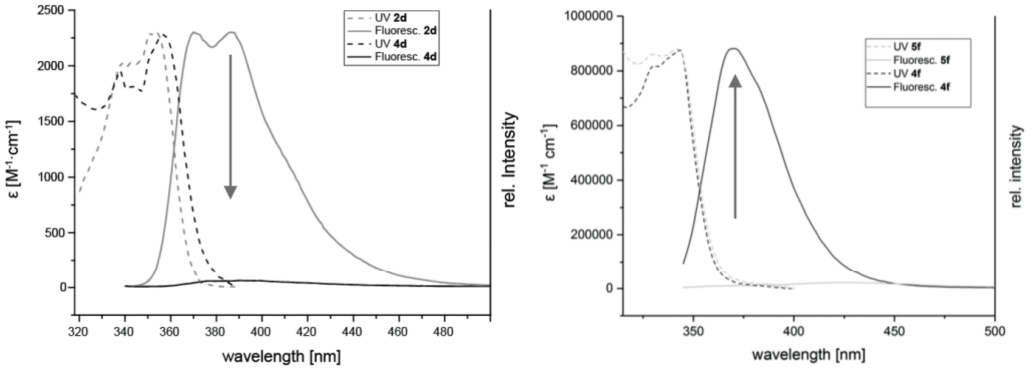

Figure 4. Normalized UV absorption and emission spectra of of **2d**/**4d** (left, excitation at 333 nm) and **5f**/**4f** (right, excitation at 340 nm) in water at 22 °C. All the emission spectra were recorded at a concentration of 0.02 mM.

Comparison of **4f** with **5f** reveals enhanced fluorescence of the rotaxane. The observed enhancement effect is stronger than in the fluorescence titration studies, as the dumbbell fluorescence is far weaker than that of the axle **2f** (Figure 4).

Conclusions

Two rotaxanes have been synthesized and characterized in water without the need for organic co-solvents. The components expose functional groups enabling their interlinking by "click" chemistry and providing desirable modularity to expand the complexity of the system. For rotaxane formation, a new azide-functionalized and water-soluble bulky stopper molecule was developed alongside a series of propargyl-terminated naphthalene guests. The substitution of the naphthalene core dictates the strength of complexation of **1** with axles **2a**–**g**, and the OEG chains reduce the tendency to self-aggregate. The optimum length of the OEG chain was investigated by using a series of naphthalene-2,6-dicarboxylate with OEG spacers of various lengths (n = 1–5), a reasonable extent of rotaxane formation being observed for n > 2, as the short-chain OEG derivatives are insoluble in water even in the presence of **1**. 2,6-Dioxynaphthalene turned out to be an ideal guest for rotaxane synthesis, as it is strongly complexed by **1**, giving hydrolytically stable rotaxanes upon stoppering with **3**.

We will further pursue this approach in our search for highly functional water-based mechanically interlocked systems. A particular focus is to explore the suitability of incorporating electrochemically addressable chromophores into such assemblies.

Experimental Section

General: All commercially available compounds were purchased and used as received unless explicitly remarked otherwise. For column chromatography, either silica gel Siliaflash® p60 (40–63 μm) from Silicycle or Alumina from Fluka, activated, neutral Brockmann Activity I or reversed-phase silica gel SiliaBond® C18 R00230B were used. TLC was performed on silica gel 60 F254 glass plates with a thickness of 0.25 mm purchased from Merck. Size-exclusion chromatography was carried out on Sephadex LH-20 using HPLC-grade methanol. ^{1}H and ^{13}C NMR spectra were recorded either with an Oxford 400 MHz or Bruker Avance III 400 NMR spectrometer equipped with a BBFO^{+} probe head, respectively, and a Bruker UltraShield 500 MHz Avance III spectrometer equipped with a BBO^{+} probe head with Z gradients or an Bruker Ascend 600 MHz Avance III HD spectrometer equipped with a 1.7 mm TCI cryoprobe head, respectively. 2D NMR spectra were either recorded with a Bruker UltraShield 500 MHz Avance III spectrometer equipped with a BBO^{+} probe head with Z gradients or with a Bruker Ascend 600 MHz Avance III HD spectrometer equipped with a 1.7 mm TCI cryoprobe head, respectively. The chemical shifts are reported in parts per million (ppm) relative to tetramethylsilane or a residual solvent peak and the J values are given in Hz. The order of coupling constants is specified by a superscript number (^{n}J). Deuteriated NMR solvents were obtained from Cambridge Isotope Laboratories, Inc. (Andover, MA, USA). All spectra were recorded at 298 K. The atom labeling used in the NMR signal assignment is as presented in Figures 2 and 3. All low-resolution mass spectra were recorded with a Bruker amaZon^{TM} X through electrospray ionization (ESI). High-resolution mass spectra (HRMS) were measured as HR-ESI-ToF-MS with a Bruker Maxis 4G spectrometer. For HPLC, a Shimadzu LC-20AT HPLC was used equipped with a diode array UV/Vis detector (SPD-M10A VP from Shimadzu, λ = 200–600 nm) and the corresponding column (Reprosher, 100 C18 Aqua, 5 μm, 125 × 2 mm, Dr. Maisch GmbH). Water filtered through a Millipak^{R} Express 40 Filter, 0.22 μm from Merck Milipore, subsequently charged with 0.01 % v/v formic acid and HPLC-grade acetonitrile from Avantor also charged with 0.01 % v/v formic acid were used as HPLC solvents. A solvent gradient starting from 10 % water/90 % acetonitrile (v/v) and changing to 5 % water/95 % acetonitrile (v/v) within 10 min was applied for HPLC measurements at a flow rate of 0.5 mL/min. UV/Vis measurements were performed with a Shimadzu UV-1800 spectrometer and fluorescence measurements were recorded with a Horiba FluoroMax-4 spectrofluorimeter using 10 × 10 mm 111-QS Hellma cuvettes at room temperature. The extinction coefficients (ε) were determined based on the UV spectra at four different concentrations (0.05, 0.025, 0.02, and 0.01 mM). All solutions were prepared and measured under air-saturated conditions.

Screening Reactions

Screening Conditions 1: A 10 mL two-neck flask was charged with the relevant oily or solid naphthalene axle **2** (1.00 μmol, 1.0 equiv.) to which water (1.55 mL) was added. Stock solutions of stopper **3** (10 mM in water; 200 μL, 2.0 equiv.) and cyclophane **1** (20 mM in water; 50.0 μL, 1.0 equiv.) were added. After flushing with argon for 10 min under vigorous stirring, a copper(II) sulfate stock solution (10 mM in water; 100 μL, 1.0 equiv.) and L-(+)-ascorbic acid sodium salt stock solution (10 mM in water; 100 μL, 1.0 equiv.) were added. The mixture was again flushed with argon for 10 min. Two hours after addition of the catalyst and reducing agent, a sample was highly diluted in water and measured by LC–ESI-MS. In the case of an incomplete conversion of the naphthalene axle or stopper, a sample was taken again after 21 h and analyzed by LC–ESI-MS.

Screening Conditions 2: The screening conditions 2 resembled those of conditions 1. The difference between the two is the amount of cyclophane added, the total concentrations of the other reactants and reagents remaining the same. The screening reactions were performed with 5.0 equiv. of cyclophane **1** (20 mM in demin. water; 250.0 μL), consequently only 1.35 mL of water were added to reach the total volume of 2.0 mL.

Screening Conditions 3: The screening conditions 3 resembled those of conditions 1. However, the reactions were performed in the presence of the co-catalyst tris(3-hydroxypropyltriazolylmethyl)amine (THPTA; 10 mM in demin. water; 100 μL, 1.0 equiv.). Consequently, only 1.45 mL of water were added to reach the total volume of 2.0 mL.

General Procedure for the Synthesis of 2a,b: A 10 mL Schlenk tube was charged with sodium hydride (60 % dispersion in mineral oil) under argon. A solution of **6a** or **6b** in dry THF was added dropwise and the foaming suspension was stirred at room temperature until hydrogen formation stopped (2 min). Then the septum was loosened, naphthalene-2,6-dicarboxylic acid dimethyl ester (**7a**) was added, and the reaction mixture was heated at 130 °C while slowly distilling off THF and the formed methanol. After 45 min reaction duration, the suspension was cooled to room temperature and was then diluted with ethyl acetate and demin. water. The aqueous phase was extracted with ethyl acetate three times. The combined organic layers were washed with brine, dried with sodium sulfate, filtered, and the solvents were removed under reduced pressure to afford a colorless solid.

Bis[2-(prop-2-yn-1-yloxy)ethyl] Naphthalene-2,6-dicarboxylate (2a): Propargyl-ethylene glycol **6a** (205 mg, 2.05 mmol, 5.0 equiv.), sodium hydride (60 % dispersion in mineral oil; 32.7 mg, 0.818 mmol, 2.0 equiv.), naphthalene-2,6-dicarboxylic acid dimethyl ester (**7a**; 99.9 mg, 0.409 mmol, 1.0 equiv.), THF (50 mL); 42 % yield (66.0 mg); colorless solid. ^{1}H NMR (400 MHz, $CDCl_3$): δ = 8.68–8.65 (m, 2 H, H_{Ar}), 8.15 [dd, $^3J_{H,H}$ = 8.4, $^4J_{H,H}$ = 1.6 Hz, 2 H, H_{Ar}], 8.01 (d, $^3J_{H,H}$ = 8.6 Hz, 2 H, H_{Ar}), 4.62–4.54 (m, 4 H, OCH_2), 4.28 (d, $^3J_{H,H}$ = 2.4 Hz, 4 H, OCH_2), 3.97–3.91 (m, 4 H, $CH_2C{\equiv}CH$), 2.47 (t, $^4J_{H,H}$ = 2.4 Hz, 2 H, $CH_2C{\equiv}CH$) ppm. ^{13}C NMR (101 MHz, $CDCl_3$): δ = 166.4, 134.8, 131.0, 129.7, 129.6, 126.2, 79.4, 75.1, 67.9, 64.4, 58.6 ppm. HRMS (ESI, +): calcd. for $C_{22}H_{20}NaO_6$ 403.1152 $[M + Na]^+$; found 403.1157.

Bis{2-[2-(prop-2-yn-1-yloxy)ethoxy]ethyl} Naphthalene-2,6-dicarboxylate (2b): Propargyl-ethylene glycol **6b** (488 mg, 3.38 mmol, 5.0 equiv.), sodium hydride (60 % dispersion in mineral oil; 27.1 mg, 0.677 mmol, 1.00 equiv.), naphthalene-2,6-dicarboxylic acid dimethyl ester (**7a**; 165 mg, 0.677 mmol, 1.00 equiv.), THF (30 mL); 14 % yield (45.0 mg); colorless solid. ^{1}H NMR (400 MHz, $CDCl_3$): δ = 8.68–8.65 (m, 2 H, H_{Ar}), 8.15 (dd, $^3J_{H,H}$ = 8.4, $^4J_{H,H}$ = 1.6 Hz, 2 H, H_{Ar}), 8.01 (d, $^3J_{H,H}$ = 8.6 Hz, 2 H, H_{Ar}), 4.62–4.54 (m, 4 H, OCH_2), 4.28 (d, $^3J_{H,H}$ = 2.4 Hz, 4 H, OCH_2), 3.97–3.91 (m, 4 H, $CH_2C{\equiv}CH$), 2.47 (t, $^4J_{H,H}$ = 2.4 Hz, 2 H, $CH_2C{\equiv}CH$) ppm. ^{13}C NMR (101 MHz, $CDCl_3$): δ = 166.4, 134.8, 131.0, 129.7, 129.6, 126.2, 79.4, 75.1, 67.9, 64.4, 58.6 ppm. HRMS (ESI, +): calcd. for $C_{26}H_{29}O_8$ 469.11857 $[M + H]^+$; found 469.1857; calcd. for $C_{26}H_{28}NaO_8$ 491.1676 $[M + Na]^+$; found 491.1682.

General Procedure for the Synthesis of 2c–e: Diethyl azodicarboxylate solution (DEAD; 40 % in toluene, 2.2 equiv.) was slowly added to a suspension of the relevant propargyl ethylene glycol derivative **6c–e** (2.0 equiv.), 2,6-naphthalenedicarboxylic acid (1.0 equiv.), and triphenylphosphine (2.2 equiv.) in dry THF under argon. The suspension turned into a clear, pale-yellow solution. After stirring the mixture for 16 h, the solvents were removed, demin. water (10 mL) was added to the crude yellow oil, and the mixture was extracted with methyl *tert*-butyl ether (3 × 100 mL). The combined organic layers were washed with brine, dried with sodium sulfate, filtered, and the solvents were removed under reduced pressure. The crude product was purified by column chromatography.

Bis{2-{2-[2-(prop-2-yn-1-yloxy)ethoxy]ethoxy}ethyl) Naphthalene-2,6-dicarboxylate (2c): Propargyl-ethylene glycol **6c** (550 mg, 2.92 mmol, 2.0 equiv.), naphthalene-2,6-dicarboxylic acid (**7b**; 316 mg, 1.46 mmol, 1.0 equiv.), triphenylphosphine (842 mg, 3.21 mmol, 2.2 equiv.), DEAD (1.40 g, 3.21 mmol, 1.47 mL, 2.2 equiv.), dry THF (45 mL); column chromatography (Al_2O_3, basic; ethyl acetate); 82 % yield (669 mg); colorless solid. ^{1}H NMR (400 MHz, $CDCl_3$): δ = 8.67–8.63 (m, 2 H, H_{Ar}), 8.14 (dd, $^3J_{H,H}$ = 8.5, $^4J_{H,H}$ = 1.5 Hz, 2 H, H_{Ar}), 8.01 (d, J = 8.5 Hz, 2 H, H_{Ar}), 4.59–4.52 (m, 4 H, $OCOCH_2$), 4.18 (d, $^4J_{H,H}$ = 2.4 Hz, 4 H, $CH_2C{\equiv}CH$), 3.92–3.84 (m, 4 H, $OCOCH_2CH_2$), 3.79–3.73 (m, 4 H, OCH_2), 3.72–3.66 (m, 12 H, OCH_2), 2.40 (t, $^4J_{H,H}$ = 2.4 Hz, 2 H, $C{\equiv}CH$) ppm. ^{13}C NMR (101 MHz, $CDCl_3$): δ = 166.5, 134.7, 130.9, 129.7, 129.6, 126.2, 79.8, 74.7, 70.9, 70.8, 70.7, 69.4, 69.3, 64.6, 58.6 ppm. HRMS (ESI, +): calcd. for $C_{30}H_{36}Na_2O_{10}$ 301.1046 $[M + 2Na]^{2+}$; found 301.1048.

Di(3,6,9,12-tetraoxapentadec-14-yn-1-yl) Naphthalene-2,6-dicarboxylate (2d): Propargyl-ethylene glycol **6d** (729 mg, 3.14 mmol, 2.0 equiv.), naphthalene-2,6-dicarboxylic acid (**7b**; 339 mg, 1.57 mmol, 1.0 equiv.), triphenylphosphine (906 mg, 3.45 mmol, 2.2 equiv.), DEAD (1.50 g, 3.45 mmol, 1.48 mL, 2.2 equiv.), dry THF (45 mL); column chromatography (rp-SiO_2 C18; water/acetone, 5:4); 64 % yield (646 mg); colorless solid. ^{1}H NMR (400 MHz, $CDCl_3$): δ = 8.68–8.63 (m, 2 H, H_{Ar}), 8.14 (dd, $^3J_{H,H}$ = 8.4, $^4J_{H,H}$ = 1.5 Hz, 2 H, H_{Ar}), 8.01 (d, $^3J_{H,H}$ = 8.6 Hz, 2 H, H_{Ar}), 4.59–4.51 (m, 4 H, $OCOCH_2$), 4.18 (d, $^4J_{H,H}$ = 2.4 Hz, 4 H, $CH_2C{\equiv}CH$), 3.93–3.86 (m, 4 H, $OCOCH_2CH_2$), 3.75–3.72 (m, 4 H, OCH_2), 3.71–3.58 (m, 20 H, OCH_2), 2.42 (t, $^4J_{H,H}$ = 2.4 Hz, 2 H, $C{\equiv}CH$) ppm. ^{13}C NMR (101 MHz, $CDCl_3$): δ = 166.6 (C_q, 2 C, $C{=}O$), 134.8 (C_q, 2 C, C_{Ar}), 131.0 (C_t, 2 C, C_{Ar}), 129.8 (C_t, 2 C, C_{Ar}), 129.7 (C_q, 2 C, C_{Ar}), 126.3 (C_t, 2 C, C_{Ar}), 79.9 (C_q, 2 C, $C{\equiv}CH$), 74.8 (C_t, 2 C, $C{\equiv}CH$), 71.0 (C_s, 2 C, CH_2), 70.9 (C_s, 2 C, CH_2), 70.9 (C_s, 2 C, CH_2), 70.9 (C_s, 2 C, CH_2), 70.7 (C_s, 2 C, CH_2), 69.5 (C_s, 2 C, CH_2), 69.3 (C_s, 2 C, CH_2), 64.7 (C_s, 2 C, CH_2), 58.6 (C_s, 2 C, CH_2) ppm. HRMS (ESI, +): calcd. for $C_{34}H_{44}NaO_{12}$ 667.2729 $[M + Na]^+$; found 667.2725.

Di(3,6,9,12,15-pentaoxaoctadec-17-yn-1-yl) Naphthalene-2,6-dicarboxylate (2e): Propargyl-ethylene glycol **6e** (558 mg, 2.02 mmol, 2.0 equiv.), naphthalene-2,6-dicarboxylic acid (**7b**; 218 mg, 1.01 mmol, 1.0 equiv.), triphenylphosphine (583 mg, 2.22 mmol, 2.2 equiv.), DEAD (967 mg, 2.22 mmol, 1.02 mL, 2.2 equiv.), dry THF (30 mL); column chromatography (rp-SiO_2 C18; water/acetone, 5:4); 43 % yield (322 mg); colorless solid. ^{1}H NMR (400 MHz, $CDCl_3$): δ = 8.68–8.63 (m, 2 H, H_{Ar}), 8.14 (dd, $^3J_{H,H}$ = 8.5,

$^4J_{H,H}$ = 1.6 Hz, 2 H, H_{Ar}), 8.01 (d, $^3J_{H,H}$ = 8.6 Hz, 2 H, H_{Ar}), 4.58–4.52 (m, 4 H, OCOCH_2), 4.19 (d, $^4J_{H,H}$ = 2.4 Hz, 4 H, CH_2C≡CH), 3.92–3.86 (m, 4 H, OCOCH$_2$CH_2), 3.77–3.72 (m, 4 H, OCH_2), 3.72–3.58 (m, 28 H, OCH_2), 2.42 (t, $^4J_{H,H}$ = 2.4 Hz, 2 H, C≡C*H*) ppm. ^{13}C NMR (101 MHz, $CDCl_3$): δ = 166.5 (C_q, 2 C, *C*=O), 134.7 (C_q, 2 C, C_{Ar}), 130.9 (C_t, 2 C, C_{Ar}), 129.7 (C_t, 2 C, C_{Ar}), 129.6 (C_q, 2 C, C_{Ar}), 126.2 (C_t, 2 C, C_{Ar}), 100.1, 79.8 (C_q, 2 C, *C*≡CH), 77.4 (C_s, 2 C, *C*H_2), 74.7 (C_t, 2 C, C≡*C*H), 70.9 (C_s, 2 C, *C*H_2), 70.8 (C_s, 2 C, *C*H_2), 70.8 (C_s, 2 C, *C*H_2), 70.8 (C_s, 2 C, *C*H_2), 70.7 (C_s, 2 C, *C*H_2), 70.6 (C_s, 2 C, *C*H_2), 69.4 (C_s, 2 C, *C*H_2), 69.2 (C_s, 2 C, *C*H_2), 64.6 (C_s, 2 C, *C*H_2), 58.5 (C_s, 2 C, *C*H_2) ppm. HRMS (ESI, +): calcd. for $C_{38}H_{52}NaO_{14}$ 755.3249 [M + Na]$^+$; found 755.3239.

2,2′-[({[{[{[Naphthalene-2,6-diylbis(oxy)]bis(ethane-2,1-diyl)}bis(oxy))bis(ethane-2,1-diyl)]bis(oxy)}bis(ethane-2,1-diyl))bis(oxy)]bis(ethan-1-ol) (7f): 2,6-Dihydroxynaphthalene (1.0 g, 6.24 mmol, 1 equiv.) was dissolved in CH_3CN (80 mL) and 2-{2-[2-(2-hydroxyethoxy)ethoxy]ethoxy}ethyl toluene-*p*-sulfonate (5.0 g, 14 mmol, 2.3 equiv.) followed by Cs_2CO_3 (8.1 g, 25 mmol 4.0 equiv.) were added. The mixture was immediately bubbled with Ar for 10 min and heated at reflux for 16 h. After cooling to room temp., the salts were filtered off, the filter cake was washed with acetone, and the solvents were removed. The crude oil was purified by column chromatography [silica gel, TBME/acetone (1:1) → acetone] to give a colorless oil, which solidified upon standing. Yield: 44 % (1.40 g). ^{1}H NMR (400 MHz, $CDCl_3$): δ = 7.60 (d, $^3J_{H,H}$ = 8.8 Hz, 2 H, H_{Ar}), 7.14 (dd, $^3J_{H,H}$ = 8.8, $^4J_{H,H}$ = 2.5 Hz, 2 H, H_{Ar}), 7.09 (d, $^4J_{H,H}$ = 2.5 Hz, 2 H, H_{Ar}), 4.32–4.09 (m, 4 H, OCH_2), 4.00–3.85 (m, 4 H, OCH_2), 3.83–3.46 (m, 24 H, OCH_2), 3.11 (br. s, 2 H, O*H*) ppm. ^{13}C NMR (101 MHz, $CDCl_3$): δ = 155.39, 129.87, 128.26, 119.34, 107.26, 72.59, 70.94, 70.78, 70.73, 70.46, 69.91, 67.58, 61.85 ppm. HRMS (ESI, +): calcd. for $C_{26}H_{40}NaO_{10}$ 535.2514 [M + Na]$^+$; found 535.2520.

2,6-Bis[(3,6,9,12-tetraoxapentadec-14-yn-1-yl)oxy]naphthalene (2f): NaH (60 % dispersion in mineral oil; 234 mg, 5.84 mmol, 4.0 equiv.) was added to a solution of **7f** (748 mg, 1.46 mmol, 1.0 equiv.) in THF (10 mL) under Ar. After completion of H_2 evolution, propargyl bromide (80 % in toluene, 480 µL, ca. 4.4 mmol, ca. 3 equiv.) was added slowly, the ice bath was removed, and the mixture was stirred for 3 h. It was then quenched by the addition of MeOH (5 mL) and subjected to silica gel column chromatography (TBME → TBME/5 % EtOH). During evaporation of the product fraction, precipitation was observed. The precipitate was filtered off and washed with a small amount of TBME to give 300 mg of white flakes. A second fraction of around 300 mg was obtained by cooling to 4 °C overnight, followed by filtration. Both fractions were combined and recrystallized from TBME. Yield: 54 % (460 mg); white flakes. ^{1}H NMR (400 MHz, $CDCl_3$): δ = 7.61 (d, $^3J_{H,H}$ = 8.8 Hz, 2 H, H_{Ar}), 7.14 (dd, $^3J_{H,H}$ = 8.8, $^4J_{H,H}$ = 2.5 Hz, 2 H, H_{Ar}), 7.09 (d, $^4J_{H,H}$ = 2.5 Hz, 2 H, H_{Ar}), 4.24–4.20 (m, 4 H, OCH_2), 4.19 (d, $^4J_{H,H}$ = 2.4 Hz, 4 H, OCH_2), 3.96–3.84 (m, 4 H, OCH_2), 3.79–3.72 (m, 4 H, OCH_2), 3.72–3.62 (m, 16 H, OCH_2), 2.41 (t, $^4J_{H,H}$ = 2.4 Hz, 2 H, C≡C*H*) ppm. ^{13}C NMR (101 MHz, $CDCl_3$): δ = 155.5, 129.9, 128.3, 119.4, 107.3, 79.8, 74.6, 71.0, 70.8, 70.8, 70.6, 69.9, 69.3, 67.6, 58.4 ppm. HRMS (ESI, +): calcd. for $C_{32}H_{44}NaO_{10}$ 611.2827 [M + Na]$^+$; found 611.2821.

***N*^{2},*N*^{6}-Di(3,6,9,12-tetraoxapentadec-14-yn-1-yl)naphthalene-2,6-dicarboxamide (2g):** 3,6,9,12-Tetraoxapentadec-14-yn-1-amine (0.60 g, 2.6 mmol, 2.2 equiv.) was placed in a flask and dissolved in CH_2Cl_2 (10 mL). Dry Et_3N was added (1.0 mL), followed by the portionwise addition of naphthalene-2,6-dicarbonyl dichloride (299 mg, 1.18 mmol, 1 equiv.). After complete addition the mixture was stirred overnight and filtered through silica gel (elution with acetone). The filtrate was evaporated and purified by column chromatography (RP-C18 silica, MeOH/H_2O, 2:1). Yield: 84 % (636 mg); waxy solid. ^{1}H NMR (400 MHz, CD_2Cl_2): δ = 8.43–8.33 (m, 2 H, H_{Ar}), 8.03 (d, ^3J = 8.4 Hz, 2 H, H_{Ar}), 7.95 (dd, ^3J = 8.4, ^4J = 1.7 Hz, 2 H, H_{Ar}), 7.06 (br. s, 2 H, CONH), 4.15 (d, ^4J = 2.4 Hz, 4 H, OCH_2), 3.83–3.45 (m, 32 H, OCH_2), 2.51 (t, J = 2.4 Hz, 2 H, C≡C*H*) ppm. ^{13}C NMR (101 MHz, CD_2Cl_2): δ = 167.2, 134.3, 134.0, 129.6, 127.4, 125.1, 80.1, 74.6, 70.9, 70.7, 70.6, 70.1, 69.5, 58.6, 40.4 ppm. HRMS (ESI, +): calcd. for $C_{34}H_{46}N_2NaO_{10}$ 665.3045 [M + Na]$^+$; found 665.3054.

3,5-Bis[(trimethylsilyl)ethynyl]aniline (9): 3,5-Diiodoaniline (**8**, 2.50 g, 7.25 mmol, 1.0 equiv.), bis(triphenylphosphine)palladium(II) dichloride (38 mg, 54 µmol, 0.75 mol-%), copper(I) iodide (21 mg, 0.11 mmol, 1.5 mol-%), and triphenylphosphine (29 mg, 0.11 mmol, 1.5 mol-%) were placed in a flask. Dry THF (50 mL) was added, followed by dry trimethylamine (5 mL). The suspension was degassed with Ar for 15 min and trimethylsilylacetylene (3.1 mL, 22 mmol, 3.0 equiv.) was added. The reaction was stirred at room temperature overnight and then it was filtered through a cotton plug to remove the precipitated salts. The filter cake was washed with a small amount of EtOAc and the filtrate was evaporated and the residue purified by column chromatography (silica gel, cyclohexane/DCM, 1:1) to give the desired compound as a yellowish oil (1.50 g, 5.25 mmol, 73 %). ^{1}H NMR (400 MHz, CD_3CN): δ = 6.75 (t, $^4J_{H,H}$ = 1.4 Hz, 1 H, H_{Ar}), 6.67 (d, $^4J_{H,H}$ = 1.4 Hz, 2 H, H_{Ar}), 4.33 (s, 2 H, NH_2), 0.21 [s, 18 H, Si(CH_3)$_3$] ppm. ^{13}C NMR (101 MHz, CD_3CN): δ = 149.3, 124.7, 124.4, 118.4, 105.4, 94.5, –0.2 ppm. HRMS (ESI, +): calcd. for $C_{16}H_{24}NSi_2$ 286.1442 [M + H]$^+$; found 286.1444.

2,2′-[({[{[{[{[5-Amino-1,3-phenylene)bis(1*H*-1,2,3-triazole-4,1-diyl)]bis(ethane-2,1-diyl)}bis(oxy))bis(ethane-2,1-diyl)]-bis(oxy)}bis(ethane-2,1-diyl))bis(oxy)]bis(ethan-1-ol) (10): 3,5-Bis[(trimethylsilyl)ethynyl]aniline (**9**; 1.34 g, 4.69 mmol, 1.0 equiv.) and 2-{2-[2-(2-azidoethoxy)ethoxy]ethoxy}ethan-1-ol (2.11 g, 9.61 mmol, 2.05 equiv.) were placed in a round-bottomed flask and dissolved in a mixture of acetone and water (1:1, 60 mL). K_2CO_3 (2.59 g, 18.8 mmol, 4.0 equiv.) and sodium ascorbate (929 mg, 4.69 mmol, 1.0 equiv.) were added, followed by $CuSO_4$ (376 mg, 2.35 mmol, 0.5 equiv.) to give a yellow-brownish suspension. The mixture was stirred at room temperature for 2 h and subsequently filtered through a short column of basic alumina, which was eluted with EtOH to remove copper salts. The solvent of the filtrate was then removed to give a brownish oil, which was directly used without further purification (2.10 g, 3.62 mmol, 77 %). ^{1}H NMR (400 MHz, CD_3CN): δ = 8.17 (s, 2 H, $H_{triazole}$), 7.57 (t, $^4J_{H,H}$ = 1.5 Hz, 1 H, H_{Ar}), 7.15 (d, $^4J_{H,H}$ = 1.5 Hz, 2 H, H_{Ar}), 4.55 (t, $^3J_{H,H}$ = 5.0 Hz, 4 H, CH_2), 3.89 (t, $^3J_{H,H}$ = 5.0 Hz, 4 H, OCH_2), 3.59–3.57 (m, 4 H, OCH_2), 3.56–3.51 (m, 16 H, OCH_2), 3.44–3.41 (m, 4 H, OCH_2) ppm. ^{13}C NMR (101 MHz, CD_3CN): δ = 149.9, 148.0, 133.4, 122.4, 112.7, 111.7, 73.2, 71.1, 71.1, 70.9, 69.9, 61.9, 51.0 ppm. HRMS (ESI, +): calcd. for $C_{26}H_{41}N_7O_8$ 580.3089 [M + H]$^+$; found 580.3094.

2,2′-[({[{[{[{[5-Azido-1,3-phenylene)bis(1*H*-1,2,3-triazole-4,1-diyl)]bis(ethane-2,1-diyl)}bis(oxy))-bis(ethane-2,1-diyl)]bis(oxy)}bis(ethane-2,1-diyl))bis(oxy)]bis(ethan-1-ol) (3): The aniline derivative **10** (460 mg, 790 µmol) was dissolved in a mixture of conc. aq. HCl (5.0 mL) and water (5.0 mL). The mixture was cooled to 0 °C and solid $NaNO_2$ (82 mg, 1.2 mmol, 1.5 equiv.) was added in small portions. It was then stirred at 0 °C for 20 min, before the addition of solid NaN_3 (155 mg, 2.38 mmol, 3.0 equiv.) in small portions at 0 °C. When the addition was complete, the reaction was warmed to room temperature and stirred for 1 h. The reaction mixture was then neutralized with solid $NaHCO_3$, diluted with water (20 mL), and extracted with EtOAc (5 × 50 mL). The combined organic phases were dried with Na_2SO_4 and the solvents evaporated. The crude product was obtained as an amber oil, which was purified by column chromatography (Al_2O_3 neutral, EtOAc/EtOH, 9:1 → 7:3) to give a colorless oil. (410 mg, 677 µmol, 85 %).

The compound proved to be bench-stable, showing only traces of decomposition products and slight discoloration after several weeks. ^{1}H NMR (500 MHz, MeOD): δ = 8.50 (s, 2 H, $H_{triazole}$), 8.10 (t, $^4J_{H,H}$ = 1.4 Hz, 1 H, H_{Ar}), 7.54 (d, $^4J_{H,H}$ = 1.4 Hz, 2 H, H_{Ar}), 4.69–4.63 (t, $^3J_{H,H}$ = 5.0 Hz, 4 H, CH_2), 4.02–3.87 (t, $^3J_{H,H}$ = 5.0 Hz, 4 H, OCH_2), 3.68–3.61 (m, 8 H, OCH_2), 3.60–3.57 (m, 8 H, OCH_2), 3.57–3.53 (m, 4 H, OCH_2), 3.50–3.45 (m, 4 H, OCH_2) ppm. ^{13}C NMR (126 MHz, MeOD): δ = 146.0 (C_q, 2 C, C_{Ar}), 141.8 (C_q, 1 C, C_{Ar}), 133.0 (C_q, 2 C, C_{Ar}), 122.5 (C_t, 2 C, C_{Ar}), 119.0 (C_t, 1 C, C_{Ar}), 115.1 (C_t, 2 C, C_{Ar}), 72.2 (C_s, 2 C, CH_2), 70.1 (C_s, 2 C, CH_2), 70.1 (C_s, 2 C, CH_2), 70.0 (C_s, 2 C, CH_2), 70.0 (C_s, 2 C, CH_2), 68.9 (C_s, 2 C, CH_2), 60.8 (C_s, 2 C, CH_2), 50.3 (C_s, 2 C, CH_2) ppm. HRMS (ESI, +): calcd. for $C_{26}H_{39}N_9NaO_8$ 628.2814 [M + Na]$^+$; found 628.2825.

Rotaxane 4d: In a 50 mL two-necked flask, stopper **3** (36.3 mg, 060 µmol, 2.0 equiv.), naphthalene rod **2d** (19.3 mg, 30 µmol, 1.0 equiv.), and cyclophane **1** (150 mg, 150 µmol, 5.0 equiv.) were dissolved in miliQ water (6.0 mL) under argon. The resulting pale-orange solution was degassed by flushing with argon for 15 min. Afterwards, a copper(II) sulfate solution (10 mM in water, 3.00 mL, 30 µmol, 1.0 equiv.), an L-(+)-ascorbic acid sodium salt solution (10 mM in water, 3.00 mL, 30 µmol, 1.0 equiv.), and tris(3-hydroxypropyltriazolylmethyl)amine (THPTA; 10 mM in water, 3.00 mL, 30 µmol, 1.0 equiv.) were added and the solution was degassed again for 5 min. After stirring at room temperature for 2 h, LC–ESI-MS was performed, which indicated the full conversion of stopper **3**. After stirring for 3 h and 20 min, the solvent was removed under reduced pressure. The solid crude product was dissolved in methanol (2.0 mL) and subjected to short column chromatography (Al_2O_3, basic; methanol) to separate the copper salts. Further purification was performed by size-exclusion chromatography (Sephadex LH20, methanol). The fractions containing rotaxane were combined, the eluate was concentrated in vacuo, and the size-exclusion procedure was repeated twice. The remaining twice-stoppered rod (7 % according to ^{1}H NMR analysis after three size-exclusion procedures) was separated from the rotaxane by washing the solid product mixture with a small amount (0.3 mL) of acetone. Finally, the product was dissolved in acetonitrile/water (7:1) and passed through an ion-exchange column (DOWEX, 1X8 400 Cl) to afford 59.0 mg of product. According to the ^{1}H NMR spectrum, the product contains 22 % of the free cyclophane, resulting in a calculated yield of 59 % for the pure rotaxane. ^{1}H NMR (600 MHz, MeOD): δ = 8.59 (s, 2 H, 15-H), 8.53 (s, 4 H, 9-H), 8.36 (t, $^4J_{H,H}$ = 1.5 Hz, 2 H, 12-H), 8.22 (d, $^4J_{H,H}$ = 1.5 Hz, 4 H, 13-H), 7.17–7.15 (m, 2 H, 28-H), 7.14 (s, 2 H, 30-H), 6.84 (s, 8 H, G-H), 6.67 (d, J = 4.3 Hz, $H_{impurity}$), 6.61 (s, G-$H_{free\ cycloph}$), 5.47 (d, $^3J_{H,H}$ = 8.4 Hz, 2 H, 29-H), 4.71 (s, 4 H, 17-H), 4.68–4.64 (m, 8 H, 8-H), 4.49–4.45 (m, 4 H, 25-H), 3.97 (t, $^3J_{H,H}$ = 5.0 Hz, 8 H, 7-H), 3.95–3.89 (m, K-$H_{free\ cycloph}$), 3.83–3.81 (m, 4 H, 24-H), 3.78–3.39 [m, 112 H, 1-H (8 H), 2-H (8 H), 3-H (8 H), 4-H (8 H), 5-H (8 H), 6-H (8 H), 18-H (4 H), 19-H (4 H), 20-H (4 H), 21-H (4 H), 22-H (4 H), 23-H (4 H), B-H (8 H), C-H (8 H), I-H (24 H)], 2.99 [br. s (NOESY), 8 H, D-H], 2.78 (s, D-$H_{free\ cycloph}$), 2.69–2.62 (m, 8 H, K-H), 1.77 (s, L-$H_{free\ cycloph}$), 1.33 (t, $^3J_{H,H}$ = 7.2 Hz, 12 H, A-H), 1.30–1.29 (m, A-$H_{free\ cycloph}$), 1.00–0.98 (m, 8 H, L-H) ppm. ^{13}C NMR (151 MHz, MeOD): δ = 167.0 (C_q, 2 C, C-26), 155.0 (C_q, 8 C, C-H), 154.9 (C_q, 8 C, C-$H_{cy\ free}$) (cy free = free cyclophane), 147.2 (C_q, 2 C, C-16), 147.0 (C_q, 4 C, C-10), 139.4 (C_q, 2 C, C-14), 136.9 (C_q, 4 C, C-$J_{cy\ free}$), 136.5 (C_q, 4 C, C-J), 134.9 (C_q, 2 C, C-31), 134.6 (C_q, 4 C, C-11), 131.1 (C_t, 2 C, C-30), 130.6 (C_t, 2 C, C-29), 129.8 (C_q, 2 C, C-27), 125.9 (C_t, 2 C, C-28), 124.2 (C_t, 4 C, C-9), 123.5 (C_t, 2 C, C-12), 123.3 (C_t, 2 C, C-15), 117.4 (C_t, 4 C, C-13), 105.4 (C_t, 8 C, C-$G_{cy\ free}$), 104.1 (C_t, 8 C, C-G), 73.6 (C_s, 4 C, C-K), 72.9 (C_s, 4 C, C-D), 71.7 (C_s, 2 C, C-19), 71.7 (C_s, 2 C, C-21), 71.7 (C_s, 2 C, C-23), 71.5 (C_s, 8 C, C-1, C-3), 71.5 (C_s, 4 C, C-5), 71.4 (C_s, 4 C, C-6), 71.4 (C_s, 8 C, C-2, C-4), 71.1 (C_s, 6 C, C-18, C-20, C-22), 70.4 (not assigned; corr. in HMQC with rotaxane sign. 3.97 ppm), 70.3 (C_s, 4 C, C-7), 65.7 (C_s, 2 C, C_{25}), 65.1 (C_s, 2 C, C_{17}), 62.2 (not assigned; corr. in HMQC with rotaxane sign. 3.57 ppm), 57.1 (C_s, 4 C, C-B), 57.0 (C_s, 4 C, C-$B_{cy\ free}$), 56.9 (C_s, 4 C, C-$C_{cy\ free}$), 56.9 (C_s, 4 C, C-C), 56.8 (C_p, 8 C, OCH_3, C-24), 56.6 (C_p, 8 C, C-I), 51.7 (C_s, 4 C, C-8), (49.8), (45.6), 45.1 (C_q, 2 C, C-$E_{cy\ free}$), (45.0), 44.6 (C_q, 2 C, C_E), (30.5), 30.4 (not assigned; corr. in HMQC with free cyclophane sign. 1.71 ppm), (30.2), (29.5), (28.4), (27.6), 27.2 (C_s, 4 C, C-$L_{cy\ free}$), 26.4 (C_s, 4 C, C-L), 7.6 (C_s, 4 C, C-A), 7.5 (C_s, 4 C, C-$A_{cy\ free}$) ppm. The signal for C_q (expected at ca. 141 ppm) next to the spiro center was not observed; signals in brackets correspond to impurity. HRMS (ESI, +): calcd. for $C_{144}H_{206}N_{20}NaO_{40}$ 959.4860 [M + Na –2Cl]$^{3+}$; found 959.4876.

Rotaxane 4f: A solution of naphthalene axle **4f** (11.8 mg, 0.0200 mmol, 1.0 equiv.) and cyclophane **1** (106 mg, 0.100 mmol, 5.0 equiv.) in water (4.0 mL) was prepared. The stopper **3** (26.6 mg, 0.044 mmol, 2.2 equiv.) was added to a flask and dissolved in water (1 mL). The cyclophane/axle solution was then added. Copper(II) sulfate (3.2 mg, 0.020 mmol, 1.0 equiv.) was added, followed by tris(3-hydroxypropyltriazolylmethyl)amine (8.7 mg, 0.020 mmol, 1.0 equiv.). After complete dissolution of these materials, sodium ascorbate (8.1 mg, 0.040 mmol, 2.0 equiv.) was added, giving a yellow solution. LC–ESI-MS indicated complete conversion after 30 min. The mixture was then directly loaded onto a Sephadex® LH-20 column, which was eluted with MeOH. It was then further purified on silica gel (ACN/0.5 M NH_4HCO_3/MeOH = 10:8:2). The solvent of the product fractions was removed and the resulting salt–product mixture was heated at 60 °C and 0.1 mBar for 24 h, followed by ion-exchange on DOWEX® 1X8 (MeOH, chloride form). The rotaxane was obtained as a colorless solid (10.9 mg, 3.81 µmol, 19.1 %). ^{1}H NMR (600 MHz, MeOD): δ = 8.62 (s, 2 H, 15-H), 8.55 (s, 4 H, 9-H), 8.38 (s, J = 1.7 Hz, 2 H, 12-H), 8.24 (s, 4 H, 13-H), 6.76 (s, 8 H, G-H), 6.12 (dd, ^3J = 8.8, ^4J = 2.6 Hz, 2 H, 27-H), 5.88 (dd, ^3J = 8.8, ^4J = 2.6 Hz, 2 H, 28-H), 5.79 (d, ^4J = 2.6 Hz, 2 H, 26-H), 4.71 (s, 4 H, 17-H), 4.66 (t, J = 5.1 Hz, 8 H, 8-H), 3.96 (t, J = 5.1 Hz, 8 H, 7-H), 3.77–3.73 (m, 4 H, H_{TEG}), 3.72–3.60 (m, H_{TEG} + I-H), 3.60–3.54 (m, H_{TEG}), 3.47–3.44 (m, 8 H, H_{TEG}), 3.02–2.96 (m, 8 H, K-H), 1.30 (t, J = 7.2 Hz, 12 H, A-H), 1.26–1.20 (m, 8 H, L-H) ppm. Signals for B-H and C-H are broad and overlapping (δ = 3.4–3.6 ppm), NOESY cross-peaks with A-H, D-H cannot be clearly identified, probably overlapping and broad (δ = 2.8–3.1 ppm), weak NOESY cross-peaks with B/A-H. ^{13}C NMR (151 MHz, MeOD): δ = 155.9 (C_q, 2 C, C-30), 155.1 (C_q, 8 C, C-H), 147.3 (C_q, 2 C, C-16), 147.2 (C_q, 4 C, C-10), 139.6 (C_q, 2 C, C-14), 137.2 (C_q, 4 C, C-J), 134.7 (C_q, 4 C, C-11), 130.5 (C_q, 2 C, C-29), 129.3 (C_t, 2 C, C-28), 124.3 (C_t, 4 C, C-9), 123.6 (C_t, 2 C, C-12), 123.6 (C_t, 2 C, C-15), 119.0 (C_t, 2 C, C-27), 117.6 (C_t, 4 C, C-13), 108.0 (C_t, 2 C, C-26), 104.8 (C_t, 8 C, C-G), 73.8 (C_s, C_{TEG}), 73.3 (C_s, 4 C, C-K), 72.0 (C_s, C_{TEG}), 71.8 (C_s, C_{TEG}), 71.8 (C_s, C_{TEG}), 71.8 (C_s, C_{TEG}), 71.7 (C_s, C_{TEG}), 71.6 (C_s, C_{TEG}), 71.6 (C_s, C_{TEG}), 71.5 (C_s, C_{TEG}), 71.3 (C_s, C_{TEG}), 70.9 (C_s, C_{TEG}), 70.4 (C_s, 4 C, C-7), 68.4 (C_s, C_{TEG}), 65.2 (C_s, 2 C, C-17), 62.3 (C_s, C_{TEG}), 57.2 (C_s, C_{TEG}), 57.0 (C_p, 8 C, C-I), 51.8 (C_s, 4 C, C-8), 44.6 (C_q, 2 C, C_E), 29.8 (no clear cross-peaks in HMQC or HMBC), 26.7 (C_s, 4 C, C-L), 7.7 (C_p, 4 C, C-A) ppm. Carbon signals C-B/C/D of the spiro-piperidinium and C-F were not observed; HRMS (ESI, +): calcd. for $C_{142}H_{207}N_{20}O_{38}$ 933.4955 [M + H – 2Cl]$^{3+}$; found 933.4961.

Procedure for the Synthesis of Dumbbell 5d: In a 25 mL of two-necked flask, stopper **3** (78.7 mg, 30 µmol, 2.70 equiv.) and axle **2d** (31.0 mg, 48.1 µmol, 1.0 equiv.) were dissolved in a 5:2 mixture of miliQ water and methanol (3.5 mL). The resulting solution was degassed by flushing with argon gas for 10 min. Afterwards, copper(II) sulfate (7.75 mg, 48.1 µmol, 1.0 equiv.) and L-(+)-ascorbic acid sodium salt (9.53 mg, 48.1 µmol, 1.0 equiv.) was added and the solution was degassed again for a further 5 min. After stirring at room temperature for 18 h, LC–ESI-MS indicated full conversion of

axle **2d**. The solvents were removed under reduced pressure and the crude product was purified by short column chromatography (Al_2O_3, basic, EtOAc/MeOH = 7:1). The fractions containing the target compound were concentrated in vacuo and were subjected to preparative TLC (Al_2O_3, EtOAc/MeOH = 7:1), and the isolated compound was analyzed by ^{1}H NMR spectroscopy. One hour after concentration of the pure target compound on a rotary evaporator, the ester bonds of dumbbell **5d** were entirely cleaved, as indicated by the single signal in the LC–ESI-MS T.I.C. chromatogram, which corresponds to the proton adduct of the decomposition product (m/z = 838). ^{1}H NMR (400 MHz, MeOD): δ = 8.71 (s, 2 H, 15-H), 8.68 (d, $^4J_{H,H}$ = 1.1 Hz, 2 H, 30-H), 8.61 (s, 4 H, 9-H), 8.47 (t, $^4J_{H,H}$ = 1.5 Hz, 2 H, 12-H), 8.35 (d, $^4J_{H,H}$ = 1.5 Hz, 4 H, 13-H), 8.12 (d, $^4J_{H,H}$ = 1.0 Hz, 4 H, 28-H, 29-H), 4.78 (s, 4 H, 17-H), 4.71–4.68 (m, 8 H, 8-H), 3.99 (s, 4 H), 3.99–3.97 (m, 8 H, 7-H), 3.79–3.74 (m, 4 H, 25-H), 3.73–3.69 (m, 4 H, 24-H), 3.69–3.45 (m, 66 H), 3.49–3.43 (m, 8 H) ppm. Due to no available 2D NMR spectra, the peaks of dumbbell **5d** were assigned with the help of the spectra of the corresponding reactant axle **2d**, stopper **3**, and rotaxane **4d**.

Procedure for the Synthesis of Dumbbell 5f: Axle **2f** (49 mg, 0.083 mmol, 1 equiv.) and B (0.11 g, 0.18 mmol, 2.2 equiv.) were placed in a flask and MeOH/H_2O (2:1, 6 mL) was added. Sodium ascorbate was then added (86 mg, 0.41 mmol, 5 equiv.), followed by $CuSO_4$ (10 mg, 0.041 mmol, 0.5 equiv.). The mixture was stirred for 1 day and then evaporated. The crude was suspended in MeOH and filtered to remove insoluble salts. The filtrate was purified by chromatography [silica gel RP C-18, H_2O/MeOH (1:1) → H_2O/MeOH (1:4)] followed by size-exclusion chromatography (Sephadex LH-20, MeOH) to give the desired compound as a colorless oil (21 mg, 12 μmol, 14 %). ^{1}H NMR (600 MHz, MeOD): δ = 8.53 (s, 2 H, 15-H), 8.46 (s, 4 H, 9-H), 8.28 (t, ^4J = 1.5 Hz, 2 H, 12-H), 8.13 (d, ^4J = 1.5 Hz, 4 H, 13-H), 7.40 (d, ^3J = 8.9 Hz, 2 H, 28-H), 6.92 (d, ^4J = 2.5 Hz, 2 H, 26-H), 6.87 (dd, ^3J = 8.8, ^4J = 2.5 Hz, 2 H, 27-H), 4.70 (s, 4 H, 17-H), 4.64 (t, ^3J = 5.0 Hz, 8 H, 8-H), 4.04–3.99 (m, 4 H, 25-H), 3.95 (t, ^3J = 5.0 Hz, 8 H, 7-H), 3.81–3.77 (m, 4 H, 24-H), 3.71–3.69 (m, 4 H, H_{TEG}), 3.68–3.61 (m, 28 H, H_{TEG}), 3.61–3.58 (m, 8 H, H_{TEG}), 3.58–3.55 (m, 16 H, H_{TEG}), 3.54–3.51 (m, 8 H, H_{TEG}), 3.46–3.42 (m, 8 H, H_{TEG}) ppm; peaks of trace impurities between 1.0–1.7 ppm showed no correlations to **5f** in the HSQC and HMBC spectra. ^{13}C NMR (151 MHz, MeOD): δ = 156.6 (C_q, 2 C, C-30), 147.3 (C_q, 2 C, C-16), 147.1 (C_q, 4 C, C-10 or C-11), 139.5 (C_q, 2 C, C-14), 134.6 (C_q, 4 C, C-10 or C-11), 131.2 (C_q, 2 C, C-29), 129.3 (C_t, 2 C, C-28), 124.3 (C_t, 4 C, C-9), 123.5 (C_t, 2 C, C-12), 123.4 (C_t, 2 C, C-15), 120.0 (C_s, 2 C, C-27), 117.6 (C_t, 4 C, C-13), 108.0 (C_t, 2 C, C-26), 73.7 (C_s, C_{TEG}), 71.9 (C_s, C_{TEG}), 71.8 (C_s, C_{TEG}), 71.8 (C_s, C_{TEG}), 71.8 (C_s, C_{TEG}), 71.7 (C_s, C_{TEG}), 71.7 (C_s, C_{TEG}), 71.6 (C_s, C_{TEG}), 71.6 (C_s, C_{TEG}), 71.5 (C_s, C_{TEG}), 71.1 (C_s, C_{TEG}), 71.0 (C_s, 2 C, C-24), 70.4 (C_s, 4 C, C-7), 68.7 (C_s, 2 C, C-25), 65.2 (C_s, 2 C, C-17), 62.3 (C_s, C_{TEG}), 51.8 (C_s, 4 C, C-8) ppm. HRMS (ESI, +): calcd. for $C_{84}H_{122}N_{18}Na_2O_{26}$ 922.4281 $[M + 2Na]^{2+}$; found 922.4295.

Acknowledgments

The authors acknowledge financial support by the Swiss National Science Foundation (SNF), the National Center of Competence in Research (NCCR), through Molecular Systems Engineering, and the Swiss Nanoscience Institute (SNI).

Keywords: Rotaxanes · Click chemistry · Cyclophanes · Host–guest systems

[1] M. Asakawa, P. R. Ashton, V. Balzani, A. Credi, C. Hamers, G. Mattersteig, M. Montalti, A. N. Shipway, N. Spencer, J. F. Stoddart, M. S. Tolley, M. Venturi, A. J. P. White, D. J. Williams, *Angew. Chem. Int. Ed.* **1998**, *37*, 333–337; *Angew. Chem.* **1998**, *110*, 357.
[2] D. A. Leigh, M. Á. F. Morales, E. M. Pérez, J. K. Y. Wong, C. G. Saiz, A. M. Z. Slawin, A. J. Carmichael, D. M. Haddleton, A. M. Brouwer, W. J. Buma, G. W. H. Wurpel, S. León, F. Zerbetto, *Angew. Chem. Int. Ed.* **2005**, *44*, 3062–3067; *Angew. Chem.* **2005**, *117*, 3122–3127.
[3] Y.-L. Zhao, W. R. Dichtel, A. Trabolsi, S. Saha, I. Aprahamian, J. F. Stoddart, *J. Am. Chem. Soc.* **2008**, *130*, 11294–11296.
[4] P. Liu, C. Chipot, X. Shao, W. Cai, *J. Phys. Chem. C* **2012**, *116*, 4471–4476.
[5] S. Grunder, P. L. McGrier, A. C. Whalley, M. M. Boyle, C. Stern, J. F. Stoddart, *J. Am. Chem. Soc.* **2013**, *135*, 17691–17694.
[6] M. Juríček, J. C. Barnes, N. L. Strutt, N. A. Vermeulen, K. C. Ghooray, E. J. Dale, P. R. McGonigal, A. K. Blackburn, A.-J. Avestro, J. F. Stoddart, *Chem. Sci.* **2014**, *5*, 2724–2731.
[7] J. Beswick, V. Blanco, G. D. Bo, D. A. Leigh, U. Lewandowska, B. Lewandowski, K. Mishiro, *Chem. Sci.* **2015**, *6*, 140–143.
[8] J. Sun, Y. Wu, Y. Wang, Z. Liu, C. Cheng, K. J. Hartlieb, M. R. Wasielewski, J. F. Stoddart, *J. Am. Chem. Soc.* **2015**, *137*, 13484–13487.
[9] N. Zhu, K. Nakazono, T. Takata, *Chem. Commun.* **2016**, *52*, 3647–3649.
[10] M. C. Jiménez, C. Dietrich-Buchecker, J.-P. Sauvage, *Angew. Chem. Int. Ed.* **2000**, *39*, 3284–3287; *Angew. Chem.* **2000**, *112*, 3422.
[11] J.-P. Collin, C. Dietrich-Buchecker, P. Gaviña, M. C. Jimenez-Molero, J.-P. Sauvage, *Acc. Chem. Res.* **2001**, *34*, 477–487.
[12] Y. Liu, A. H. Flood, P. A. Bonvallet, S. A. Vignon, B. H. Northrop, H.-R. Tseng, J. O. Jeppesen, T. J. Huang, B. Brough, M. Baller, S. Magonov, S. D. Solares, W. A. Goddard, C.-M. Ho, J. F. Stoddart, *J. Am. Chem. Soc.* **2005**, *127*, 9745–9759.
[13] J. Wu, K. C.-F. Leung, D. Benítez, J.-Y. Han, S. J. Cantrill, L. Fang, J. F. Stoddart, *Angew. Chem. Int. Ed.* **2008**, *47*, 7470–7474; *Angew. Chem.* **2008**, *120*, 7580.
[14] P. G. Clark, M. W. Day, R. H. Grubbs, *J. Am. Chem. Soc.* **2009**, *131*, 13631–13633.
[15] G. Du, E. Moulin, N. Jouault, E. Buhler, N. Giuseppone, *Angew. Chem. Int. Ed.* **2012**, *51*, 12504–12508; *Angew. Chem.* **2012**, *124*, 12672.
[16] C. J. Bruns, J. Li, M. Frasconi, S. T. Schneebeli, J. Iehl, H.-P. Jacquot de Rouville, S. I. Stupp, G. A. Voth, J. F. Stoddart, *Angew. Chem. Int. Ed.* **2014**, *53*, 1953–1958; *Angew. Chem.* **2014**, *126*, 1984.
[17] C. J. Bruns, J. F. Stoddart, *Acc. Chem. Res.* **2014**, *47*, 2186–2199.
[18] J. D. Badjić, V. Balzani, A. Credi, S. Silvi, J. F. Stoddart, *Science* **2004**, *303*, 1845–1849.
[19] S. Saha, A. H. Flood, J. F. Stoddart, S. Impellizzeri, S. Silvi, M. Venturi, A. Credi, *J. Am. Chem. Soc.* **2007**, *129*, 12159–12171.
[20] V. Serreli, C.-F. Lee, E. R. Kay, D. A. Leigh, *Nature* **2007**, *445*, 523–527.
[21] A. Carlone, S. M. Goldup, N. Lebrasseur, D. A. Leigh, A. Wilson, *J. Am. Chem. Soc.* **2012**, *134*, 8321–8323.
[22] B. Lewandowski, G. D. Bo, J. W. Ward, M. Papmeyer, S. Kuschel, M. J. Aldegunde, P. M. E. Gramlich, D. Heckmann, S. M. Goldup, D. M. D'Souza, A. E. Fernandes, D. A. Leigh, *Science* **2013**, *339*, 189–193.
[23] Z. Meng, J.-F. Xiang, C.-F. Chen, *Chem. Sci.* **2014**, *5*, 1520–1525.
[24] F. Lohmann, J. Weigandt, J. Valero, M. Famulok, *Angew. Chem. Int. Ed.* **2014**, *53*, 10372–10376; *Angew. Chem.* **2014**, *126*, 10540.
[25] B. Hesseler, M. Zindler, R. Herges, U. Lüning, *Eur. J. Org. Chem.* **2014**, 3885–3901.
[26] C. Cheng, P. R. McGonigal, S. T. Schneebeli, H. Li, N. A. Vermeulen, C. Ke, J. F. Stoddart, *Nat. Nanotechnol.* **2015**, *10*, 547–553.
[27] G. Ragazzon, M. Baroncini, S. Silvi, M. Venturi, A. Credi, *Nat. Nanotechnol.* **2015**, *10*, 70–75.
[28] L. Fang, S. Basu, C.-H. Sue, A. C. Fahrenbach, J. F. Stoddart, *J. Am. Chem. Soc.* **2011**, *133*, 396–399.
[29] M. J. Gresser, J. A. Myers, P. D. Boyer, *J. Biol. Chem.* **1982**, *257*, 12030–12038.
[30] H. Noji, R. Yasuda, M. Yoshida, K. Kinosita, *Nature* **1997**, *386*, 299–302.
[31] R. Yasuda, H. Noji, M. Yoshida, K. Kinosita, H. Itoh, *Nature* **2001**, *410*, 898–904.
[32] H. Itoh, A. Takahashi, K. Adachi, H. Noji, R. Yasuda, M. Yoshida, K. Kinosita, *Nature* **2004**, *427*, 465–468.
[33] R. Watanabe, R. Iino, H. Noji, *Nat. Chem. Biol.* **2010**, *6*, 814–820.
[34] F. Jon Kull, E. P. Sablin, R. Lau, R. J. Fletterick, R. D. Vale, *Nature* **1996**, *380*, 550–555.

[35] N. Hirokawa, Y. Noda, Y. Tanaka, S. Niwa, *Nat. Rev. Mol. Cell Biol.* **2009**, *10*, 682–696.
[36] C. V. Sindelar, K. H. Downing, *Proc. Natl. Acad. Sci. USA* **2010**, *107*, 4111–4116.
[37] R. D. Astumian, I. Derényi, *Biophys. J.* **1999**, *77*, 993–1002.
[38] T. D. Pollard, E. Shelton, R. R. Weihing, E. D. Korn, *J. Mol. Biol.* **1970**, *50*, 91–97, IN24.
[39] J. T. Finer, R. M. Simmons, J. A. Spudich, *Nature* **1994**, *368*, 113–119.
[40] H. L. Sweeney, A. Houdusse, *Annu. Rev. Biophys.* **2010**, *39*, 539–557.
[41] G. V. Oshovsky, D. N. Reinhoudt, W. Verboom, *Angew. Chem. Int. Ed.* **2007**, *46*, 2366–2393; *Angew. Chem.* **2007**, *119*, 2418–2445.
[42] R. Ludwig, *Angew. Chem. Int. Ed.* **2001**, *40*, 1808–1827; *Angew. Chem.* **2001**, *113*, 1856–1876.
[43] S. Anderson, T. D. W. Claridge, H. L. Anderson, *Angew. Chem. Int. Ed. Engl.* **1997**, *36*, 1310–1313; *Angew. Chem.* **1997**, *109*, 1367.
[44] H. Onagi, C. J. Easton, S. F. Lincoln, *Org. Lett.* **2001**, *3*, 1041–1044.
[45] R. B. Hannak, G. Färber, R. Konrat, B. Kräutler, *J. Am. Chem. Soc.* **1997**, *119*, 2313–2314.
[46] Y. Akae, H. Okamura, Y. Koyama, T. Arai, T. Takata, *Org. Lett.* **2012**, *14*, 2226–2229.
[47] X. Chi, X. Ji, D. Xia, F. Huang, *J. Am. Chem. Soc.* **2015**, *137*, 1440–1443.
[48] H. Wang, H. Xing, X. Ji, *RSC Adv.* **2016**, *6*, 740–744.
[49] G. Yu, X. Zhou, Z. Zhang, C. Han, Z. Mao, C. Gao, F. Huang, *J. Am. Chem. Soc.* **2012**, *134*, 19489–19497.
[50] V. Ramalingam, A. R. Urbach, *Org. Lett.* **2011**, *13*, 4898–4901.
[51] D. Tuncel, M. Katterle, *Chem. Eur. J.* **2008**, *14*, 4110–4116.
[52] S. Senler, B. Cheng, A. E. Kaifer, *Org. Lett.* **2014**, *16*, 5834–5837.
[53] J. Winn, A. Pinczewska, S. M. Goldup, *J. Am. Chem. Soc.* **2013**, *135*, 13318–13321.
[54] I. Smukste, D. B. Smithrud, *J. Org. Chem.* **2003**, *68*, 2547–2558.
[55] S. Yu, J. Yuan, J. Shi, X. Ruan, Y. Wang, S. Gao, Y. Du, *J. Mater. Chem. B* **2015**, *3*, 5277–5283.
[56] S. B. Ferguson, E. M. Seward, F. Diederich, E. M. Sanford, A. Chou, P. Inocencio-Szweda, C. B. Knobler, *J. Org. Chem.* **1988**, *53*, 5593–5595.
[57] S. B. Ferguson, E. M. Sanford, E. M. Seward, F. Diederich, *J. Am. Chem. Soc.* **1991**, *113*, 5410–5419.
[58] D. B. Smithrud, T. B. Wyman, F. Diederich, *J. Am. Chem. Soc.* **1991**, *113*, 5420–5426.
[59] D. B. Smithrud, E. M. Sanford, I. Chao, S. B. Ferguson, D. R. Carcanague, J. D. Evanseck, K. N. Houk, F. Diederich, *Pure Appl. Chem.* **1990**, *62*, 2227–2236.
[60] D. R. Benson, J. Fu, C. K. Johnson, S. W. Pauls, D. A. Williamson, *J. Org. Chem.* **1998**, *63*, 9935–9945.
[61] S. Anderson, H. L. Anderson, W. Clegg, *Chem. Commun.* **1998**, 2379–2380.
[62] S. Anderson, R. T. Aplin, T. D. W. Claridge, T. Goodson III, A. C. Maciel, G. Rumbles, J. F. Ryan, H. L. Anderson, *J. Chem. Soc. Perkin Trans. 1* **1998**, 2383–2398.
[63] S. Anderson, H. L. Anderson, *Angew. Chem. Int. Ed. Engl.* **1996**, *35*, 1956–1959; *Angew. Chem.* **1996**, *108*, 2075.
[64] P. N. Taylor, A. J. Hagan, H. L. Anderson, *Org. Biomol. Chem.* **2003**, *1*, 3851–3856.
[65] J. Rotzler, S. Drayss, O. Hampe, D. Häussinger, M. Mayor, *Chem. Eur. J.* **2013**, *19*, 2089–2101.
[66] F. Diederich, D. R. Carcanague, *Angew. Chem. Int. Ed. Engl.* **1990**, *29*, 769–771; *Angew. Chem.* **1990**, *102*, 836.
[67] T. Marti, B. R. Peterson, A. Fürer, T. Mordasini-Denti, J. Zarske, B. Jaun, F. Diederich, V. Gramlich, *Helv. Chim. Acta* **1998**, *81*, 109–144.
[68] V. V. Rostovtsev, L. G. Green, V. V. Fokin, K. B. Sharpless, *Angew. Chem. Int. Ed.* **2002**, *41*, 2596–2599; *Angew. Chem.* **2002**, *114*, 2708.
[69] C. W. Tornøe, C. Christensen, M. Meldal, *J. Org. Chem.* **2002**, *67*, 3057–3064.
[70] J. E. Hein, V. V. Fokin, *Chem. Soc. Rev.* **2010**, *39*, 1302–1315.
[71] J. Rotzler, M. Mayor, *Chem. Soc. Rev.* **2013**, *42*, 44–62.
[72] P. R. Aston, P. T. Glink, J. F. Stoddart, P. A. Tasker, A. J. P. White, D. J. Williams, *Chem. Eur. J.* **1996**, *2*, 729–736.
[73] C. Ke, R. A. Smaldone, T. Kikuchi, H. Li, A. P. Davis, J. F. Stoddart, *Angew. Chem. Int. Ed.* **2013**, *52*, 381–387; *Angew. Chem.* **2013**, *125*, 399.
[74] R. Chakrabarty, P. J. Stang, *J. Am. Chem. Soc.* **2012**, *134*, 14738–14741.
[75] P. Thordarson, *Chem. Soc. Rev.* **2011**, *40*, 1305–1323.
[76] T. R. Chan, R. Hilgraf, K. B. Sharpless, V. V. Fokin, *Org. Lett.* **2004**, *6*, 2853–2855.
[77] V. Hong, S. I. Presolski, C. Ma, M. G. Finn, *Angew. Chem. Int. Ed.* **2009**, *48*, 9879–9883; *Angew. Chem.* **2009**, *121*, 10063.

Received: May 8, 2017

Supporting Information. Assembly of [2]Rotaxanes in Water

Eur. J. Org. Chem. **2017** · ISSN 1099–0690

https://doi.org/10.1002/ejoc.201700640

SUPPORTING INFORMATION

Title: Assembly of [2]Rotaxanes in Water
Author(s): Yves Aeschi, Sylvie Drayss-Orth, Michal Valášek, Felix Raps, Daniel Häussinger, Marcel Mayor*

Table of Contents

Synthetic Procedures for Structures 6a-e

General procedure for the syntheses of 6a-e

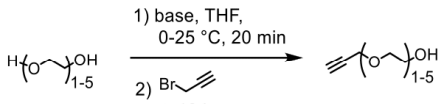

11a: n = 1
11b: n = 2
11c: n = 3
11d: n = 4
11e: n = 5

6a: n = 1
6b: n = 2
6c: n = 3
6d: n = 4
6e: n = 5

A 100 mL Schlenk tube was charged with the appropriate ethylene glycol derivative which was then diluted with dry THF (10% vv) under argon atmosphere. The solution was cooled to 0 °C with an ice-bath and base was then added portion-wise at 0 °C. Afterwards, the solution was allowed to warm up to room temperature and was stirred at this temperature for 20 min. Propargyl bromide solution (80% in toluene, 1.0 eq) was added dropwise and the reaction mixture was stirred for 18 hrs at room temperature. The solvent was removed under reduced pressure and the crude oil was purified via column chromatography.

2-(prop-2-yn-1-yloxy)ethan-1-ol (6a)

Ethylene glycol (7.76 g, 125 mmol, 6.99 mL, 5.0 eq), potassium hydroxide (3.30 g, 50.0 mmol, 2.0 eq), propargyl bromide solution (3.71 g, 25.9 mmol, 2.69 mL, 1.0 eq); column chromatography (SiO_2; dichloromethane: methanol 96:4); 66% yield (1.64 g); colorless oil.

^{1}H NMR (400 MHz, Chloroform-*d*): δ = 4.21 (d, $^4J_{H,H}$ = 2.4 Hz, 2H, CH_2C≡CH), 3.80 – 3.75 (m, 2H, CH_2), 3.69 – 3.64 (m, 2H, CH_2), 2.46 (t, $^4J_{H,H}$ = 2.4 Hz, 1H, C≡C*H*), 2.08 (s, 1H, O*H*) ppm. The spectroscopic data are in agreement with those previously reported.[1]

2-(2-(prop-2-yn-1-yloxy)ethoxy)ethan-1-ol (6b)

Diethylene glycol (9.65 g, 90.0 mmol, 8.69 mL, 2.0 eq), potassium *tert*-butoxide (5.26 g, 45.4 mmol, 1.01 eq), propargyl bromide solution (6.69 g, 45.0 mmol, 4.85 mL, 1.0 eq); column chromatography (SiO_2; ethyl acetate); 11% yield (700 mg); colorless oil.

^{1}H NMR (400 MHz, Chloroform-*d*): δ = 4.20 (d, $^4J_{H,H}$ = 2.4 Hz, 2H, CH_2C≡CH), 3.78 – 3.66 (m, 6H, CH_2), 3.64 – 3.57 (m, 2H, CH_2), 2.44 (t, $^4J_{H,H}$ = 2.4 Hz, 1H, C≡C*H*) ppm. The spectroscopic data are in agreement with those previously reported.[2]

2-(2-(2-(prop-2-yn-1-yloxy)ethoxy)ethoxy)ethan-1-ol (6c)

Triethylene glycol (9.01 g, 59.4 mmol, 8.04 mL, 3.0 eq), sodium hydride 60% dispersion in mineral oil (800 mg, 20.0 mmol, 1.01 eq), propargyl bromide solution (2.94 g, 19.8 mmol, 2.13 mL, 1.0 eq); column chromatography (SiO_2; ethyl acetate); 78% yield (2.92 g); colorless oil.

^{1}H NMR (400 MHz, Chloroform-*d*): δ = 4.20 (d, $^4J_{H,H}$ = 2.4 Hz, 2H, CH_2C≡C), 3.75 – 3.64 (m, 10H, CH_2), 3.64 – 3.58 (m, 2H, CH_2OH), 2.43 (t, $^4J_{H,H}$ = 2.4 Hz, 1H, C≡C*H*) ppm. The spectroscopic data are in agreement with those previously reported.[3]

3,6,9,12-tetraoxapentadec-14-yn-1-ol (6d)

Tetraethylene glycol (25.0 g, 129 mmol, 22.3 mL, 2.80 eq), sodium hydride 60% dispersion in mineral oil (1.00 g, 41.7 mmol, 2.24 eq), propargyl bromide solution (2.76 g, 18.6 mmol, 2.00 mL, 1.00 eq); column chromatography (SiO_2; ethyl acetate); 90% yield (3.90 g); colorless oil.

^{1}H NMR (400 MHz, Chloroform-*d*): δ = 4.21 (d, $^4J_{H,H}$ = 2.4 Hz, 2H, CH_2C≡C), 3.77 – 3.64 (m, 14H, CH_2), 3.64 – 3.59 (m, 2H, CH_2), 2.64 (s, 1H, O*H*), 2.43 (t, $^4J_{H,H}$ = 2.4 Hz, 1H, C≡C*H*) ppm. The spectroscopic data are in agreement with those previously reported.[4]

3,6,9,12,15-pentaoxaoctadec-17-yn-1-ol (6e)

Pentaethylene glycol (1.70 g, 7.11 mmol, 1.50 mL, 2.8 eq), sodium hydride 60% dispersion in mineral oil (101 mg, 2.51 mmol, 0.99 eq), propargyl bromide solution (378 mg, 2.54 mmol, 0.274 mL, 1.0 eq); column chromatography (SiO_2; ethyl acetate, 5% methanol); 41% yield (286 mg); colorless oil.

^{1}H NMR (400 MHz, Chloroform-*d*): δ = 4.21 (d, $^4J_{H,H}$ = 2.4 Hz, 2H, CH_2C≡CH), 3.75 – 3.64 (m, 18H, CH_2), 3.64 – 3.58 (m, 2H, CH_2), 2.43 (t, $^4J_{H,H}$ = 2.4 Hz, 1H, C≡C*H*) ppm. The spectroscopic data are in agreement with those previously reported.[5]

^{1}H NOESY Spectrum of Rotaxane 4d

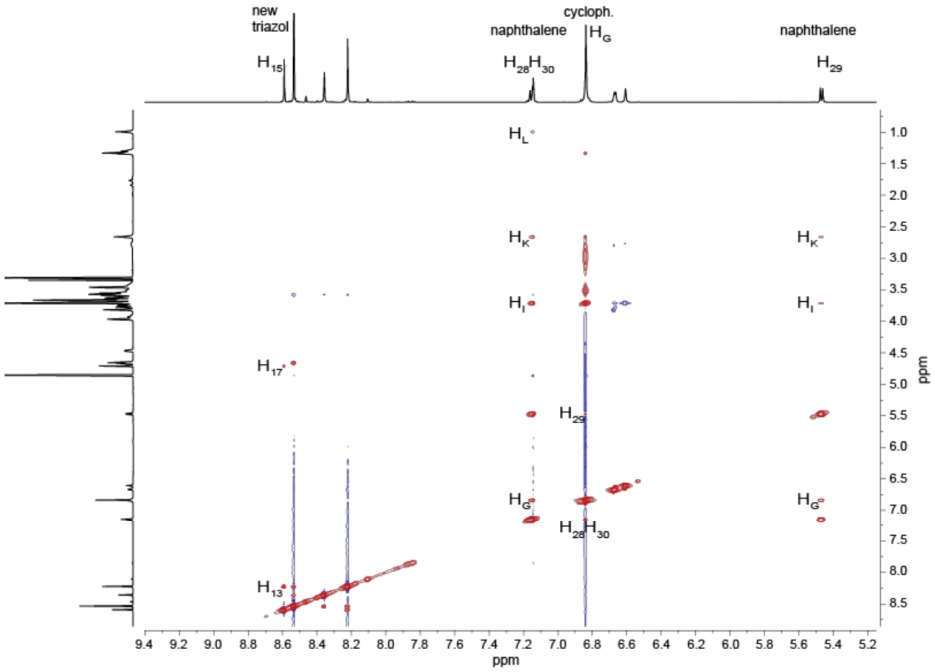

Figure 1.1: Partial ^{1}H NOESY spectrum (600 MHz, 298 K, methanol-*d4*) of rotaxane **4d** in which the most significant crosspeaks are labeled which confirm the interlocked structure.

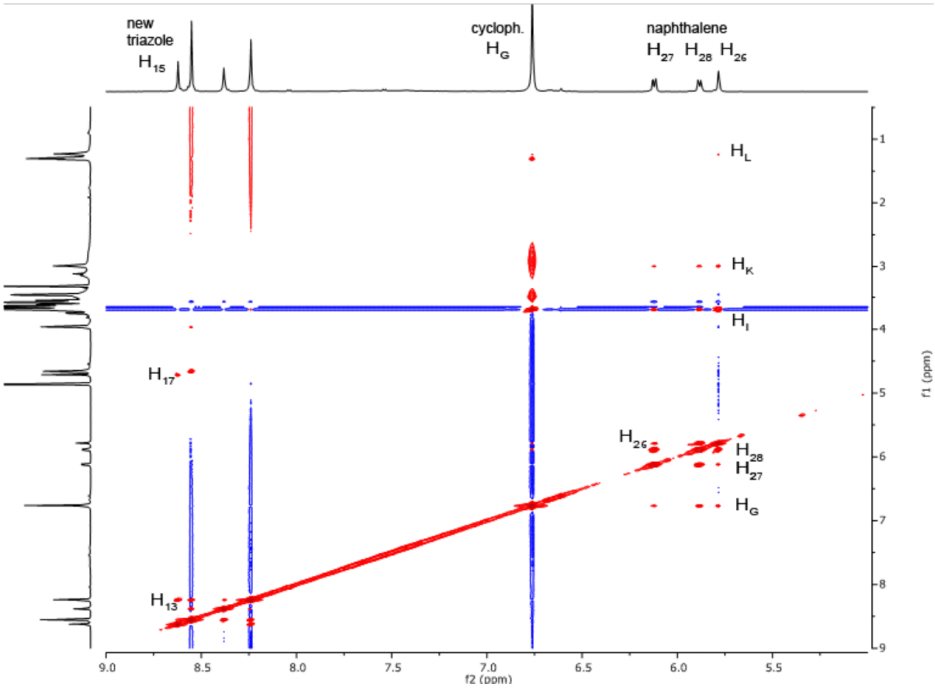

Figure 1.2: Partial ^{1}H NOESY spectrum (600 MHz, 298 K, methanol-*d4*) of rotaxane **4f** in which the crosspeaks are labeled which confirm the interlocked structure.

Fluorescence Binding Studies for 2c-e

Binding studies were performed by adding aliquots of a host **1** solution to the respective naphthalene derivative **2c-e** solution and recording the changes in fluorescence intensity. For each run a 0.0666 mM stock solution of **2c** was prepared by dissolving 1.00 µmol (0.556 mg) in 15.0 mL of water. Naphthalene derivative stock solutions of **2d** and **2e** with a concentration of 0.1 mM were prepared by dissolving 1.00 µmol of **2d** (0.645 mg) and **2e** (0.733 mg), respectively in 10.0 mL of water. Each guest stock solution was diluted to the measurement concentration c = 20.0 µM solutions with a starting volume V = 2.00 mL and fluorescence measurement was performed which gives the starting intensity without host. For the following measurements with aliquots of host, the guest concentration had to be kept constant. Consequently, the host solution contained the same concentration of guest. To obtain the host solution with a concentration of 400 µM (20 eq, 2.5 mL total volume) and 20.0 µM of the relevant guest, 1.07 mg of **1** were dissolved in the relevant amount of guest stock

solution and nanopure water. After each addition of the appropriate amount of host solution to the relevant guest solution, it was waited for four minutes before the fluorescence spectra were recorded in a quartz cuvette at 22 °C with the excitation wavelength of 333 nm. Following instrumental parameters were used: excitation slit width 2.00 nm (front entrance and exit); emission slit width 1.00 nm (front entrance and exit); integration time 0.100 s. For each guest, the titration studies were performed three times. In each titration series, the host equivalents were consistently added: 1) 0.0 eq; 2) 0.1 eq; 3) 0.3 eq; 4) 0.5 eq; 5) 0.7 eq; 6) 0.9 eq; 7) 1.0 eq; 8) 1.2 eq; 9) 1.4 eq; 10) 1.6 eq; 11) 1.8 eq; 12) 2.2 eq; 13) 2.6 eq; 14) 3.0 eq; 15) 3.4 eq; 16) 3.8 eq; 17) 4.2 eq; 18) 5.0 eq; 19) 5.5 eq; 20) 6.0 eq; 21) 7.0 eq; 22) 8.0 eq; 23) 10 eq and 24) 20 eq.

As for each series the independent variables (total concentration of host $[H]_0$) were identical, the association constants (K_a) were determined from nonlinear regression analysis with concatenate fitting. The applied fit function was used as described by Thordarson:[6]

$$F_{obs} = F_0 + \frac{\Delta F}{2[G]_0}\left([H]_0 + [G]_0 + \frac{1}{K_a} - \sqrt{\left([H]_0 + [G]_0 + \frac{1}{K_a}\right)^2 - 4[H]_0[G]_0}\right)$$

F_{obs} the observed fluorescence; $F_{obs} \mathrel{\widehat{=}} y$; dependent variable

F_0 fluorescence of guest solution before the guest is added; constant

ΔF maximal fluorescence quench, here $\Delta F \mathrel{\widehat{=}} F_0$, negative value; parameter

$[G]_0$ total concentration of the guest; constant

$[H]_0$ total concentration of the host; $[H]_0 \mathrel{\widehat{=}} x$; independent variable

K_a association constant; parameter

Table 1: Association constants and statistical values (reduced χ^2 and adjusted R^2) of inclusion complexes **1·2c**, **1·2d** and **1·2e**. The errors are given as standard errors.

	1·2c	**1·2d**	**1·2e**
K_a values [x 10^5 M^{-1}]	1.7	1.4	1.2
red. χ^2	0,01172	0,01468	0,00469
adj. R^2	0,97701	0,97271	0,99165

1·2c:

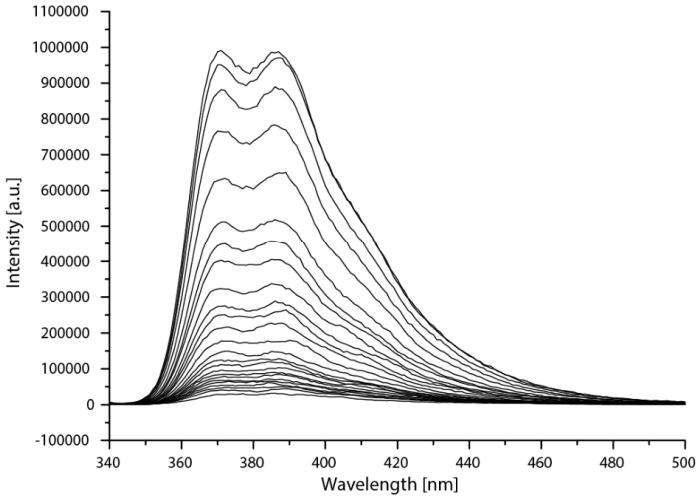

Figure 2: Titration of 20.0 µM **2c** with cyclophane **1** in water at 22 °C (λ_{exc} = 333 nm). Fluorescence spectra correspond to added host equivalents, top down: **1)** 0.0 eq; **2)** 0.1 eq; **3)** 0.3 eq; **4)** 0.5 eq; **5)** 0.7 eq; **6)** 0.9 eq; **7)** 1.0 eq; **8)** 1.2 eq; **9)** 1.4 eq; **10)** 1.6 eq; **11)** 1.8 eq; **12)** 2.2 eq; **13)** 2.6 eq; **14)** 3.0 eq; **15)** 3.4 eq; **16)** 3.8 eq; **17)** 4.2 eq; **18)** 5.0 eq; **19)** 5.5 eq; **20)** 6.0 eq; **21)** 7.0 eq; **22)** 8.0 eq; **23)** 10 eq **and 24)** 20 eq.

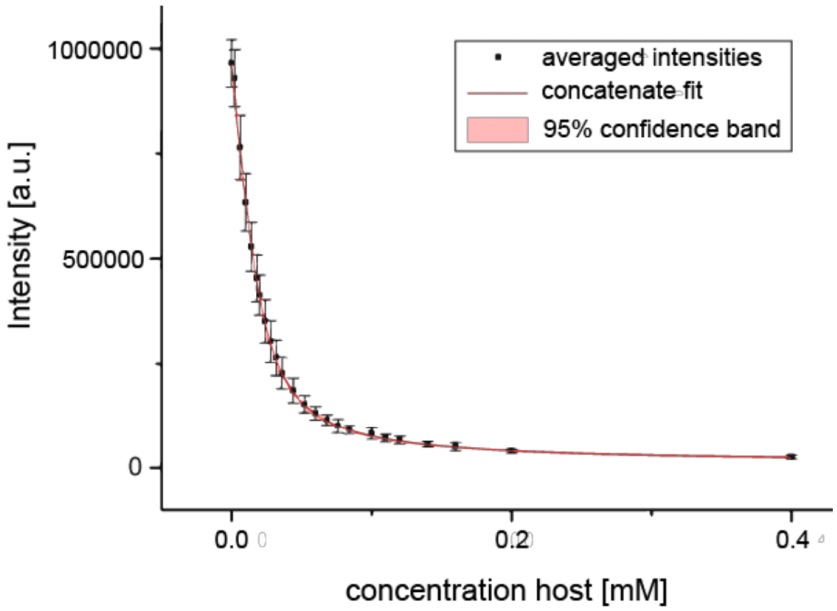

Figure 3: Concatenate fitting curve of the titration with guest **2c**.

1·2d:

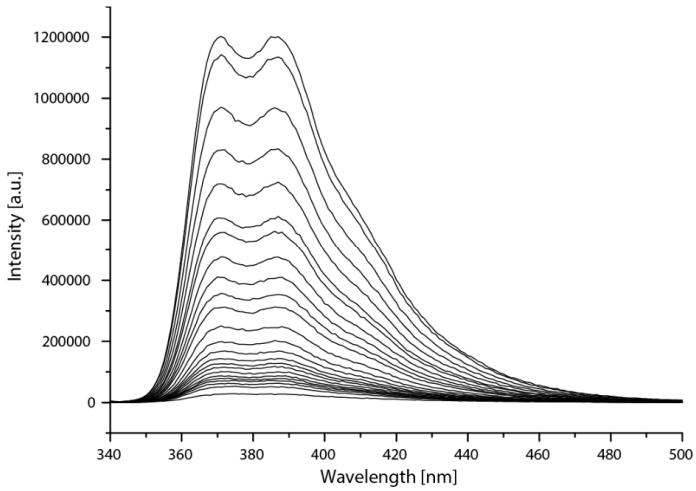

Figure 4: Titration of 20.0 μM **2d** with cyclophane **1** in water at 22 °C (λ_{exc} = 333 nm). Fluorescence spectra correspond to added host equivalents, top down: **1)** 0.0 eq; **2)** 0.1 eq; **3)** 0.3 eq; **4)** 0.5 eq; **5)** 0.7 eq; **6)** 0.9 eq; **7)** 1.0 eq; **8)** 1.2 eq; **9)** 1.4 eq; **10)** 1.6 eq; **11)** 1.8 eq; **12)** 2.2 eq; **13)** 2.6 eq; **14)** 3.0 eq; **15)** 3.4 eq; **16)** 3.8 eq; **17)** 4.2 eq; **18)** 5.0 eq; **19)** 5.5 eq; **20)** 6.0 eq; **21)** 7.0 eq; **22)** 8.0 eq; **23)** 10 eq **and 24)** 20 eq.

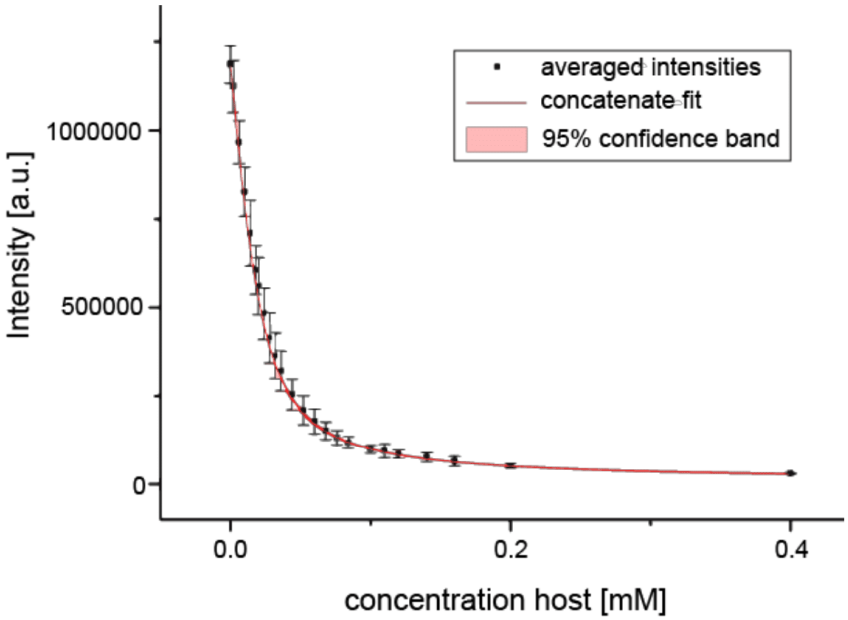

Figure 5: Concatenate fitting curve of the titration with guest **2d**.

1·2e:

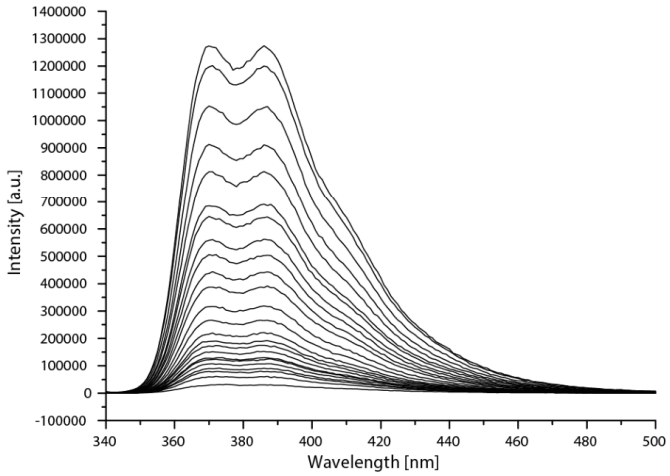

Figure 6: Titration of 20.0 μM **2e** with cyclophane **1** in water at 22 °C (λ_{exc} = 333 nm). Fluorescence spectra correspond to added host equivalents, top down: **1)** 0.0 eq**; 2)** 0.1 eq**; 3)** 0.3 eq**; 4)** 0.5 eq**; 5)** 0.7 eq**; 6)** 0.9 eq**; 7)** 1.0 eq**; 8)** 1.2 eq**; 9)** 1.4 eq**; 10)** 1.6 eq**; 11)** 1.8 eq**; 12)** 2.2 eq**; 13)** 2.6 eq**; 14)** 3.0 eq**; 15)** 3.4 eq**; 16)** 3.8 eq**; 17)** 4.2 eq**; 18)** 5.0 eq**; 19)** 5.5 eq**; 20)** 6.0 eq**; 21)** 7.0 eq**; 22)** 8.0 eq**; 23)** 10 eq **and 24)** 20 eq.

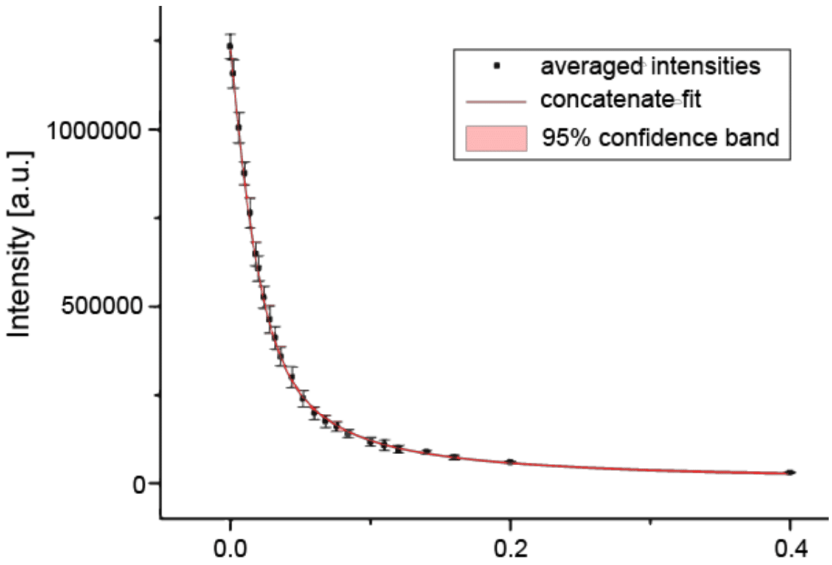

Figure 7: Concatenate fitting curve of the titration with guest **2e**.

Fluorescence Binding Studies for 2f

A 20.0 μM stock solution of **2f** was prepared by dissolving 0.59 mg of the compound in 50.0 mL of water, for **1** a 1.60 mM stock solution was prepared by dissolving 10.6 mg of **1** in 6.00 mL of H_2O. 1.00 mL of each stock solution were added to a quartz cuvette and the fluorescence intensity was recorded (excitation wavelength 340 nm). Aliquots of naphthalene stock solution were removed and replaced by 10.0 μM **2f** stock solution. After each step the fluorescence intensity was recorded. All solutions were handled at 22 °C. The following host equivalents were examined: 1) 0.0 eq; 2) 0.1 eq; 3) 0.3 eq; 4) 0.5 eq; 5) 0.7 eq; 6) 0.9 eq; 7) 1.0 eq; 8) 1.2 eq; 9) 1.4 eq; 10) 1.6 eq; 11) 1.8 eq; 12) 2.2 eq; 13) 2.6 eq; 14) 3 eq; 15) 3.4 eq; 16) 3.8 eq; 17) 4.2 eq; 18) 5.0 eq; 19) 5.5 eq; 20) 6 eq; 21) 8 eq; 22) 10 eq; 23) 20 eq; 24) 40 eq; 25) 80 eq.

The series was repeated four times with varying data quality i.e. the fluorescence intensities of consecutive host concentrations did not continuously decrease or increase. Association constants ranging between 10^4 - $4*10^4$ M^{-1} were obtained by nonlinear regression analysis of the titrations with erratic variations between individual titration runs. Variation of experimental parameters (emission and excitation slit widths, lower naphthalene axle concentrations) did not lead to any improvement. Figures **9** and **10** show a representative example of a titration and the corresponding nonlinear fit.

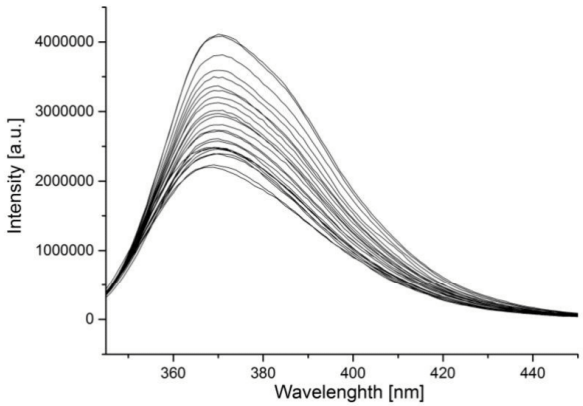

Figure 8: Titration of 10.0 μM **2e** with cyclophane **1** in water at 22 °C (λ_{exc} = 340 nm). Fluorescence spectra correspond to added host equivalents, bottom up: **1)** 0.0 eq; **2)** 0.1 eq; **3)** 0.3 eq; **4)** 0.5 eq; **5)** 0.7 eq; **6)** 0.9 eq; **7)** 1.0 eq; **8)** 1.2 eq; **9)** 1.4 eq; **10)** 1.6 eq; **11)** 1.8 eq; **12)** 2.2 eq; **13)** 2.6 eq; **14)** 3 eq; **15)** 3.4 eq; **16)** 3.8 eq; **17)** 4.2 eq; **18)** 5.0 eq; **19)** 5.5 eq; **20)** 6 eq; **21)** 8 eq; **22)** 10 eq; **23)** 20 eq; **24)** 40 eq; **25)** 80 eq

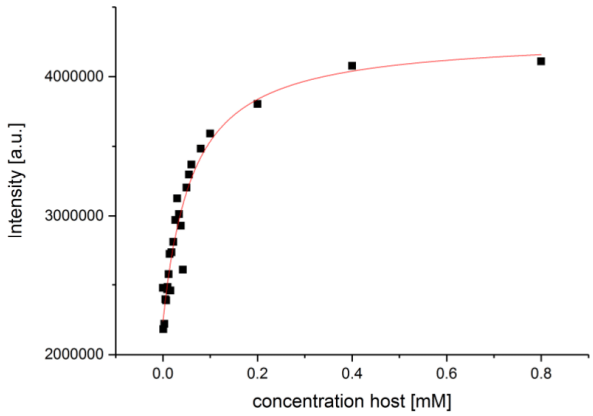

Figure 9: Nonlinear fit for titration curve, Intensity at 370 nm vs. concentration of **1**.

The data was fitted to the following function which was derived from equations given by Thordarson:[6]

$$F_{obs} = \frac{F_0}{[G]_0}\left([G]_0 - 0.5\left([G]_0 + [H]_0 + \frac{1}{K_a} - \sqrt{\left([H]_0 + [G]_0 + \frac{1}{K_a}\right)^2 - 4[H]_0[G]_0}\right)\right)$$
$$+ \frac{F_S}{[G]_0}0.5\left([G]_0 + [H]_0 + \frac{1}{K_a} - \sqrt{\left([H]_0 + [G]_0 + \frac{1}{K_a}\right)^2 - 4[H]_0[G]_0}\right)$$

F_{obs} the observed fluorescence; $F_{obs} \mathrel{\widehat{=}} y$; dependent variable

F_0 fluorescence of guest solution in absence of host; constant

F_S Fluorescence intensity at saturation; constant

$[G]_0$ total concentration of the guest; constant

$[H]_0$ total concentration of the host; $[H]_0 \mathrel{\widehat{=}} x$; independent variable

K_a association constant; parameter

Fluorescence binding studies for 2g

For **2g** an explorative titration run was conducted analogously to **2c-e** with slightly different host-guest ratios. **2g** exhibits the same quenching behavior as **2c-e** except for the very low binding strength to **1**, which makes fluorescence titration an unsuitable means for accurate determination of K_a.[7]

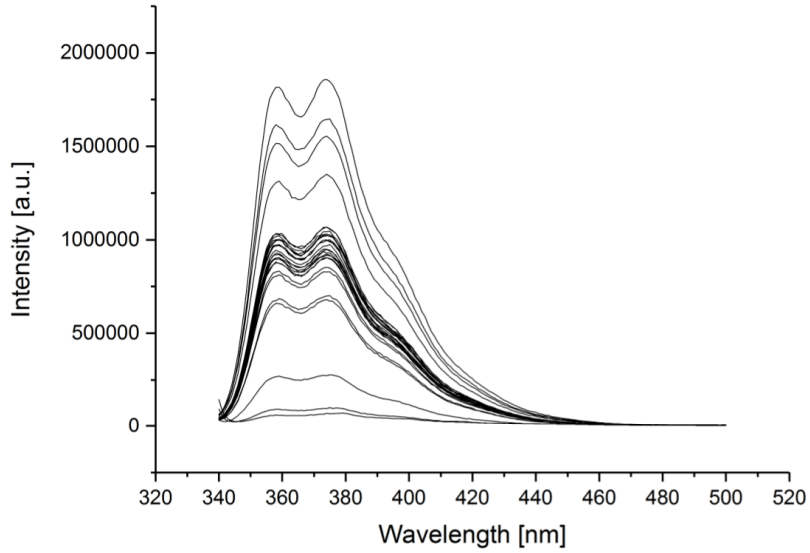

Figure 10: Titration of 20.0 µM **2g** with cyclophane **1** in water at 22 °C (λ_{exc} = 343 nm). Fluorescence spectra correspond to added host equivalents, top down: **1)** 0.0 eq; **2)** 0.1 eq; **3)** 0.3 eq; **4)** 0.5 eq; **5)** 0.7 eq; **6)** 0.9 eq; **7)** 1.0 eq; **8)** 1.2 eq; **9)** 1.4 eq; **10)** 1.6 eq; **11)** 1.8 eq; **12)** 2.2 eq; **13)** 2.6 eq; **14)** 3 eq; **15)** 3.4 eq; **16)** 3.8 eq; **17)** 4.2 eq; **18)** 5.0 eq; **19)** 5.5 eq; **20)** 6 eq; **21)** 7 eq; **22)** 8 eq; **23)** 10 eq; **24)** 20 eq; **25)** 100 eq **26)** 260 eq **27)** 440 eq.

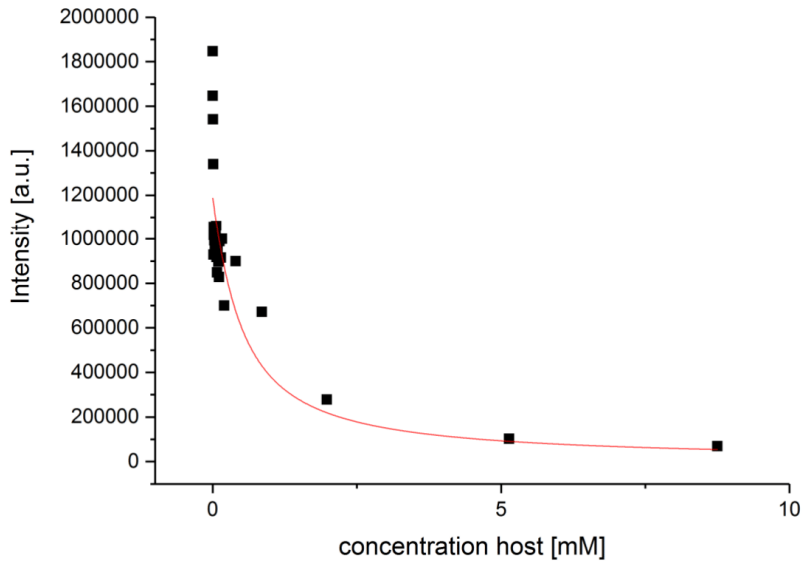

Figure 11: Titration curve of **2g** with **1** nonlinear fit

ITC measurements

Isothermal titration calorimetry (ITC) experiments were performed at 298 K using a Malvern PEAQ-ITC instrument. Experiments were carried out in Millipore Milli-Q water. In a standard experiment, the host cyclophane **1** solution (0.1 mM, 50 µM) in water was placed into the calorimeter cell (200 µL) and 20 aliquots (2 µL) of guest axle **2c-f** solution (1-2 mM) in water were added via a computer-automated syringe at 150 s intervals. Heat changes were recorded after each addition. Dilution heats were subtracted from the titration data prior to curve fitting. Every titration was done at least three times. The first smaller injection (0.8 µL) was discarded from each data set to remove the effect of guest diffusion across the syringe tip during the equilibration process. Titration curves were fitted with the one binding site model using PEAQ-ITC Analysis software supplied by MicroCal. Association constants (*Ka*) were calculated from the corresponding binding isotherms (Figures **13**-**17**).

Association constants for the pseudorotaxane formation of naphthalene-2,6-dicarboxylate axles **2c-e** range from 1.04×10^5 to 1.41×10^5 M^{-1} and confirm the 1:1 stoichiometry of the complex. The small changes of the K_a value observed for the series of these naphthalene axles **2c-e** are within

the experimental error limits, suggesting that the K_a value for the pseudorotaxane formation event is independent of the axle composition. The binding isotherms in figures **13**-**15** show strong binding between host **1** and guest **2c-e** molecules, where intense signals for and exothermic process are observed until the saturation point is reached. As expected, the binding is enthalpically driven by a ΔH value range from -32.9 to -45.4 kJ mol^{-1} for an entropic cost in the range of from -98.66 to -32.68 J K^{-1} mol^{-1} in ΔS. The free energy of the pseudorotaxane formation ΔG at 298 K ranged from -28.7 to -29.4 kJ mol^{-1}. By contrast, the binding isotherm in figures **16** and **17** is characteristic of a weaker binding between host and guest molecules. Association constants for the pseudorotaxane formation of naphthalene-2,6-dicarboxamide **2g** and 2,6-dioxynaphthalene **2f** axles were found to be 2.51×10^3 M^{-1} and 5.08×10^4 M^{-1}, respectively.

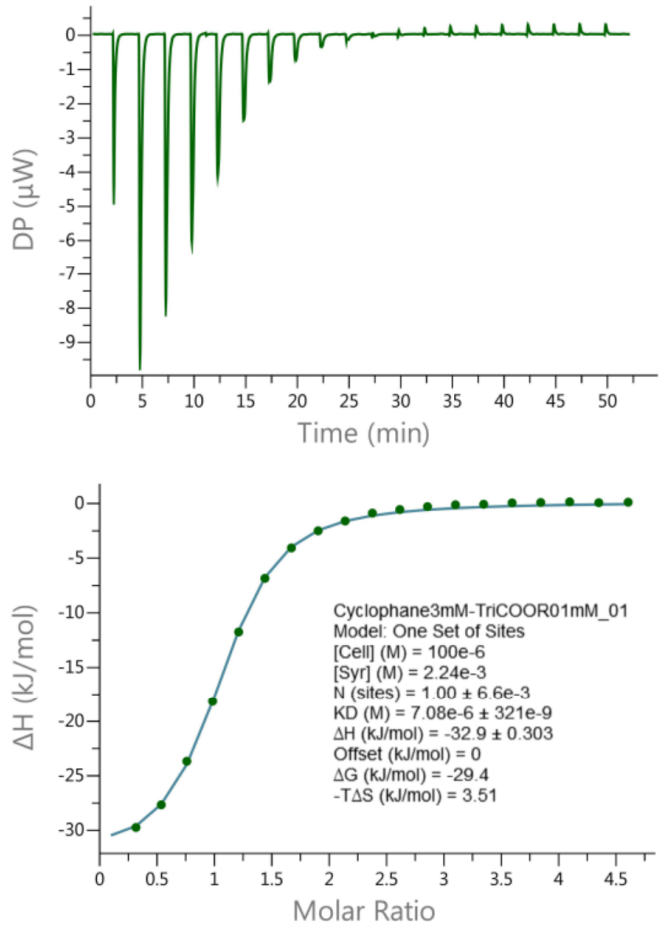

Figure 13: ITC binding isotherm of cyclophane **1** with guest Propargyl-Triethyleneglycol naphthalene-2,6-dicarboxylate axle **2c** in water at 298 K. ΔG = -29.4 kJ mol^{-1}, ΔH = -32.9±0.3 kJ mol^{-1}, ΔS = -98.66 J K^{-1} mol^{-1}, KD = 7.08±0.32 × 10^{-6} M. The association constant was determined by ITC to be 1.41±0.06 × 10^{5} M^{-1}.

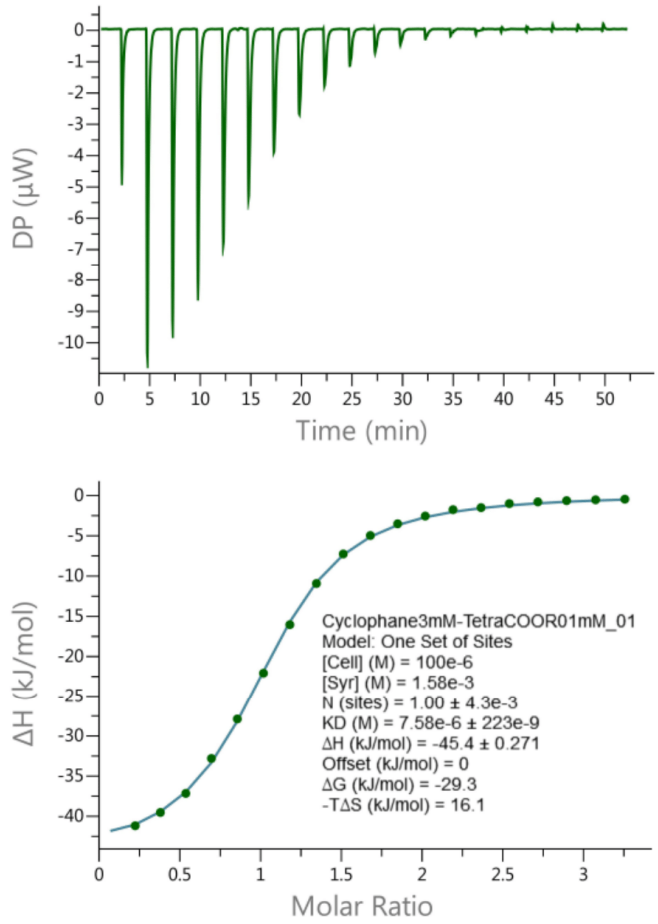

Figure 14. ITC binding isotherm of cyclophane **1** with guest Propargyl-Tetraethyleneglycol naphthalene-2,6-dicarboxylate axle **2d** in water at 298 K. ΔG = -29.3 kJ mol^{-1}, ΔH = -45.4±0.3 kJ mol^{-1}, ΔS = -54.03 J K^{-1} mol^{-1}, K_D = 7.58±0.22 × 10^{-6} M. The association constant was determined by ITC to be 1.32±0.04 × 10^5 M^{-1}.

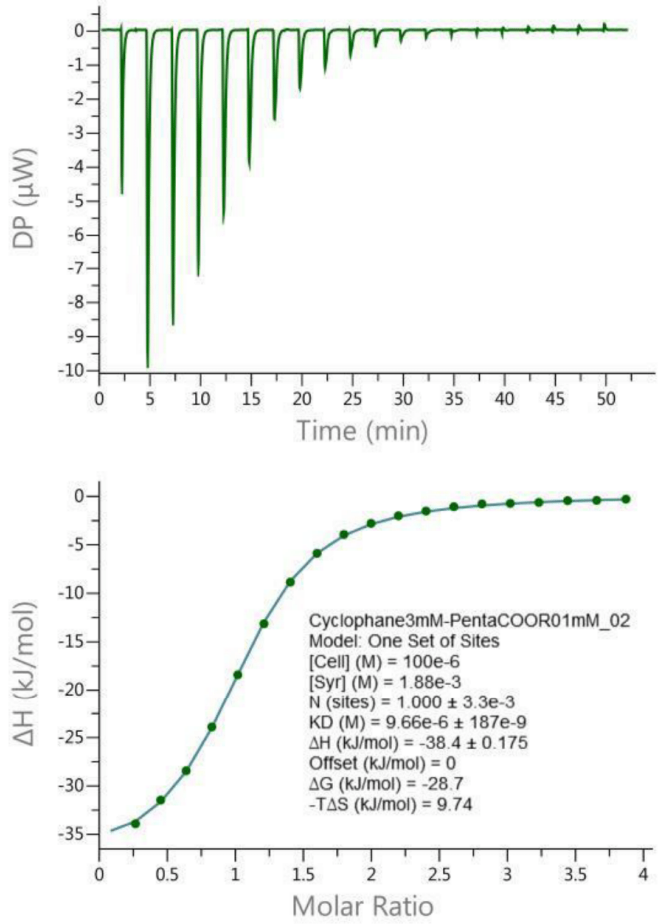

Figure 15. ITC binding isotherm of cyclophane **1** with guest Propargyl-Pentaethyleneglycol naphthalene-2,6-dicarboxylate axle **2e** in water at 298 K. ΔG = -28.7 kJ mol^{-1}, ΔH = -38.4±0.2 kJ mol^{-1}, ΔS = -32.68 J K^{-1} mol^{-1}, K_D = 9.66±0.19 × 10^{-6} M. The association constant was determined by ITC to be 1.04±0.02 × 10^5 M^{-1}.

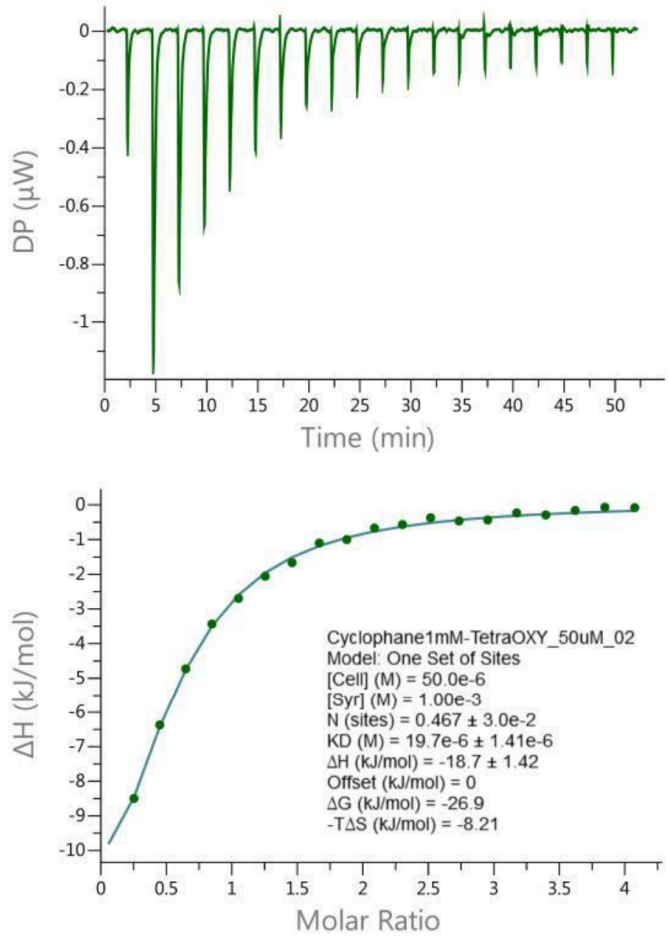

Figure 16. ITC binding isotherm of cyclophane **1** with guest Propargyl-Tetraethyleneglycol-2-6-dioxynaphthalene axle **2f** in water at 298 K. ΔG = -26.9 kJ mol^{-1}, disentanglement of enthalpic and entropic contributions is not applicable due to lack of sigmoid curve shape. $K_D = 19.70 \pm 1.41 \times 10^{-6}$ M. The association constant was determined by ITC to be $5.08 \pm 0.34 \times 10^{4}$ M^{-1}.

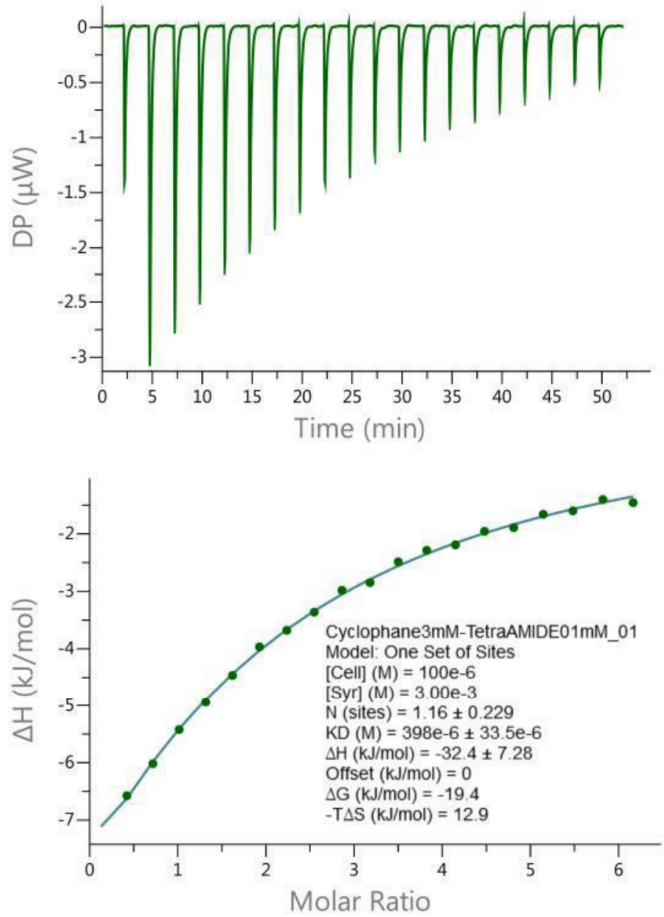

Figure 17. ITC binding isotherm of cyclophane **1** with guest Propargyl-Tetraethyleneglycol naphthalene-2,6-dicarboxamide axle **2g** in water at 298 K. ΔG = -19.4 kJ.mol-1, disentanglement of enthalpic and entropic contributions is not applicable due to lack of sigmoid curve shape. K_D = 398.0±33.5 × 10^{-6} M. The association constant was determined by ITC to be 2.51±0.21 × 10^3 M^{-1}.

Screening Reactions

General Procedure of Screening Reactions

The solid or respectively oily axles **2a-b** and **2c-e** were directly weighted into the reaction flask, before the appropriate amounts of cyclophane, stopper and catalyst system (Table **2**) were added from aqueous stock solutions allowing convenient preparation of the reaction mixtures. After two hours, a sample was taken, diluted with water and analyzed via LC-ESI-MS. In case of the longer polyethylene glycol spacers n = 3 - 5, stopper **3** was entirely consumed indicating reaction completion, whereas in case of n = 1 and 2, the chromatograms exhibit a signal with a retention time (t_R) of 6.5 min corresponding to **3**. The chromatograms recorded of samples taken after 21 hours revealed no further decrease of the stopper signal. Even after prolonged reaction times the stopper was not completely consumed. Furthermore, no signal for the corresponding axles **2a** and **2b**, was observed in the LC-MS traces, which reflects their insolubility in water. The recorded LC-ESI-MS chromatograms were analyzed by extracting the m/z values of rotaxanes **4a-e** and dumbbells **5a-e** either in the form of their corresponding proton or sodium ion adducts and m/z values for cyclophane from the total ion chromatogram (T.I.C) (see chromatograms in Figure **18**-**24**). The peaks were then integrated, the obtained integrals corresponding to the same compound were summed up, e.g. proton and sodium ion adduct of rotaxane (traces b and c in Figure **2**), and used for evaluation.

Table 2: Overview of the total concentrations and equivalents of reactants and reagents of the CuAAC screening reactions under three different conditions.*

Cond.	cyclophane	axle	stopper	$CuSO_4$	Na ascorb.	THPTA
1	0.5 mM (1.0 eq)	0.5 mM (1.0 eq)	1.0 mM (2.0 eq)	0.5 mM (1.0 eq)	0.5 mM (1.0 eq)	–
2	2.5 mM (5.0 eq)	0.5 mM (1.0 eq)	1.0 mM (2.0 eq)	0.5 mM (1.0 eq)	0.5 mM (1.0 eq)	–
3	0.5 mM (1.0 eq)	0.5 mM (1.0 eq)	1.0 mM (2.0 eq)	0.5 mM (1.0 eq)	0.5 mM (1.0 eq)	0.5 mM (1.0 eq)

* All reactions were performed at room temperature and under argon atmosphere.

Evaluation of Results

The following chromatograms contain the results obtained by HPLC-ESI-MS from the screening reactions under three different conditions with each of the five different axles **2a-e** after a certain time. In each series the topmost chromatogram corresponds to the total ion current trace (T.I.C.), whereas the chromatograms below represent the extracted ion chromatograms of the majorly observed ions in the T.I.C. (proton and sodium adducts of rotaxane and dumbbell and the doubly charged cyclophane). The results (see table **3** – **9**) represent the extracted ion current ratios between formed rotaxane compared to dumbbell.

***Penta*-EG naphthalene ester axle:**

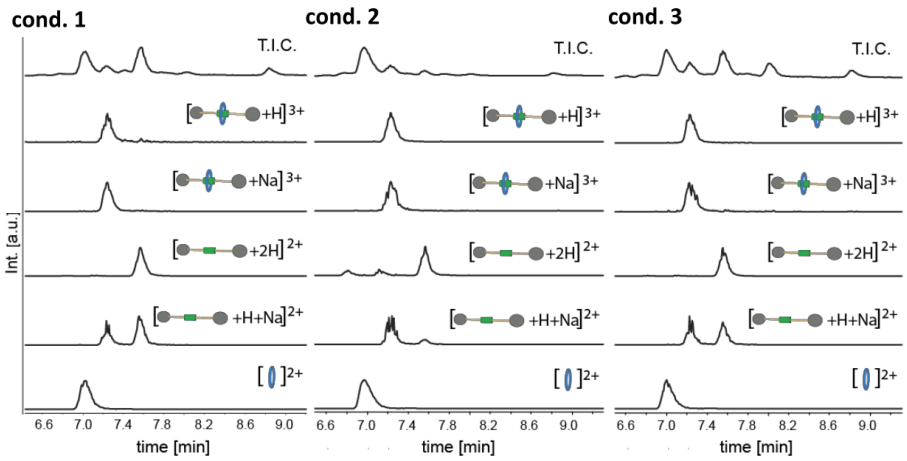

Figure 18: Screening reactions after **two hours** with ***penta*-EG naphthalene ester axle 2e** under the three different conditions 1-3. A signal for stopper **3** is not observed; the low signal with retention time t_R = 8.0 min and t_R = 8.9 min corresponds to some single-stoppered and non-consumed axle **2e**, respectively.

Table 3: Semiquantified results of the screening reactions with ***penta*-EG naphthalene ester axle** under three different conditions after **two hours**.

	condition 1	condition 2	condition 3
rotaxane/ dumbbell	0.33	2.63	0.47

***Tetra*-EG naphthalene ester axle:**

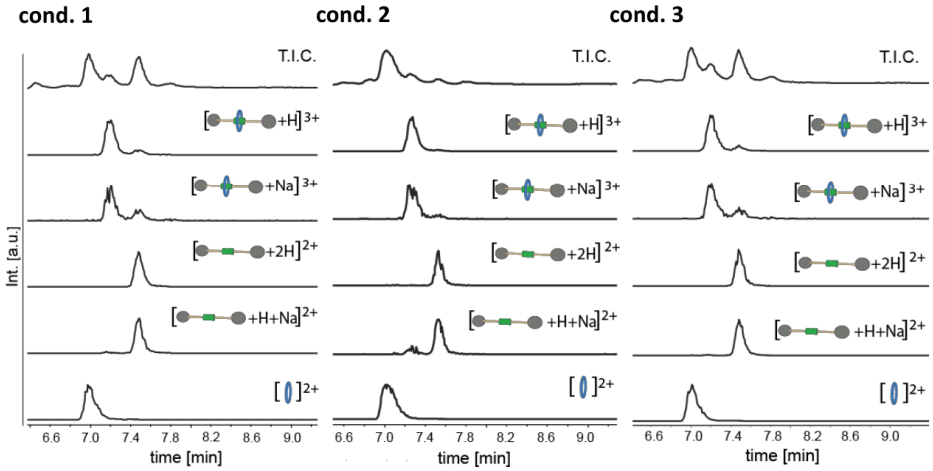

Figure 19: Screening reactions after **two hours** with ***tetra*-EG naphthalene ester axle** under the three different conditions 1-3. A signal corresponding to either axle **2d** or stopper **3**, respectively, is not observed in either of the three T.I.C.s, which indicates complete conversion of **2d**.

Table 4: Semiquantified results of the screening reactions with ***tetra*-EG naphthalene ester axle** under three different conditions after **two hours**.

	condition 1	condition 2	condition 3
rotaxane/ dumbbell	0.43	1.40	0.56

***Tri*-EG naphthalene ester axle, 2h:**

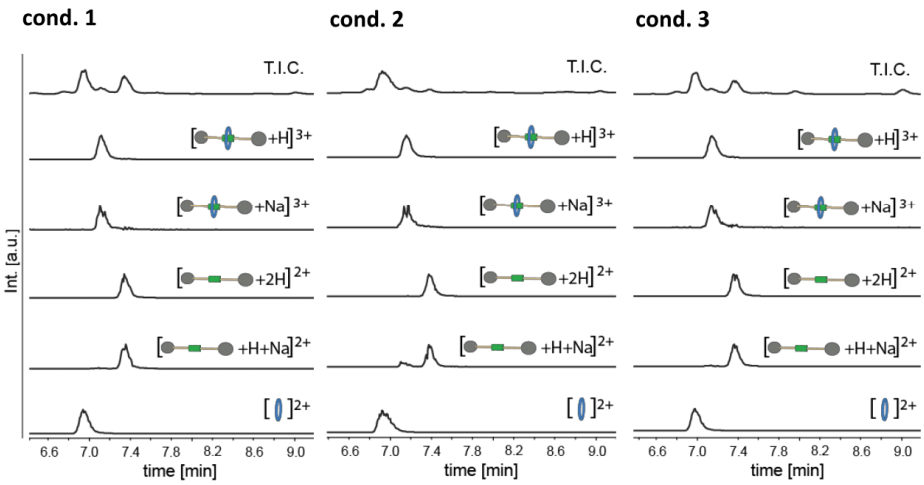

Figure 20: Screening reactions after **two hours** with ***tri*-EG naphthalene ester axle** under the three different conditions 1-3. A signal corresponding to stopper **3** (t_R = 6.5 min) is not observed in neither of the three T.I.C.s, whereas the low signal under condition 3 indicates some non-consumed axle **2c** (t_R = 9.0 min).

Table 5: Semiquantified results of the screening reactions with ***tri*-EG naphthalene ester axle** under three different conditions after **two hours**.

	condition 1	condition 2	condition 3
rotaxane/ dumbbell	0.35	2.04	0.31

***Di*-EG naphthalene ester axle, 2 hours:**

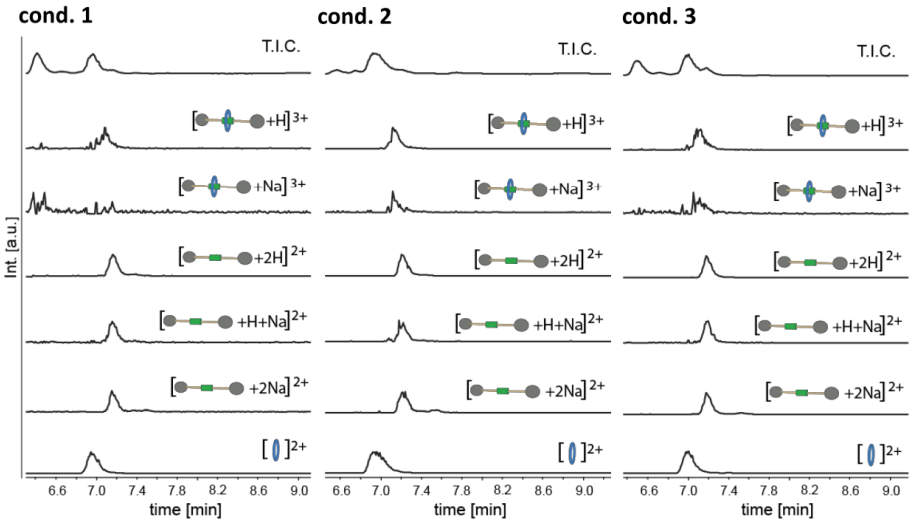

Figure 21: Screening reactions after **two hours** with ***di*-EG naphthalene ester axle** under the three different conditions 1-3. The signal at t_R = 6.5 min in each T.I.C. corresponds to stopper **3** and indicates incomplete conversion after two hours; axle **2b** cannot be observed due to its insolubility in pure water.

Table 6: Semiquantified results of the screening reactions with ***di*-EG naphthalene ester axle** under three different conditions after **two hours**.

	condition 1	condition 2	condition 3
rotaxane/ dumbbell	0.14	0.44	0.19

***Di*-EG naphthalene ester axle, 21 hours:**

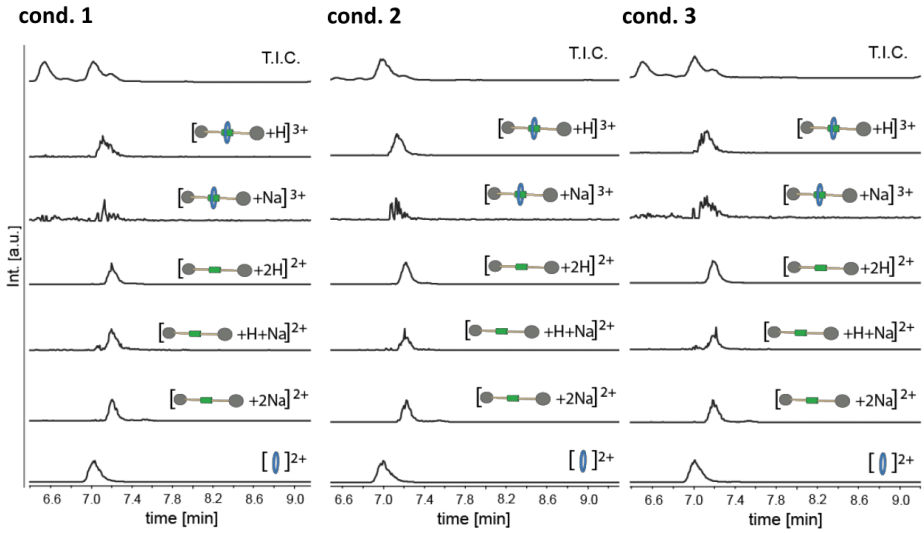

Figure 22: Screening reactions after **21 hours** with ***di*-EG naphthalene ester axle** under the three different conditions 1-3. The signal at t_R = 6.5 min in each T.I.C. corresponds to stopper **3** and indicates incomplete conversion after two hours; axle **2b** cannot be observed due to its insolubility in pure water.

Table 7: Semiquantified results of the screening reactions with ***di*-EG naphthalene ester axle** under three different conditions after **21 hours**.

	condition 1	condition 2	condition 3
rotaxane/ dumbbell	0.12	0.50	0.22

***Mono*-EG naphthalene ester axle, 2 hours:**

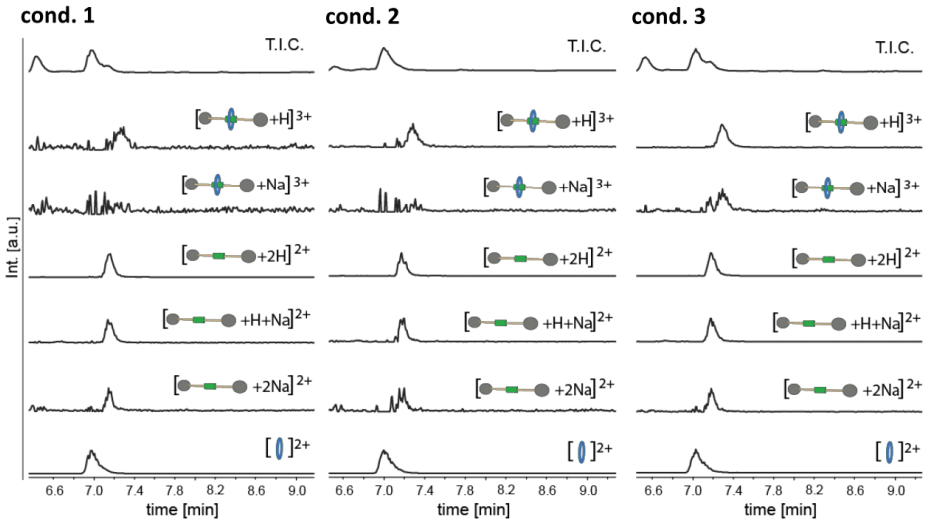

Figure 23: Screening reactions after **two hours** with ***mono*-EG naphthalene ester axle** under the three different conditions 1-3. The signal at t_R = 6.5 min in each T.I.C. corresponds to stopper **3** and indicates incomplete conversion after two hours; axle **2a** cannot be observed due to its insolubility in pure water.

Table 8: Semiquantified results of the screening reactions with ***mono*-EG naphthalene ester axle** under three different conditions after **two hours**.

	condition 1	**condition 2**	**condition 3**
rotaxane/ dumbbell	0.02	0.15	0.13

***Mono*-EG naphthalene ester axle, 21 hours:**

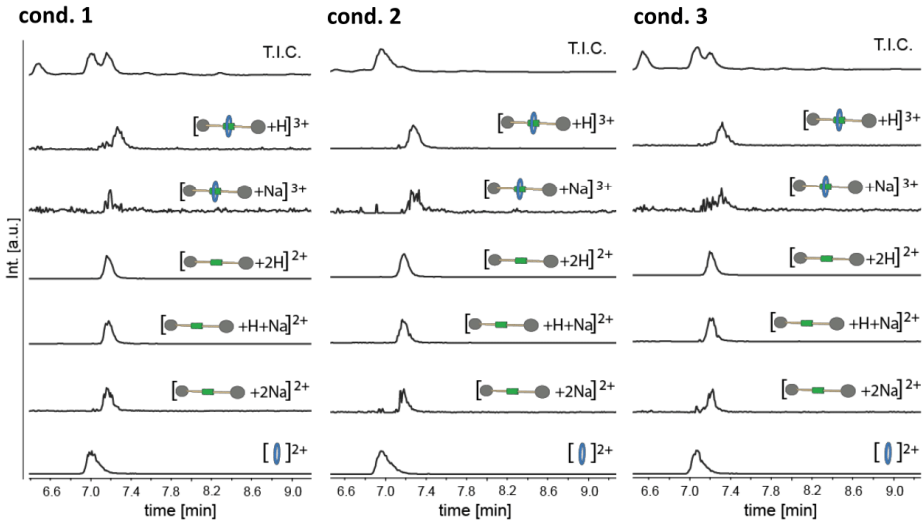

Figure 24: Screening reactions after **two hours** with ***mono*-EG naphthalene ester axle** under the three different conditions 1-3. The signal at t_R = 6.5 min in each T.I.C. corresponds to stopper **3** and indicates incomplete conversion after two hours; axle **2a** cannot be observed due to its insolubility in pure water.

Table 9: Semiquantified results of the screening reactions with ***mono*-EG naphthalene ester axle** under three different conditions after **21 hours**.

	condition 1	**condition 2**	**condition 3**
rotaxane/ dumbbell	0.02	0.15	0.09

^{1}H NMR Spectrum of 2a

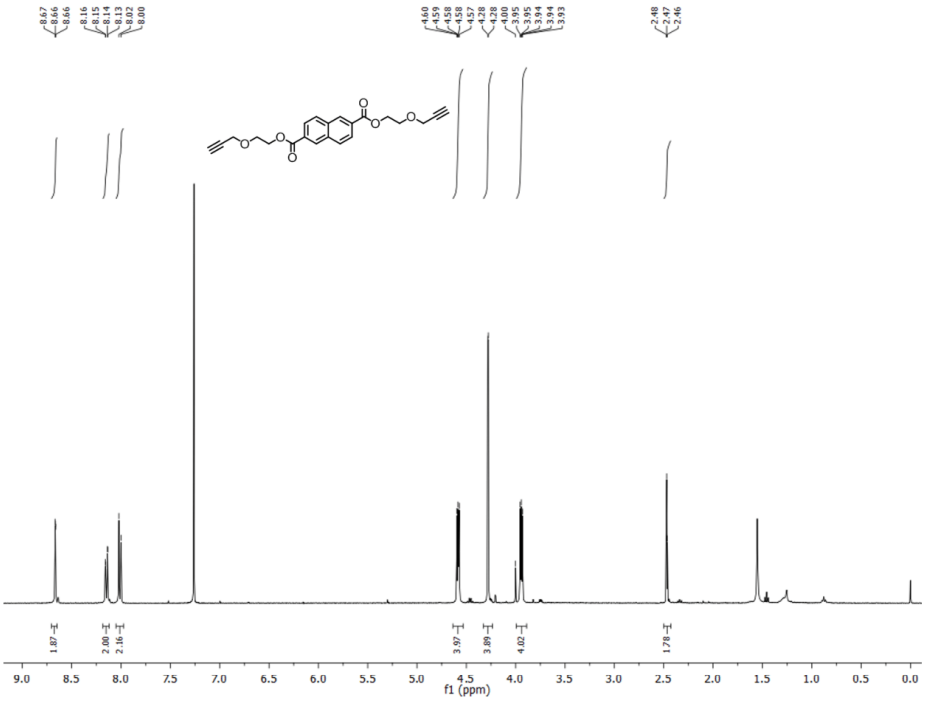

^{13}C NMR Spectrum of 2a

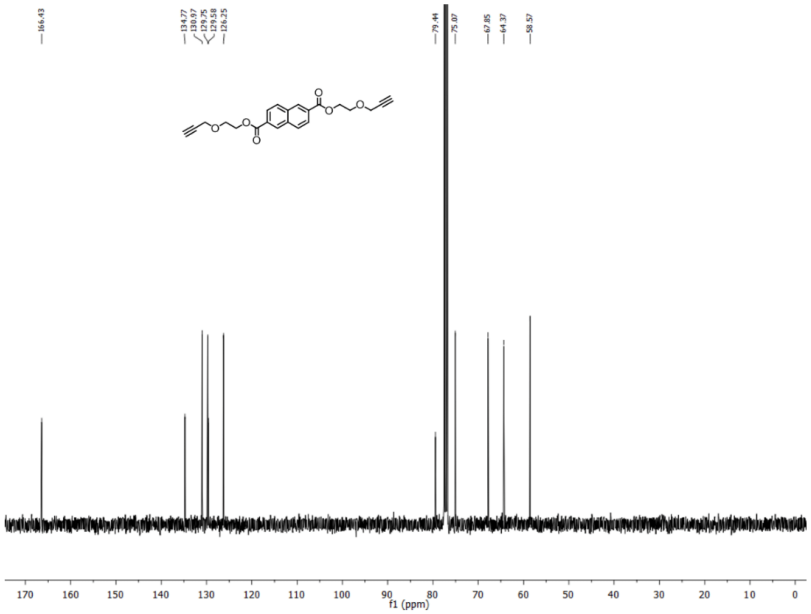

^{1}H NMR Spectrum of 2b

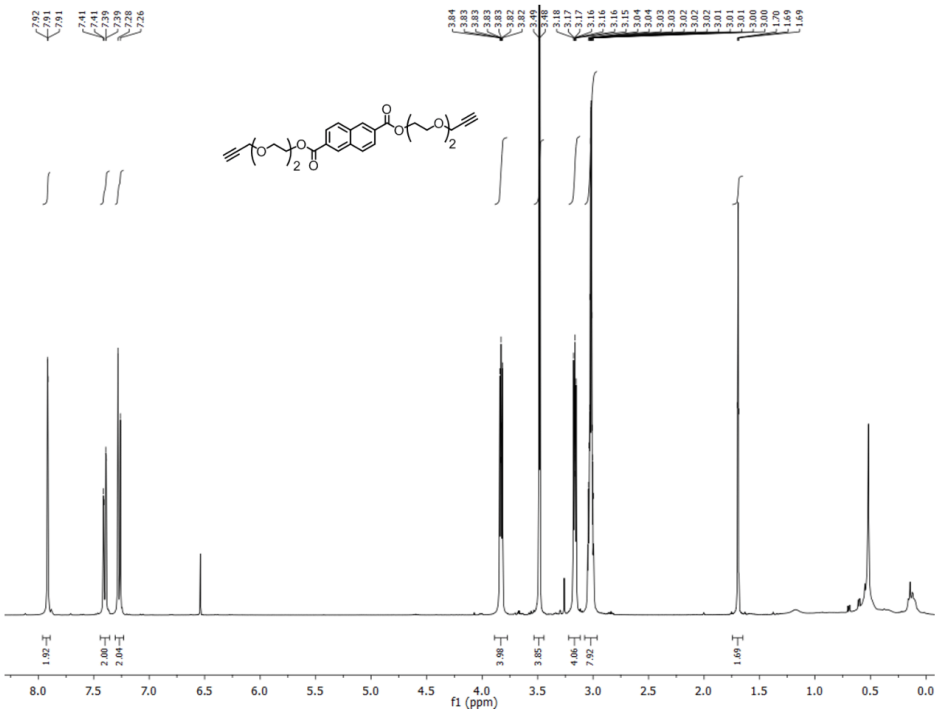

^{13}C NMR Spectrum of 2b

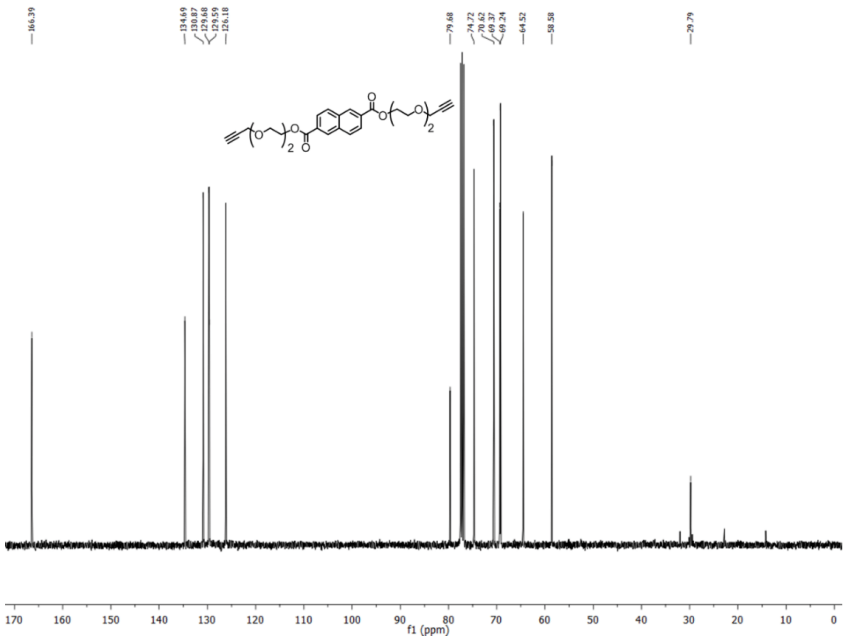

^{1}H NMR Spectrum of 2c

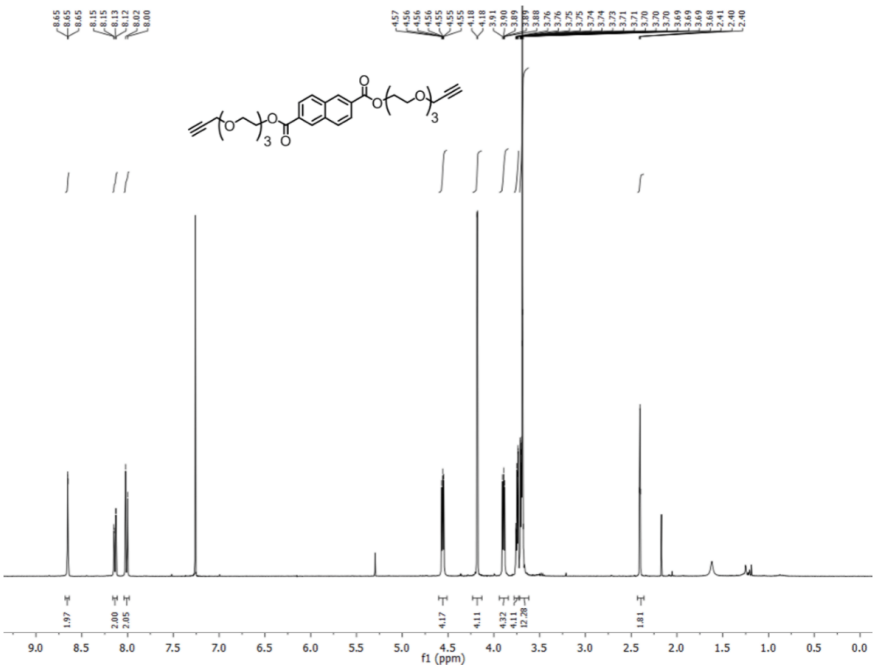

^{13}C NMR Spectrum of 2c

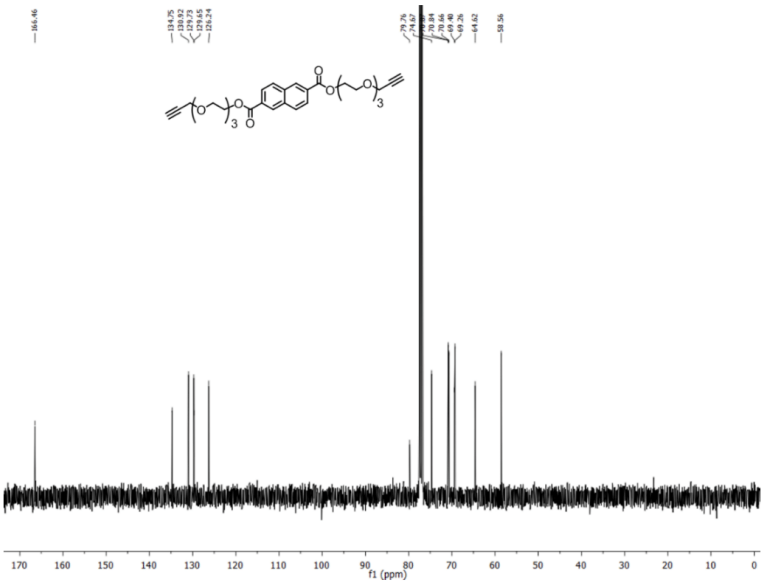

^{1}H NMR Spectrum of 2d

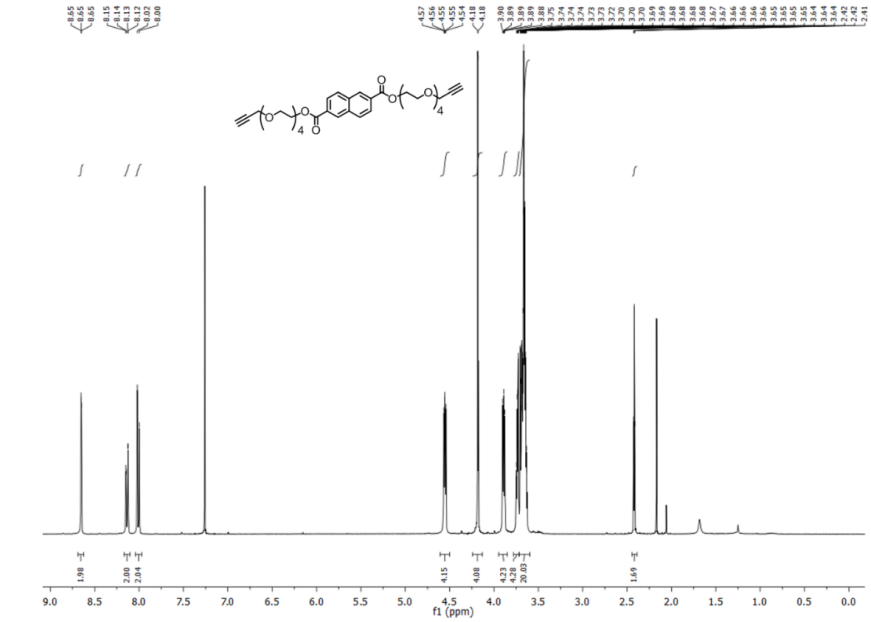

^{13}C NMR Spectrum of 2d

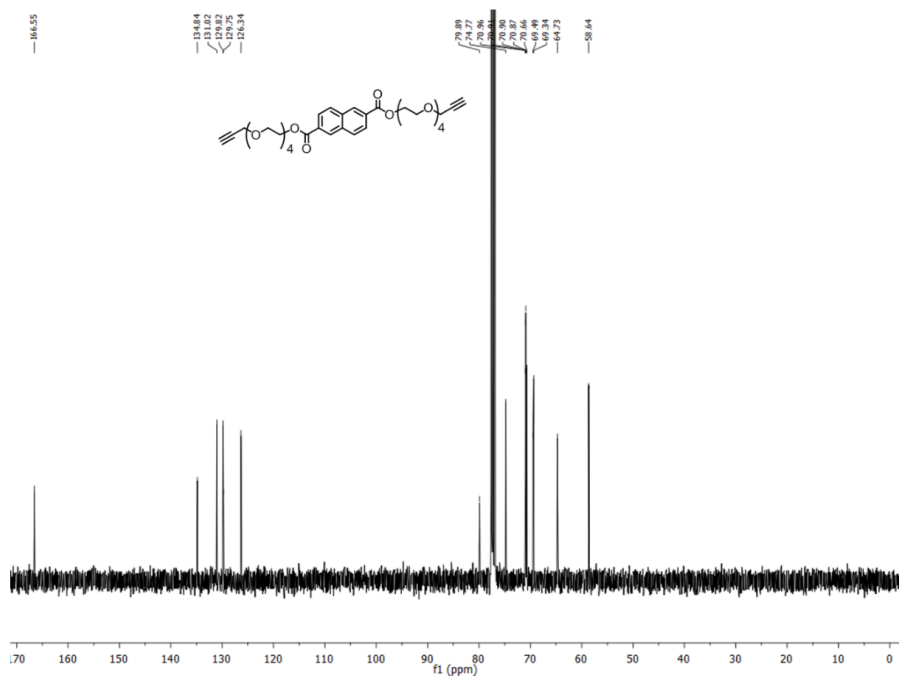

^{1}H NMR Spectrum of 2e

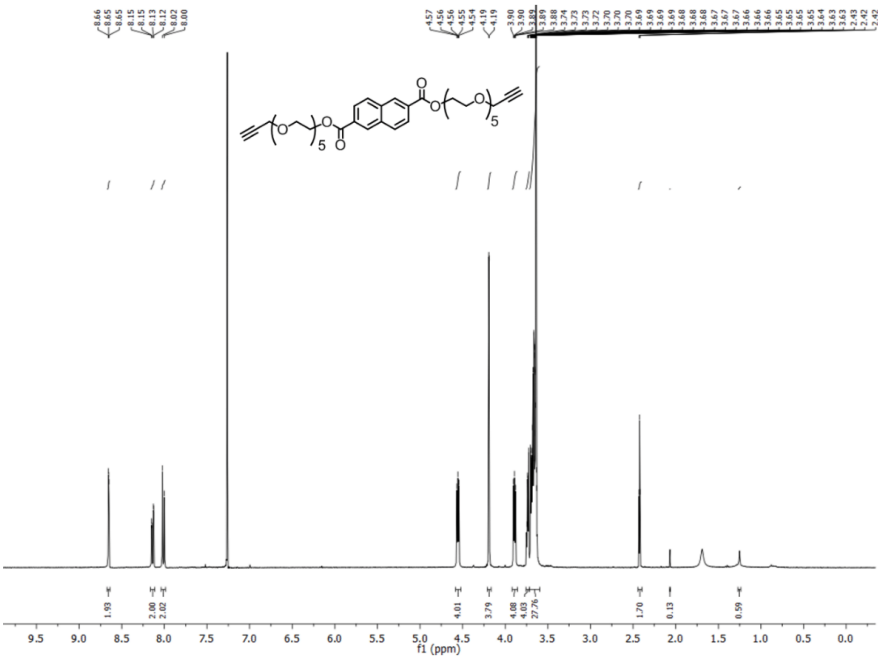

^{13}C NMR Spectrum of 2e

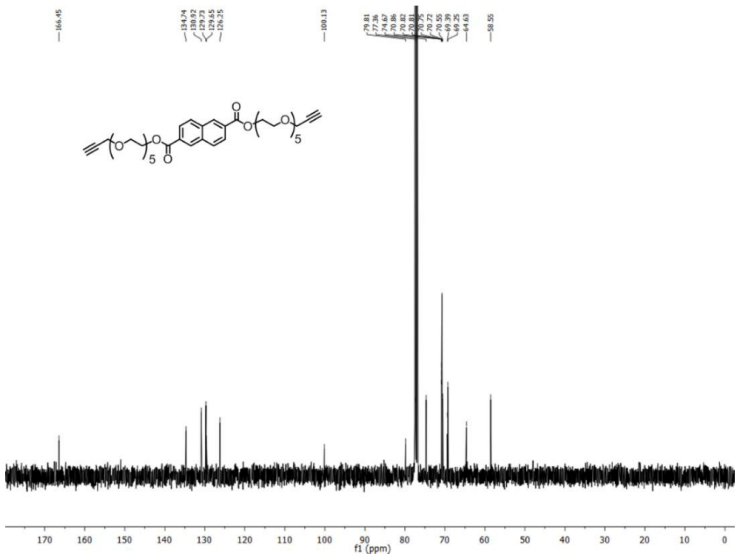

^{1}H NMR Spectrum of 2f

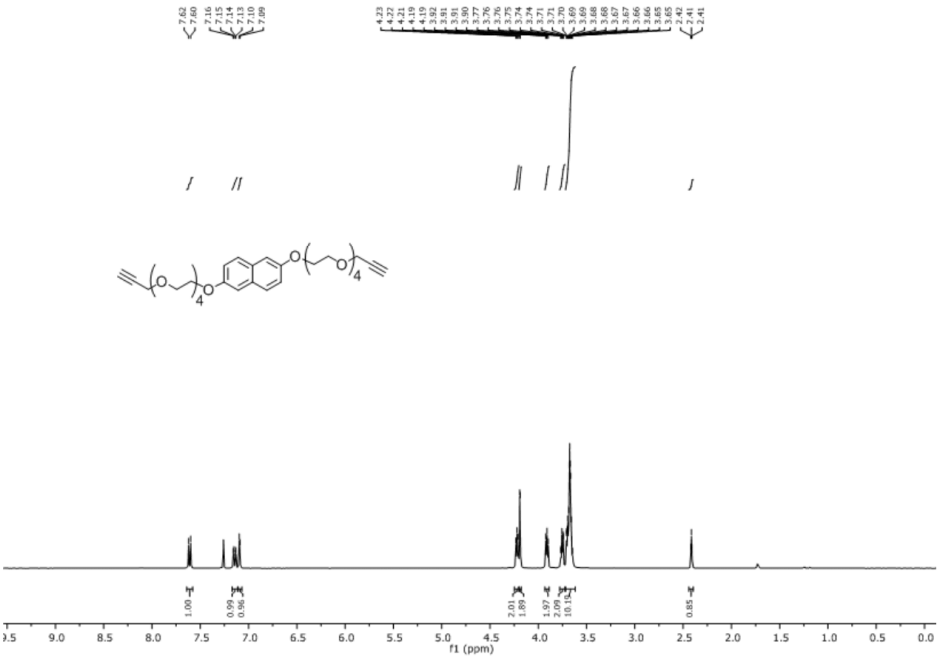

^{13}C NMR Spectrum of 2f

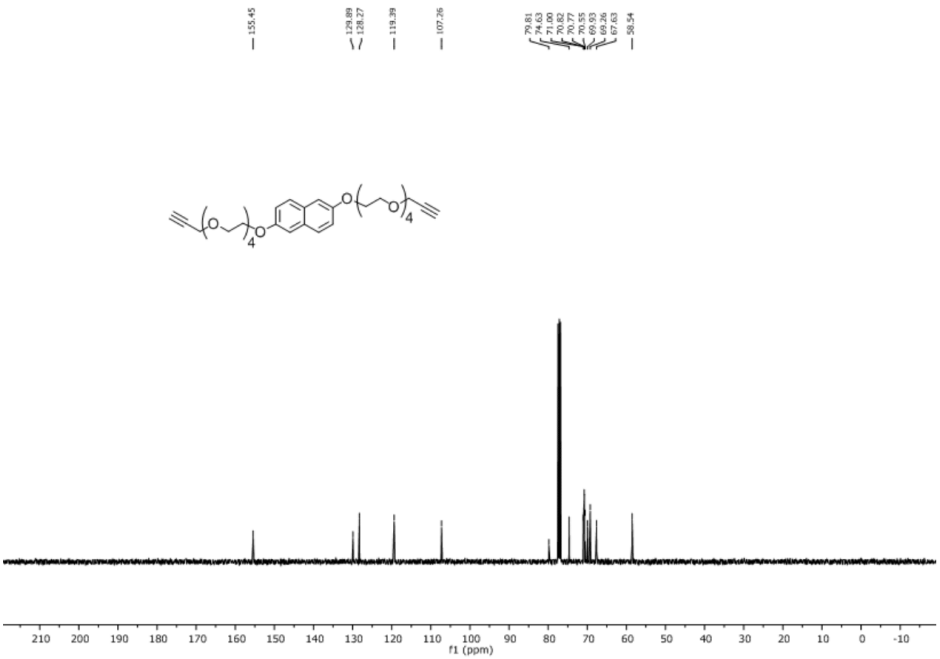

^{1}H NMR Spectrum of 2g

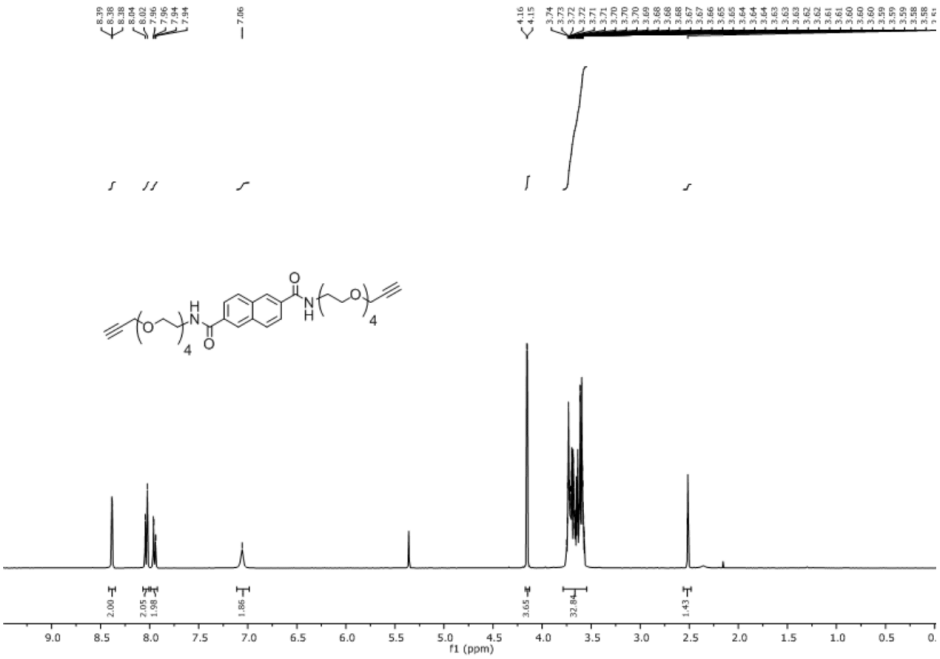

^{13}C NMR Spectrum of 2g

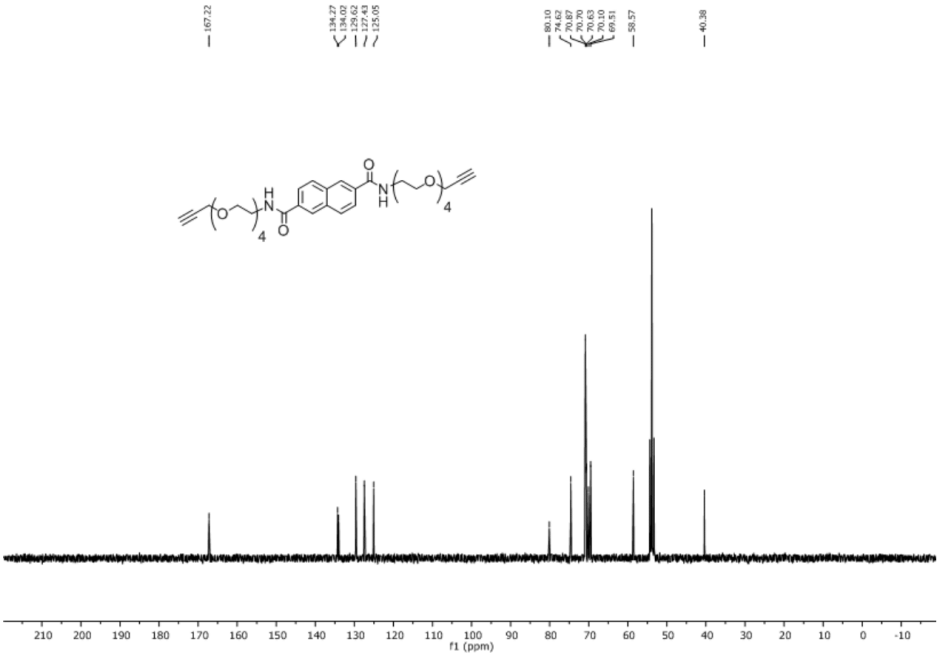

^{1}H NMR Spectrum of 7f

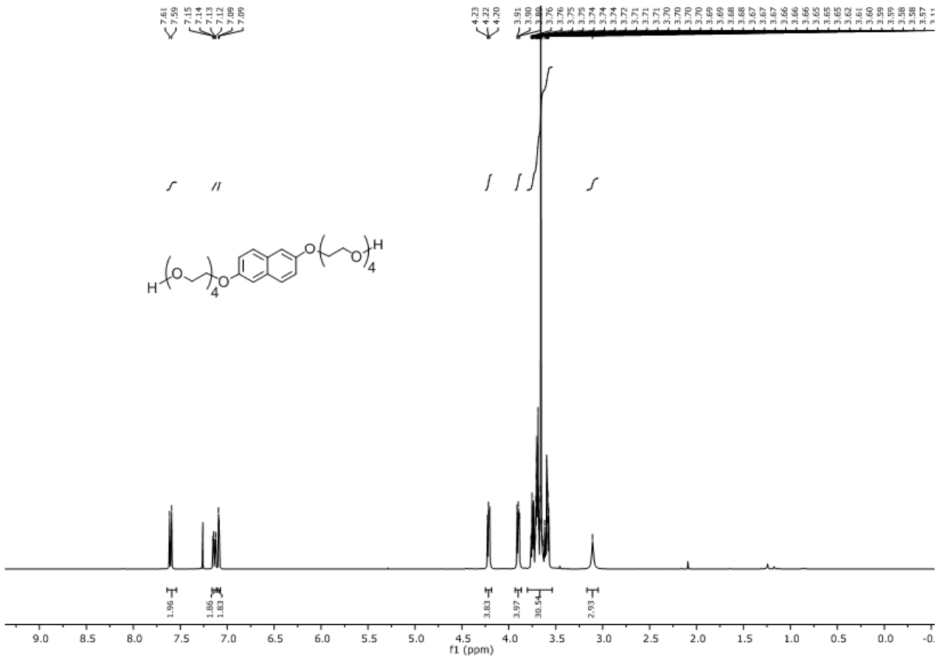

^{13}C NMR Spectrum of 7f

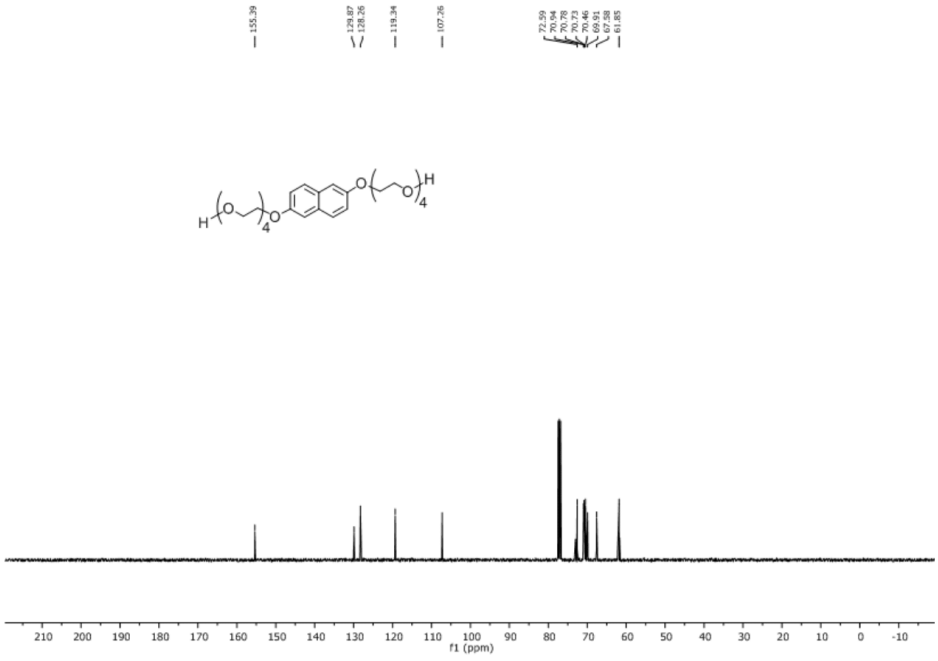

^{1}H NMR Spectrum of 9

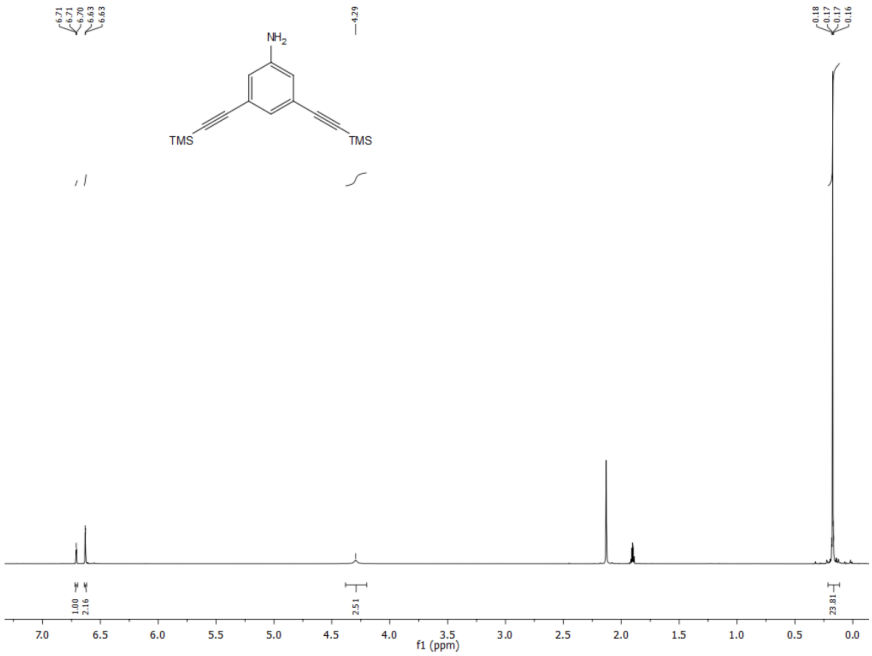

^{13}C NMR Spectrum of 9

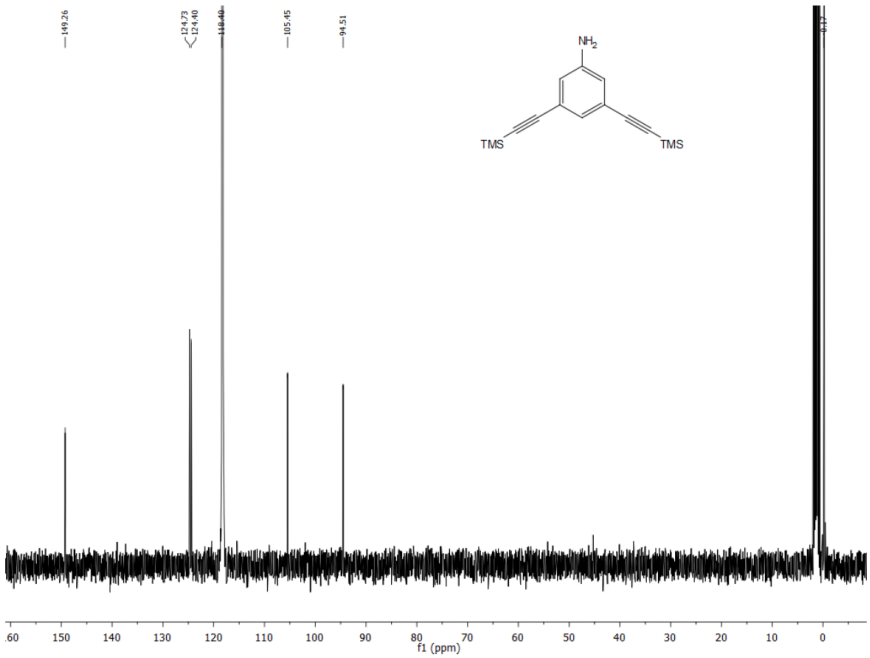

^{1}H NMR Spectrum of 10

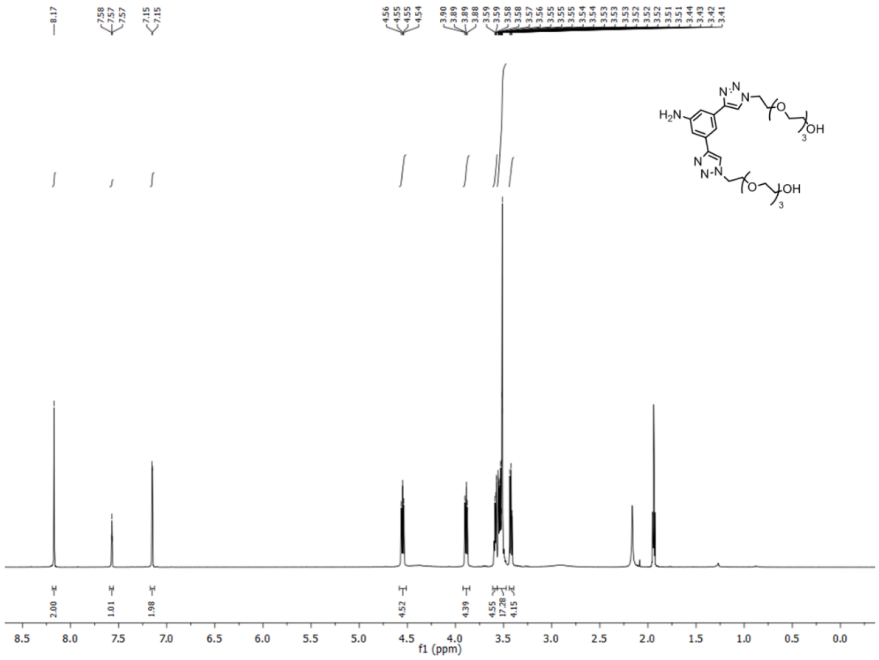

^{13}C NMR Spectrum of 10

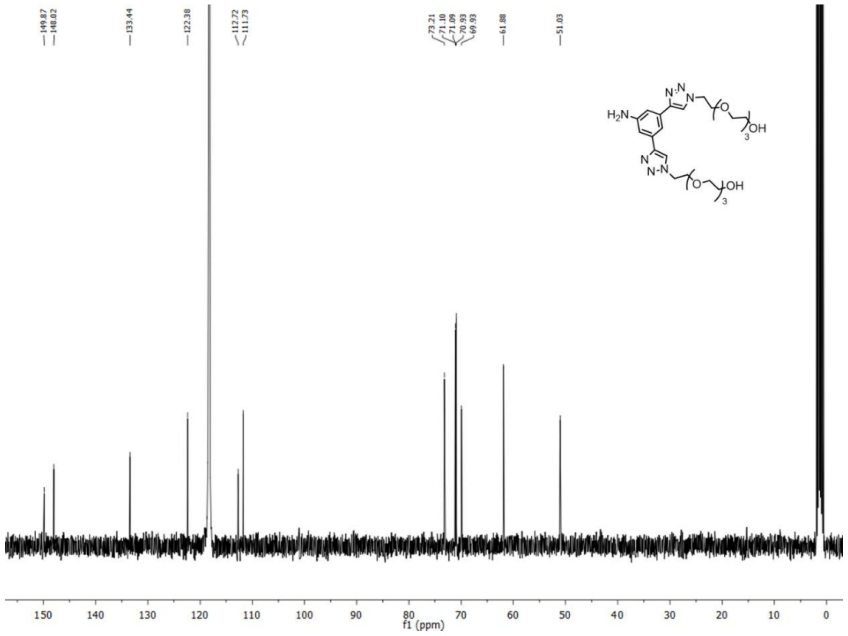

^{1}H NMR Spectrum of 3

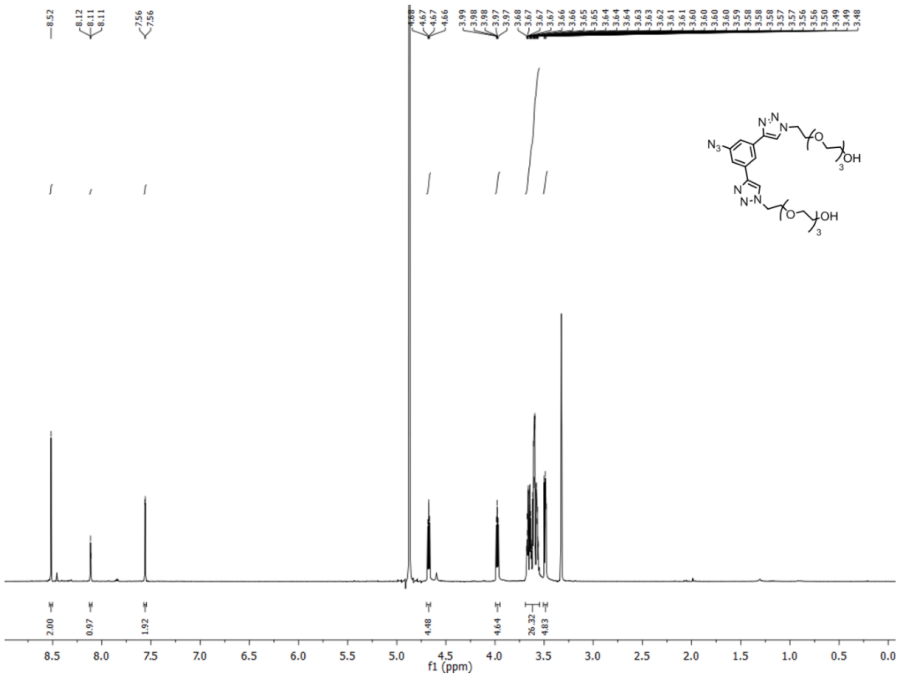

^{13}C NMR Spectrum of 3

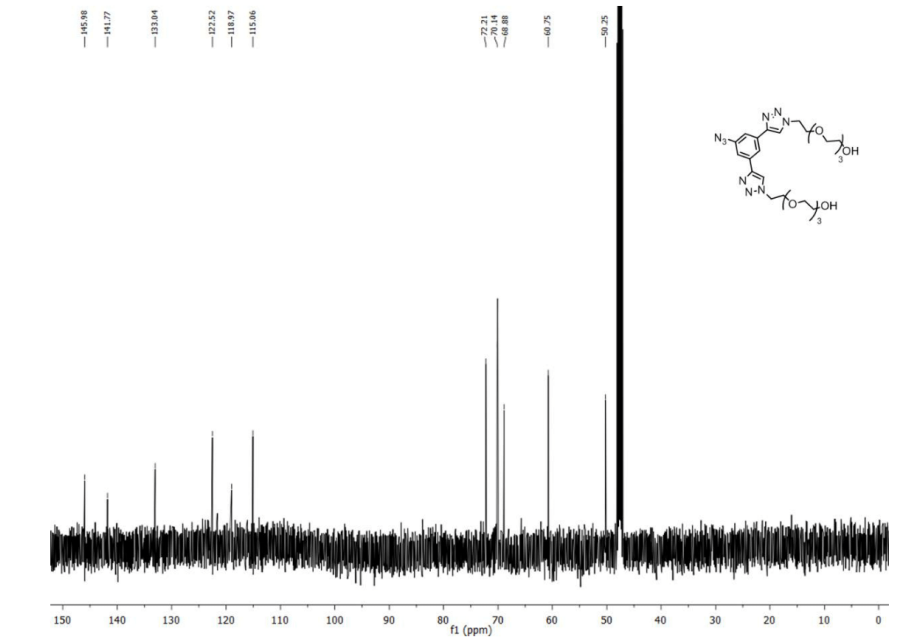

^{1}H NMR Spectrum of 4d

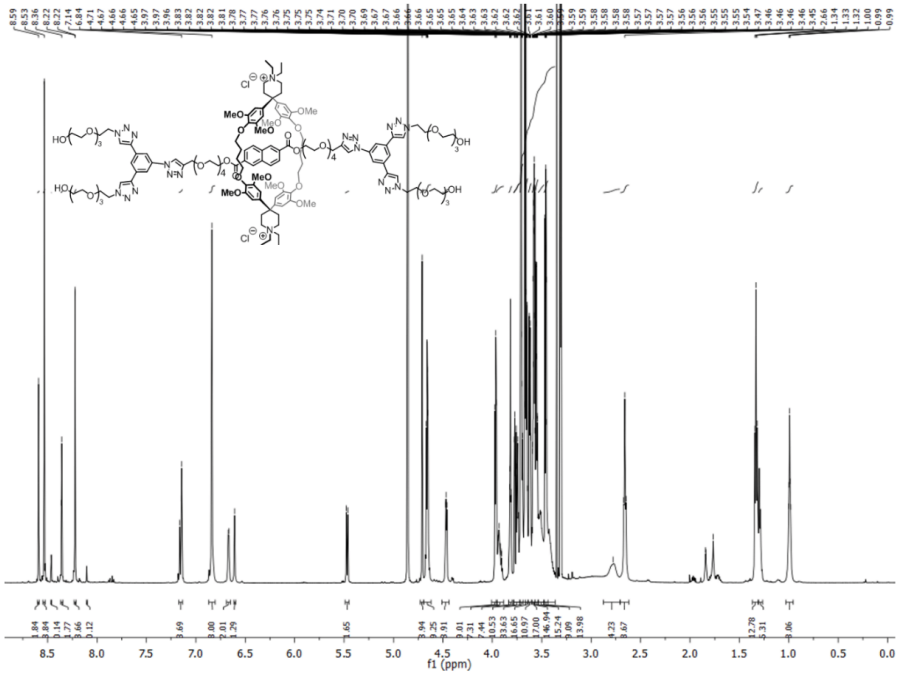

^{13}C NMR Spectrum of 4d

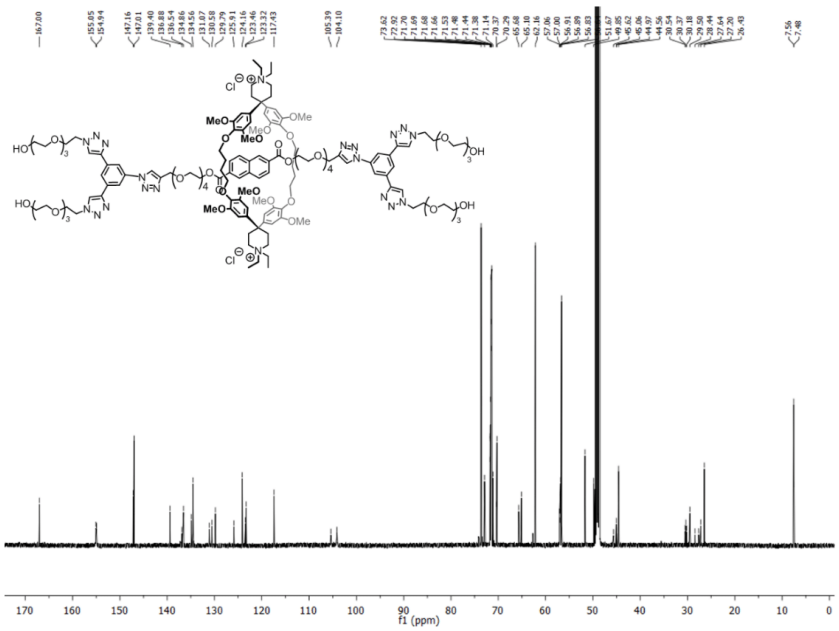

^{1}H NMR Spectrum of 4f

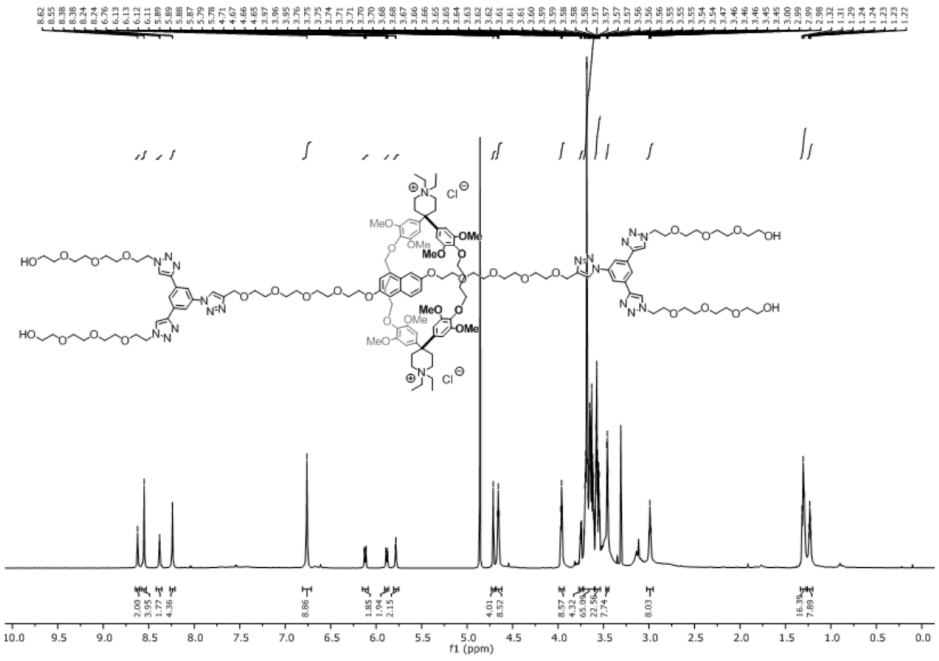

^{13}C NMR Spectrum of 4f

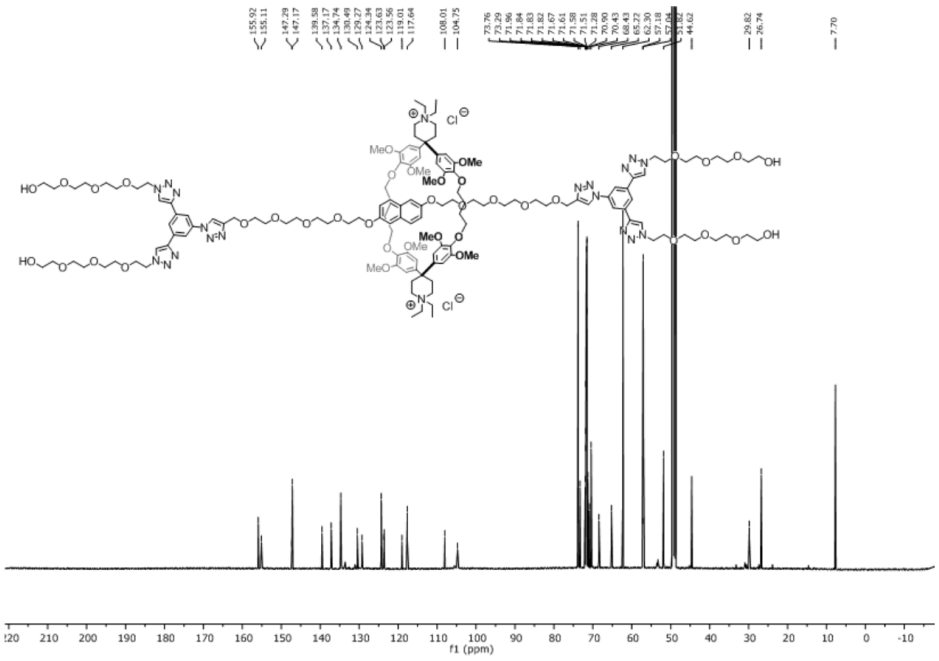

^{1}H NMR Spectrum of 5d

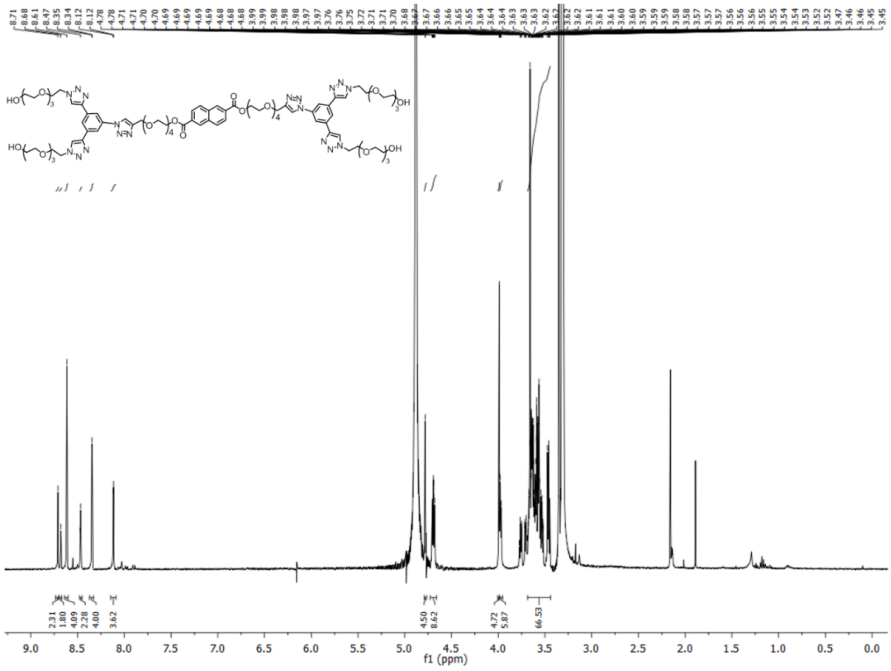

^{1}H NMR Spectrum of 5f

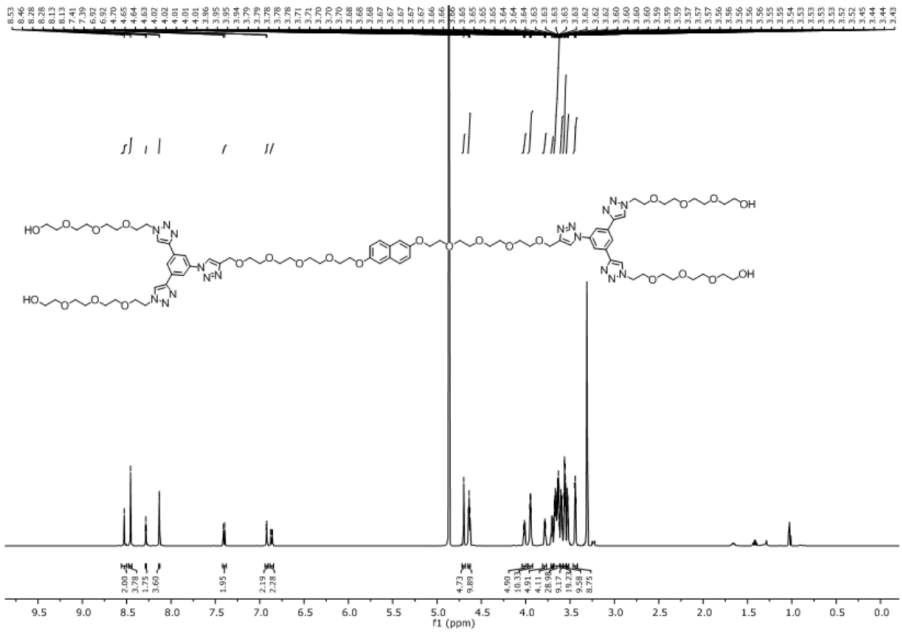

^{13}C NMR Spectrum of 5f

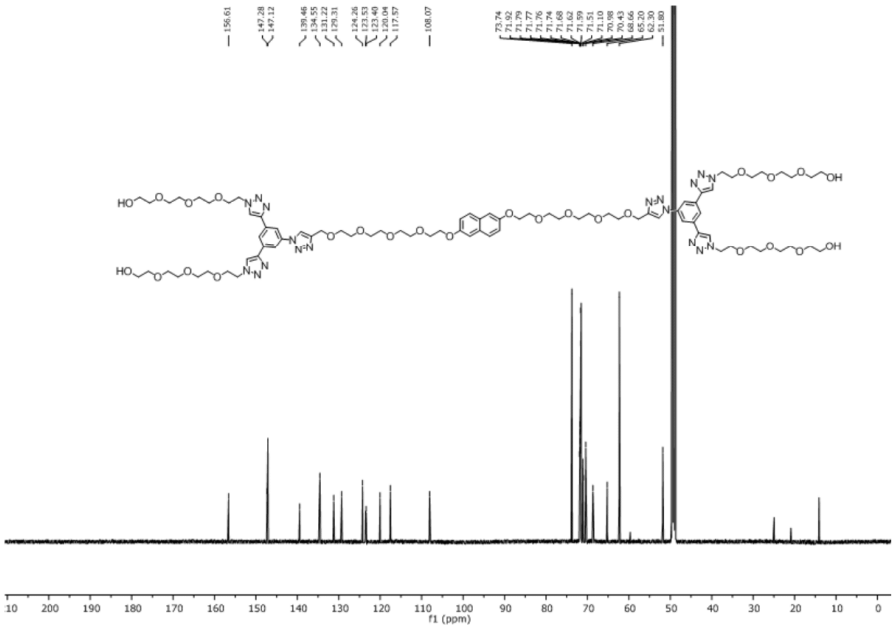

References

[1] T. Mayer, M. E. Maier, *Eur. J. Org. Chem.* **2007**, *2007*, 4711–4720.

[2] G. Jayamurugan, O. Dumele, J.-P. Gisselbrecht, C. Boudon, W. B. Schweizer, B. Bernet, F. Diederich, *J. Am. Chem. Soc.* **2013**, DOI 10.1021/ja312084s.

[3] D. Mertz, C. J. Ochs, Z. Zhu, L. Lee, S. N. Guntari, G. K. Such, T. K. Goh, L. A. Connal, A. Blencowe, G. G. Qiao, et al., *Chem. Commun.* **2011**, *47*, 12601–12603.

[4] S. Asano, J. Gavrilyuk, D. R. Burton, C. F. Barbas, *ACS Med. Chem. Lett.* **2014**, *5*, 133–137.

[5] J. Diot, M. I. García-Moreno, S. G. Gouin, C. O. Mellet, K. Haupt, J. Kovensky, *Org. Biomol. Chem.* **2008**, *7*, 357–363.

[6] P. Thordarson, in *Supramol. Chem.*, John Wiley & Sons, Ltd, **2012**.

[7] P. Thordarson, *Chem Soc Rev* **2011**, *40*, 1305–1323.

Aqueous Assembly of Zwitterionic Daisy Chains

ChemPubSoc Europe

DOI: 10.1002/chem.201803944

CHEMISTRY A European Journal Full Paper

Supramolecular Chemistry |Hot Paper|

Aqueous Assembly of Zwitterionic Daisy Chains

Yves Aeschi,[a, b] Sylvie Drayss-Orth,[a] Michal Valášek,[c] Daniel Häussinger,[a] and Marcel Mayor*[a, b, c, d]

Abstract: The synthesis and characterization of zwitterionic molecular [*c*2]- and [*a*2]-daisy chains are described, relying on recognition of a positively charged cyclophane and a negatively charged oligo(phenylene-ethynylene) (OPE) rod in aqueous medium. For this purpose, syntheses of an acetylene-functionalized macrocyclic receptor and a water-soluble OPE-rod as the guest component are presented, from which a heteroditopic daisy chain monomer was prepared. This monomer aggregated strongly in water/methanol 4:1 and formed molecular daisy chains, which were isolated as interlocked species from a stoppering reaction at 1 mM concentration. The cyclic dimer [*c*2] was the main product with an isolated yield of 30% and consisted of a mixture of diastereomers, as evidenced by ^{1}H NMR spectroscopy.

Introduction

Synthesis of rotaxanes, catenanes, and derived structures thereof, from dynamic host–guest assemblies has been accomplished by employment of various strategies.[1] A plethora of such mechanically interlocked super-structures are known to date, which upon introduction of stimuli-responsive features have enabled chemists to obtain elaborate molecular machines.[2–4] The stupendous development in this field was recently appreciated by awarding a Nobel Prize for the achievements in this research area. Introduction of rotaxane-type supramolecular subunits or even supramolecular machinery in materials chemistry[4,5] and molecular electronics[6–8] may give rise to the development of functional materials with unprecedented physical and/or chemical properties.

Covalently bound host–guest conjugates result in the formation of supramolecular daisy chains,[9–16] if the molecular structures are designed appropriately to rule out unimolecular self-complexation and formation of non-interlinked, intermolecular aggregates.[16] Due to the hermaphroditic nature of daisy chains, only one component is required for supramolecular complex formation, which is appealing for the construction of molecular devices because it is possible to obtain aggregates of different sizes by rational design, as demonstrated by the synthesis of linear and cyclic molecular muscles,[12–14,17–19] polymers[11,20–22] and gels.[13,23,24] Most daisy chains are based on recognition features that have only limited applicability in water, either due to limited solubility or functional disruption of the recognition site. This is striking considering that hydrophobic self-assembly is widespread in the biological realm, often in combination with other driving forces, such as hydrogen-bonding, donor–acceptor and electrostatic interactions,[25–27] which generate a sheer limitless modular pool of supramolecular assemblies. Furthermore, exploitation of the hydrophobic effect as a driving force for supramolecular assembly is particularly appealing because no specialized recognition site is required and, thus, any hydrophobic surfaces would aggregate in aqueous environment. Limitations for hydrophobic assembly are mainly the solubility of host–guest complexes in aqueous environment in combination with sterically matching hydrophobic sites; these two parameters are often challenging to implement simultaneously. In addition, the lack of inherent specificity of hydrophobic interactions requires that lipophilic und hydrophilic properties are carefully balanced to avoid undesired aggregation modes.

In the context of daisy chains, aqueous assembly is so far mostly limited to systems based on cyclodextrin receptors.[16] In spite of the wide availability and well-established chemistry,[28,29] their synthetic modifiability is limited. Therefore, an alternative, synthetically modifiable receptor for aqueous media is desirable. The series of cyclophanes synthesized and extensively characterized by Diederich and co-workers[30,31] bind strongly to hydrophobic guests and show a high degree of synthetic flexibility.[32–35] Rotaxane syntheses with these cyclophanes have been accomplished[36–39] and high association

[a] Y. Aeschi, Dr. S. Drayss-Orth, Dr. D. Häussinger, Prof. Dr. M. Mayor
Department of Chemistry, University of Basel
St. Johanns-Ring 19, 4056 Basel (Switzerland)
E-mail: marcel.mayor@unibas.ch

[b] Y. Aeschi, Prof. Dr. M. Mayor
Swiss Nanoscience Institute, University of Basel
Klingelbergstrasse 82, 4056 Basel (Switzerland)

[c] Dr. M. Valášek, Prof. Dr. M. Mayor
Institute for Nanotechnology (INT)
Karlsruhe Institute of Technology (KIT)
P. O. Box 3640, 76021 Karlsruhe (Germany)

[d] Prof. Dr. M. Mayor
Lehn Institute of Functional Materials (LIFM)
School of Chemistry, Sun Yat-Sen University (SYSU)
Guangzhou 510275 (P. R. China)

Supporting information and the ORCID identification number(s) for the author(s) of this article can be found under: https://doi.org/10.1002/chem.201803944.

[24] A. Goujon, T. Lang, G. Mariani, E. Moulin, G. Fuks, J. Raya, E. Buhler, N. Giuseppone, *J. Am. Chem. Soc.* **2017**, *139*, 14825 – 14828.
[25] B. W. Ninham, V. Yaminsky, *Langmuir* **1997**, *13*, 2097 – 2108.
[26] M. Vendruscolo, C. M. Dobson, *Nat. Chem. Biol.* **2013**, *9*, 216 – 217.
[27] J. J. McManus, P. Charbonneau, E. Zaccarelli, N. Asherie, *Curr. Opin. Colloid Interface Sci.* **2016**, *22*, 73 – 79.
[28] J. Szejtli, *Chem. Rev.* **1998**, *98*, 1743 – 1754.
[29] T. Girek, *J. Inclusion Phenom. Macrocyclic Chem.* **2012**, *74*, 1 – 21.
[30] F. Diederich, *Angew. Chem. Int. Ed. Engl.* **1988**, *27*, 362 – 386; *Angew. Chem.* **1988**, *100*, 372 – 396.
[31] S. B. Ferguson, E. M. Sanford, E. M. Seward, F. Diederich, *J. Am. Chem. Soc.* **1991**, *113*, 5410 – 5419.
[32] F. Diederich, D. R. Carcanague, *Angew. Chem. Int. Ed. Engl.* **1990**, *29*, 769 – 771; *Angew. Chem.* **1990**, *102*, 836 – 838.
[33] E. M. Seward, R. B. Hopkins, W. Sauerer, S. W. Tam, F. Diederich, *J. Am. Chem. Soc.* **1990**, *112*, 1783 – 1790.
[34] D. R. Benson, R. Valentekovich, F. Diederich, *Angew. Chem. Int. Ed. Engl.* **1990**, *29*, 191 – 193; *Angew. Chem.* **1990**, *102*, 213 – 216.
[35] J. Rotzler, S. Drayss, O. Hampe, D. Häussinger, M. Mayor, *Chem. Eur. J.* **2013**, *19*, 2089 – 2101.
[36] S. Anderson, R. T. Aplin, T. D. W. Claridge, T. Goodson III, A. C. Maciel, G. Rumbles, J. F. Ryan, H. L. Anderson, *J. Chem. Soc. Perkin Trans. 1* **1998**, 2383 – 2398.
[37] P. N. Taylor, A. J. Hagan, H. L. Anderson, *Org. Biomol. Chem.* **2003**, *1*, 3851.
[38] S. Anderson, T. D. W. Claridge, H. L. Anderson, *Angew. Chem. Int. Ed. Engl.* **1997**, *36*, 1310 – 1313; *Angew. Chem.* **1997**, *109*, 1367 – 1370.
[39] Y. Aeschi, S. Drayss-Orth, M. Valášek, F. Raps, D. Häussinger, M. Mayor, *Eur. J. Org. Chem.* **2017**, 4091 – 4103.
[40] D. R. Benson, J. Fu, C. K. Johnson, S. W. Pauls, D. A. Williamson, *J. Org. Chem.* **1998**, *63*, 9935 – 9945.
[41] M. Meldal, C. W. Tornøe, *Chem. Rev.* **2008**, *108*, 2952 – 3015.
[42] K. D. Hänni, D. A. Leigh, *Chem. Soc. Rev.* **2010**, *39*, 1240 – 1251.
[43] C. Clavel, C. Romuald, E. Brabet, F. Coutrot, *Chem. Eur. J.* **2013**, *19*, 2982 – 2989.
[44] Y. Wang, J. Sun, Z. Liu, M. S. Nassar, Y. Y. Botros, J. F. Stoddart, *Chem. Sci.* **2017**, *8*, 2562 – 2568.
[45] K. Kitagawa, A. Inoue, H. Shinokubo, K. Oshima, *Angew. Chem. Int. Ed.* **2000**, *39*, 2481 – 2483; *Angew. Chem.* **2000**, *112*, 2594 – 2596.
[46] A. Krasovskiy, P. Knochel, *Angew. Chem. Int. Ed.* **2004**, *43*, 3333 – 3336; *Angew. Chem.* **2004**, *116*, 3396 – 3399.
[47] K. J. Edgar, S. N. Falling, *J. Org. Chem.* **1990**, *55*, 5287 – 5291.
[48] T. R. Chan, R. Hilgraf, K. B. Sharpless, V. V. Fokin, *Org. Lett.* **2004**, *6*, 2853 – 2855.
[49] S. J. Cantrill, G. J. Youn, J. F. Stoddart, D. J. Williams, *J. Org. Chem.* **2001**, *66*, 6857 – 6872.
[50] F. Coutrot, C. Romuald, E. Busseron, *Org. Lett.* **2008**, *10*, 3741 – 3744.
[51] J. Voignier, J. Frey, T. Kraus, M. Buděšínský, J. Cvačka, V. Heitz, J.-P. Sauvage, *Chem. Eur. J.* **2011**, *17*, 5404 – 5414.
[52] E. M. G. Jamieson, F. Modicom, S. M. Goldup, *Chem. Soc. Rev.* **2018**, *47*, 5266 – 5311.

Manuscript received: August 2, 2018
Accepted manuscript online: September 10, 2018
Version of record online: November 8, 2018

Supporting Information. Aqueous Assembly of Zwitterionic Daisy Chains

CHEMISTRY
A European Journal

Supporting Information

Aqueous Assembly of Zwitterionic Daisy Chains

Yves Aeschi,[a, b] Sylvie Drayss-Orth,[a] Michal Valášek,[c] Daniel Häussinger,[a] and Marcel Mayor*[a, b, c, d]

chem_201803944_sm_miscellaneous_information.pdf

Supporting information

Aggregation studies of $CyOMe_8$ * 2 Cl and 3 * 2 Na

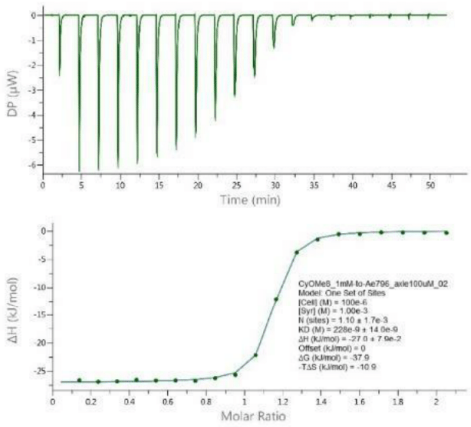

Figure SI 1. ITC binding isotherm of **$CyOMe_8$ * 2 Cl** (1 mM) and **3 * 2 Na** (0.1 mM) in water at 298 K.

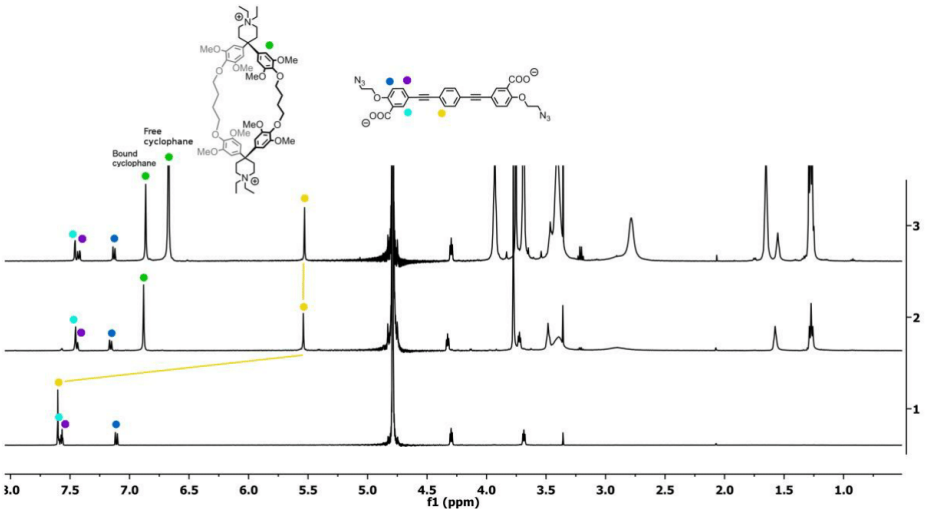

Figure SI 2. ^{1}H-NMR spectra (500 MHz, D_2O) of a 0.5 mM solution of **3 * 2 Na** with 5 eq of **$CyOMe_8$ * 2 Cl** (top), 1 eq (middle), 0 eq (bottom).

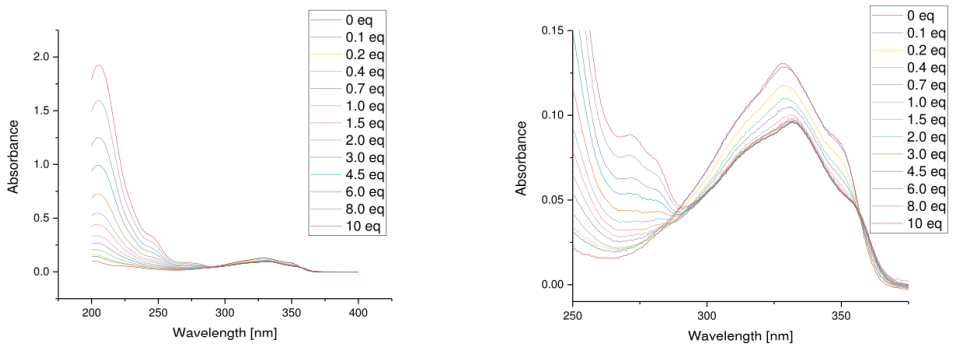

Figure SI 3. Dependence of absorbance of **3 * 2 Na** (1.5 μM) in H_2O upon titration with **CyOMe$_8$ * 2 Cl**. A slight red-shift of the near-UV absorption maximum and a decline in absorbance were observed upon complexation (0 eq: λ_{max} = 328 nm, A = 0.131, 10 eq: λ_{max} = 332 nm, A = 0.096).

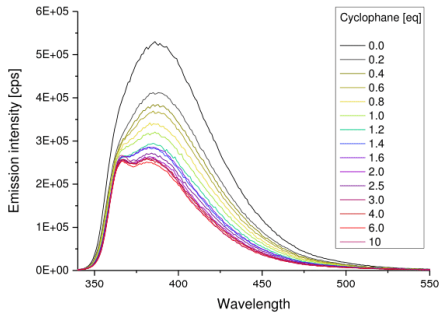

Figure SI 4. Fluorescence quenching titration of **3 * 2 Na** (3 μM) with **CyOMe$_8$ * 2 Cl.**

Characterization of 1

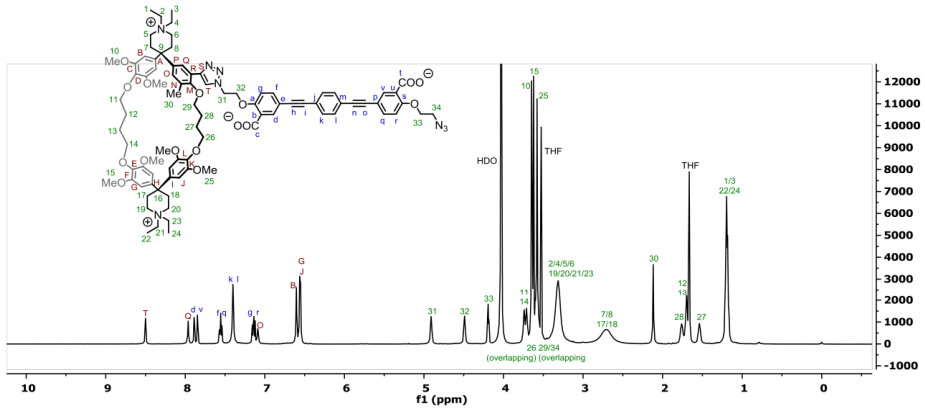

Figure SI 5. Molecular structure and ^{1}H-NMR (600 MHz, THF-d_8:D_2O = 4:1, 26 mM) assignment of **1**.

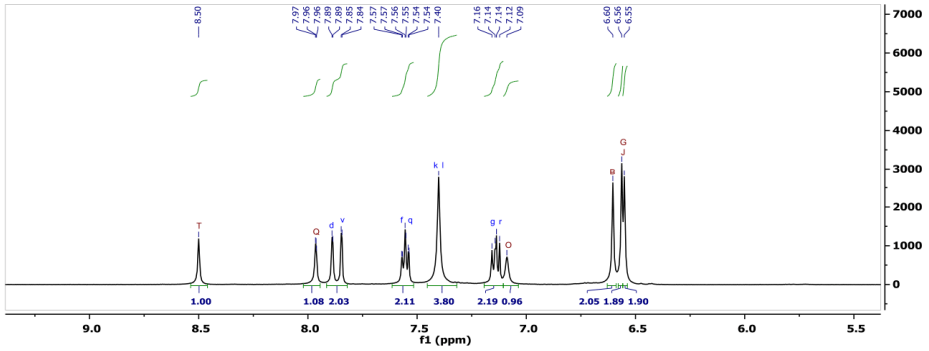

Figure SI 6. Expanded aromatic region of ^{1}H-NMR spectra (600 MHz, THF-d_8:D_2O = 4:1, 26 mM) of **1**.

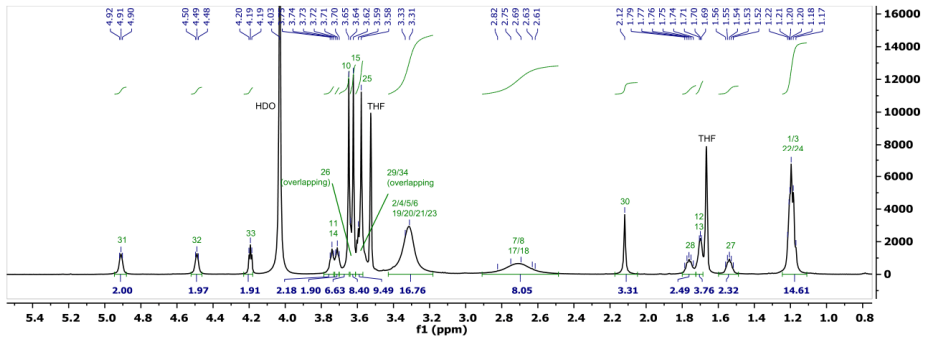

Figure SI 7. Expanded aliphatic region of ^{1}H-NMR spectra (600 MHz, THF-d_8:D_2O = 4:1, 26 mM) of **1**.

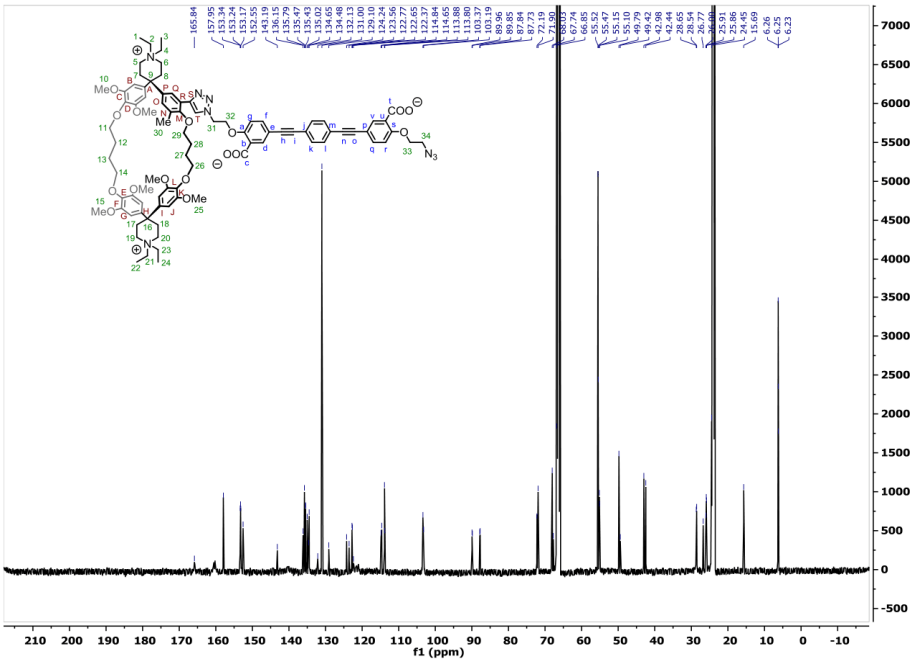

Figure SI 8. Full range ^{13}C-NMR spectrum (126 MHz, THF-d_8:D_2O = 4:1, 26 mM) of **1**.

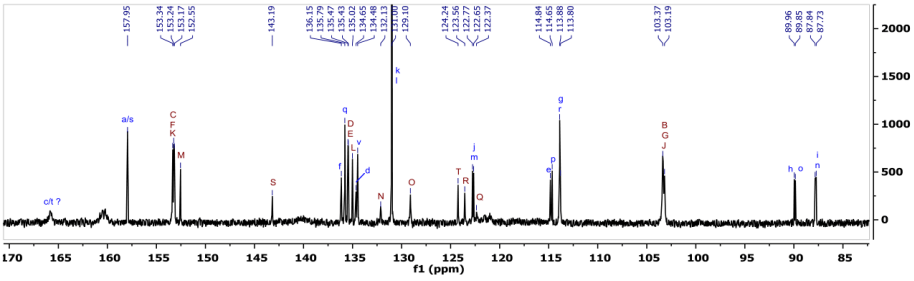

Figure SI 9. Aromatic and acetylenic region and assignment of ^{13}C-NMR spectrum (126 MHz, THF-d_8:D_2O = 4:1, 26 mM) of **1**.

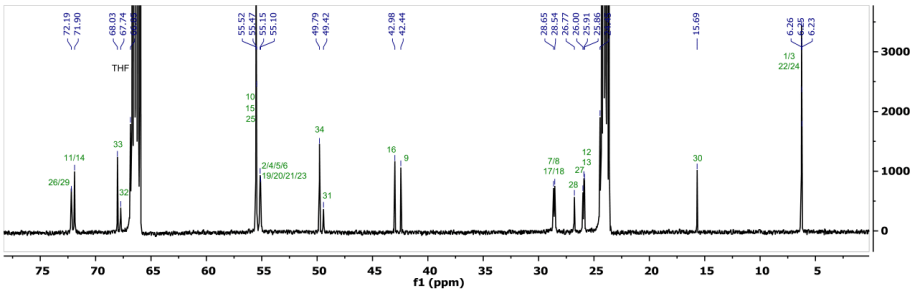

Figure SI 10. Aliphatic region and assignment of ^{13}C-NMR spectra (126 MHz, THF-d_8:D_2O 4:1, 26 mM) of **1**.

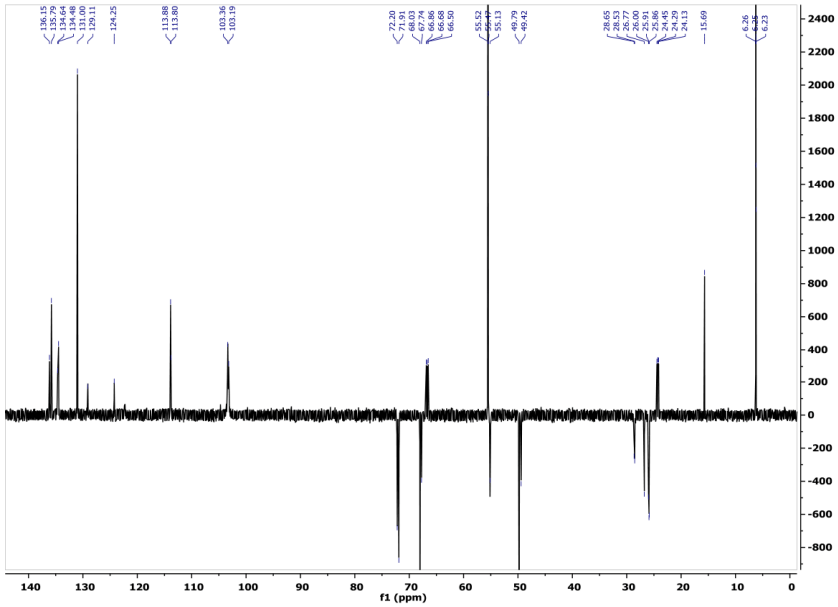

Figure SI 11. DEPT-135 spectrum (126 MHz, THF-d_8:D_2O = 4:1, 26 mM) of **1**.

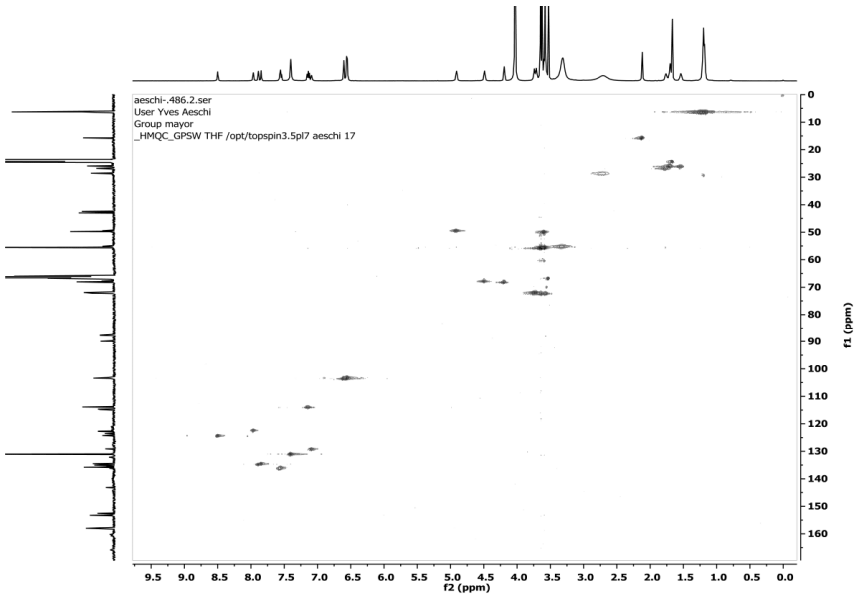

Figure SI 12. HMQC spectrum (126 MHz, THF-d_8:D_2O = 4:1, 26 mM) of **1**.

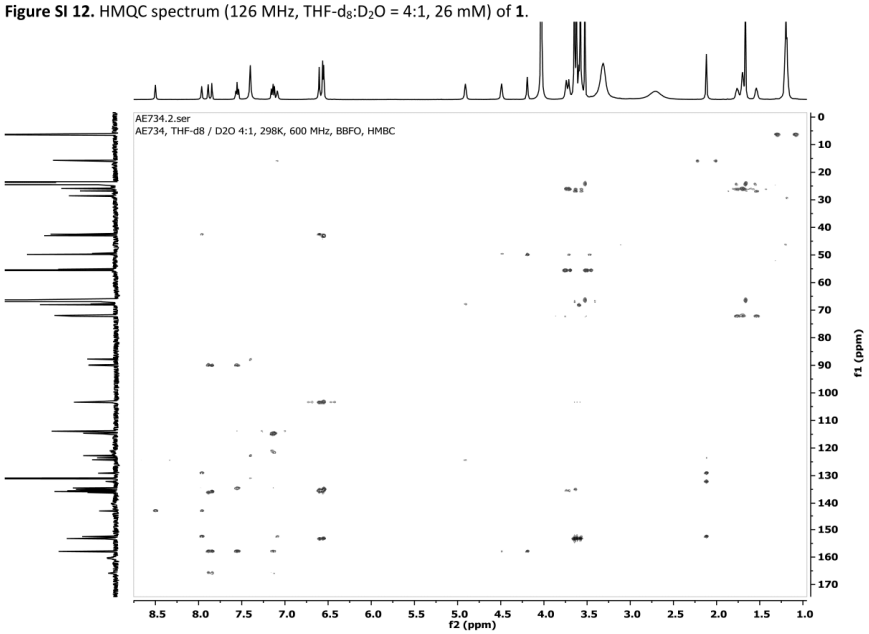

Figure SI 13. HMBC spectrum (126 MHz, THF-d_8:D_2O = 4:1, 26 mM) of **1**.

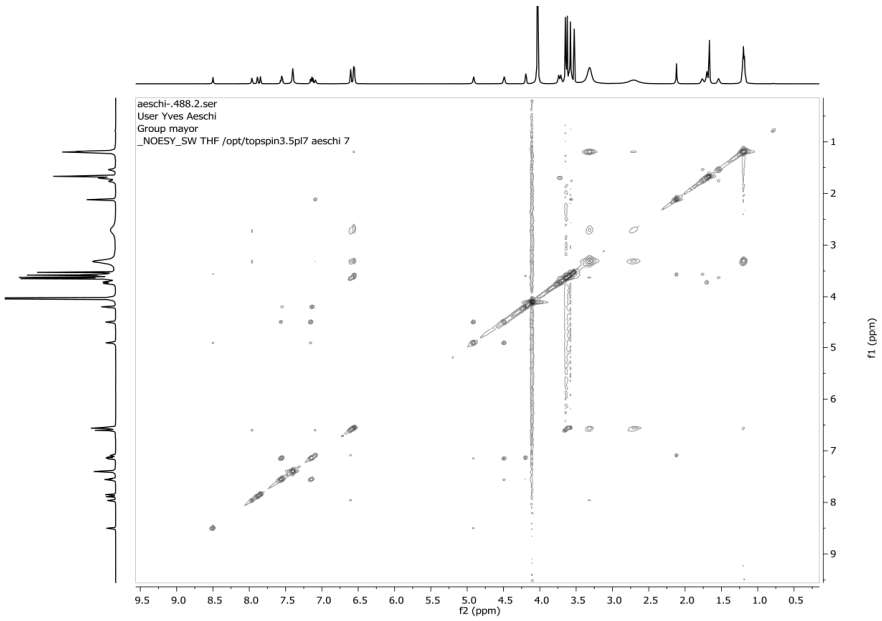

Figure SI 14. NOESY (500 MHz, THF-d_8:D_2O = 4:1, 26 mM) of **1**.

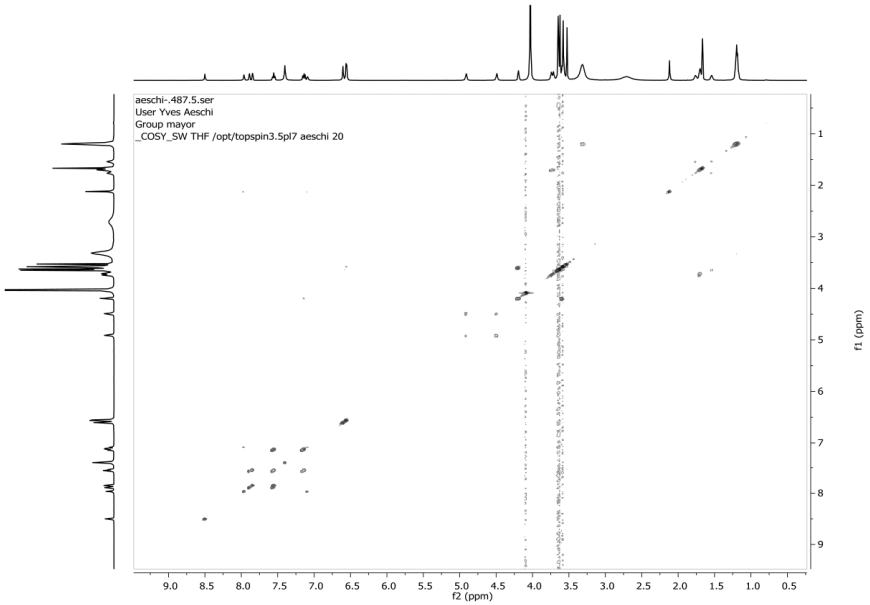

Figure SI 15. COSY (500 MHz, THF-d_8:D_2O =4:1, 26 mM) of **1.**

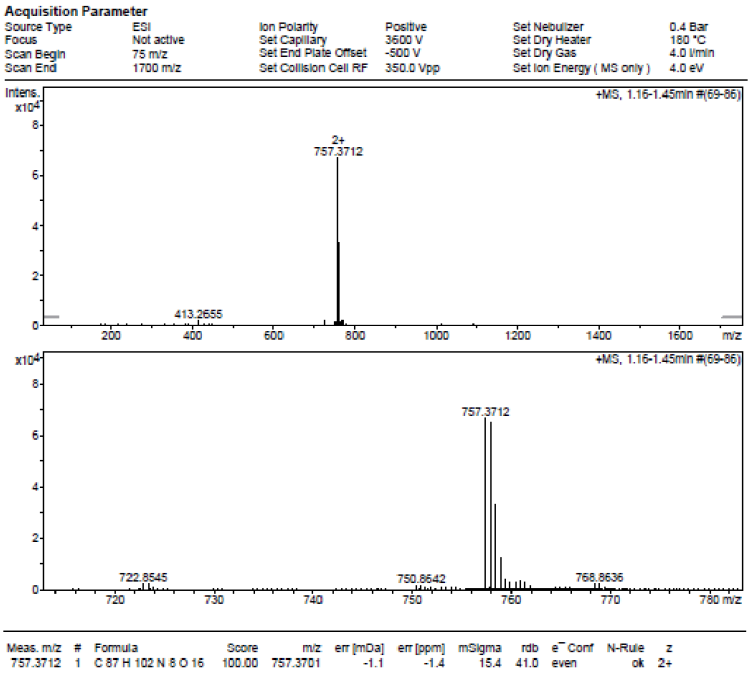

Figure SI 16. ESI-ToF HRMS of **1**.

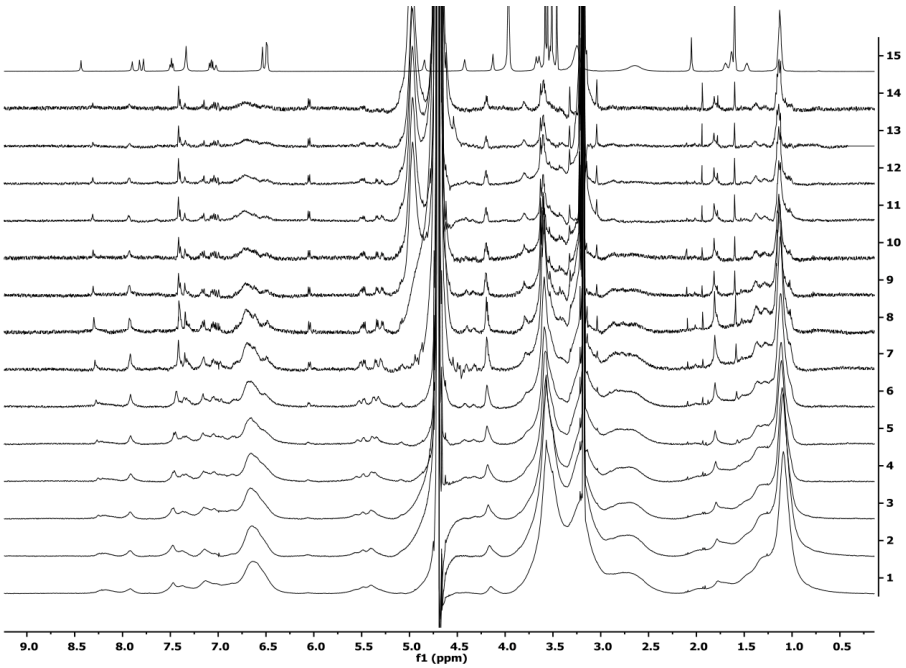

Figure SI 17. Full range ^{1}H-NMR dilution series of **1** (500 MHz, 298 K, MeOD/D_2O 1:4, 1-10 were recorded with 128 scans, 11-14 with 1024 scans, 15 was measured in THF-d_8/D_2O 4:1). 1: 10 mM; 2: 6.7 mM; 3: 4.4 mM; 4: 3.0 mM; 5: 2.0 mM; 6: 1.3 mM; 7: 0.88 mM; 0.59 mM; 9: 0.39 mM; 10: 0.26 mM; 11: 0.17 mM; 12: 0.12 mM; 13: 0.08 mM; 14: 0.05 mM, 15: 26 mM

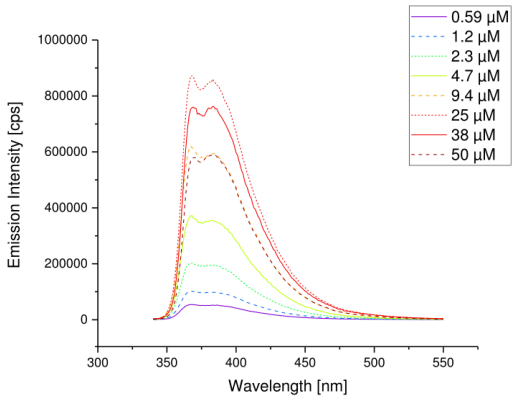

Figure SI 18. Concentration-dependent fluorescence of **1**, selected spectra. An inner filter effect becomes apparent by the lower emission intensity towards higher concentrations due to the absorption of the excitation light at higher optical densities. These emission spectra, after inner filter correction, are the basis for the plots in **Figure SI 19**.

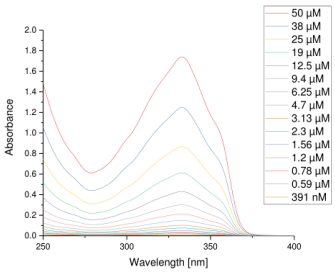

Figure SI 19. Concentration-dependent UV-Vis absorption spectra of **1**. Neither any change in spectral shape nor shift in the absorption maximum was observed. The optical density at 332 nm was used for inner filter correction of the emission intensity (**Figure SI 20**).

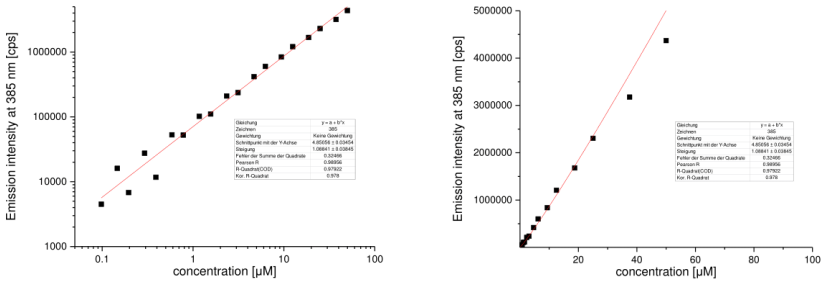

Figure SI 20. Fluorescence aggregation studies of **1** in 1:4 MeOH/H_2O from 0.1 µM to 50 µM (λ_{ex} = 332 nm) (combination of two individual dilution series). Emission intensity vs. concentration; left: doubly logarithmic plot; right: plot with linear axes. No critical aggregation concentration was deduced from these plots. Measurements tended to stray at low concentration. Emission intensities above 1 µM were corrected for the inner filter effect according to the following equation.[1]

$$\frac{F_0}{F} = \frac{2.303 * A_{ex} * \Delta x * 10^{A_{ex} * x}}{1 - 10^{-A_{ex} * \Delta x}}$$

F_0 : Ideal emission intensity

F : Measured emission intensity

A_{ex} : Absorption at excitation wavelength

Δx : Width of the emission beam (0.25 mm)

x : Optical path length until emergence of the emission beam (0.5 cm)

[1] B. C. MacDonald, S. J. Lvin, H. Patterson, *Anal. Chim. Acta* **1997**, *338*, 155–162.

Characterization of 2

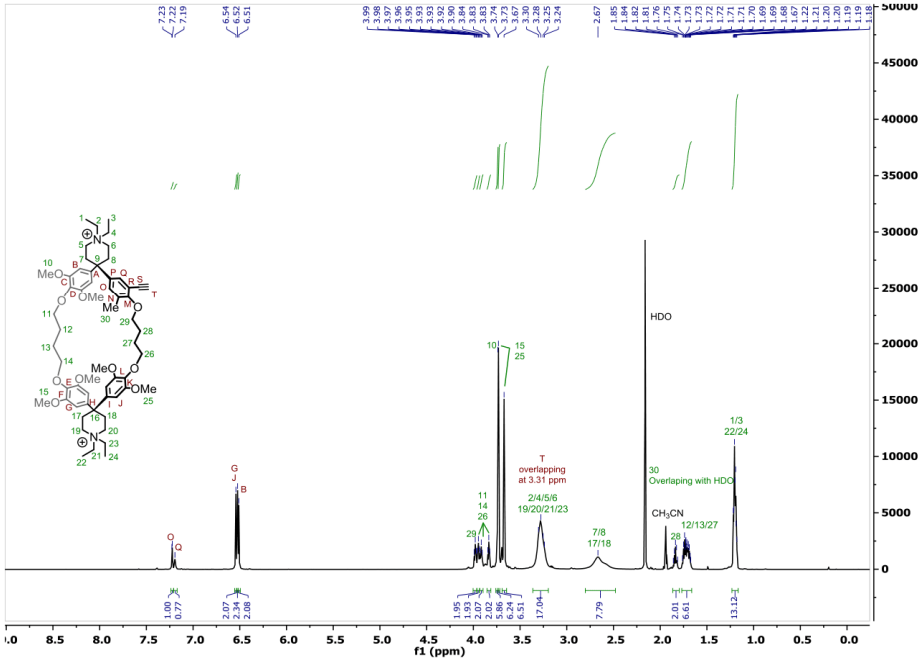

Figure SI 21. ^{1}H-NMR (600 MHz, CD_3CN) spectrum of **2** with full assignment.

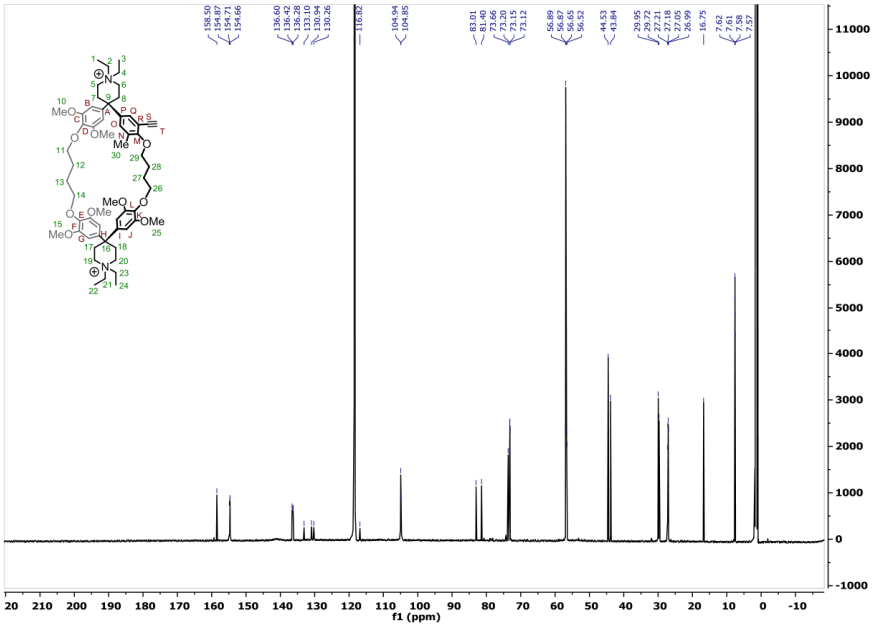

Figure SI 22. Full range ^{13}C-NMR (126 MHz, CD_3CN) spectrum of **2**.

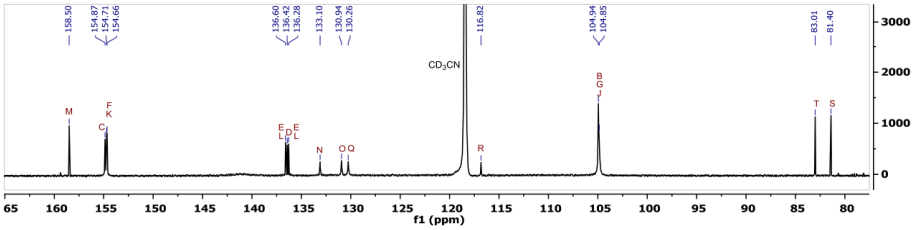

Figure SI 23. ^{13}C-NMR spectrum (126 MHz, CD_3CN) of **2**, aromatic and acetylenic regions.

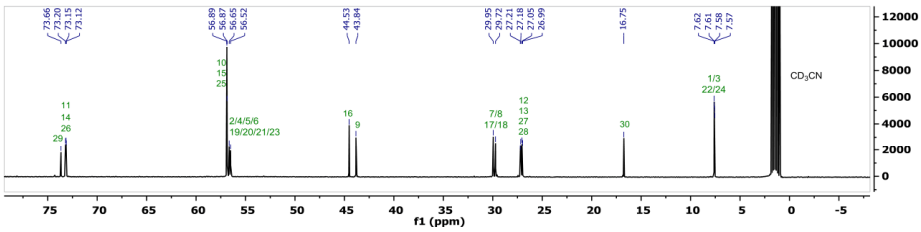

Figure SI 24. ^{13}C-NMR spectrum (126 MHz, CD_3CN) of **2**, aliphatic region.

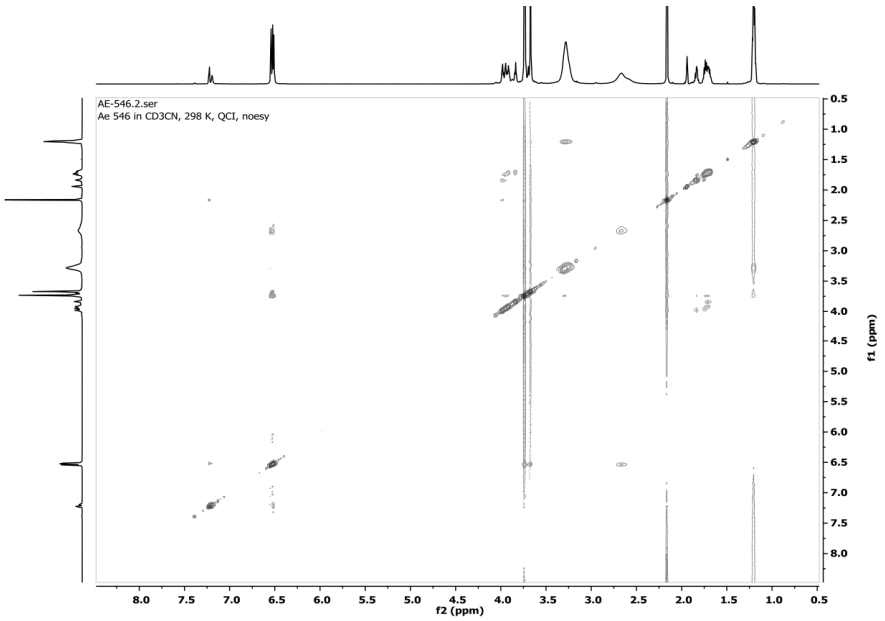

Figure SI 25. NOESY (600 MHz, CD_3CN) of **2**.

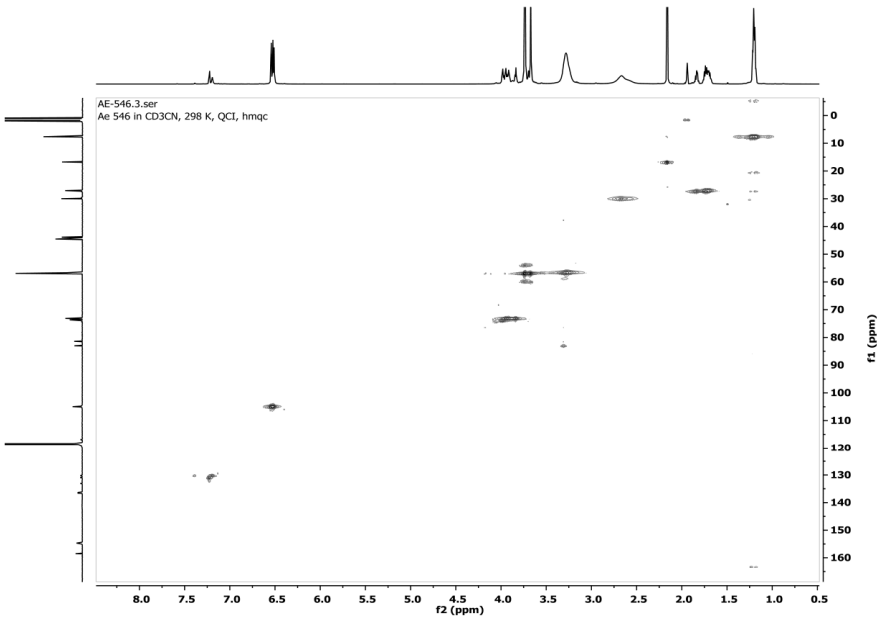

Figure SI 26. HMQC spectrum (600 MHz, CD_3CN) of **2**.

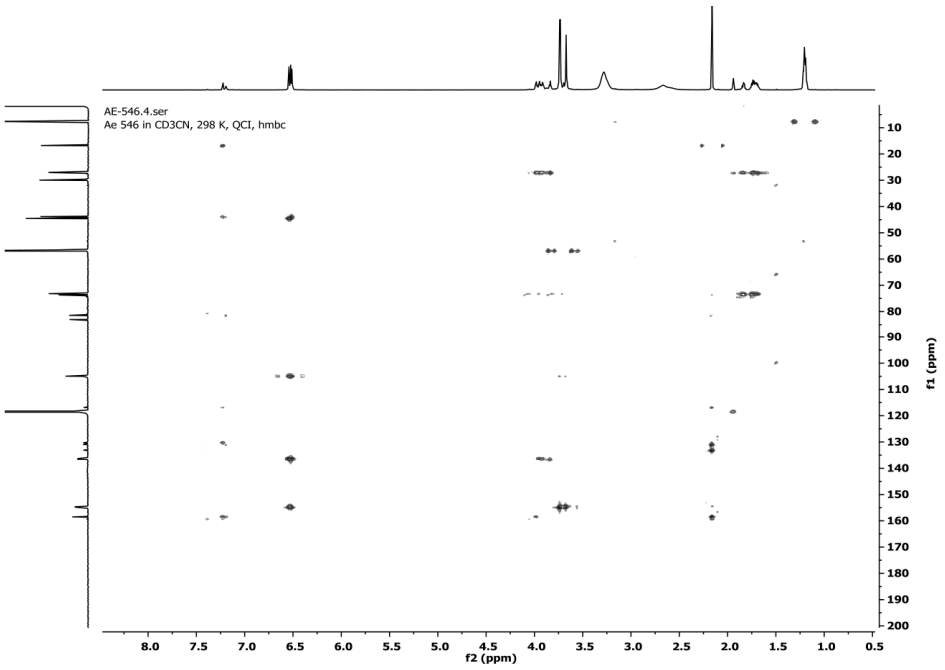

Figure SI 27. HMBC spectrum (600 MHz, CD_3CN) of **2**.

Mass Spectrum SmartFormula Report

Analysis Info

Analysis Name	E:\new acq data for data analysis\Ae MeOCy_ac_q 003.d	Acquisition Date	27.07.2016 16:56:38
Method	hn Direct_Infusion_pos mode_75-1700 mid 4eV.m	Operator	hn
Sample Name	Yves Aeschi	Instrument / Ser#	maXis 4G 21243
Comment	Ae MeOCy ac q, ca. 10 ug/ml MeOH		

Acquisition Parameter

Source Type	ESI	Ion Polarity	Positive	Set Nebulizer	0.4 Bar
Focus	Not active	Set Capillary	3600 V	Set Dry Heater	180 °C
Scan Begin	75 m/z	Set End Plate Offset	-500 V	Set Dry Gas	4.0 l/min
Scan End	1700 m/z	Set Collision Cell RF	350.0 Vpp	Set Ion Energy (MS only)	4.0 eV

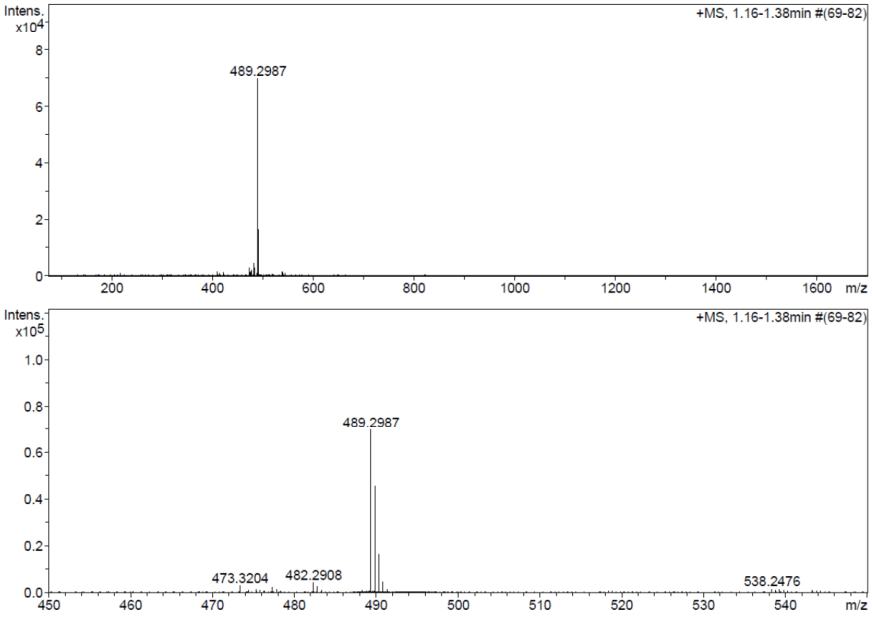

Meas. m/z	#	Formula	Score	m/z	err [mDa]	err [ppm]	mSigma	rdb	e⁻ Conf	N-Rule	z
489.2987	1	C 59 H 82 N 2 O 10	100.00	489.2979	-0.8	-1.7	4.8	20.0	even	ok	2+

Figure SI 28. ESI-ToF HRMS of **2**.

Characterization of 3 and 3 * 2 Na

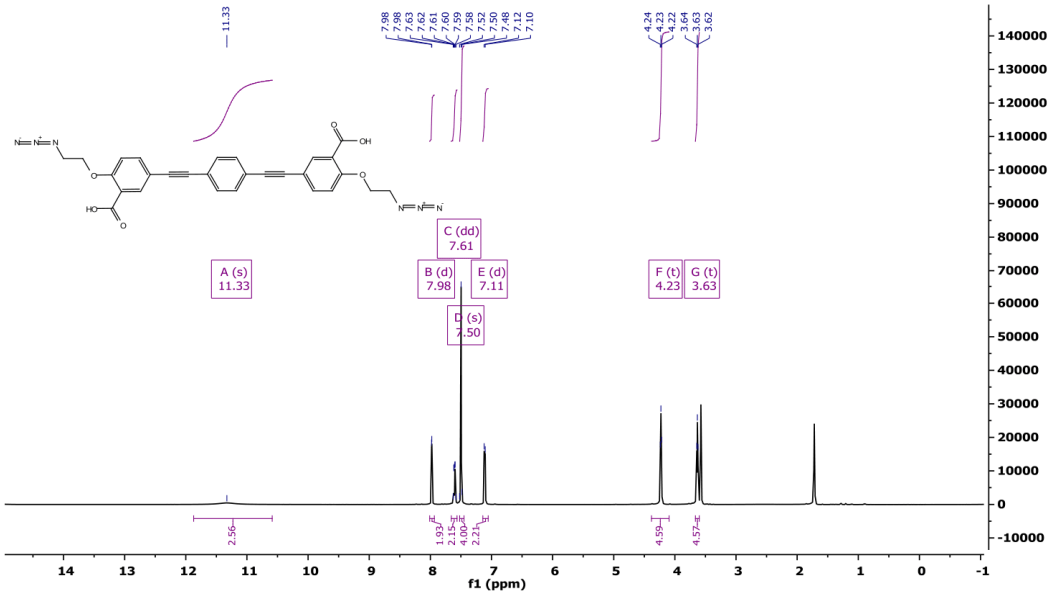

Figure SI 29. ^{1}H-NMR spectrum (500 MHz, THF-d_8) of **3**.

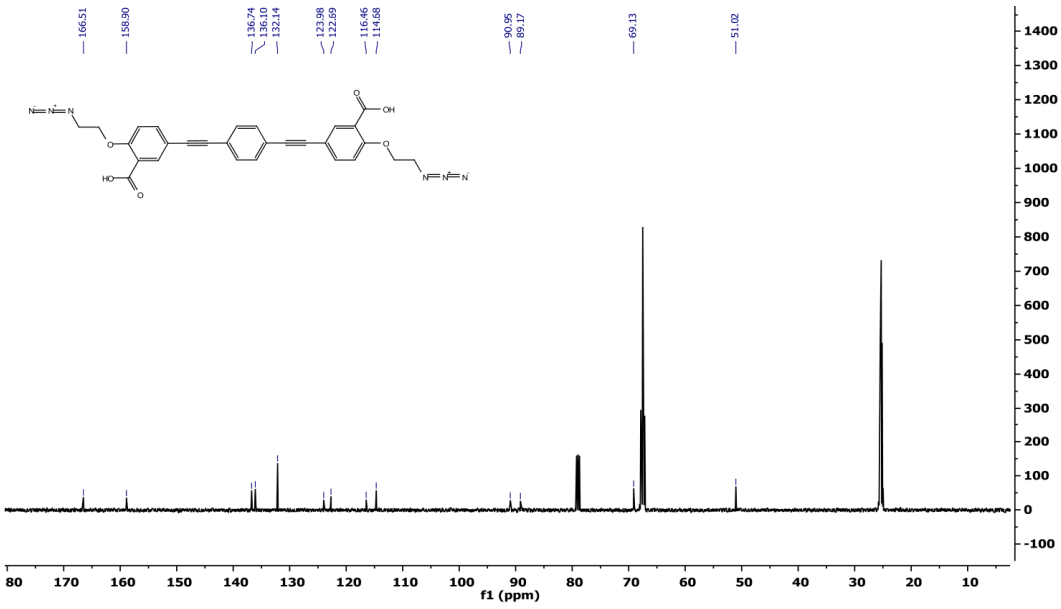

Figure SI 30. ^{13}C-NMR spectrum (101 MHz, THF-d_8) of **3.**

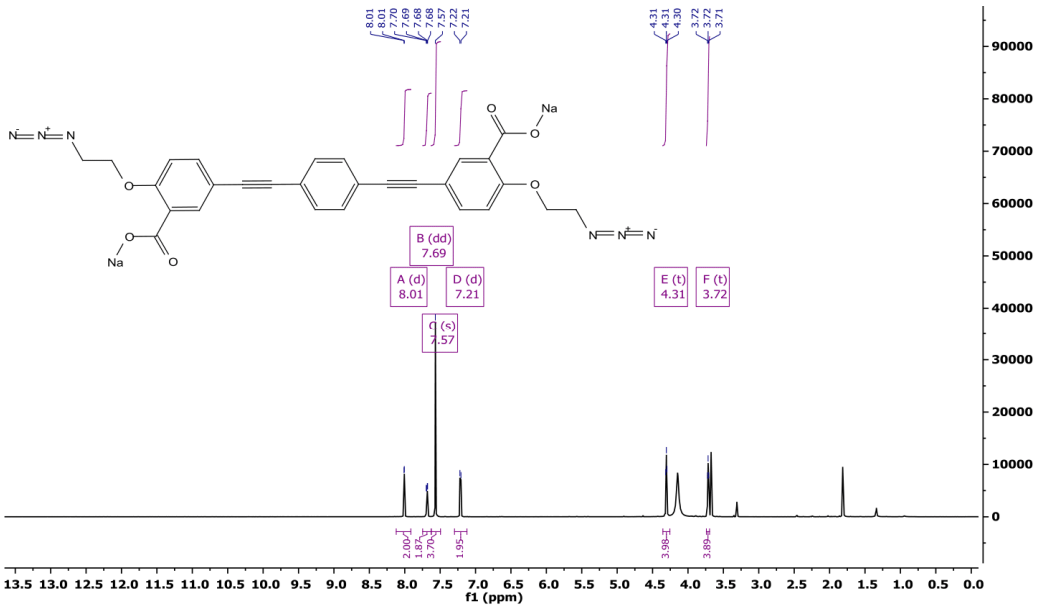

Figure SI 31. ^{1}H-NMR spectrum (600 MHz, THF-d_8/MeOD = 3:1) of **3 * 2 Na.**

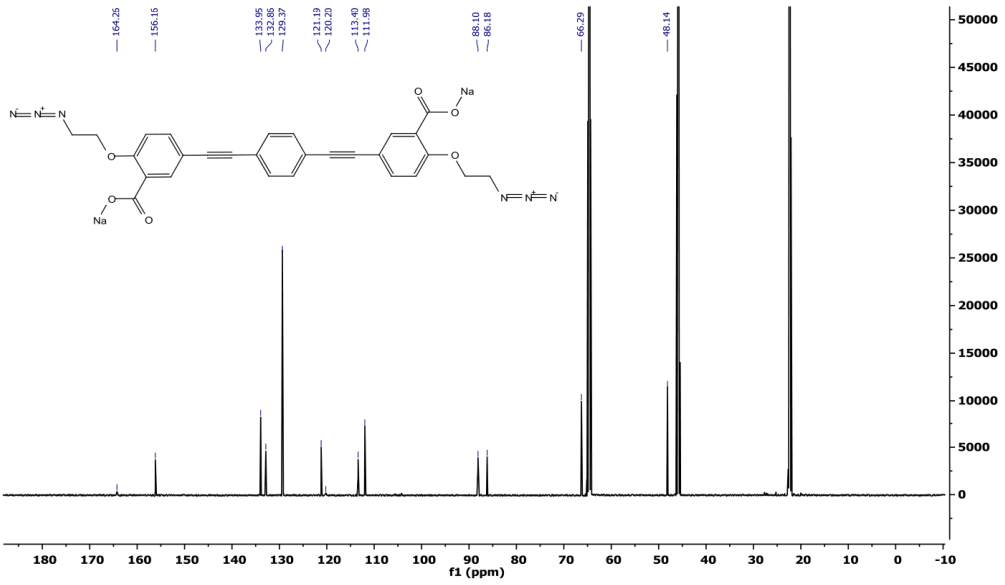

Figure SI 32. ^{13}C-NMR spectrum (126 MHz, THF-d_8/MeOD = 3:1) of **3 * 2 Na.**

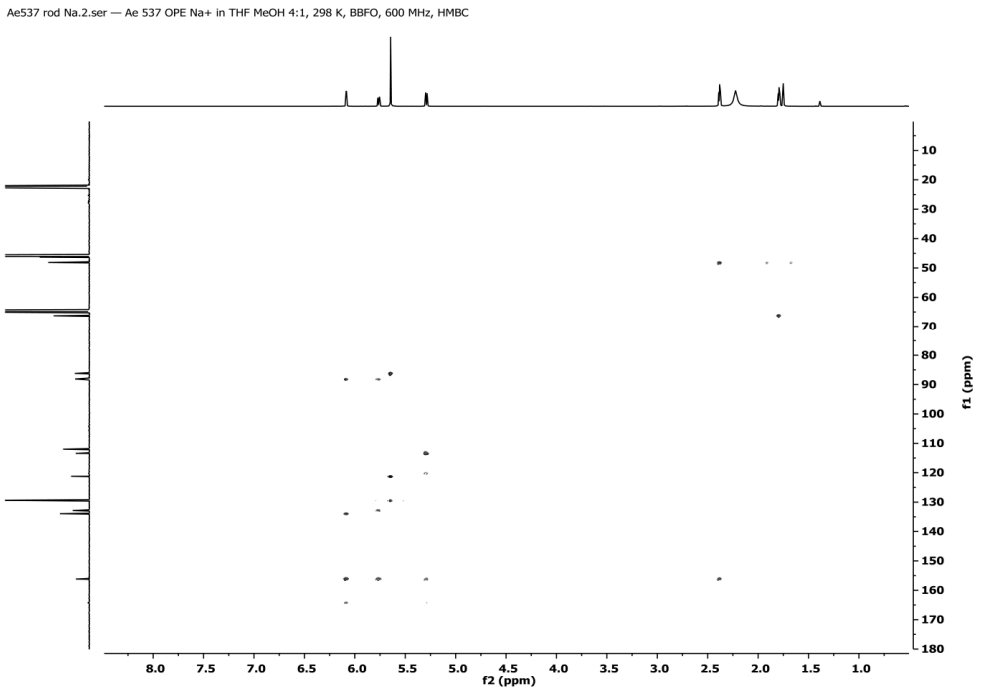

Figure SI 33. HMBC spectrum (600 MHz, THF-d_8/MeOD = 3:1) of **3 * 2 Na.**

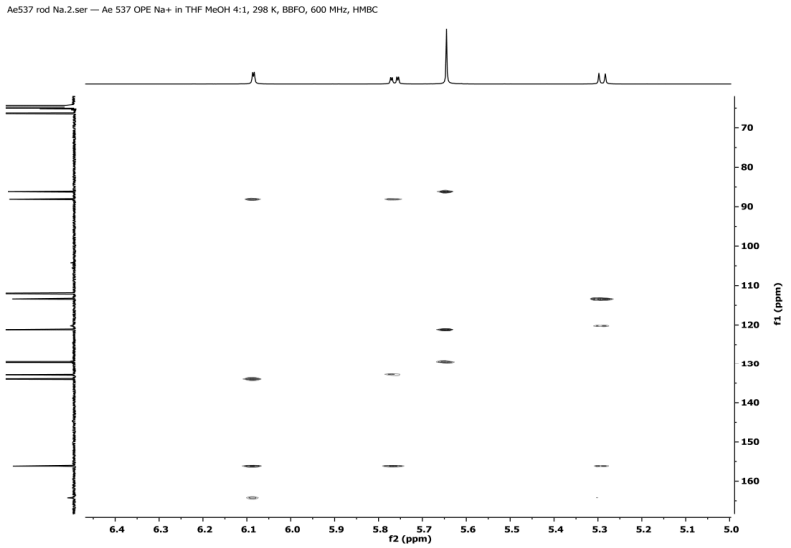

Figure SI 34. HMBC spectrum (600 MHz, THF-d_8/MeOD = 3:1) of **3 * 2 Na**, which revealed the missing ^{13}C-resonance with a low intensity at 120.2 ppm.

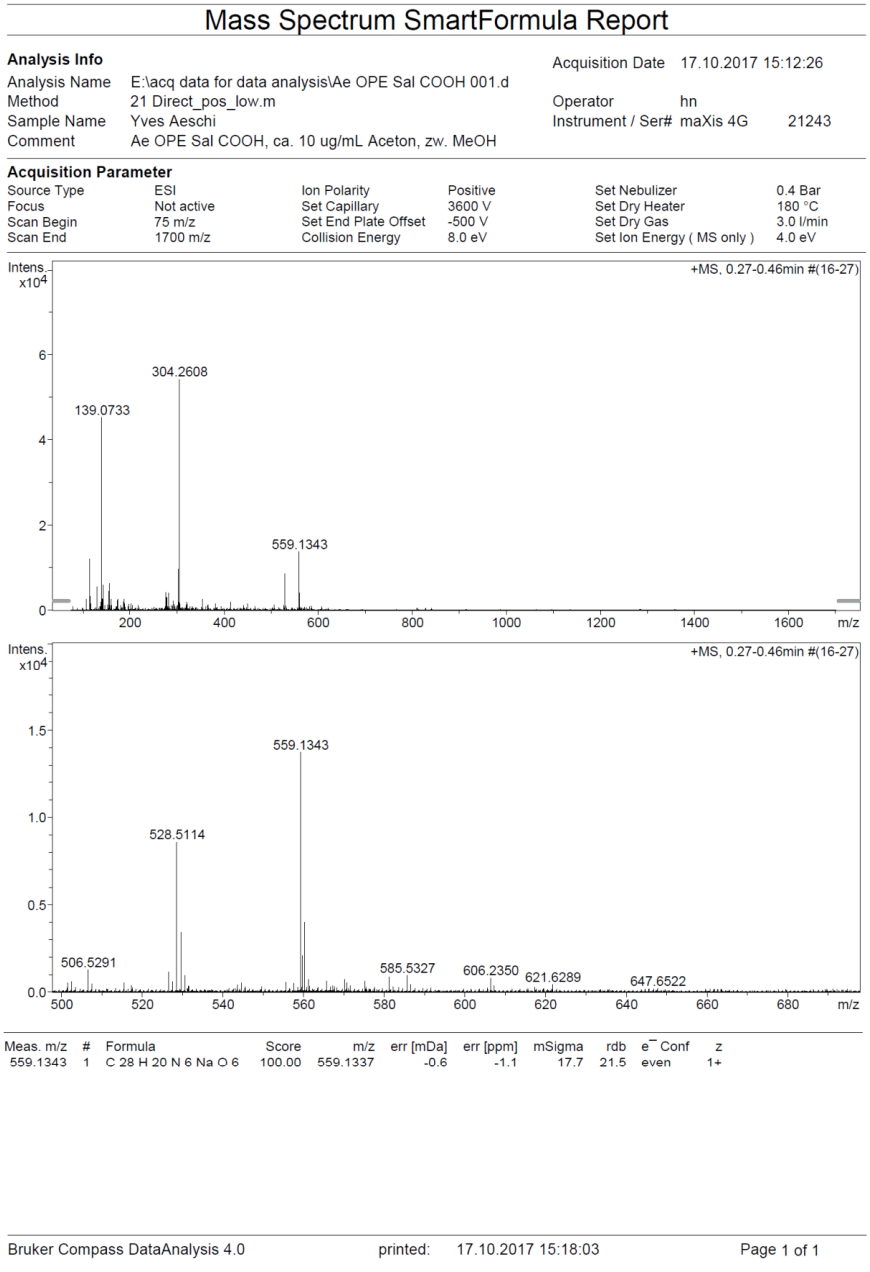

Figure SI 35. ESI-ToF HRMS of **3**.

Characterization of 4

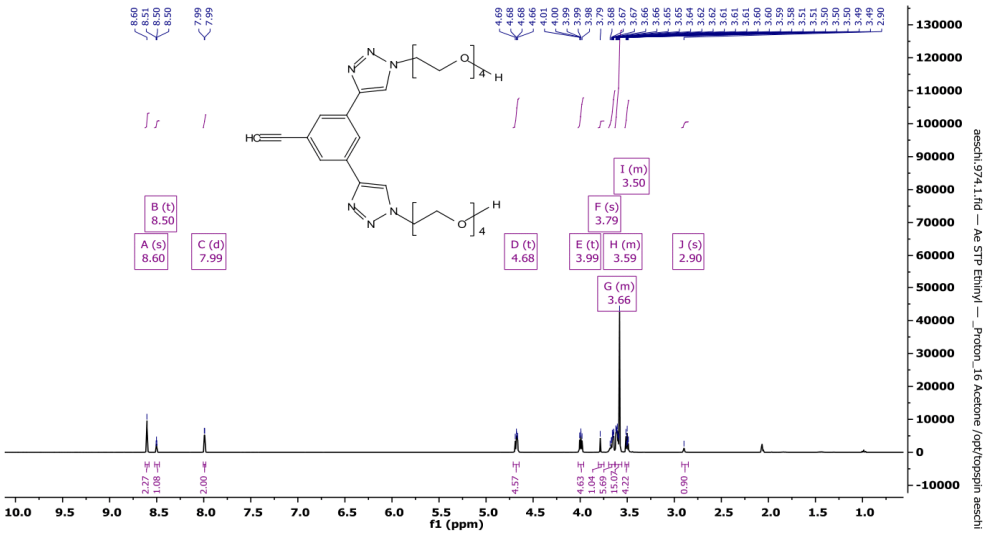

Figure SI 36. ^{1}H-NMR spectrum (400 MHz, Acetone-d_6) of **4**.

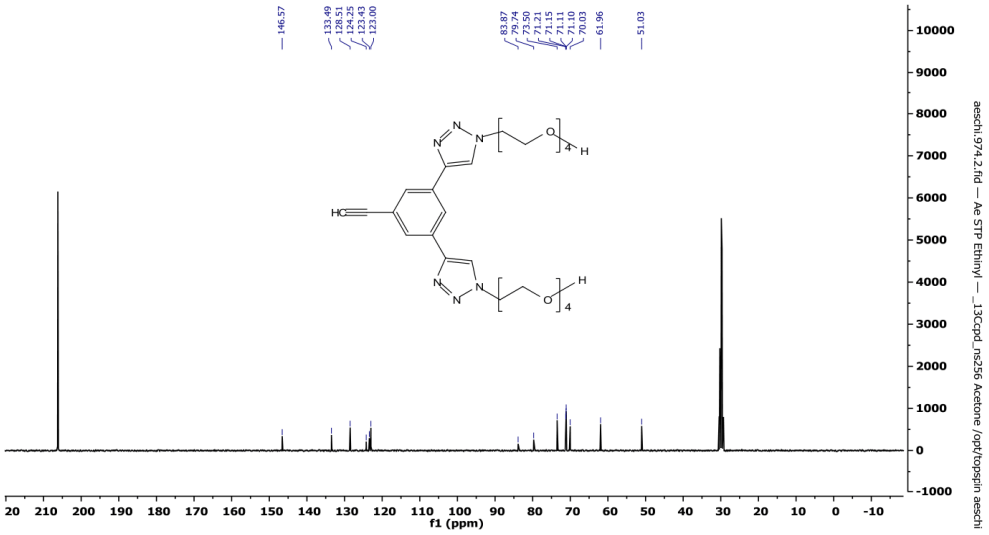

Figure SI 37. ^{13}C-NMR spectrum (101 MHz, Acetone-d_6) of **4**.

Acquisition Parameter

Source Type	ESI	Ion Polarity	Positive	Set Nebulizer	0.4 Bar
Focus	Not active	Set Capillary	3600 V	Set Dry Heater	180 °C
Scan Begin	75 m/z	Set End Plate Offset	-500 V	Set Dry Gas	4.0 l/min
Scan End	1700 m/z	Collision Energy	8.0 eV	Set Ion Energy (MS only)	4.0 eV

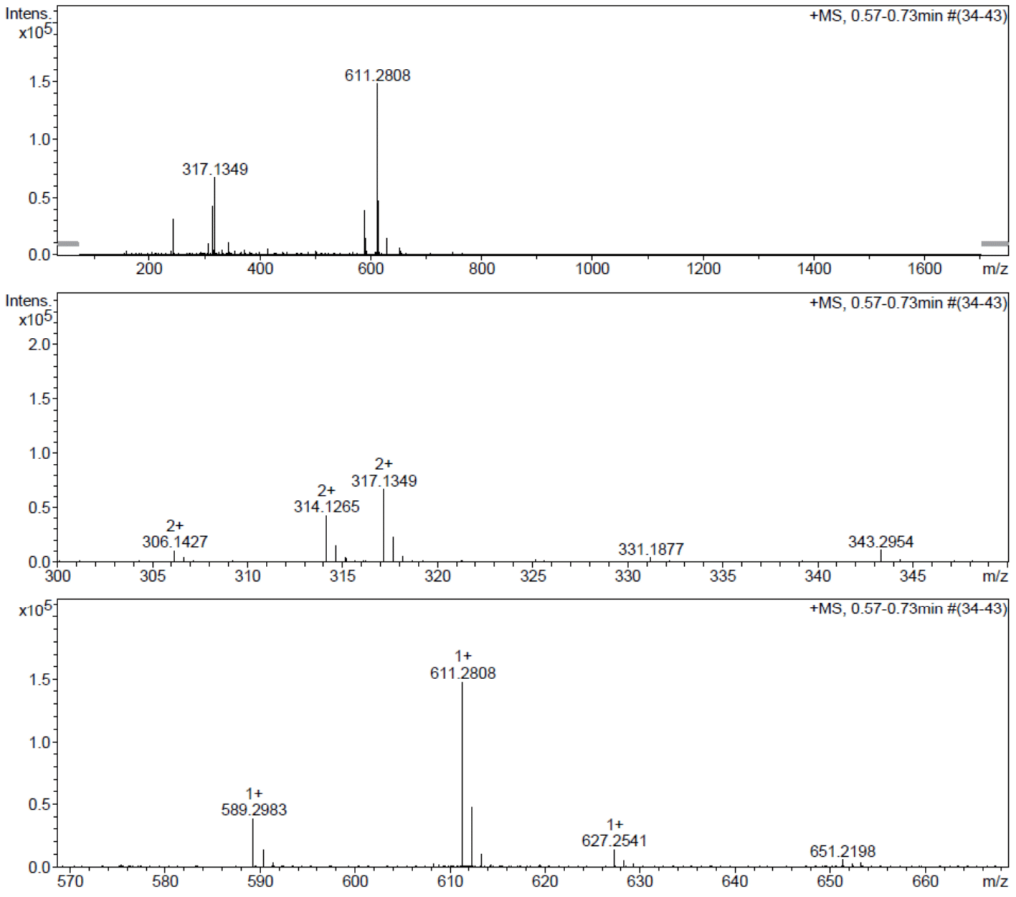

Meas. m/z	#	Formula	Score	m/z	err [mDa]	err [ppm]	mSigma	rdb	e¯ Conf	z
306.1427	1	C 28 H 41 N 6 Na O 8	100.00	306.1436	0.9	2.9	31.3	11.0	even	2+
314.1265	1	C 24 H 43 K N 6 Na 2 O 8	100.00	314.1282	1.7	5.5	37.7	5.0	even	
317.1349	1	C 28 H 40 N 6 Na 2 O 8	100.00	317.1346	-0.3	-0.9	2.0	11.0	even	
589.2983	1	C 28 H 41 N 6 O 8	100.00	589.2980	-0.2	-0.4	14.0	11.5	even	1+
611.2808	1	C 28 H 40 N 6 Na O 8	100.00	611.2800	-0.8	-1.3	5.0	11.5	even	
627.2541	1	C 28 H 40 K N 6 O 8	100.00	627.2539	-0.2	-0.3	4.9	11.5	even	

Figure SI 38. ESI-ToF HRMS of **4**.

Preparative and analytical HPLC details of 5

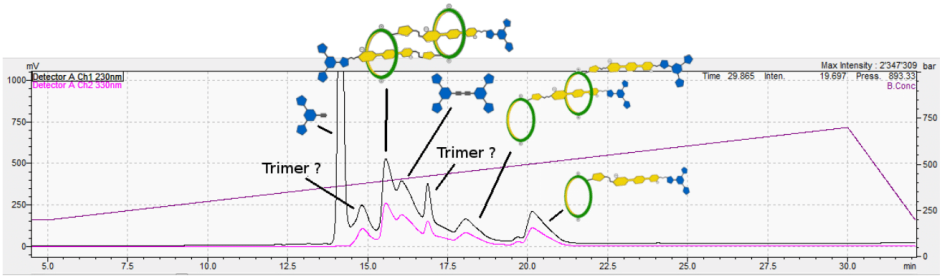

Figure SI 39. Preparative HPLC chromatogram (RP-C18, H_2O:CH_3CN = 20-70 % in 25 min, 0.1 % HCOOH) of the crude mixture of the daisy chain stoppering reaction.

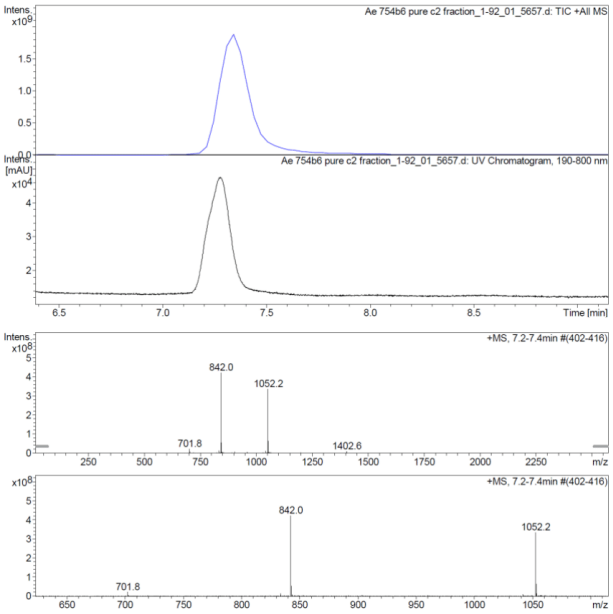

Figure SI 40. Analytical RP-C18/ESI-MS chromatogram of **5-[*c2*]**.

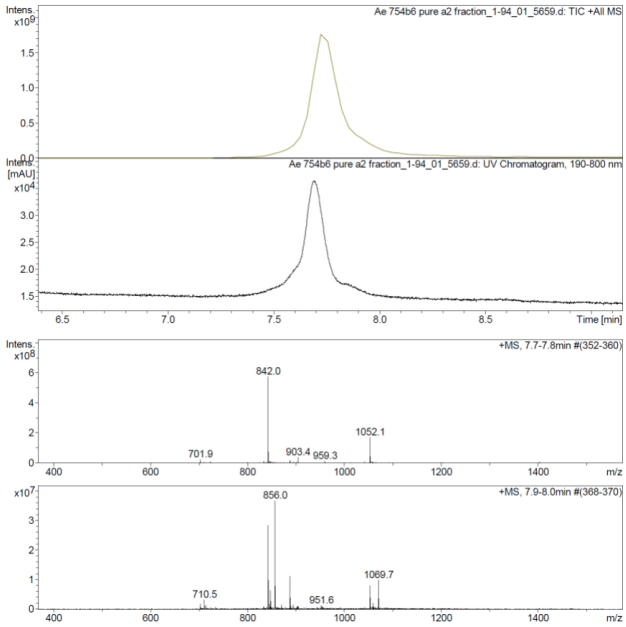

Figure SI 41. Analytical RP-C18/ESI-MS chromatogram of **5-[*α*2]**.

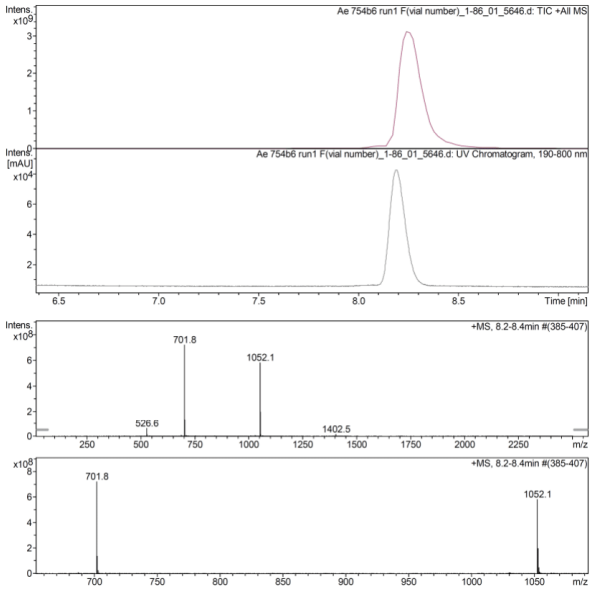

Figure SI 42. Analytical RP-C18/ESI-MS chromatogram of **5-[*α*1]**.

Characterization of the daisy chains 5-[*a*1]/[*a*2]/[*c*2]

5-[*c*2]

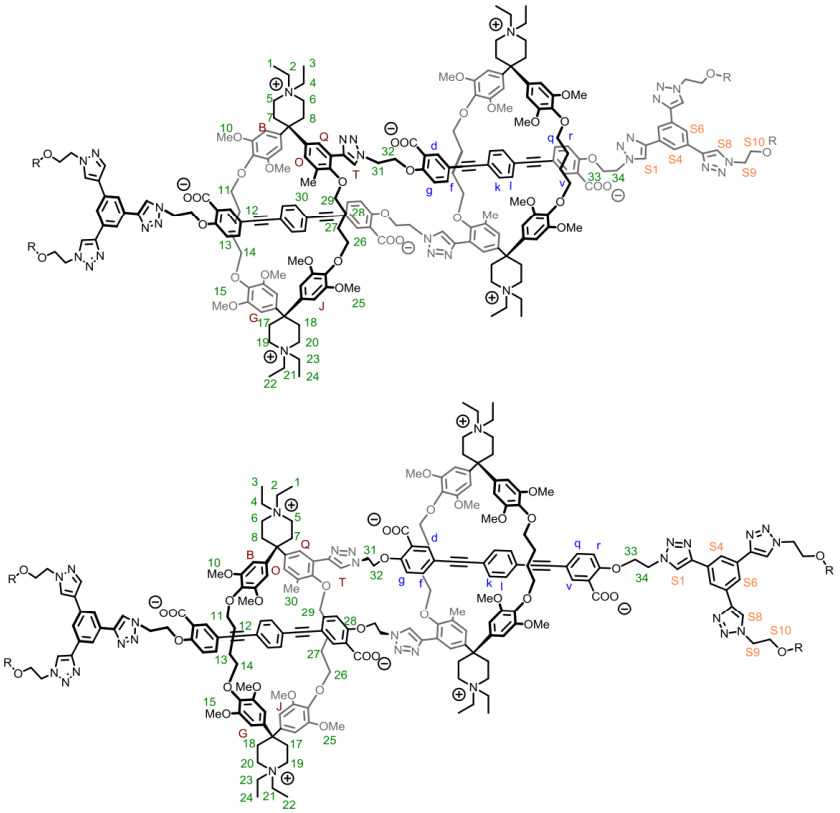

Figure SI 43. Molecular structures of the **5-[*c*2]**-diasteromers including atom numbering, C_i-symmetric meso (top) and C_2-symmetric chiral (bottom).

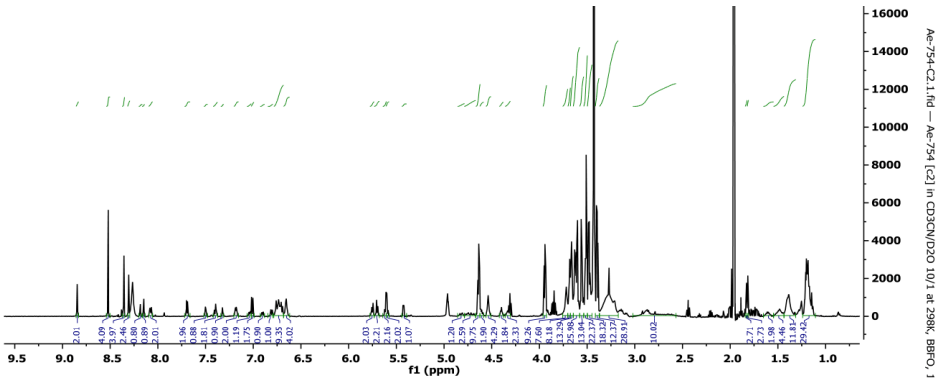

Figure SI 44. Full range ^{1}H-NMR spectrum (600 MHz, 10:1 = CD_3CN/D_2O) of **5-[*c*2]**.

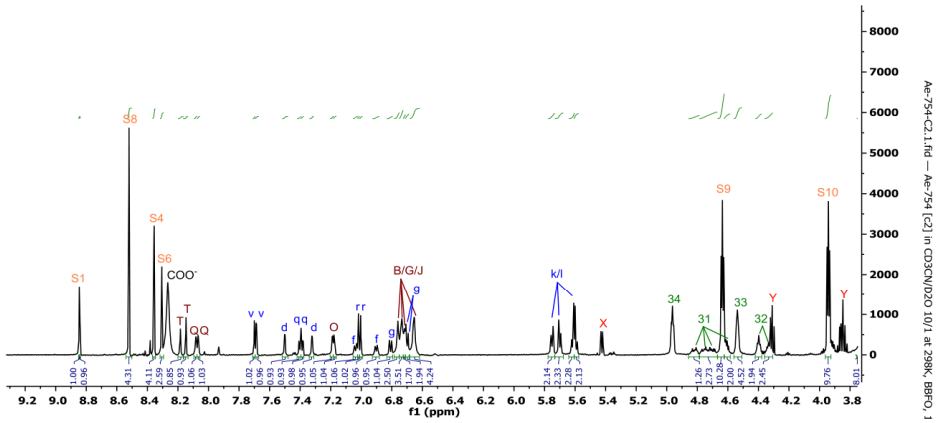

Figure SI 45. ^{1}H-NMR spectrum (600 MHz, 10:1 = CD_3CN/D_2O), aromatic & low field aliphatic region of **5-[*c*2]**.

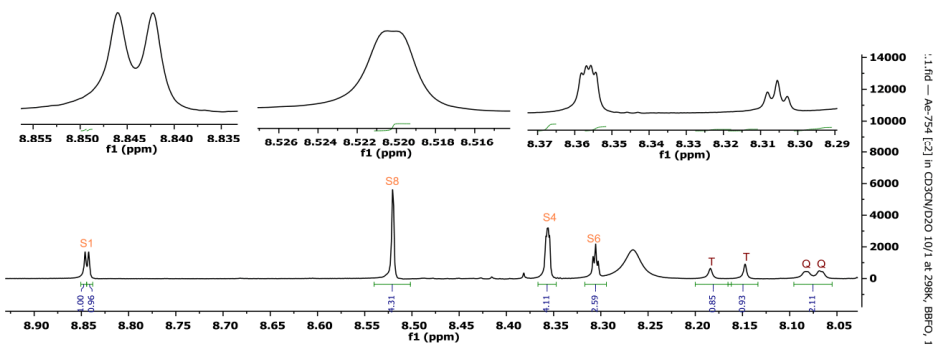

Figure SI 46. ^{1}H-NMR spectrum (600 MHz, 10:1 = CD_3CN/D_2O), low field aromatic peaks of **5-[*c*2]** to visualize the doubling of the stopper peaks due to the presence of two diastereomers.

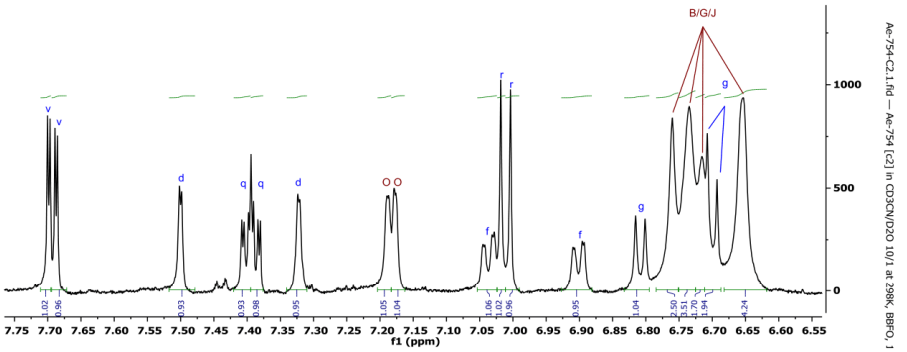

Figure SI 47. ^{1}H-NMR spectrum (600 MHz, 10:1 = CD_3CN/D_2O), aromatic region of **5-[*c2*]**. Most aromatic peaks are doubled and the differences of chemical shift between doubled grows smaller, the more remote from the molecular center they are located.

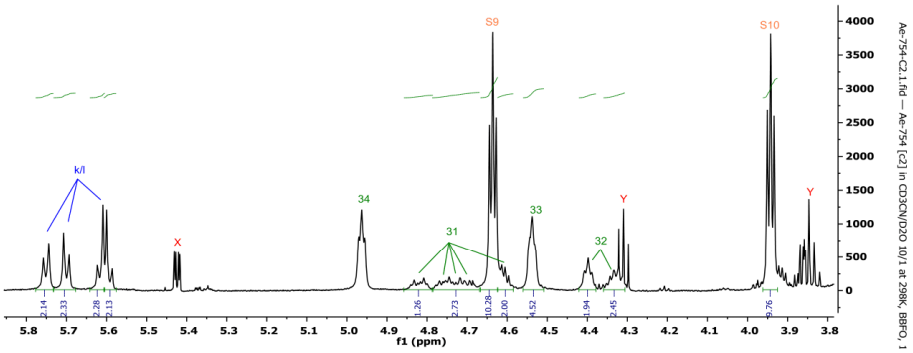

Figure SI 48. ^{1}H-NMR spectrum (600 MHz, 10:1 = CD_3CN/D_2O), high field aromatic region and low-field aliphatics of **5-[*c2*]**. X could not be assigned and did not exhibit any cross-peaks in the NOESY spectrum, DOSY revealed the diffusion coefficient of the same order of magnitude as the formate and solvent peaks. Y belongs to a trace amount of the acetylene-homocoupled stopper **4**.

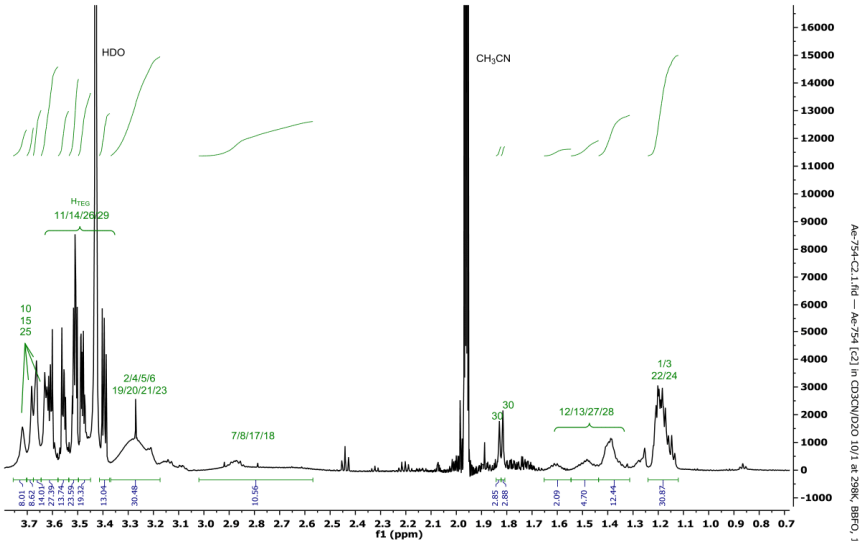

Figure SI 49. ^{1}H-NMR spectrum (600 MHz, 10:1 = CD_3CN/D_2O), high field aromatic region and low-field aliphatics of **5-[*c2*]**.

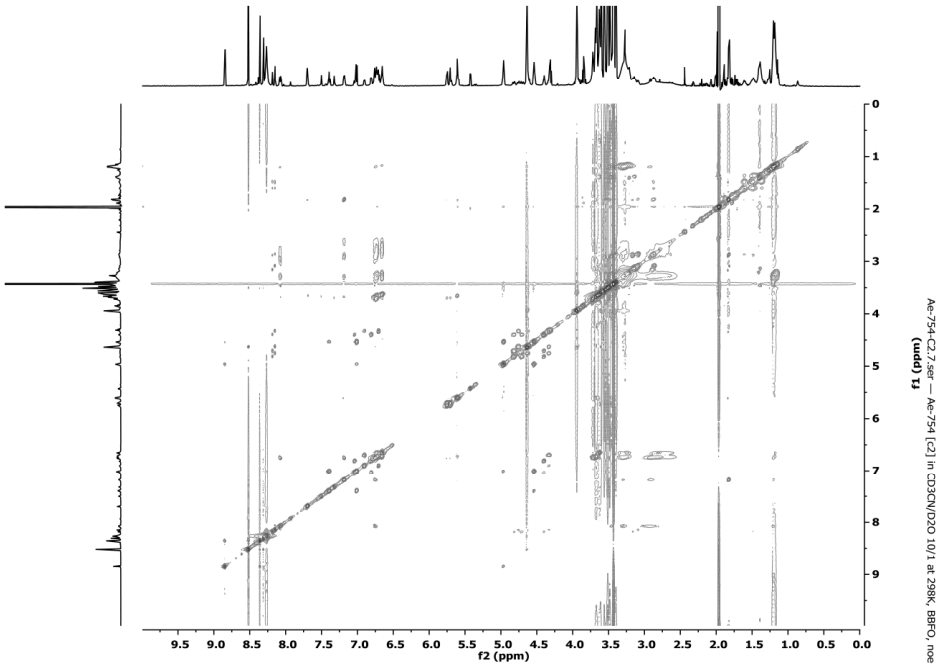

Figure SI 50. Full range NOESY (600 MHz, 10:1 CD_3CN/D_2O) of **5-[*c2*]**.

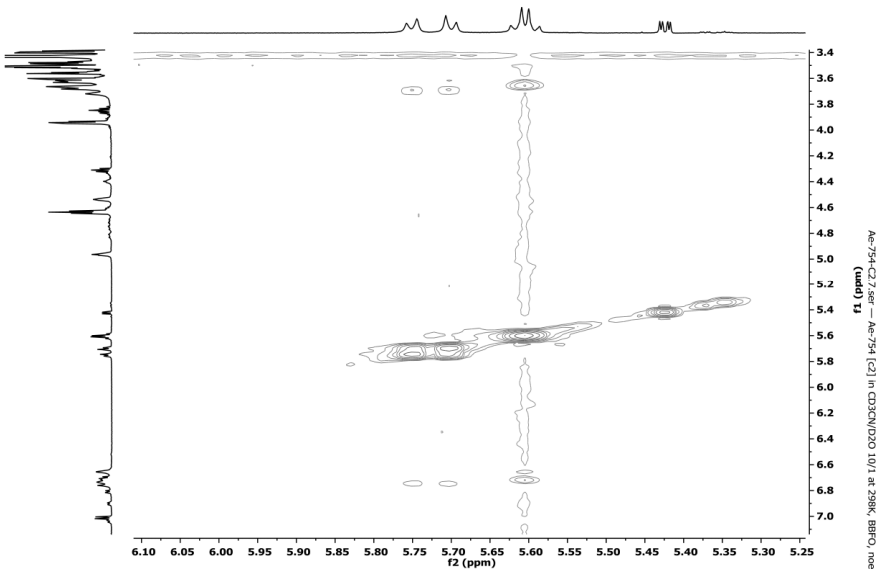

Figure SI 51. NOESY of **5-[*c2*]** of the phenylene protons k & l to B, G and J (cyclophane aryl) and 10, 15, 25 (cyclophane methoxy).

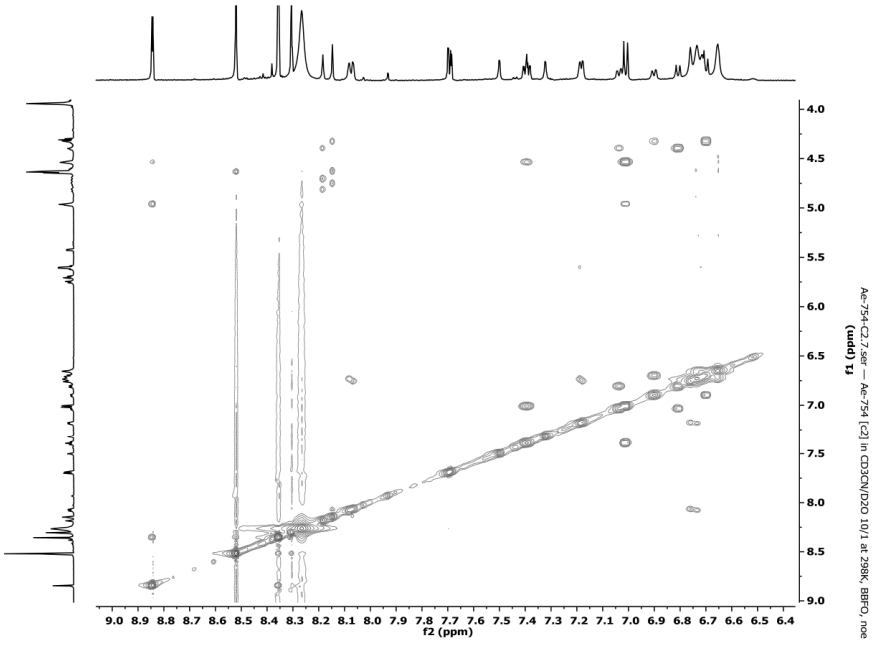

Figure SI 52. NOESY of **5-[*c2*]**, aromatic region.

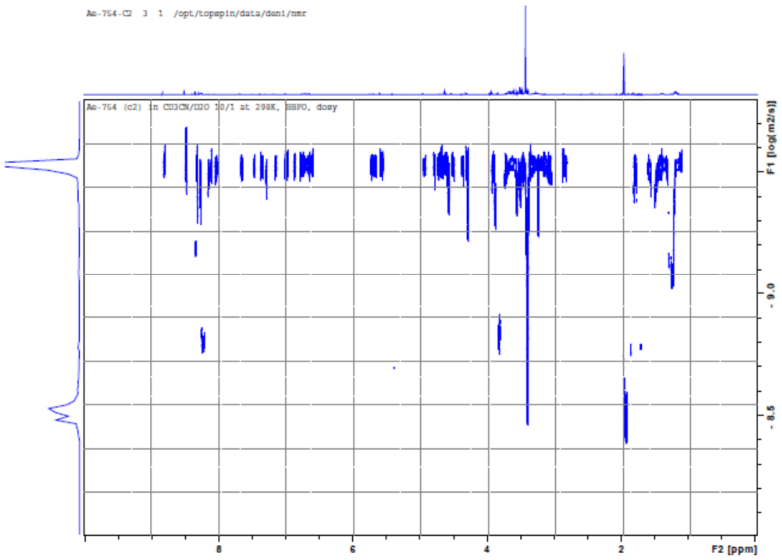

Figure SI 53. DOSY-NMR (600 MHz, CD_3CN/D_2O = 10:1)**.** of **5-[*c2*].**

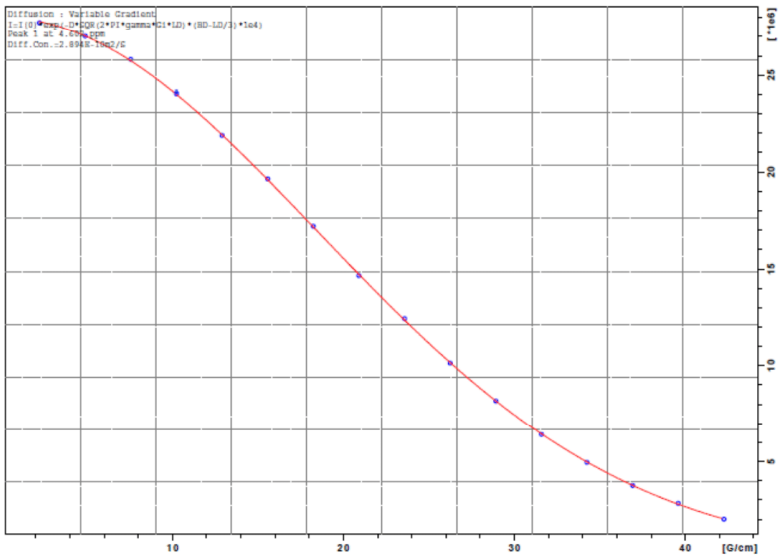

Figure SI 54. Fitting curve of the DOSY-NMR. A diffusion coefficient of 2.90 * 10^{-10} m^2s^{-1} was obtained, as evaluated from the triplet S9 at about 4.6 ppm.

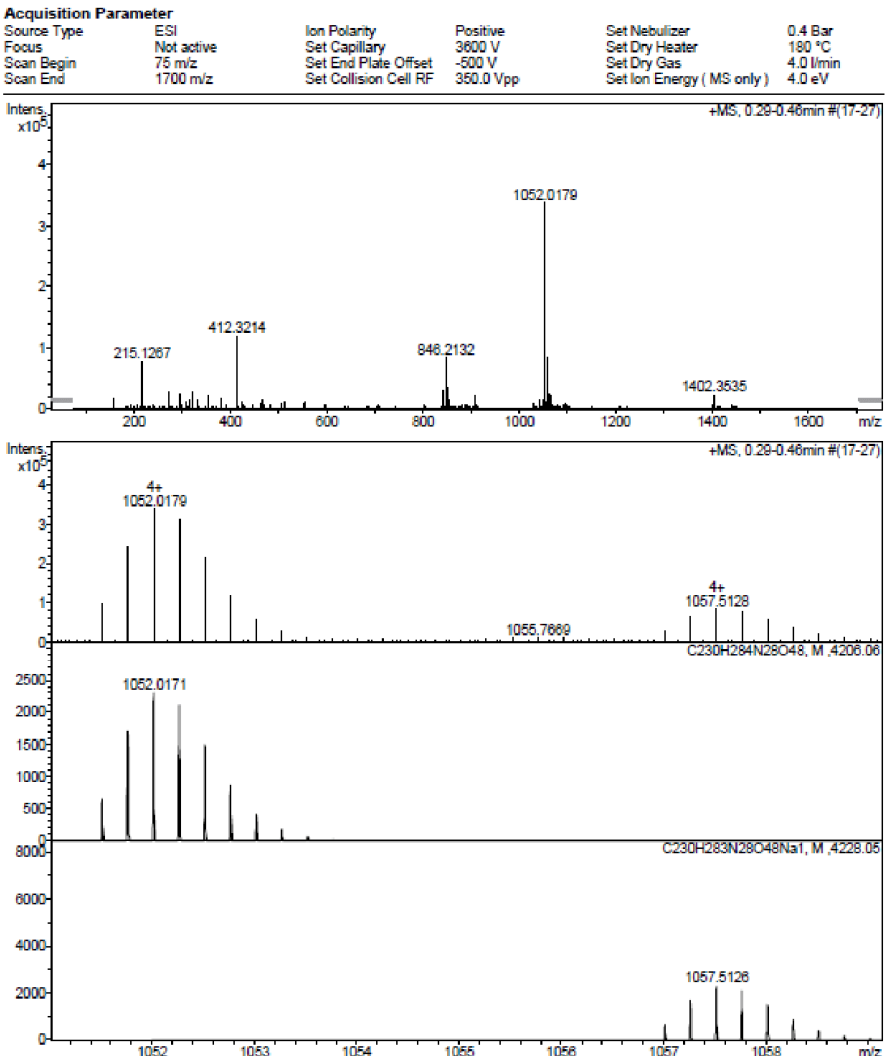

Figure SI 55. Full-range ESI-TOF HRMS spectrum (top) of **5-[*c*2]** with simulated isotopic patterns of $[M+4H]^{4+}$ and $[M+3H+Na]^{4+}$ (bottom).

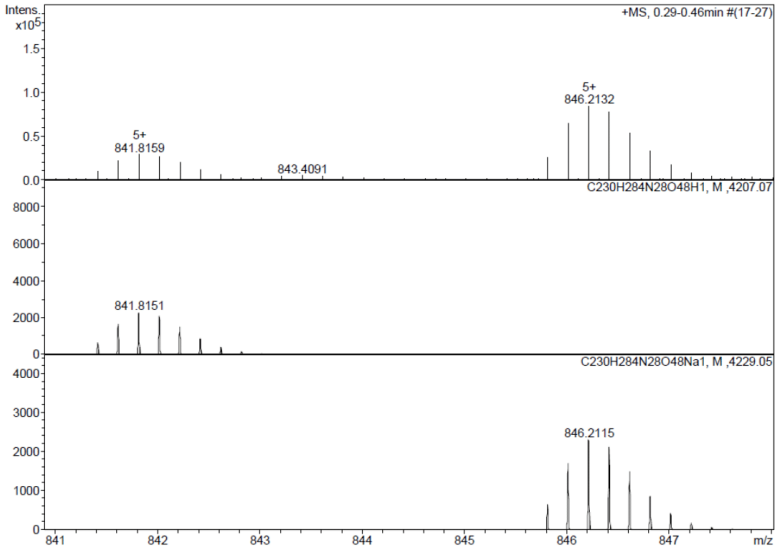

Figure SI 56. Partial ESI-TOF HRMS spectrum (top) of **5-[*c2*]** with simulated isotopic patterns of $[M+5H]^{5+}$ and $[M+4H+Na]^{5+}$.

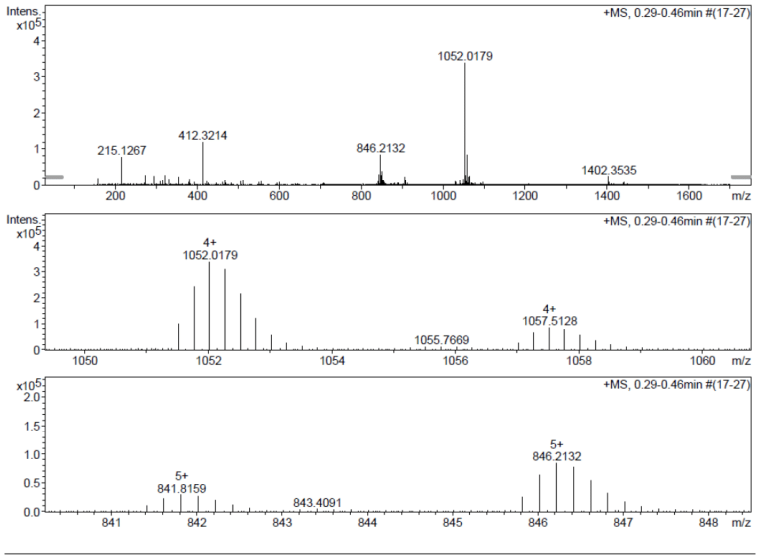

Meas. m/z	#	Formula	Score	m/z	err [mDa]	err [ppm]	mSigma	rdb	e⁻ Conf	N-Rule	z
841.4143	1	C 230 H 285 N 28 O 48	100.00	841.4139	-0.4	-0.5	248.2	102.5	even	ok	5+
845.8113	1	C 230 H 284 N 28 Na O 48	100.00	845.8103	-1.1	-1.2	246.9	102.5	even	ok	
1051.5157	1	C 230 H 284 N 28 O 48	100.00	1051.5155	-0.2	-0.2	12.2	103.0	even	ok	4+
1057.0112	1	C 230 H 283 N 28 Na O 48	100.00	1057.0110	-0.2	-0.2	34.9	103.0	even	ok	

Figure SI 57. Calculated and measured m/z of **5-[*c2*]** (ESI-TOF HRMS).

5-[*a*2]

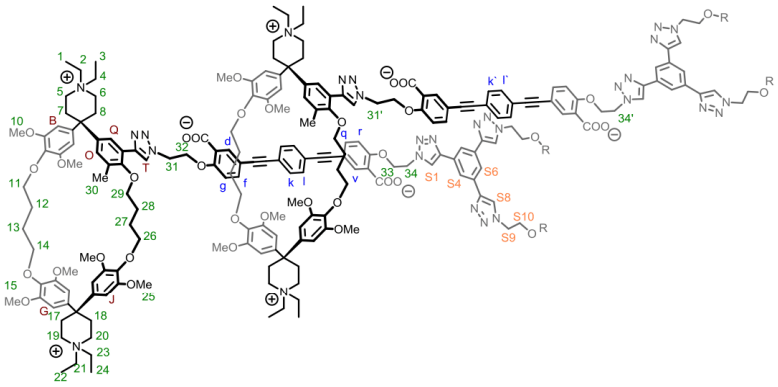

Figure SI 58. Molecular structure and atom numbering of **5-[*a*2]**

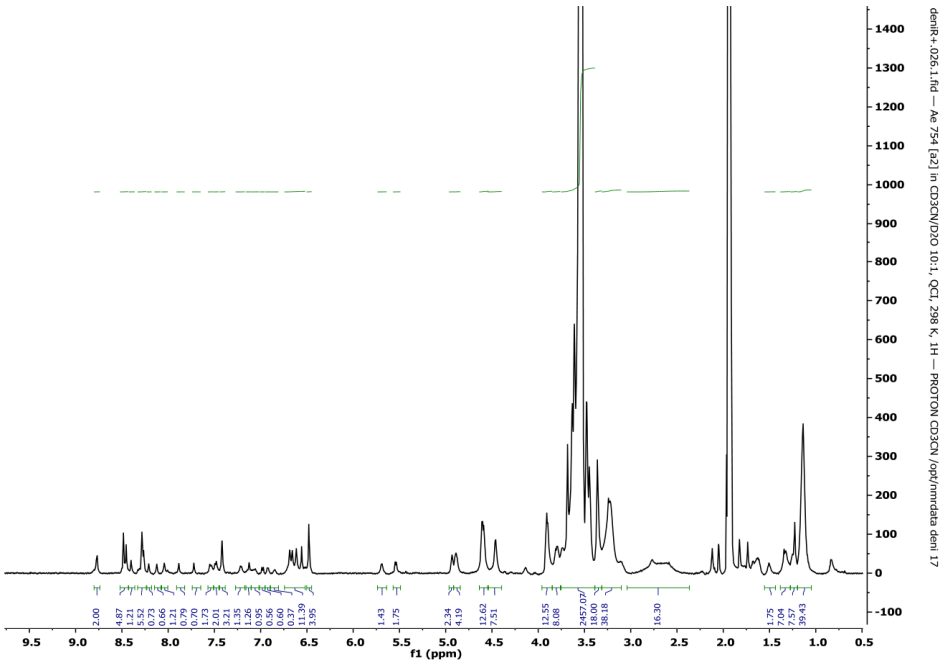

Figure SI 59. Full range ^{1}H-NMR spectrum (600 MHz, CD_3CN/D_2O = 10:1) of **5-[*a*2]**. It proved to be challenging to obtain reasonably-resolved spectra for this substance. Assignments in the following expansions are only partially given as far as conclusions in analogy to **5-[*c*2]** or **5-[*a*1]**, based on chemical shift or integration ratios could be drawn.

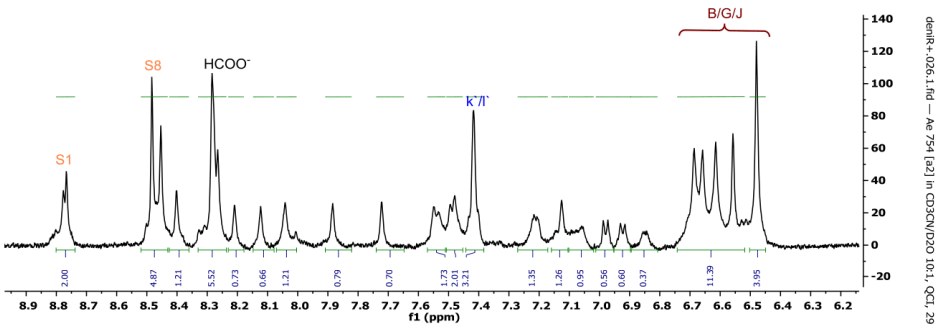

Figure SI 60. Aromatic ^{1}H-NMR spectrum (600 MHz, CD_3CN/D_2O 10:1) range of **5-[*a*2].**

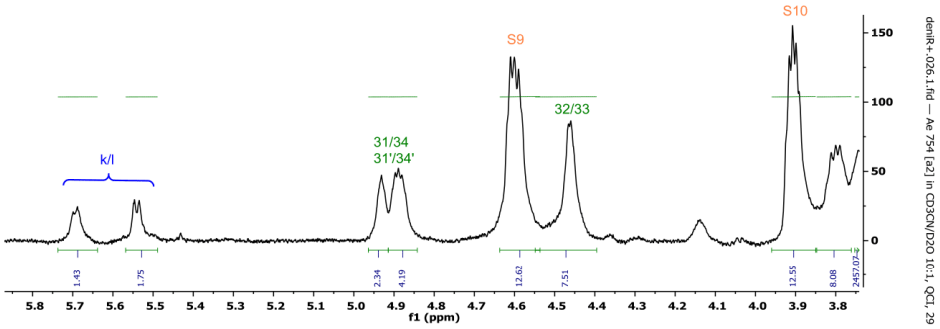

Figure SI 61. Low field aliphatic ^{1}H-NMR spectrum (600 MHz, CD_3CN/D_2O 10:1) range of **5-[*a*2].**

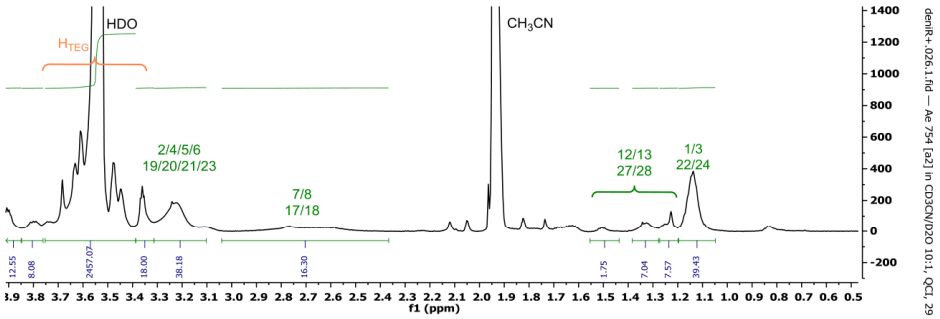

Figure SI 62. Aromatic ^{1}H-NMR spectrum (600 MHz, CD_3CN/D_2O 10:1) range of **5-[*a*2].**

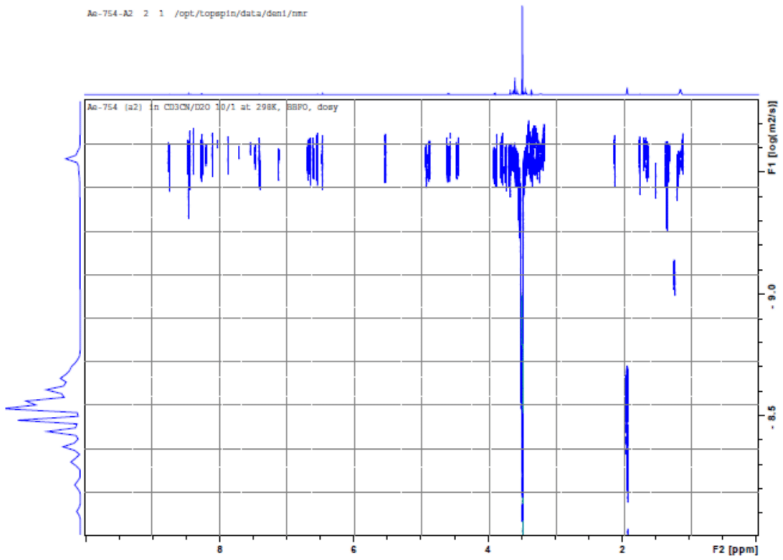

Figure SI 63. DOSY-NMR (600 MHz, CD_3CN/D_2O = 10:1)**.** of **5-[*a*2].**

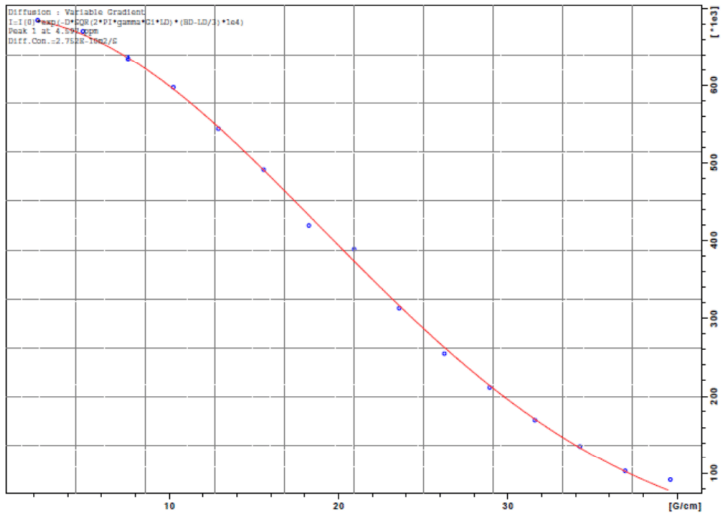

Figure SI 64. Fitting curve of the DOSY-NMR. A diffusion coefficient of 2.75 × 10^{-10} m^2s^{-1} was obtained, as evaluated from the triplet S9 at about 4.6 ppm.

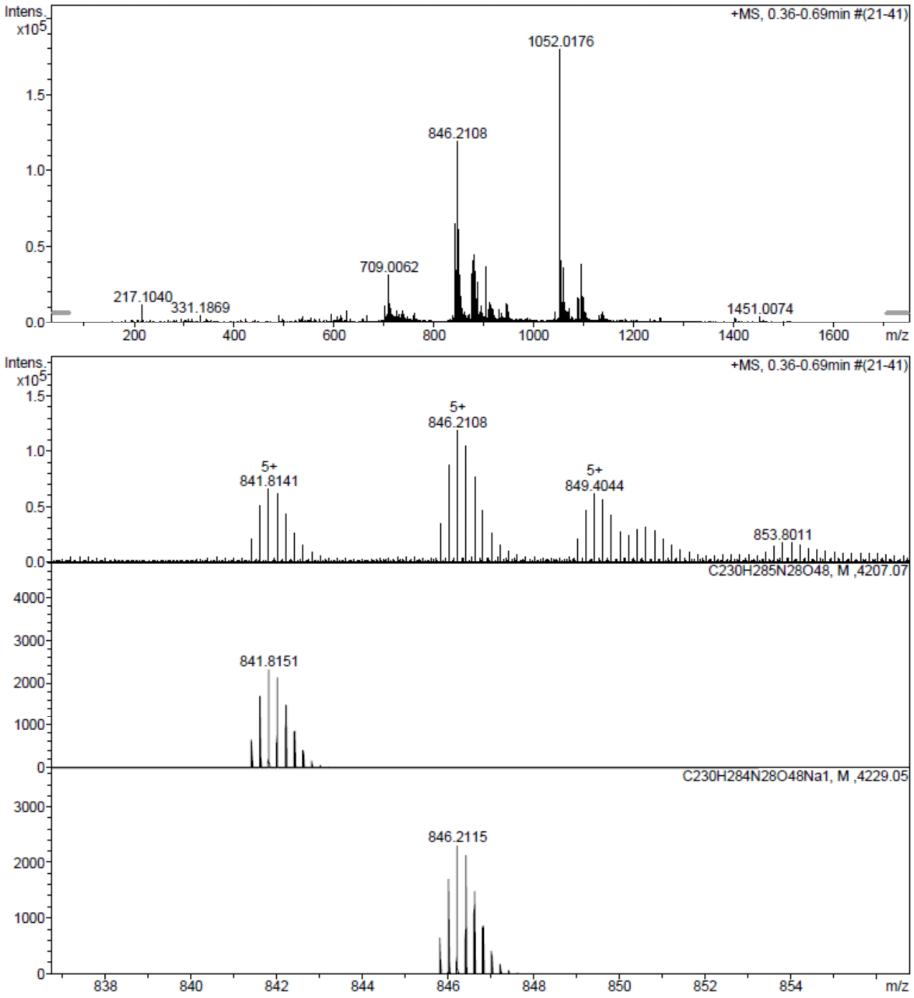

Figure SI 65. Full-range ESI-TOF HRMS spectrum (top) of **5-[*a*2]** with simulated isotopic patterns of $[M+5H]^{5+}$ and $[M+4H+Na]^{5+}$ (bottom).

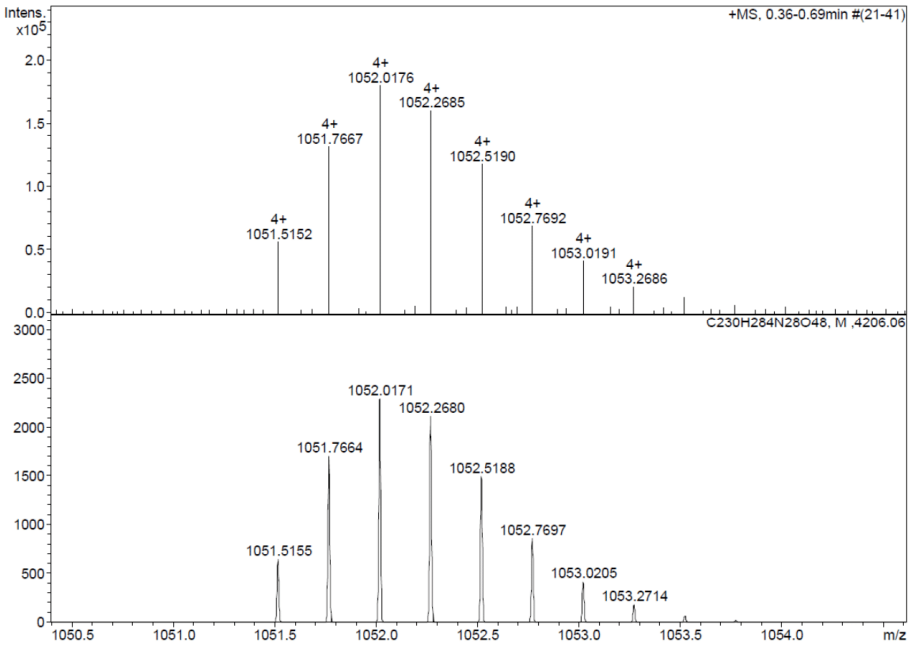

Figure SI 66. Partial ESI-TOF HRMS spectrum (top) of **5-[*a*2]** with simulated isotopic patterns of $[M+4H]^{4+}$ (bottom).

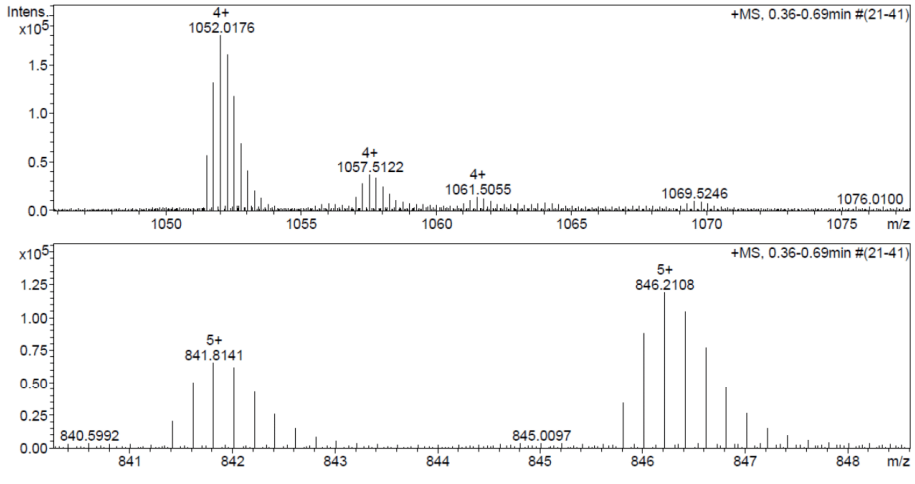

Meas. m/z	#	Formula	Score	m/z	err [mDa]	err [ppm]	mSigma	rdb	e¯ Conf	z
841.4123	1	C 230 H 285 N 28 O 48	100.00	841.4139	1.5	1.8	248.2	102.5	even	5+
845.8089	1	C 230 H 284 N 28 Na O 48	100.00	845.8103	1.3	1.6	248.3	102.5	even	
1051.5152	1	C 230 H 284 N 28 O 48	96.44	1051.5155	0.4	0.4	27.5	103.0	even	4+

Figure SI 67. Calculated and measured m/z of **5-[*a*2]** (ESI-TOF HRMS).

5-[*a*1]

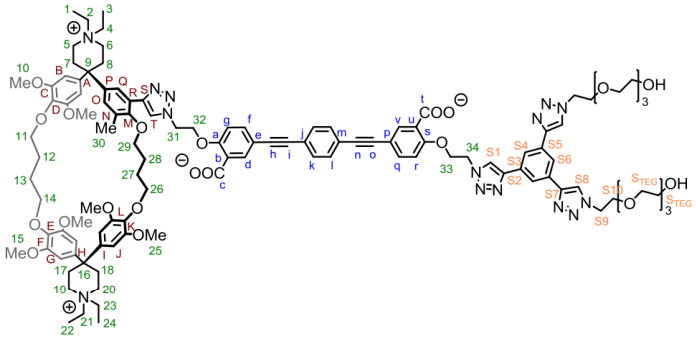

Figure SI 68. Molecular structure and atom numbering of **5-[*a*1]**

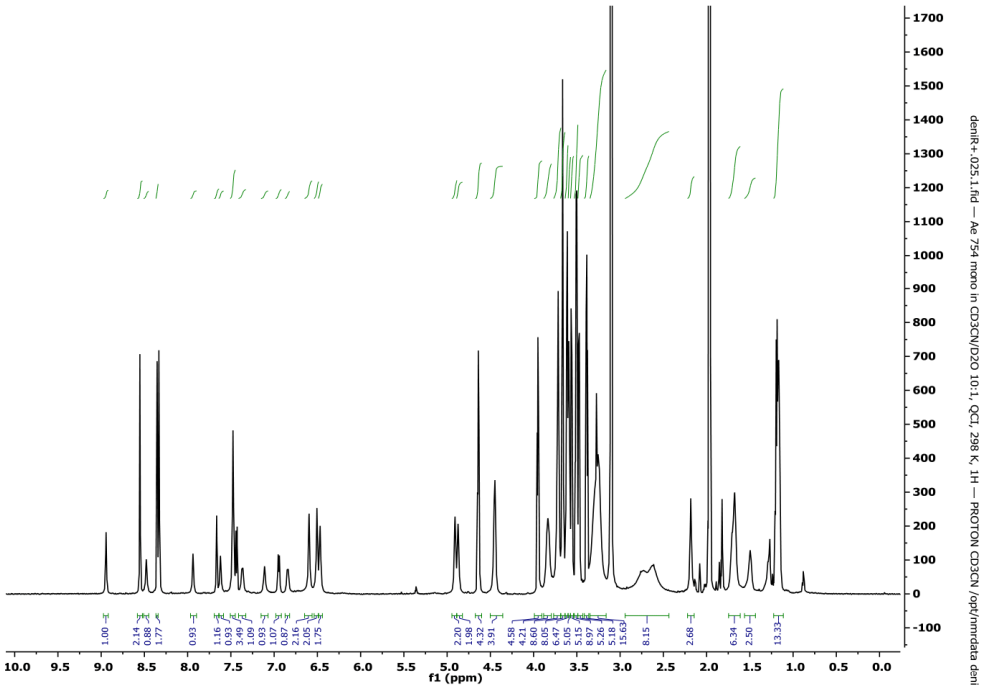

Figure SI 69. Full range ^{1}H-NMR spectrum (600 MHz, CD_3CN/D_2O = 10:1) of **5-[*a*1]**.

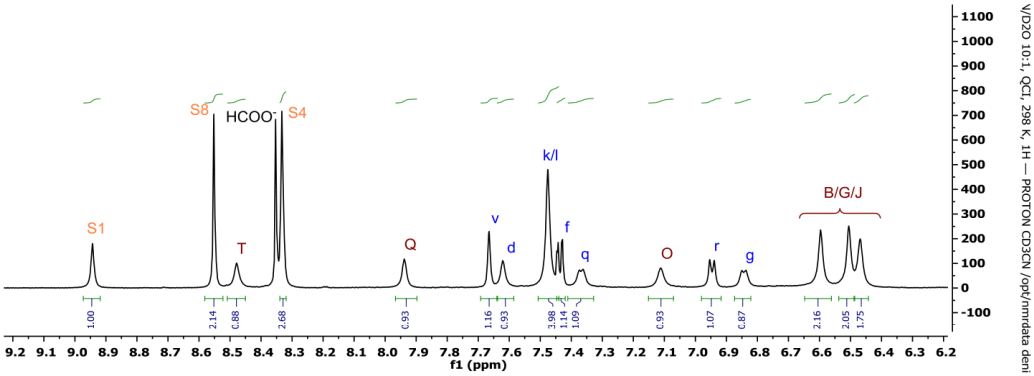

Figure SI 70. ^{1}H-NMR spectrum (600 MHz, CD_3CN/D_2O = 10:1) of **5-[*a*1]**, aromatic range.

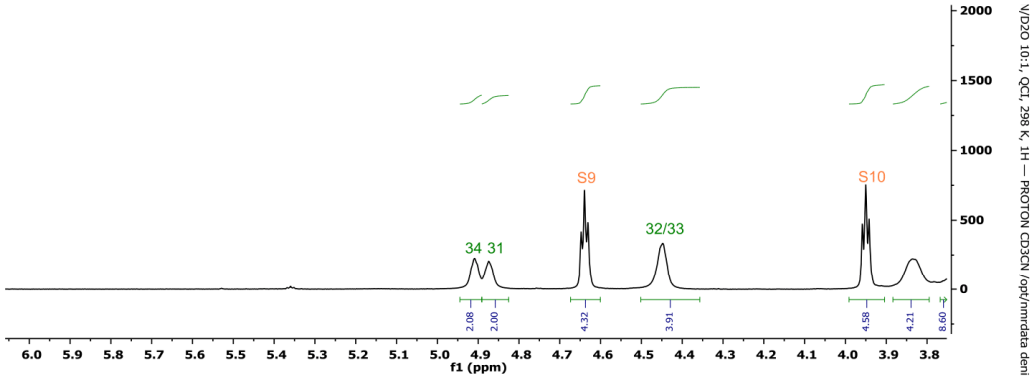

Figure SI 71. ^{1}H-NMR spectrum (600 MHz, CD_3CN/D_2O 10:1) of **5-[*a*1]**, low-field aliphatic range. Aromatic signals at δ = 5.2-5.6 ppm are absent compared to **5-[*c*2]** or **5-[*a*2]**.

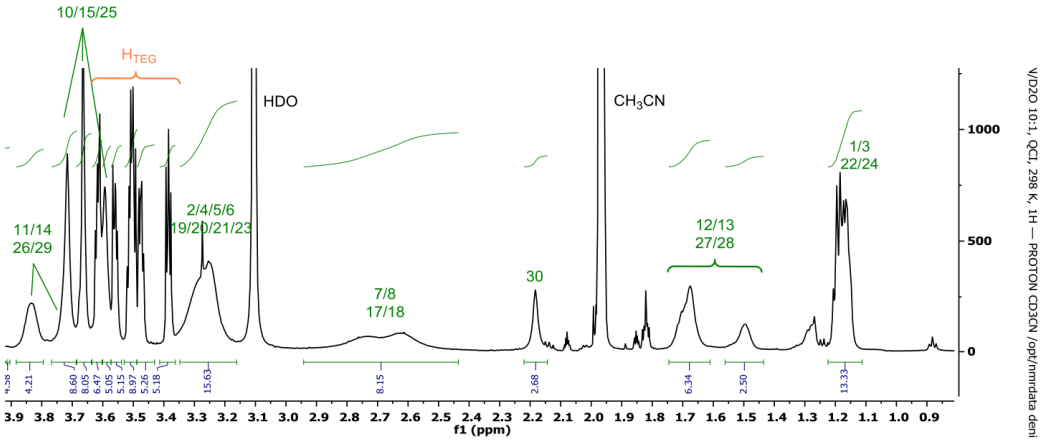

Figure SI 72. ^{1}H-NMR spectrum (600 MHz, CD_3CN/D_2O = 10:1) of **5-[*α*1]**, high-field aliphatic range.

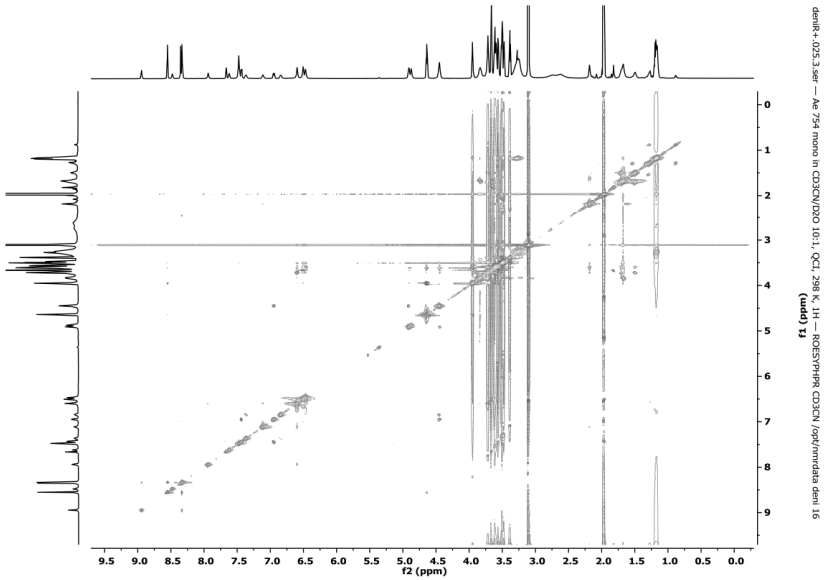

Figure SI 73. ROESY (600 MHz, $CD_3CN:D_2O$ = 10:1) of **5-[*α*1]**.

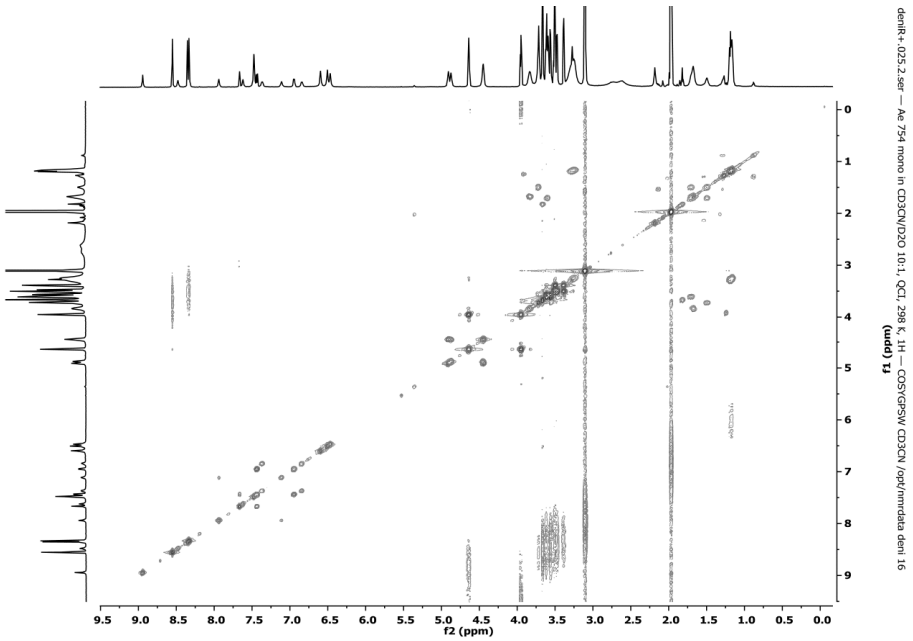

Figure SI 74. COSY (600 MHz, $CD_3CN:D_2O$ = 10:1) of **5-[*α*1]**.

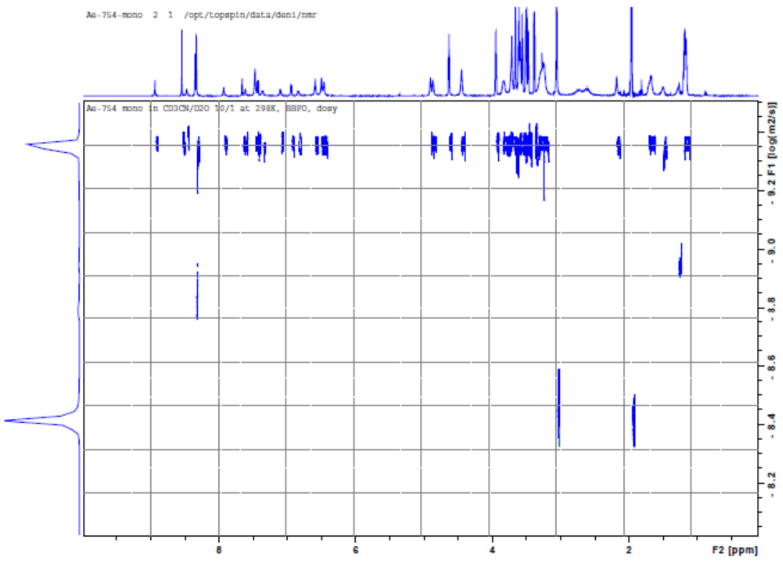

Figure SI 75. DOSY-NMR (600 MHz, CD_3CN/D_2O = 10:1) of **5-[*α*1]**

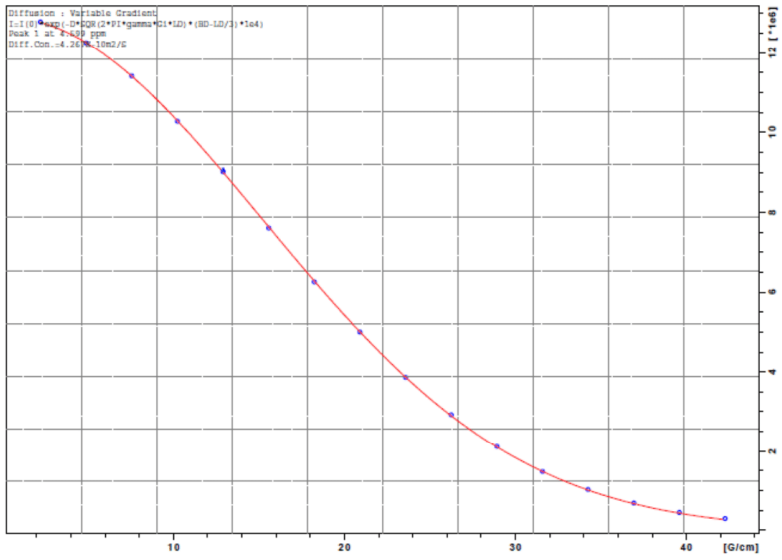

Figure SI 76. Fitting curve of the DOSY-NMR. A diffusion coefficient of 4.27 × 10^{-10} m^2s^{-1} was obtained, as evaluated from the triplet S9 at about 4.6 ppm.

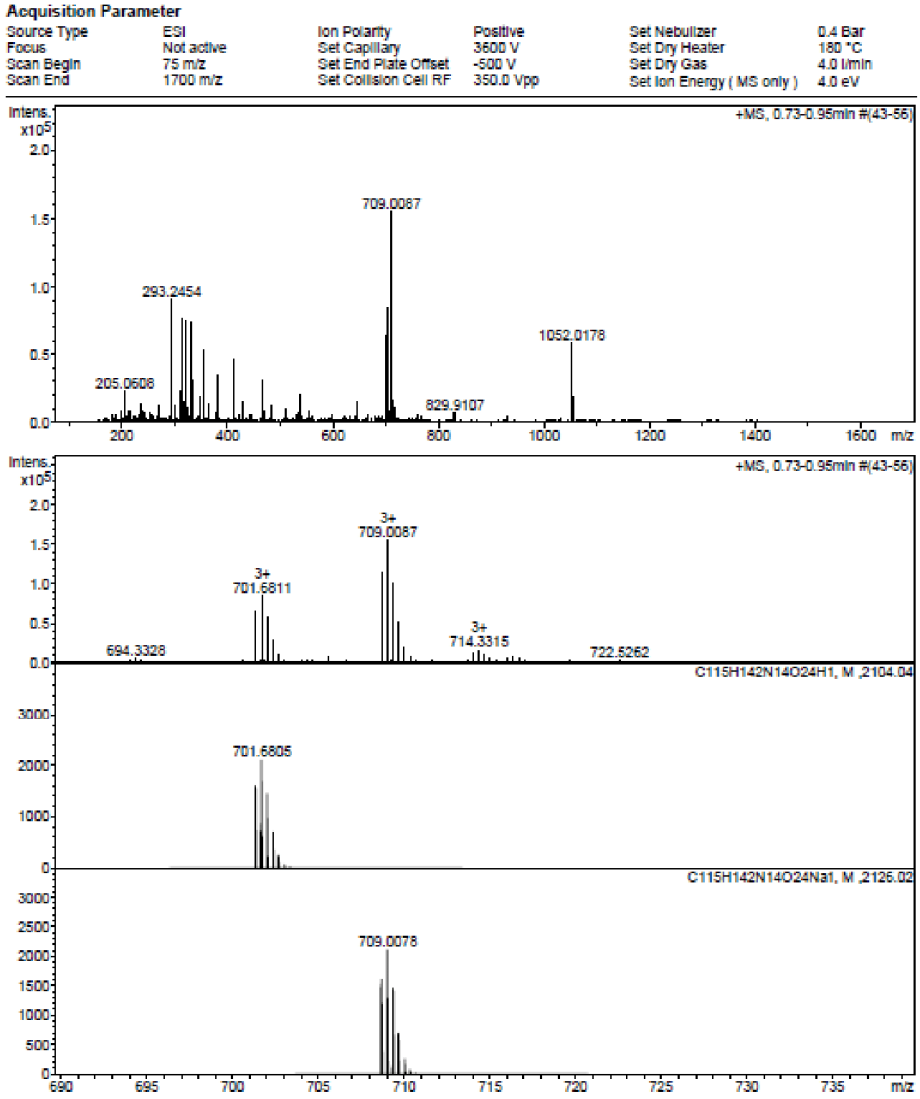

Figure SI 77. Full-range ESI-TOF HRMS spectrum (top) of **5-[*α*1]** with simulated isotopic patterns of $[M+3H]^{3+}$ and $[M+2H+Na]^{3+}$ (bottom).

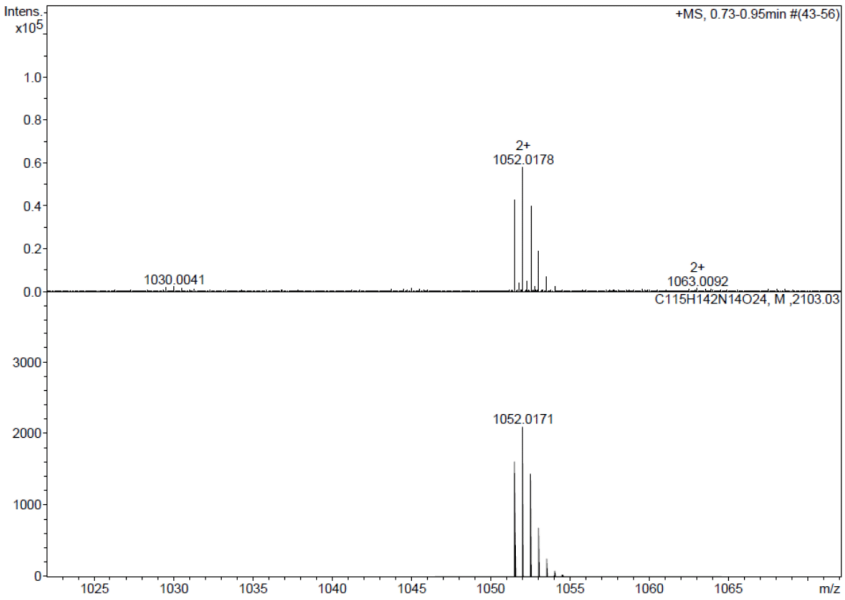

Figure SI 78. Partial ESI-TOF HRMS spectrum (top) of **5-[*a*1]** with simulated isotopic patterns of $[M+2H]^{2+}$ (bottom).

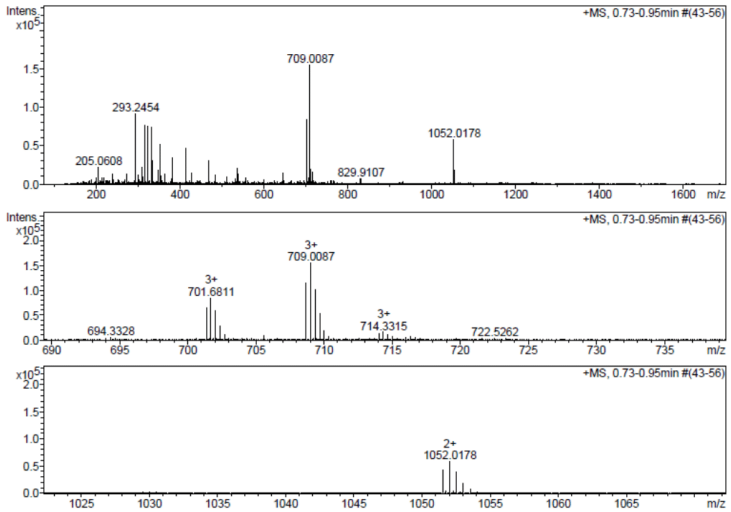

Meas. m/z	#	Formula	Score	m/z	err [mDa]	err [ppm]	mSigma	rdb	e⁻ Conf	N-Rule	z
701.3469	1	C 115 H 143 N 14 O 24	100.00	701.3461	-0.8	-1.2	6.8	51.5	even	ok	3+
708.6742	1	C 115 H 142 N 14 Na O 24	100.00	708.6734	-0.8	-1.2	14.0	51.5	even	ok	
713.9979	1	C 115 H 142 K N 14 O 24	100.00	713.9981	0.1	0.2	135.8	51.5	even	ok	
1051.5158	1	C 115 H 142 N 14 O 24	100.00	1051.5155	-0.3	-0.3	10.6	52.0	even	ok	2+

Figure SI 79. Calculated and measured m/z of **5-[*a*1]** (ESI-TOF HRMS

Experimental details and synthetic procedures

Commercially available compounds were used as received unless indicated otherwise. Dry THF was freshly distilled from sodium/benzophenone. Other dry solvents were prepared by slow overnight stirring over freshly activated molecular sieves (3 Å). For flash chromatography, SiliCycle SiliaFlash® p60 (40-63 μM) was used, size exclusion chromatography was conducted on Sephadex® LH-20 columns, which were regenerated with approx. 10 column volumes of 1-5 % ammonia in MeOH/H_2O 1:1 followed by MeOH/H_2O 1:1 until the eluate was neutral or 0.2 M NH_4HCO_3 in MeOH/H_2O 1:1 after usage. ^1H and ^{13}C NMR spectra were recorded with Bruker Avance III NMR spectrometers operating at 400, 500, or 600 MHz proton frequencies. All instruments were equipped either with a direct-observe 5 mm BBFO smart probe or an indirect-detection 5 mm BBI probe (500 MHz) or a five-channel cryogenic 5 mm QCI probe (600 MHz). All probes were equipped with actively shielded z-gradients (10 A). Spectra at 400 MHz were recorded at 295 K, spectra at 500 or 600 MHz were acquired at 298 K.Chemical shifts given are referenced to a solvent residual peak unless indicated otherwise. HPLC/ESI-MS was conducted on a Shimadzu LC-20AT HPLC equipped with a diode array UV/Vis detector (Shimadzu SPD-M10A, λ = 200–600 nm) and a C-18 reversed phase column (Reprospher®, 100 C18 Aqua, 5 μm, 125 × 2 mm, Dr. Maisch GmbH) with a gradient of 10 to 90 % CH_3CN in H_2O within 12 minutes and 0.1 % formic acid as an additive coupled to a Bruker amaZon X ESI-spectrometer. Preparative HPLC was conducted with a Shimadzu LC-20AP and a SPD-20A UV-Vis detector, and carried out on a Dr. Maisch Reprosil 100 C-18 (10 μm) column with a length of 250 mm and a diameter of 30 mm. For optical characterization, quartz fluorescence cuvettes with a 1 cm optical path length were used, which were washed with concentrated H_2SO_4 prior to use. Fluorescence spectra were recorded with a Horiba FluoroMax-4, UV-Vis spectra were recorded with a JASCO V-770. High resolution mass spectra were recorded with a Bruker M axis 4G ESI-TOF instrument or a Bruker solariX spectrometer with a MALDI source. Isothermal titration calorimetry (ITC) experiments were performed at 298 K using a Malvern PEAQ-ITC instrument. Experiments were carried out in Millipore Milli-Q water. Guest axle **3 * 2 Na** solution (0.1 mM) in water was placed into the calorimeter cell (200 μL) and 20 aliquots (2 μL) of cyclophane **CyOMe$_8$ * 2 Cl** solution (1 mM) in water were added via a computer-automated syringe at 150 s intervals. Heat changes were recorded after each addition. Dilution heats were subtracted from the titration data prior to curve fitting. Every titration was done at least three times. The first smaller injection (0.8 μL) was discarded from each data set to remove the effect of guest diffusion across the syringe tip during the equilibration process. Titration curves were fitted with the one binding site model using PEAQ-ITC Analysis software supplied by MicroCal. Association constant (K_a) was calculated from the corresponding binding isotherm. **CyOMe$_8$ * 2 Cl**,[2] 1-[4,4-bis(4-hydroxy-3,5-dimethoxyphenyl)piperidin-1-yl]ethan-1-one (**12**)[3] and [(3,5-diethynylphenyl)ethynyl]triisopropylsilane (**22**)[4] were synthesized according to literature procedures, for 4-bromo-2,6-dimethoxyphenol (**6**)[5] a literature-known procedure was slightly modified.

[2] S. Anderson, R. T. Aplin, T. D. W. Claridge, T. Goodson III, A. C. Maciel, G. Rumbles, J. F. Ryan, H. L. Anderson, *J. Chem. Soc. Perkin 1* **1998**, 2383–2398.

[3] D. R. Benson, R. Valentekovich, C. B. Knobler, F. Diederich, *Tetrahedron* **1991**, *47*, 2401–2422.

[4] F. Feng, S. H. Lee, S. W. Cho, S. Kömürlü, T. D. McCarley, A. Roitberg, V. D. Kleiman, K. S. Schanze, *Langmuir* **2012**, *28*, 16679–16691.

[5] H. Lee, D. Kim, H.-K. Lee, W. Qiu, N.-K. Oh, W.-C. Zin, K. Kim, *Tetrahedron Lett.* **2004**, *45*, 1019–1022.

Synthesis of 4-Bromo-2,6-dimethoxyphenol (**6**)

2,6-Dimethoxyphenol (33.0 g, 214 mmol) was placed in a three-necked flask which was equipped with a thermometer and a nitrogen inlet. Dichloromethane (300 mL, freshly distilled over CaH_2) and methanol (3 mL) were added and the solution was degassed with N_2 for 10 minutes. NaH (60 % dispersion in mineral oil, 86 mg, 2.1 mmol) was added under nitrogen atmosphere (The deprotonated dimethoxyphenol is sensitive to atmospheric oxygen, which results in a blue-black color of the solution if the reaction is not properly protected from oxygen). After stirring for 10 minutes at r.t., the flask was cooled to -40 °C in an acetonitrile/dry ice bath. N-Bromosuccinimide was added portionwise while maintaining a constant nitrogen flow and the temperature was monitored to stay below -25 °C. After complete addition, it was stirred for 15 minutes. The reaction mixture was then poured onto a short silica gel column, which was eluted with EtOAc. The organic solvents were removed and the crude product was dissolved in MeOH/H_2O = 1:1 (500 mL). The brown solution was cooled in the freezer to -15 °C, resulting in crystallization of cotton-like needles. The product was filtered off and washed with a cold MeOH/H_2O = 1:1 (50 mL), giving white fluffy needles (29.5 g, 59 %).

Note: Monitoring of the reaction temperature is crucial for the success of this reaction. Temperatures below -40 °C resulted in the formation of a red, insoluble mass (probably oxidation products) and poor yields of the desired compound.

^{1}H NMR (250 MHz, $CDCl_3$) δ 6.72 (s, 2H), 5.45 (s, 1H), 3.87 (s, 6H)

^{13}C NMR (63 MHz, $CDCl_3$) δ 147.7, 134.2, 111.2, 108.6, 56.6.

5-Bromo-2-(4-chlorobutoxy)-1,3-dimethoxybenzene (**7**):

4-bromo-2,6-dimethoxyphenol (**6**) (25.4 g, 109 mmol) was placed in a flask, DMF (150 mL) and 1,4-dichlorobutane (150 mL, 1.37 mol) were added. Under vigorous stirring, NaH (60 % in mineral oil, 120 mmol, 4.80 g) was added in small portions. After the H_2 evolution ceased, the mixture was heated at 110 °C for 3 h. The solvents were evaporated and the residue was partitioned between water and cyclohexane. The aqueous phase was extracted three times with cyclohexane, the combined organic phases were dried over Na_2SO_4 and evaporated. The crude product was purified on silica gel (Cyclohexane → EtOAc/cyclohexane 9:1) to give a colorless oil (33.0 g, 94 %).

^{1}H NMR (400 MHz, $CDCl_3$) δ 6.71 (s, 2H), 3.95 (t, *J* = 12.3 Hz, 2H), 3.82 (s, 6H), 3.65 (t, *J* = 6.7 Hz, 2H), 2.09 – 1.94 (m, 2H), 1.94 – 1.78 (m, 2H)

^{13}C NMR (101 MHz, $CDCl_3$) δ 154.2, 136.5, 116.2, 109.1, 72.4, 56.4, 45.0, 29.3, 27.5

HRMS (ESI, +): calcd. for $C_{12}H_{16}BrClNaO_3$ 344.9864 $[M+Na]^+$, found 344.9864.

Compound **8**:

A flask equipped with a thermometer was charged with anhydrous THF (300 mL), and cooled to -5 °C in a water/methanol (70:30)/dry ice bath. *i*-PrMgCl solution (2 M in THF, 15 mL, 30 mmol) was added, followed by *n*-butyllithium 1.6 M in hexanes (37.5 mL, 60 mmol). It was stirred at -5 °C for 15 min and then a solution of **7** (19.5 g, 60 mmol) in anhydrous THF (40 mL) was slowly cannulated such that the temperature remained within -10 to -5 °C. After 15 min, a solution of *N*-acetyl-4-piperidone in anhydrous THF (15 mL) was added dropwise such that the temperature stayed between -5 °C and 0 °C. A white precipitate was formed and stirring was continued for 15 minutes followed by quenching with saturated NH_4Cl solution. The organic phase was separated and the solvents were removed to give a first crop of the crude product. The aqueous phase was extracted twice with DCM (100 mL) and combined with the crude product obtained before, the combined organic phases were washed with water and dried over Na_2SO_4. After evaporation, the desired compound was obtained by column chromatography (SiO_2, DCM → DCM + 4 % MeOH) as a colorless oil, which crystallized upon standing (12.1 g, 52 %). The compound can be recrystallized from acetone/Et_2O (1:20).

^{1}H NMR (400 MHz, $CDCl_3$) δ 6.66 (s, 2H), 4.62 – 4.54 (m, 1H), 3.97 (t, *J* = 6.1 Hz, 2H), 3.84 (s, 6H), 3.78 – 3.68 (m, 1H), 3.65 (t, *J* = 6.7 Hz, 2H), 3.63 – 3.52 (m, 1H), 3.13 – 3.02 (m, 1H), 2.53 – 2.42 (m, 1H), 2.13 (s, 3H), 2.07 – 2.00 (m, 4H), 1.92 – 1.74 (m, 4H); 2 methylene protons of the piperidine ring are overlapping with other alkyl resonances and exhibit complex coupling patterns

^{13}C NMR (101 MHz, $CDCl_3$) δ 168.9, 153.3, 143.6, 136.2, 101.8, 72.2, 71.6, 56.2, 44.9, 42.8, 39.1, 37.8, 37.7, 29.2, 27.4, 21.4

HRMS (ESI, +): calcd. for $C_{19}H_{27}ClNO_4$ 368.1623 $[M+H]^+$, found 368.1620.

Compound **9**:

To a solution of **8** (9.80 g, 25.4 mmol) in DCM (20 mL) was given 2-methylphenol (11.1 g, 102 mmol). The mixture was cooled in an ice bath and $BF_3 \times Et_2O$ (15.7 mL, 127 mmol) was added slowly. The flask was then capped with a septum and equipped with a balloon for pressure equilibration and the mixture was stirred at 35 °C for 18 h. The flask contents were poured onto crushed ice (100 g) and stirred until the red color disappeared. It was extracted with DCM three times and the combined organic fractions were washed with saturated sodium bicarbonate solution, then dried over sodium sulfate and evaporated. The crude product was purified by flash column chromatography (Silica gel, DCM/MeOH 96:4) to give a yellowish oil, which crystallized upon standing (10.9 g, 90 %).

^{1}H NMR (400 MHz, $CDCl_3$) δ 6.95 (d, *J* = 0.9 Hz, 1H), 6.91 (dd, *J* = 8.3, 0.9 Hz, 1H), 6.73 (d, *J* = 8.3 Hz, 1H), 6.40 (s, 2H), 5.71 (s, 1H), 3.95 (t, *J* = 6.1 Hz, 2H), 3.76 (s, 6H), 3.64 (t, *J* = 6.7 Hz, 2H), 3.60 – 3.40 (m, 4H), 2.42 – 2.23 (m, 4H), 2.21 (s, 3H), 2.10 (s, 3H), 2.07 – 1.95 (m, 2H), 1.92 – 1.79 (m, 2H)

^{13}C NMR (101 MHz, $CDCl_3$) δ 169.2, 153.3, 152.6, 142.9, 137.4, 135.7, 129.7, 125.7, 124.1, 115.0, 104.8, 72.3, 56.4, 45.1, 44.7, 43.9, 38.9, 37.2, 36.3, 29.4, 27.6, 21.5, 16.4

HRMS (ESI, +): calcd. for $C_{26}H_{34}ClNNaO_5$ 498.2018 $[M+Na]^+$, found 498.2019.

Compound **10**:

Procedure A: A 5 % solution of iodine chloride in MeOH was prepared. Compound **9** (10.42 g, 21.89 mmol) was dissolved in a mixture of MeOH (220 mL), and water (110 mL) containing sodium hydroxide (1.77 g, 44.2 mmol). The mixture was cooled to 0 °C and the reaction mixture was slowly titrated with iodine chloride solution and monitored by TLC until full conversion was observed. Water (300 mL) was added and the mixture was acidified with a diluted HCl until a slightly acidic pH value was observed. It was extracted with DCM (3 x 50 mL) and the combined organic layers were washed with saturated sodium thiosulfate solution and dried over Na_2SO_4. After removal of the solvent *in vacuo*, the crude was purified by flash column chromatography (Silica gel, DCM/MeOH 98:2) to afford the desired compound as a white solid (10.0 g, 76 %).

Procedure B: Compound **9** (671 mg, 1.41 mmol), NaOH (0.11 g, 2.8 mmol) and NaI (0.42 g, 2.8 mmol) were placed in a flask and MeOH (20 mL) was added. The mixture was stirred until everything was dissolved, cooled in an ice bath followed by slow addition of NaOCl solution (13 % active chlorine, approx. 8 mL). The reaction was monitored carefully by TLC (silica gel, DCM/MeOH 95:5), until all starting material was converted and iodine started to appear on TLC. $NaHCO_3$ was then added (2.0 g), followed by TBME (150 mL). Residual iodine in the organic phase was reduced by shaking with a spatula tip of sodium dithionite. The organic phase was separated and the aqueous phase was extracted again with TBME (50 mL), the combined organic phases were washed with brine and dried over Na_2SO_4. The solvent was removed and the product was obtained as a vitreous solid (625 mg, quant.). Analytical data for the products of both procedures were equivalent.

^{1}H NMR (400 MHz, $CDCl_3$) δ 7.31 (d, *J* = 2.4, 1H), 6.91 (d, *J* = 2.4, 1H), 6.39 (s, 2H), 5.29 (s, 1H), 3.96 (t, *J* = 6.2 Hz, 2H), 3.78 (s, 6H), 3.64 (t, *J* = 6.7 Hz, 2H), 3.53 – 3.44 (m, 2H), 2.30 – 2.27 (m, 4H), 2.25 (s, 3H), 2.09 (s, 3H), 2.05 – 1.98 (m, 2H), 1.92 – 1.82 (m, 2H); one broad multiplet corresponding to two protons of the spiropiperidine ring is overlapping at δ = 3.64 ppm. Significant amounts of solvent always remained in the product after evaporation, which could only be removed by gentle heating under vacuum. Unfortunately, this caused partial decomposition of the product which became apparent by the emergence of iodine vapor and a brown discoloration of the product

^{13}C NMR (101 MHz, $CDCl_3$) δ 168.9, 153.3, 151.3, 141.7, 140.0, 135.8, 133.9, 130.2, 124.8, 104.7, 86.2, 72.2, 56.3, 44.9, 44.4, 43.6, 38.6, 37.0, 36.1, 29.3, 27.4, 21.4, 17.6

HRMS (ESI, +): calcd. for $C_{26}H_{34}ClINO_5$ 602.1165 $[M+H]^+$, found 602.1162.

Compound **11**:

Compound **10** (10.0 g, 16.6 mmol) was dissolved in DMF (140 mL) and 1,4-dichlorobutane (70 mL, 640 mmol). Sodium hydride (60 % dispersion in mineral oil, 0.764 g, 19.1 mmol) was added slowly. After the H2 gas evolution stopped, the mixture was heated at 50 °C for 3 d. Water (600 mL) was added, followed by 9 % hydrochloric acid (100 mL). After extraction with TBME (3 x 200 mL) the combined organic layers were washed with saturated sodium bicarbonate solution (200 mL) and water (2 x 200 mL), followed by drying over sodium sulfate. After removal of the solvents, the crude was purified by flash column chromatography (Silica gel, cyclohexane/EtOAc, 1:2 → EtOAc) to yield a colorless oil (10.6 g, 92 %).

^{1}H NMR (400 MHz, $CDCl_3$) δ 7.45 (d, *J* = 2.4 Hz, 1H), 6.95 (d, *J* = 2.3 Hz, 1H), 6.38 (s, 2H), 3.96 (t, *J* = 6.1 Hz, 2H), 3.85 (t, *J* = 5.9 Hz, 2H), 3.77 (s, 6H), 3.69 – 3.61 (m, 4H), 3.49 (t, *J* = 5.6 Hz, 2H), 2.33 – 2.27 (m, 4H), 2.26 (s, 3H), 2.08 (s, 3H), 2.09 – 1.94 (m, 6H), 1.90 – 1.81 (m, 2H)

^{13}C NMR (101 MHz, $CDCl_3$) δ 169.0, 155.3, 153.5, 144.0, 141.4, 135.9, 135.5, 132.1, 130.4, 104.8, 92.7, 72.3, 71.8, 56.4, 45.1, 45.1, 44.7, 43.6, 38.6, 37.0, 36.1, 29.5, 29.4, 27.7, 27.5, 21.6, 17.6

HRMS (ESI, +): calcd. for $C_{30}H_{40}Cl_2INNaO_5$ 714.1220 $[M+Na]^+$, found 714.1227.

Compound **13**:

Dry DMF (1.6 L) was degassed with N2 for 15 minutes and **11** (9.87 g, 14.3 mmol) was added, followed by **12** (6.16 g, 14.3 mmol) and dry cesium carbonate (26.9 g, 134 mmol). The reaction mixture was further degassed and stirred for 20 min at room temperature, then immersed into a preheated oil bath at 100 °C and stirred for 40 h. The solvent was removed *in vacuo* and the residue was partitioned between DCM (80 mL) and water (800 mL). The organic layer was separated and the aqueous layer was extracted with DCM (3 x 80 mL, then 2 x 40 mL). The combined organic layers were washed with 9 % hydrochloric acid (300 mL), saturated sodium bicarbonate solution (300 mL) and dried over sodium sulfate. After removal of the solvent *in vacuo*, the crude was purified by flash column chromatography (Silica gel, DCM/MeOH 97:3) to afford the target compound as a white solid, which was dried by heating at 60 °C and 3 mbar (6.13 g, 41 %).

^{1}H NMR (400 MHz, $CDCl_3$) δ 7.38 (d, *J* = 2.3 Hz, 1H), 6.90 (d, *J* = 2.3 Hz, 1H), 6.37 (s, 2H), 6.36 (s, 2H), 6.35 (s, 2H), 4.05 (t, *J* = 6.6 Hz, 2H), 4.01 (t, *J* = 6.8 Hz, 2H), 3.92 (t, *J* = 6.3 Hz, 2H), 3.84 (t, *J* = 6.3 Hz, 2H), 3.73 (s, 6H), 3.71 (s, 6H), 3.63 (s, 6H), 3.62 – 3.46 (m, br, 8H), 2.32 – 2.24 (m, br, 8H), 2.19 (s, 3H), 2.08 (s, 3H), 2.07 (s, 3H), 2.01 – 1.89 (m, 4H), 1.89 – 1.78 (m, 4H)

^{13}C NMR (101 MHz, $CDCl_3$) δ 169.1, 169.1, 155.4, 153.6, 153.4, 153.4, 144.0, 141.8, 141.8, 141.2, 136.0, 135.9, 135.5, 134.9, 132.2, 129.9, 104.9, 104.6, 104.6, 92.8, 73.1, 73.0, 72.7, 56.5, 56.4, 56.4, 45.2, 44.1, 26.7, 26.4, 26.3, 21.4, 21.4, 17.6. Resonances of the spiropiperidine methylene-carbon atoms are not observed

HRMS (MALDI, +): calcd. for $C_{53}H_{67}IN_2O_{12}$ 1050.3733 $[M]^+$, found 1050.3727.

Compound **2 * 2 PF_6**:

Compound **15** (1.50 g, 1.63 mmol) was placed in a flask and dry THF (20 mL) was added, followed by sodium carbonate (173 mg, 1.63 mmol). Iodoethane (10 mL, 125 mmol) was added and the reaction mixture was stirred for 4 d in the dark. It was evaporated to dryness and then dissolved in water (approx. 0.6 L) at 60 °C. The solution was filtered over Celite and the filter cake was washed with water at 60 °C (200 mL). A solution of potassium hexafluorophosphate (5.0 g, 27 mmol) in water (70 mL) was added under vigorous stirring, leading to the precipitation of the desired compound. The precipitate was collected by filtration and dried under vacuum (4 mbar) to give a white solid (2.00 g, 97 %).

^{1}H NMR (600 MHz, CD_3CN) δ 7.22 (d, *J* = 2.5 Hz, 1H, H-O), 7.19 (s, 1H, H-Q), 6.54 (s, 2H, H-G or J), 6.52 (s, 2H, H-G or J), 6.51 (s, 2H, H-B), 3.98 (t, *J* = 6.5 Hz, 2H, H-29), 3.95 (t, *J* = 6.7 Hz, 2H, H-11 or 14 or 26), 3.92 (t, *J* = 6.6 Hz, 2H, H-11 or 14 or 26), 3.83 (t, *J* = 5.9 Hz, 2H, H-11 or 14 or 26), 3.74 (s, 6H, H-10), 3.73 (s, 6H, H-15 or 25), 3.67 (s, 6H, H-15 or 25), 3.37 – 3.18 (m, br, 16H, H-2/4/5/6/19/20/21/23), 2.78 – 2.50 (m, br, 8H, H-7/8/17/18), 2.16 (s, 3H, H-30) 1.87 – 1.80 (m, 2H, H-28), 1.78 – 1.66 (m, 6H, H-12/13/27), 1.23 – 1.17 (m, 12H, H-1/3/22/24); H-T of the terminal acetylene at δ = 3.31 ppm is overlapping with the broad signal of the methylene protons adjacent to the ammonium center and could be identified in the HMQC spectrum

^{13}C NMR (151 MHz, CD_3CN) δ 158.50 (C-M), 154.87 (C-C), 154.71 (C-F or K), 154.66 (C-F or K), 136.60 (C-E or L), 136.42 (C-D), 136.28 (C-E or L), 133.10 (C-N), 130.94 (C-O), 130.26 (C-Q), 116.82 (C-R), 104.94 (2C, C-B or G or J), 104.85 (C-B or G or J), 83.01 (C-T), 81.40 (C-S), 73.66 (C-29), 73.20 (C-11 or 14 or 26), 73.15 (C-11 or 14 or 26), 73.12 (C-11 or 14 or 26), 56.89 (4C, C-10 or 15 or 25), 56.87 (2C, C-10 or 15 or 25), 56.65 (4C, C-2 and/or 4/5/6/19/20/21/23), 56.52 (4C, C-2 and/or 4/5/6/19/20/21/23), 44.53 (C-16), 43.84 (C-9), 29.95 (2C, C-7/8/17/18), 29.72 (2C, C-7/8/17/18), 27.21 (C-12 or 13 or 27 or 28), 27.18 (C-12 or 13 or 27 or 28), 27.05 (C-12 or 13 or 27 or 28), 26.99 (C-12 or 13 or 27 or 28), 16.75 (C-30), 7.62 (C-1 or 3 or 22 or 24), 7.61 7.62 (C-1 or 3 or 22 or 24), 7.58 7.62 (C-1 or 3 or 22 or 24), 7.57 7.62 (C-1 or 3 or 22 or 24); Resonances of C-A/H/I/P were not observed. For the atom numbering see figure 5

HRMS (ESI, +): calcd. for $C_{59}H_{82}N_2O_{10}$ 489.2979 $[M\text{-}2\ PF_6^-]^{2+}$, found 489.2987.

Butyl 2-hydroxy-5-iodobenzoate (**17**):

5-Iodosalicylic acid **16** (15.0 g, 56.8 mol) was placed in a two-necked 500 mL flask and cyclohexane (330 mL) and *n*-BuOH (78 mL) were added. Sulfuric acid (20 mL) was carefully added and the reaction flask was equipped with a Dean-Stark trap. It was heated to reflux for 2 hours and the water was removed 3 times from the Dean Stark trap during this time. The reaction mixture was cooled to r.t. and then neutralized with saturated sodium bicarbonate solution. The organic layer was separated and the aqueous phase was extracted with cyclohexane (50 mL). The combined organic phases were dried over Na_2SO_4, evaporated and the residue was purified by column chromatography (Silica gel, cyclohexane → cyclohexane/EtOAc 20:1) to give a yellowish oil (14.1 g, 78 %).

^{1}H NMR (400 MHz, $CDCl_3$) δ 10.83 (s, 1H), 8.11 (d, *J* = 2.3 Hz, 1H), 7.69 (dd, *J* = 8.8, 2.3 Hz, 1H), 6.77 (d, *J* = 8.8 Hz, 1H), 4.36 (t, *J* = 6.7 Hz, 2H), 1.81 – 1.73 (m, 2H), 1.52 – 1.42 (m, 2H), 0.99 (t, *J* = 7.4 Hz, 3H)

^{13}C NMR (101 MHz, $CDCl_3$) δ 169.2, 161.5, 144.1, 138.3, 120.2, 113.0, 80.1, 65.9, 30.7, 19.3, 13.9

HRMS (ESI, +): calcd. for $C_{11}H_{13}INaO_3$ 342.9802 $[M+Na]^+$, found 342.9799.

Compound **14**:

Compound **13** (1.58 g, 1.50 mmol), bis(triphenylphosphine)palladium(II) chloride (53 mg, 75 µmol, 5 mol%), triphenylphosphine (39 mg, 0.15 mmol, 10 mol%) and copper(I) iodide (29 mg, 0.15 mmol, 10 mol%) were placed in a flask , followed by the addition of DCM (15 mL) and Et_3N (1.0 mL). The solution was bubbled with Ar for 5 min, and then trimethylsilylacetylene (1.1 mL, 7.5 mmol) was added. The reaction was stirred for 20 h and then evaporated to dryness and redissolved in DCM. The suspension was directly purified by column chromatography (DCM→ DCM/MeOH 95:5) to give the target compound as a colorless foam. After drying at 80 °C and 4 mbar the desired compound was obtained as a colorless solid (1.37 g, 89 %).

^{1}H NMR (400 MHz, $CDCl_3$) δ: 7.15 (d, *J* = 2.4 Hz, 1H), 6.82 (d, *J* = 2.4 Hz, 1H), 6.35 (s, 4H), 6.32 (s, 2H), 4.07 (t, *J* = 6.6 Hz, 2H), 4.01 – 3.89 (m, 6H), 3.69 (s, 6H), 3.67 (s, 6H), 3.64 (s, 6H), 3.56 – 3.33 (m, br, 8H), 2.46 – 2.19 (m, br, 8H), 2.08 (s, 3H), 2.06 (s, 3H), 2.04 (s, 3H), 1.96 – 1.76 (m, 8H), 0.22 (s, 9H)

^{13}C NMR (101 MHz, $CDCl_3$) δ: 168.9, 168.9, 157.4, 153.4, 153.4, 153.3, 142.0, 141.8, 141.7, 140.7, 135.9, 135.8, 135.5, 131.5, 130.5, 129.0, 116.3, 104.9, 104.6, 104.5, 102.3, 98.4, 72.9, 72.8, 56.4, 56.4, 56.2, 45.1, 44.1, 43.6, 43.6, 38.6, 38.5, 36.9, 36.4, 35.9, 35.5, 26.7, 26.4, 26.3, 26.3, 21.5, 21.4, 16.7, 0.0. Two (-*C*H_2O-) resonances are overlapping at 72.9 ppm

HRMS (MALDI, +): calcd. for $C_{58}H_{77}N_2O_{12}Si$ 1021.5240 $[M+H]^+$, found 1021.5224.

Compound **15**:

Compound **14** (1.96 g, 1.92 mmol) was dissolved in THF (20 mL) and bubbled with Ar for 10 min. The flask was then immersed into a cooling bath at -10 °C and lithium aluminium hydride solution (1 M in THF, 11.5 ml, 11.5 mmol, 6 eq) was slowly added, followed by slow addition of DIBAL-H (1 M in hexanes, 11.5 mL, 11.5 mmol, 6 eq). The reaction mixture was stirred for 30 min and then the mixture was allowed to reach room temperature followed by stirring for an additional 30 min. The reaction was cooled to -10 °C and the remaining hydrides were quenched by careful addition of EtOAc (10 mL). Aqueous solution of NaOH (40 %) was added (50 mL) which gave a thick slurry. The organic solvents were then removed from the mixture by rotary evaporation (60 °C, 100 mbar). DCM was added (50 mL) and the whole suspension was filtered through a cotton wool to remove insoluble aluminium salts. The filter cake was suspended in DCM (50 mL) and filtered off again. The organic phase was separated from the biphasic filtrate and the aqueous phase was extracted twice with DCM. Phase separation required standing for a prolonged time (>1 h). The combined organic phases were washed with 40 % NaOH solution and water, followed by drying over anhydrous sodium carbonate. HPLC/ESI-MS indicated only partial desilylation, therefore the crude compound was dissolved in a mixture of MeOH (10 mL) and DCM (10 mL) and potassium carbonate (1.0 g) was added. It was stirred for 30 min then the solvents were evaporated. The remaining solids were suspended in DCM and the inorganic salts were filtered off. The filtrate was evaporated to give a brown solid, which was then purified by a silica gel plug column (DCM/Et_3N 95:5) to give a white foam. Drying of the foam under vacuum (3 mbar) to remove residual solvents gave a brownish, vitreous solid (1.60 g, 91 %).

^{1}H NMR (400 MHz, CD_2Cl_2) δ 7.32 (d, *J* = 2.5 Hz, 1H), 7.26 (d, *J* = 2.5 Hz, 1H), 6.65 (s, 2H), 6.64 (s, 2H), 6.62 (s, 2H), 4.22 (t, *J* = 6.4 Hz, 2H), 4.18 (t, *J* = 6.6 Hz, 2H), 4.14 (t, *J* = 6.6 Hz, 2H), 4.09 (t, *J* = 6.1 Hz, 2H), 3.91 (s, 6H), 3.90 (s, 6H), 3.86 (s, 6H), 3.29 (s, 1H), 2.74 – 2.62 (m, br, 8H), 2.60 – 2.53 (m, br, 8H), 2.53 – 2.46 (m, 4H), 2.37 (s, 3H), 2.17 – 2.09 (m, 2H), 2.09 – 1.97 (m, 6H), 1.23 (t, *J* = 7.2 Hz, 3H), 1.22 (t, *J* = 7.2 Hz, 3H)

^{13}C NMR (101 MHz, CD_2Cl_2) δ 157.5, 153.6, 153.5, 153.5, 135.8, 135.7, 135.5, 131.6, 131.1, 130.4, 115.5, 105.2, 105.1, 105.0, 81.5, 80.9, 73.1, 72.9, 72.9, 72.8, 56.4, 56.4, 52.7, 52.7, 50.6, 50.5, 45.3, 44.4, 36.8, 36.5, 26.9, 26.8, 26.7, 26.6, 16.7, 12.5. The resonances of the aromatic quaternary carbons adjacent to the piperidine rings were not observed

HRMS (ESI, +): calcd. for $C_{55}H_{74}N_2O_{10}$ 461.2666 $[M+2H]^{2+}$, found 461.2672.

Butyl 2-(2-chloroethoxy)-5-iodobenzoate (**18**):

Compound **17** (9.99 g, 31.2 mmol) and dry potassium carbonate (12.9 g, 93.6 mmol) were placed in a flask, dry DMSO (50 mL) was added, followed by 1-bromo-2-chloroethane (5.2 mL, 62 mmol). The suspension was stirred at room temperature for 3 days. Water (250 mL) and pentane (100 mL) were added and the aqueous phase was extracted two times with pentane (50 mL). The combined organic phases were evaporated and the crude compound was purified chromatographically (Silica gel, pentane/TBME 19:1 → 9:1) to give a clear oil (8.86 g, 83 %).

^{1}H NMR (400 MHz, $CDCl_3$) δ 8.05 (d, *J* = 2.4 Hz, 1H), 7.71 (dd, *J* = 8.7, 2.4 Hz, 1H), 6.73 (d, *J* = 8.8 Hz, 1H), 4.29 (t, *J* = 6.7 Hz, 2H), 4.25 (t, *J* = 6.0 Hz, 2H), 3.82 (t, *J* = 6.0 Hz, 2H), 1.79 – 1.65 (m, 2H), 1.53 – 1.36 (m, 2H), 0.97 (t, *J* = 7.4 Hz, 3H)

^{13}C NMR (101 MHz, $CDCl_3$) δ 164.8, 157.4, 141.8, 140.1, 123.7, 116.3, 83.1, 69.4, 65.3, 41.4, 30.7, 19.2, 13.7

HRMS (ESI, +): calcd. for $C_{13}H_{16}ClINaO_3$ 404.9725 $[M+Na]^+$, found 404.9728.

Butyl 2-(2-azidoethoxy)-5-iodobenzoate (**19**):

Compound **18** (8.88 g, 23.2 mmol) was placed in a flask, dry DMSO (50 mL) was added, followed by sodium azide (1.81 g, 27.8 mmol). The mixture was stirred for 2 d at 80 °C and then allowed to cool to r.t. It was poured into water (150 mL) and extracted 5 times with pentane. The combined organic phases were dried over Na_2SO_4 and evaporated, the crude oil was then purified by column chromatography (silica gel, Pentane:TBME 4:1 → 2:1) to give a colorless oil (7.92 g, 88 %).

^{1}H NMR (400 MHz, $CDCl_3$) δ 8.04 (d, *J* = 2.3 Hz, 1H), 7.71 (dd, *J* = 8.8, 2.3 Hz, 1H), 6.73 (d, *J* = 8.7 Hz, 1H), 4.29 (t, *J* = 6.7 Hz, 2H), 4.16 (t, *J* = 5.0 Hz, 2H), 3.63 (t, *J* = 5.0 Hz, 2H), 1.80 – 1.68 (m, 2H), 1.50 – 1.39 (m, 2H), 0.97 (t, *J* = 7.4 Hz, 3H)

^{13}C NMR (101 MHz, $CDCl_3$) δ 164.9, 157.5, 141.8, 140.1, 123.8, 115.9, 83.1, 68.3, 65.4, 50.2, 30.8, 19.3, 13.9

HRMS (ESI, +): calcd. for $C_{13}H_{17}IN_3NaO_3$ 412.0129 $[M+Na]^+$, found 412.0127

Compound **20**:

A solution of 1,4-diethynylbenzene (236 mg, 1.87 mmol) and **18** (1.50 g, 3.93 mmol) in THF (20 mL) and Et_3N (2.0 mL) was degassed with Ar for 10 min. Bis(triphenylphosphine)palladium dichloride (26 mg, 0.037 mmol, 2 mol%) and copper(I) iodide (7.0 mg, 0.037 mmol, 2 mol%) were added and the solution was stirred at r.t. for 30 min, followed by heating at 50 °C for 30 min. The reaction mixture was cooled to r.t. and filtered to remove Et_3NHI^-. The filter cake was washed with TBME until the filtrate was colorless. The product was obtained by a short plug column (Silica gel, toluene) to give a yellowish solid (650 mg, 55 %)

^{1}H NMR (400 MHz, $CDCl_3$) δ 7.97 (d, *J* = 2.2 Hz, 2H), 7.60 (dd, *J* = 8.6, 2.2 Hz, 2H), 7.49 (s, 4H), 6.94 (d, *J* = 8.6 Hz, 2H), 4.33 (t, *J* = 6.4 Hz, 4H), 4.31 (t, *J* = 6.0 Hz, 4H), 3.86 (t, *J* = 6.0 Hz, 4H), 1.80 – 1.72 (m, 4H), 1.53 – 1.42 (m, 4H), 0.98 (t, *J* = 7.4 Hz, 6H)

^{13}C NMR (101 MHz, $CDCl_3$) δ 165.5, 157.6, 136.3, 135.1, 131.6, 123.1, 121.9, 116.1, 113.6, 90.2, 89.0, 77.5, 77.2, 76.8, 68.2, 65.3, 50.2, 30.9, 19.4, 13.9

HRMS (MALDI, +): calcd. for $C_{36}H_{36}Cl_2O_6$ 634.1883 $[M]^+$, found 634.1883.

Ompound **21**:

Procedure A: Compound **19** (4.20 g, 10.8 mmol) was placed in a Schlenk tube, dry THF (50 mL) and Et_3N (5.0 mL) were added, followed by 1,4-diethynylbenzene (648 mg, 5.14 mmol). The solution was degassed with Ar for 10 min. Tetrakis(triphenylphosphine)palladium (6 mg, 0.05 mmol) and copper(I) iodide (2 mg, 0.1 mmol) were then added, followed by further degassing for 5 min. The reaction was heated at 50 °C for 1 d. The reaction mixture was then evaporated together with silica gel and purified by short column chromatography (Silica gel, DCM + 1 % EtOAc) to give the target compound (2.10 g, 63 %) as a yellowish solid.
Procedure B: Benzoate **20** (450 mg, 0.71 mmol) and sodium azide (460 mg, 7.08 mmol) were suspended in the mixture of toluene:DMSO (1:2, 15 mL) and heated to 120 °C for 1 h by microwave irradiation. After cooling, the vial was shaken, as a small amount of starting material stayed as a rim above the liquid layer. The vial was then heated again at 120 °C for 1 h. The residue was partitioned between DCM (40 mL) and water (300 mL), and the aqueous phase was again extracted with DCM (40 mL). The combined organic phases were washed with water (300 mL), dried over sodium sulfate and evaporated. Purification by column chromatography (Silica gel, DCM → DCM/EtOAc 97:3) afforded 220 mg (58 %) of a yellowish solid.

^{1}H NMR (400 MHz, $CDCl_3$) δ 7.95 (d, *J* = 2.2 Hz, 2H), 7.60 (dd, *J* = 8.6, 2.2 Hz, 2H), 7.49 (s, 4H), 6.94 (d, *J* = 8.6 Hz, 2H), 4.32 (t, *J* = 6.7 Hz, 4H), 4.22 (t, *J* = 5.0 Hz, 4H), 3.66 (t, *J* = 5.0 Hz, 4H), 1.75 (m, 4H), 1.57 – 1.33 (m, 4H), 0.98 (t, *J* = 7.4, 6H)

^{13}C NMR (101 MHz, $CDCl_3$) δ 165.5, 157.6, 136.3, 135.1, 131.6, 123.1, 121.9, 116.1, 113.6, 90.2, 89.0, 77.5, 77.2, 76.8, 68.2, 65.3, 50.2, 30.9, 19.4, 13.9

HRMS (MALDI, +): calcd. for $C_{36}H_{36}N_6O_6$ 648.2691 $[M]^+$, found 648.2690.

Compound **3**:

A solution of sodium hydroxide (1.20 g, 30.0 mmol) in water (3 mL) was prepared and diluted with MeOH (10 mL). Afterwards **22** (1.20 g, 1.85 mmol) was added, followed by THF (20 mL) and a clear solution was obtained, which was stirred for 20 h at room temperature. The solvents were then removed in vacuo and the crude product was suspended in water (15 mL) and acidified with 5 % HCl until a pH < 2 was reached. After stirring for 20 min, the precipitate was filtered off and washed with water (2 × 40 mL), MeOH (2 × 10 mL) and Et_2O (20 mL) to give a white solid (0.98 g, 99 %).

^{1}H NMR (500 MHz, THF-d_8 + 2 drops of $CDCl_3$) δ 11.33 (s, 2H), 7.98 (d, *J* = 2.3 Hz, 2H), 7.61 (dd, *J* = 8.6, 2.3 Hz, 2H), 7.50 (s, 4H), 7.11 (d, *J* = 8.7 Hz, 2H), 4.23 (t, *J* = 5.0 Hz, 4H), 3.63 (t, *J* = 4.9 Hz, 4H)

^{13}C NMR (126 MHz, THF 2 drops of $CDCl_3$) δ 166.5, 158.9, 136.7, 136.1, 132.1, 124.0, 122.7, 116.5, 114.7, 91.0, 89.2, 69.1, 51.0

HRMS (ESI, +): calcd. for $C_{28}H_{20}N_6NaO_6$ 559.1337 $[M+Na]^+$, found 559.1343.

Compound **3 * 2 Na**:

Carboxylic acid **3** (300 mg, 0.56 mmol) was placed in a flask and *i*-PrOH was added (15 mL) followed by THF (5 mL). The suspension was sonicated and 10 % aqueous sodium hydroxide (0.6 mL) was added. It was stirred for 90 min and the solids were filtered off. The crude disodium salt was redissolved in ethanol/water (1:1, approx. 50 mL) and concentrated to a volume of 5 mL, during the course of which the disodium salt of **3** precipitated. The precipitate was washed with water (2 × 2mL) and air-dried to give the desired compound as a white solid (240 mg, 74 %)

^{1}H NMR (600 MHz, THF-d_8/MeOD 3:1) δ 8.01 (d, *J* = 2.3 Hz, 2H), 7.69 (dd, *J* = 8.6, 2.3 Hz, 2H), 7.57 (s, 4H), 7.21 (d, *J* = 8.7 Hz, 2H), 4.31 (t, *J* = 4.9 Hz, 4H), 3.72 (t, *J* = 4.9 Hz, 4H)

^{13}C NMR (151 MHz, THF-d_8/MeOD 3:1) δ 164.26, 156.16, 133.95, 132.86, 129.37, 121.19, 120.20 (low intensity, identified by HMBC), 113.40, 111.98, 88.10, 86.18, 66.29, 48.14

HRMS was identical to **3.**

Compound **23**:

[(3,5-Diethynylphenyl)ethynyl]triisopropylsilane **22** (445 mg, 1.45 mmol) was dissolved in acetone (20 mL) and 11-azido-3,6,9-trioxadodecanol (1.10 g, 5.07 mmol) was added, the solution was degassed with Ar for 5 min, then tetrakis(acetonitrile)copper(I)-hexafluorophosphate (54 mg, 0.15 mmol) and tris[(1-benzyl-1*H*-1,2,3-triazol-4-yl)methyl]amine (77 mg, 0.15 mmol) were added. It was stirred for 20 min and then the compound was adsorbed on silica gel and purified by column chromatography (Silica gel, EtOAc/Acetone 1:1 -> acetone → acetone 10 % EtOH) to give the desired product as a clear oil (1.0 g, 93 %).

^{1}H NMR (400 MHz, CD_3CN) δ 8.36 (d, *J* = 1.6 Hz, 1H), 8.33 (s, 2H), 7.89 (d, *J* = 1.6 Hz, 2H), 4.57 (t, *J* = 5.0 Hz, 4H), 3.90 (t, *J* = 5.0 Hz, 4H), 3.63 – 3.56 (m, 4H), 3.57 – 3.47 (m, 16H), 3.45 – 3.38 (m, 4H), 2.85 (t, *J* = 5.8 Hz, 2H), 1.17 (s, 21H)

^{13}C NMR (101 MHz, CD_3CN) δ 145.4, 132.0, 127.4, 123.9, 122.1, 121.8, 106.2, 90.8, 72.0, 69.8 (4C), 69.7 (4C), 68.6, 60.6, 49.9, 17.7, 10.8

HRMS (ESI, +): calcd. for $C_{37}H_{60}N_6NaO_8Si$ 767.4134 $[M+Na]^+$, found 767.4130.

Compound **4**:

Compound **23** (983 mg, 1.32 mmol) was dissolved in THF (10 mL) and tetrabutylammonium fluoride solution in THF (1 M, 4.0 mL, 4.0 mmol) was added. It was stirred for 6 h and then silica gel was added and the solvent was removed in vacuo. The desired compound was obtained by column chromatography (Silica gel, acetone → acetone/EtOH 9:1) as a yellowish oil (615 mg, 79 %).

^{1}H NMR (400 MHz, Acetone-d_6) δ 8.60 (s, 2H), 8.50 (t, *J* = 1.6 Hz, 1H), 7.99 (d, *J* = 1.6 Hz, 2H), t (t, *J* = 5.0 Hz, 4H), 3.99 (t, *J* = 5.0 Hz, 4H), 3.79 (s, 1H), 3.70 – 3.63 (m, 4H), 3.63 – 3.56 (m, 16H), 3.52 – 3.48 (m, 4H), 2.90 (s, 2H)

^{13}C NMR (101 MHz, Acetone) δ 146.6, 133.5, 128.5, 124.2, 123.4, 123.0, 83.9, 79.7, 73.5, 71.2, (4C), 71.1 (4C), 70.0, 62.0, 51.0

HRMS (ESI, +): calcd. for $C_{28}H_{41}N_6O_8$ 589.2980 $[M+H]^+$, found 589.2983.

Compound **1 * 2 HCOOH**:

Cyclophane **2** (80 mg, 63 µmol) and azide **3** (202 mg, 378 µmol, 6 eq) were placed in a flask and DMF (2.0 mL) was added, followed by Et_3N (0.2 mL). While degassing with Ar it was stirred for 10 min giving a clear solution. Tris[(1-benzyl-1*H*-1,2,3-triazol-4-yl)methyl]amine (3.34 mg, 6.3 µmol, 10 mol%) and tetrakis(acetonitrile)copper(I)-hexafluorophosphate (2.35 mg, 6.3 µmol, 10 mol%) were added and the yellow solution was stirred until **2** was completely consumed according to HPLC/ESI-MS analysis, which took approximately 24 h. The mixture was then directly applied onto a size exclusion column (Sephadex LH-20, MeOH/H_2O 1:1, 0.20 M NH_4HCO_3) to separate a large part of excess **3**. The solvent was removed from the product fraction by rotary evaporation (bath temperature 25 °C, by the end of evaporation *n*-butanol was added to prevent foaming). Final purification was achieved by dividing the reaction batch into two equal portions, which were purified by preparative HPLC (RP-C18, 5 % to 90 % CH_3CN in H_2O in 13 minutes) to obtain **1 * 2 HCOOH** as a white solid in varying yields between 30 and 64 %. Analytical samples of the zwitterionic compound for NMR studies were prepared by neutralization of the conjugate acid with NH_4CO_3 and subsequent desalting by size exclusion chromatography (Sephadex LH-20, MeOH/H_2O 1:1).

^{1}H NMR (600 MHz, THF-d_8 : D_2O 4:1) δ 8.50 (s, 1H, H-T), 7.96 (s, 1H, H-Q), 7.89 (d, *J* = 2.3 Hz, 1H, H-d), 7.85 (d, *J* = 2.3 Hz, 1H, H-v), 7.56 (dd, *J* = 9.2, 2.3 Hz, 1H, H-f), 7.55 (dd, *J* = 9.2, 2.3 Hz, 1H, H-q), 7.40 (s, 4H, H-k,l), 7.15 (d, *J* = 8.8 Hz, 1H, H-g), 7.13 (d, *J* = 8.7 Hz, 1H, H-r), 7.09 (s, 1H, H-O), 6.60 (s, 2H, H-B), 6.56 (s, 2H, H-G or H-J), 6.55 (s, 2H, H-G or H-J), 4.91 (t, *J* = 4.8 Hz, 2H, H-31), 4.49 (t, *J* = 4.7 Hz, 2H, H-32), 4.19 (t, *J* = 4.8 Hz, 2H, H-33), 3.75 (t, *J* = 6.1 Hz, 2H, H-11 or 14), 3.71 (t, *J* = 5.8 Hz, 2H, H-11 or 14), 3.65 (s, 6H, H-10), 3.63 (m, overlapping, 2H, H-26), 3.62 (s, 6H, H-15), 3.59 (m, overlapping, 4H, H-29/34), 3.58 (s, 6H, H-25), 3.31 (m, br, 16H, H-2/4/5/6/19/20/21/23), 2.72 (m, br, 8H, H-7/8/17/18), 2.12 (s, 3H, H-30), 1.76 (m, Hz, 2H, H-28), 1.70 (m, 4H, H-12/13), 1.54 (m, 2H, H-27), 1.35 – 1.01 (m, 12H, H-1/3/22/24)

^{13}C NMR (126 MHz, THF-d_8 : D_2O 4:1) δ 157.95 (C-a/s), 153.34 (C-C or F or K), 153.24 (C-C or F or K), 153.17 (C-C or F or K), 152.55 (C-M), 143.19 (C-S), 136.15 (C-f), 135.79 (C-q), 135.47 (C-D or L), 135.43 (C-D or E), 135.02 (C-L), 134.65 (C-d), 134.48 (C-v), 132.13 (C-N), 131.00 (C-k/l), 129.10 (C-O), 124.24 (C-T), 123.56 (C-R), 122.77 (C-j or m), 122.65 (C-j or m), 122.37 (C-Q), 114.84 (C-e), 114.65 (C-p), 113.88 (C-g or r), 113.80 (C-g or r), 103.37 (2C, C-B/G or J), 103.19 (C-G or J), 89.96(C-h), 89.85 (C-o), 87.84 (C-i or n), 87.73 (C-i or n), 72.19 (C-26/29), 71.90 (C-11/14), 68.03 (C-33), 67.74 (C-32), 55.52 (2C, C-10 or 15 or 25), 55.47 (C-10 or 15 or 25), 55.15 (4C, C-2 and/or 4/5/6/19/20/21/23), 55.10 (4C, C-2 and/or 4/5/6/19/20/21/23), 49.79 (C-34), 49.42 (C-31), 42.98 (C-16), 42.44 (C-9), 28.65 (2C, C7/8/17/18), 28.54 (2C, C7/8/17/18), 26.77 (C-28), 26.00 (C-27), 25.91 (C-12 or 13), 25.86 (C-12 or 13), 15.69 (C-30), 6.26 (2C, C-1/3/22/24), 6.25 (C-1/3/22/24), 6.23 (C-1/3/22/24); Resonances of the quaternary carbon atoms A/H/I/P/u/p were not observed, assignments of c/t is unclear.

HRMS (ESI, +): calcd. for $C_{87}H_{102}N_8O_{16}$ 757.3701 $[M]^{2+}$, found 757.3712.

Analytical data of compounds 6-11, 13-15, 17-21 & 23

^{1}H- and ^{13}C-NMR spectra of **6**

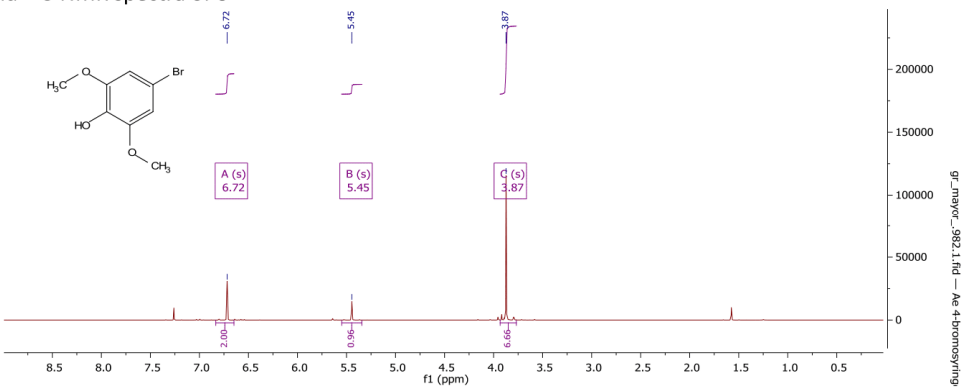

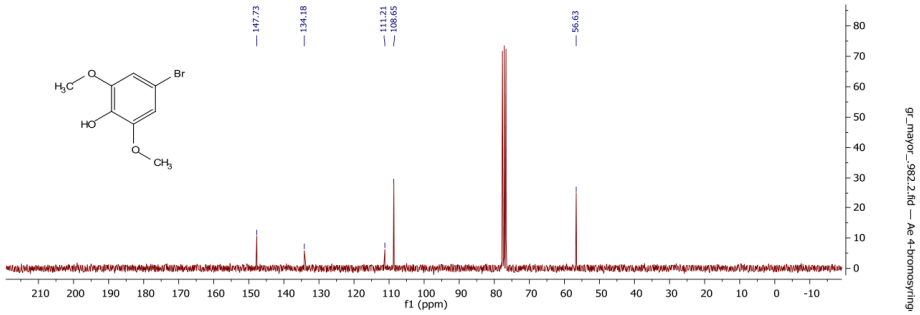

Mass Spectrum SmartFormula Report

Analysis Info

Analysis Name	N:\new acq data\Ae 493 001.d	Acquisition Date	30.03.2016 08:45:56
Method	hn Direct_Infusion_pos mode_75-1700 mid 4eV.m	Operator	hn
Sample Name	Yves Aeschi	Instrument / Ser#	maXis 4G 21243
Comment	Ae 493, ca. 10 ug/ml MeOH		

Acquisition Parameter

Source Type	ESI	Ion Polarity	Positive	Set Nebulizer	0.4 Bar
Focus	Not active	Set Capillary	3600 V	Set Dry Heater	180 °C
Scan Begin	75 m/z	Set End Plate Offset	-500 V	Set Dry Gas	4.0 l/min
Scan End	1700 m/z	Set Collision Cell RF	350.0 Vpp	Set Ion Energy (MS only)	4.0 eV

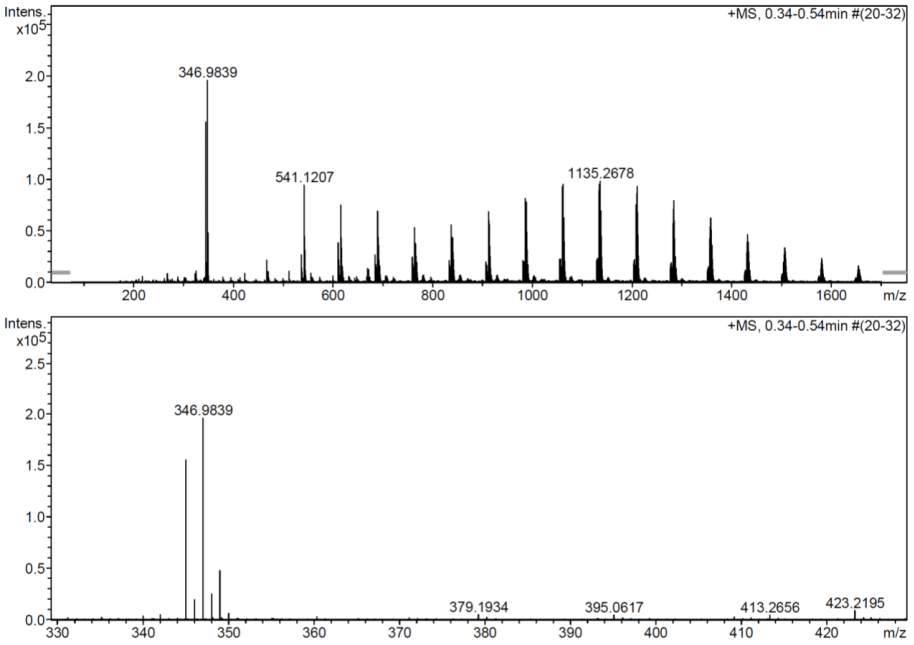

Meas. m/z	#	Formula	Score	m/z	err [mDa]	err [ppm]	mSigma	rdb	e⁻ Conf	N-Rule	z
344.9861	1	C 12 H 16 Br Cl Na O 3	100.00	344.9864	0.3	0.8	11.8	3.5	even	ok	1+

^{1}H-, ^{13}C-NMR spectra and HRMS of **7**

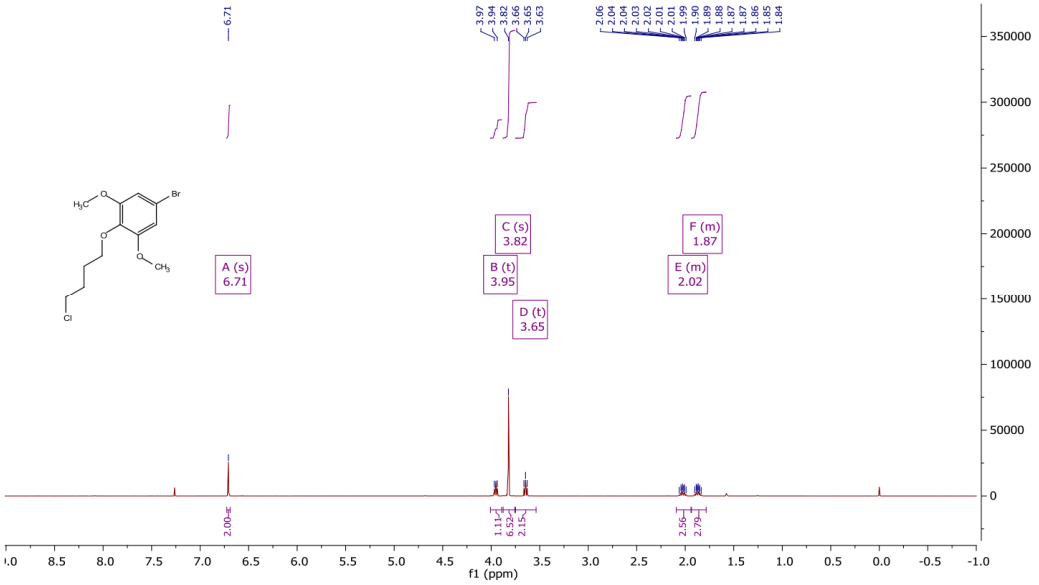

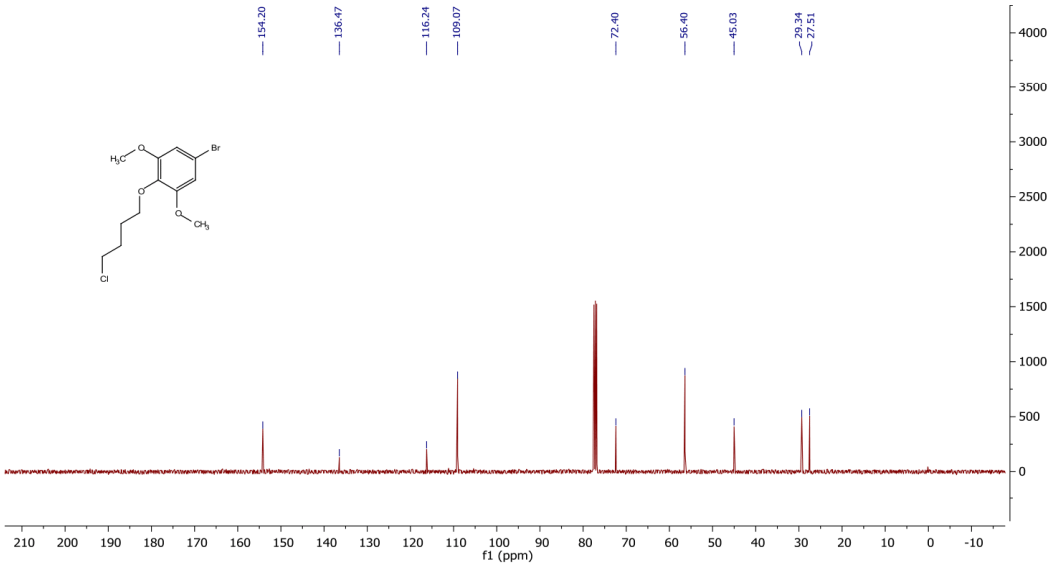

^{1}H-, ^{13}C-NMR spectra and HRMS of **8**

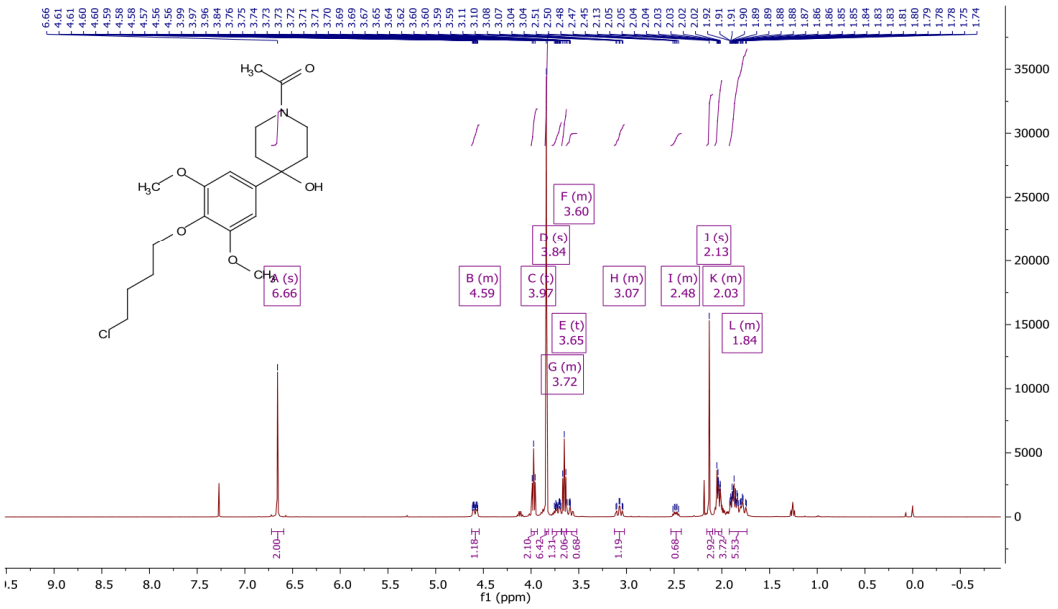

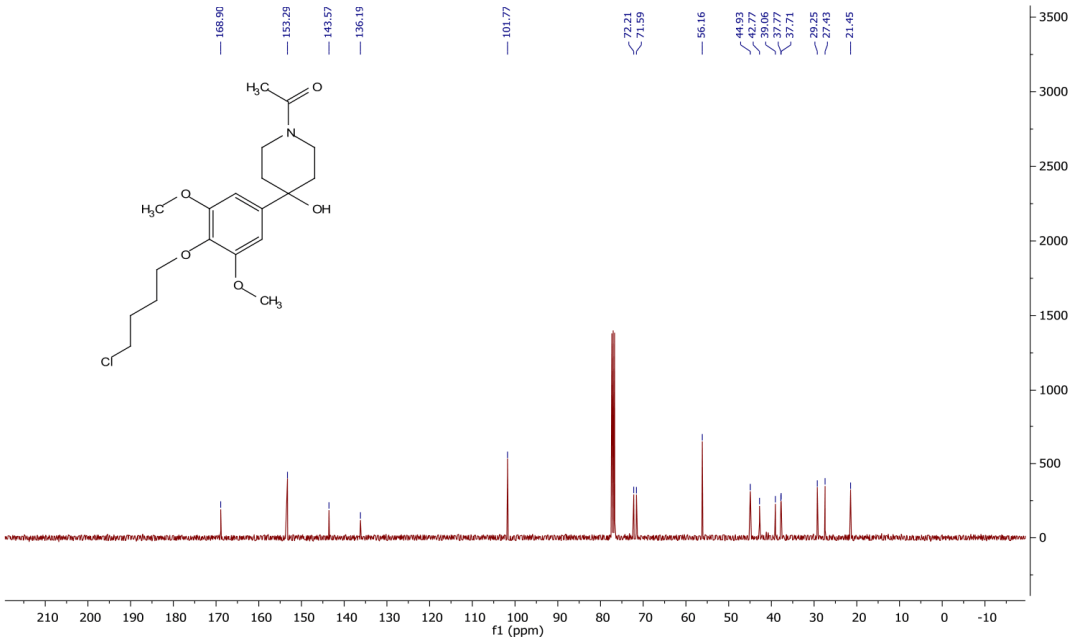

SI-60

^{1}H-, ^{13}C-NMR spectra and HRMS of **9**

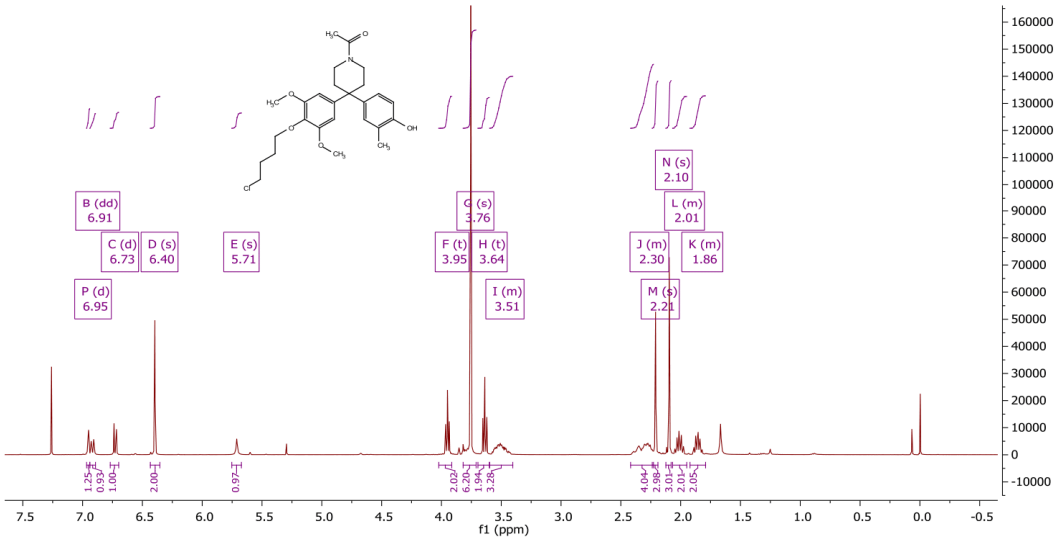

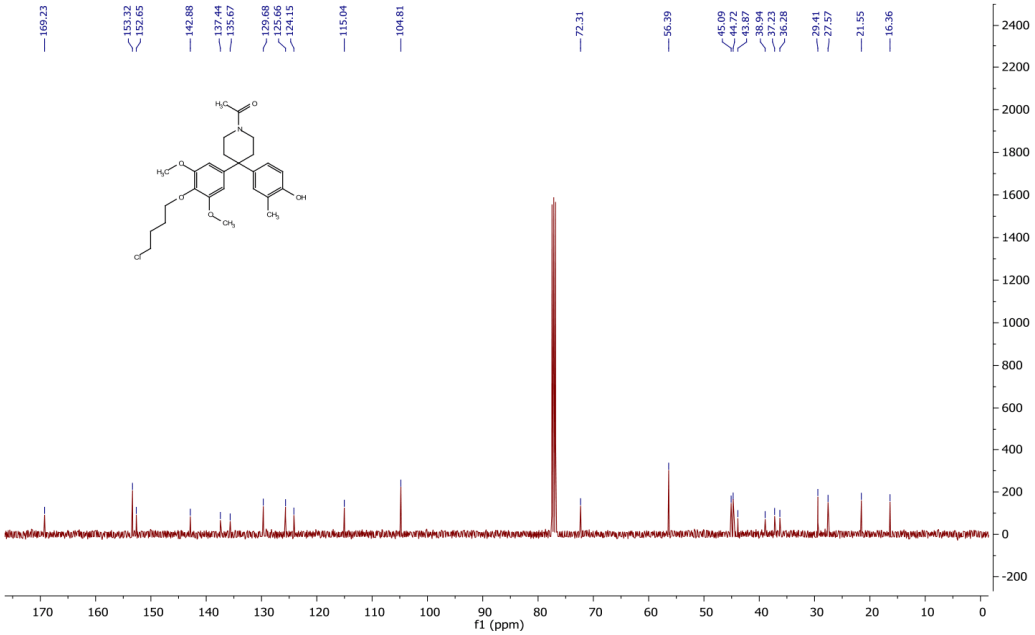

Mass Spectrum SmartFormula Report

Analysis Info

Analysis Name	N:\new acq data\Ae 401 003.d.d	Acquisition Date	13.11.2015 17:19:18
Method	hn Direct_Infusion_pos mode_75-1700 low 4eV.m	Operator	hn
Sample Name	Yves Aeschi	Instrument / Ser#	maXis 4G 21243
Comment	Ae 401, ca. 1 ug/ml MeCN		

Acquisition Parameter

Source Type	ESI	Ion Polarity	Positive	Set Nebulizer	0.4 Bar
Focus	Not active	Set Capillary	3600 V	Set Dry Heater	180 °C
Scan Begin	75 m/z	Set End Plate Offset	-500 V	Set Dry Gas	3.0 l/min
Scan End	1700 m/z	Set Collision Cell RF	350.0 Vpp	Set Ion Energy (MS only)	4.0 eV

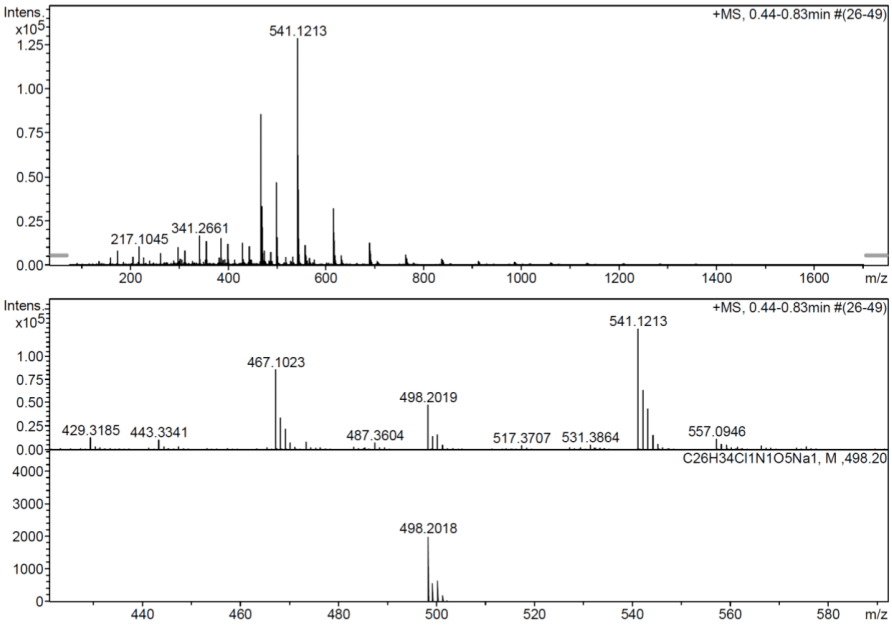

Meas. m/z	#	Formula	Score	m/z	err [mDa]	err [ppm]	mSigma	rdb	e⁻ Conf	N-Rule	z
498.2019	1	C 26 H 34 Cl N Na O 5	100.00	498.2018	-0.2	-0.3	17.3	9.5	even	ok	1+

^{1}H-, ^{13}C-NMR spectra and HRMS of **10.**

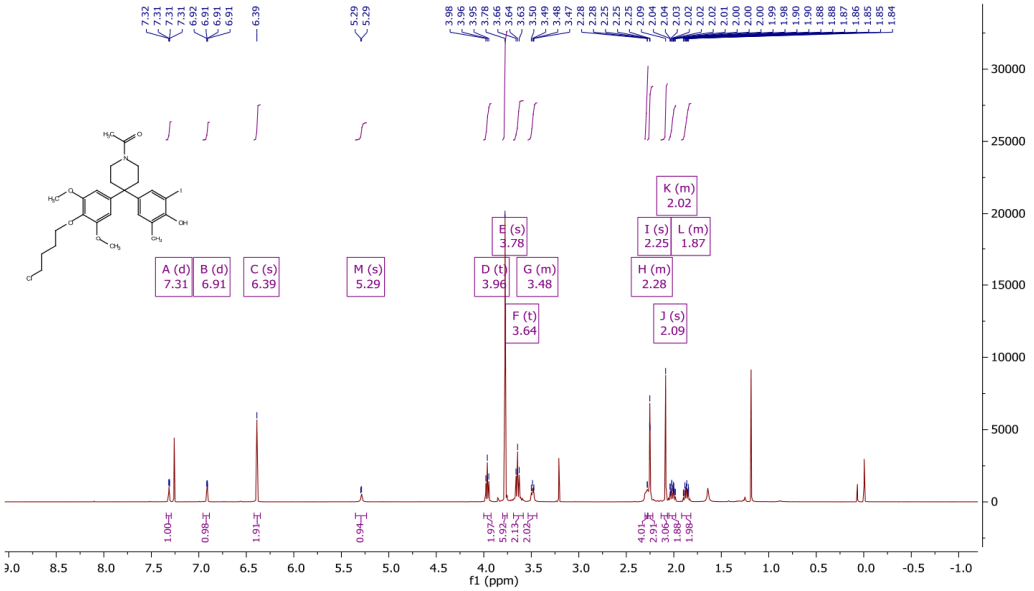

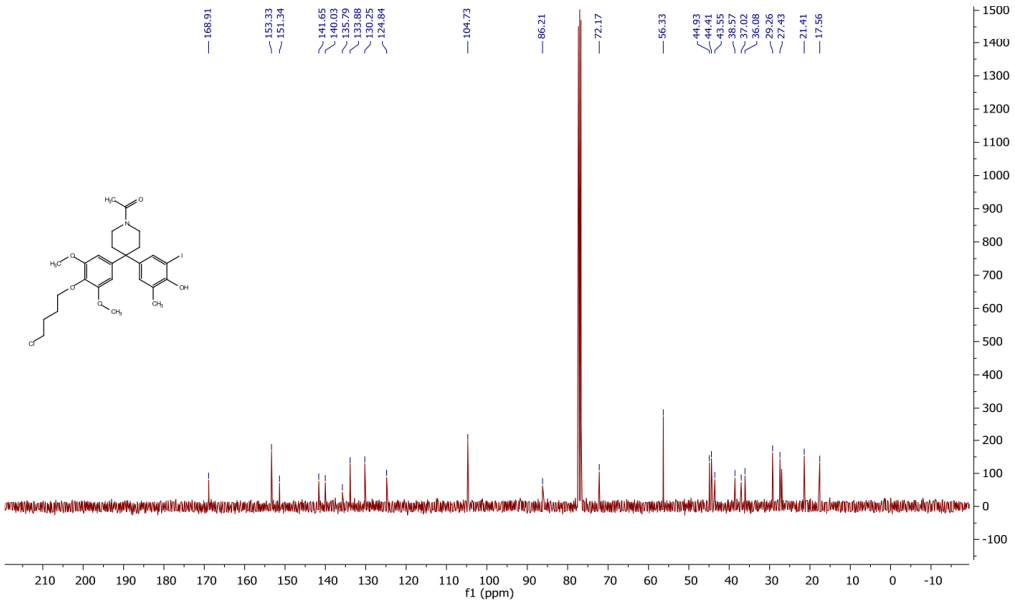

Mass Spectrum SmartFormula Report

Analysis Info

Analysis Name	N:\new acq data\Ae 417 002.d	Acquisition Date	16.11.2015 14:40:23
Method	hn Direct_Infusion_pos mode_75-1700 mid 4eV.m	Operator	hn
Sample Name	Yves Aeschi	Instrument / Ser#	maXis 4G 21243
Comment	Ae 417, ca. 10 ug/ml MeCN, mit HCOOH		

Acquisition Parameter

Source Type	ESI	Ion Polarity	Positive	Set Nebulizer	0.4 Bar
Focus	Not active	Set Capillary	3600 V	Set Dry Heater	180 °C
Scan Begin	75 m/z	Set End Plate Offset	-500 V	Set Dry Gas	4.0 l/min
Scan End	1700 m/z	Set Collision Cell RF	350.0 Vpp	Set Ion Energy (MS only)	4.0 eV

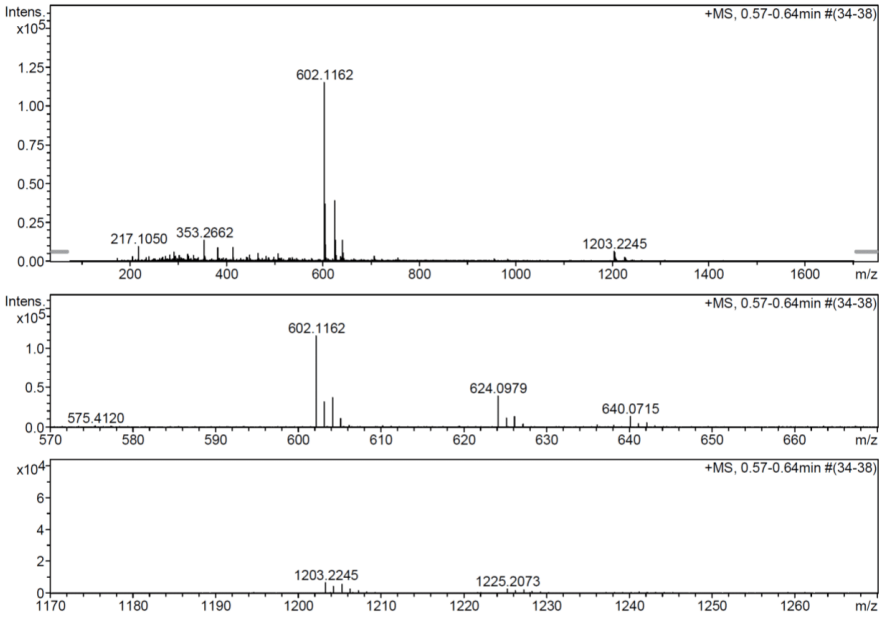

Meas. m/z	#	Formula	Score	m/z	err [mDa]	err [ppm]	mSigma	rdb	e⁻ Conf	N-Rule	z
602.1162	1	C 26 H 34 Cl I N O 5	100.00	602.1165	0.2	0.4	24.3	9.5	even	ok	1+
624.0979	1	C 26 H 33 Cl I N Na O 5	100.00	624.0984	0.6	0.9	10.1	9.5	even	ok	
640.0715	1	C 26 H 33 Cl I K N O 5	100.00	640.0724	0.8	1.3	20.9	9.5	even	ok	
1203.2245	1	C 52 H 67 Cl 2 I 2 N 2 O 10	100.00	1203.2257	1.1	0.9	14.1	18.5	even	ok	
1225.2073	1	C 52 H 66 Cl 2 I 2 N 2 Na O 10	100.00	1225.2076	0.3	0.2	39.4	18.5	even	ok	

^{1}H-, ^{13}C-NMR spectra and HRMS of **11**

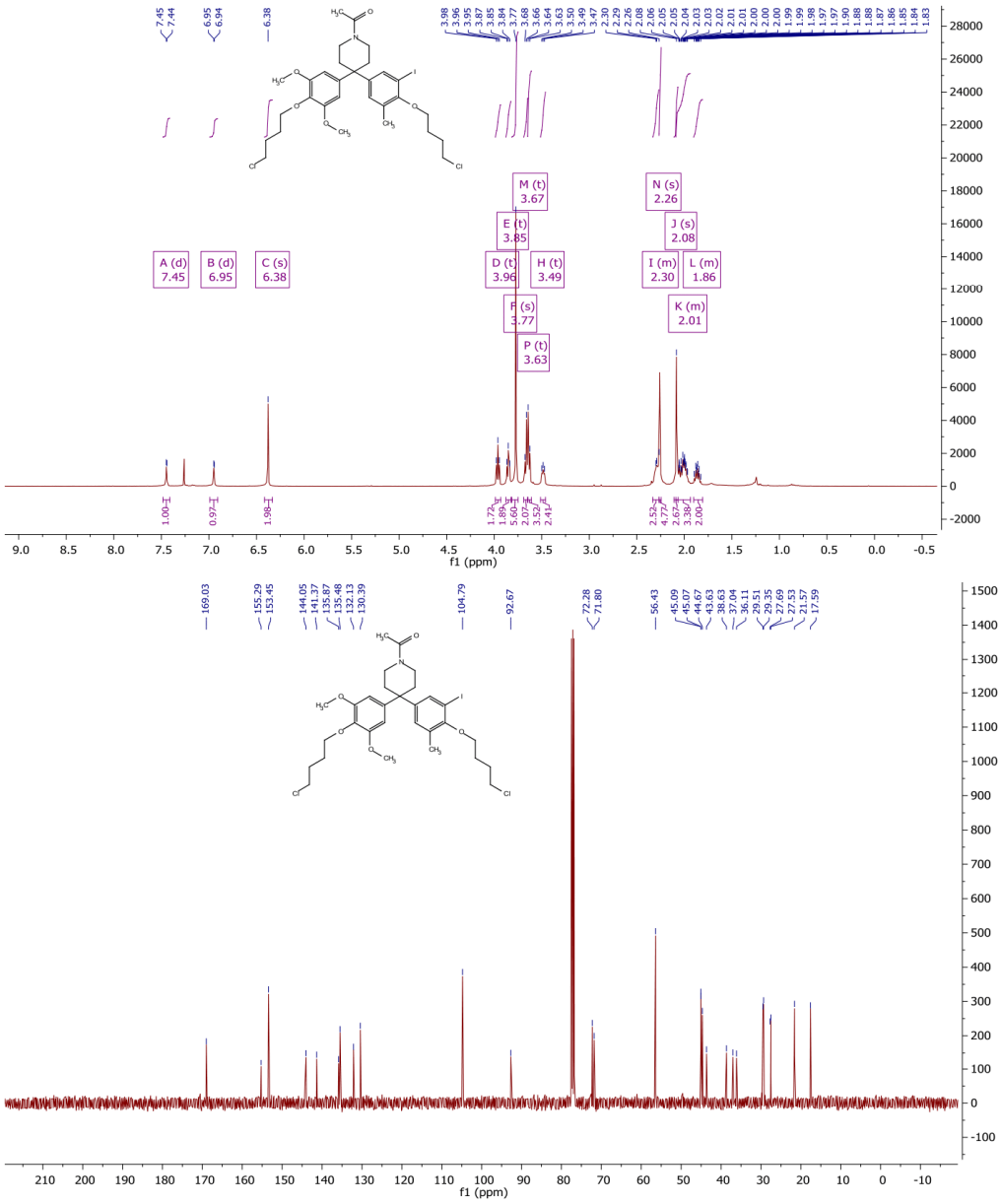

Mass Spectrum SmartFormula Report

Analysis Info

Analysis Name	N:\new acq data\Ae 345 001.d	Acquisition Date	16.07.2015 09:27:08
Method	hn Direct_Infusion_pos mode_75-2000 high 4eV.m	Operator	hn
Sample Name	Yves Aeschi, Ae 345	Instrument / Ser#	maXis 4G 21243
Comment	ca 10 ug/mL MeCN		

Acquisition Parameter

Source Type	ESI	Ion Polarity	Positive	Set Nebulizer	0.4 Bar
Focus	Not active	Set Capillary	3600 V	Set Dry Heater	180 °C
Scan Begin	75 m/z	Set End Plate Offset	-500 V	Set Dry Gas	4.0 l/min
Scan End	2000 m/z	Set Collision Cell RF	1000.0 Vpp	Set Ion Energy (MS only)	4.0 eV

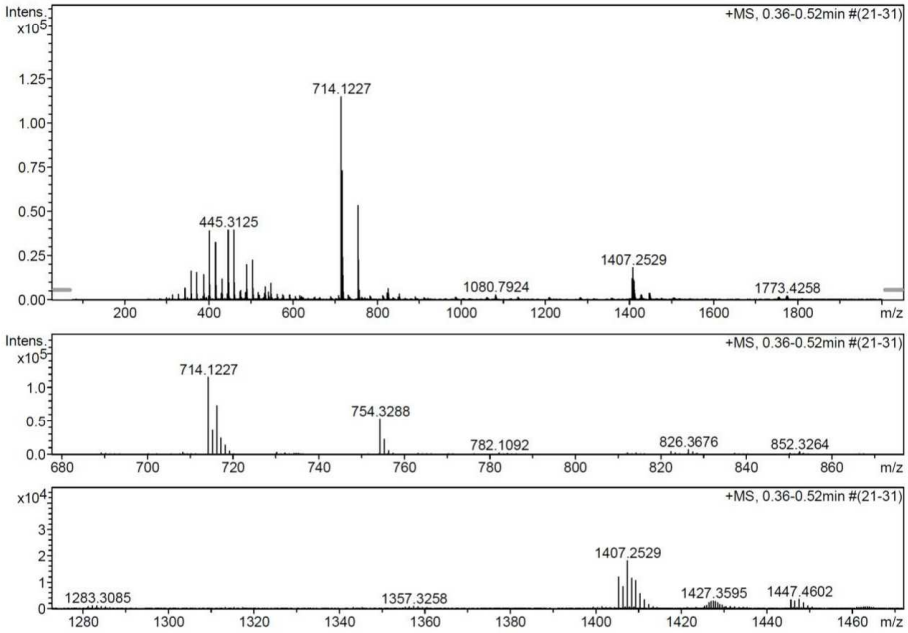

Meas. m/z	#	Formula	Score	m/z	err [mDa]	err [ppm]	mSigma	rdb	e⁻ Conf	N-Rule	z
714.1227	1	C 30 H 40 Cl 2 I N Na O 5	100.00	714.1220	-0.6	-0.9	28.7	9.5	even	ok	1+
1405.2543	1	C 60 H 80 Cl 4 I 2 N 2 Na O 10	100.00	1405.2549	0.6	0.4	13.7	18.5	even	ok	

Mass Spectrum SmartFormula Report

Analysis Info

Analysis Name	N:\new acq data\Ae 494 002.d	Acquisition Date	30.03.2016 09:55:22
Method	hn Direct_Infusion_pos mode_75-1700 mid 4eV.m	Operator	hn
Sample Name	Yves Aeschi	Instrument / Ser#	maXis 4G 21243
Comment	Ae 494, ca. 5 ug/ml MeOH		

Acquisition Parameter

Source Type	ESI	Ion Polarity	Positive	Set Nebulizer	0.4 Bar
Focus	Not active	Set Capillary	3600 V	Set Dry Heater	180 °C
Scan Begin	75 m/z	Set End Plate Offset	-500 V	Set Dry Gas	4.0 l/min
Scan End	1700 m/z	Set Collision Cell RF	350.0 Vpp	Set Ion Energy (MS only)	4.0 eV

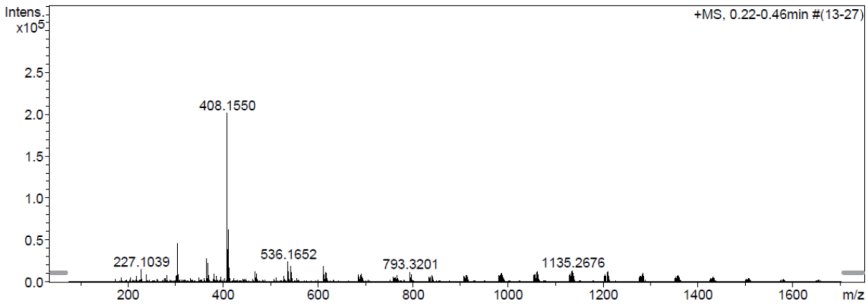

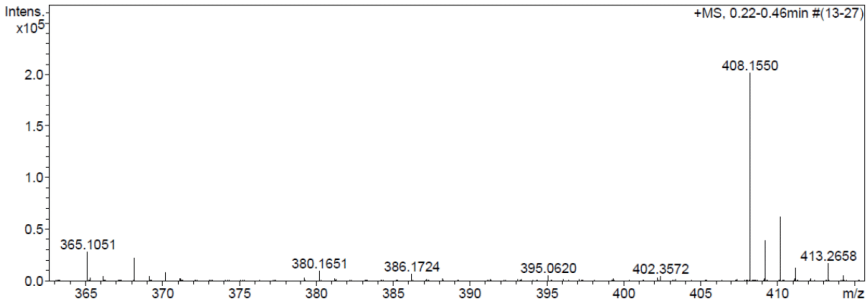

Meas. m/z	#	Formula	Score	m/z	err [mDa]	err [ppm]	mSigma	rdb	e⁻ Conf	N-Rule	z
368.1620	1	C 19 H 27 Cl N O 4	100.00	368.1623	0.3	0.9	9.6	6.5	even	ok	1+
386.1724	1	C 19 H 29 Cl N O 5	100.00	386.1729	0.5	1.3	12.5	5.5	even	ok	
408.1550	1	C 19 H 28 Cl N Na O 5	100.00	408.1548	-0.2	-0.5	20.8	5.5	even	ok	
793.3201	1	C 38 H 56 Cl 2 N 2 Na O 10	100.00	793.3204	0.3	0.4	9.1	10.5	even	ok	

^{1}H-, ^{13}C-NMR spectra and HRMS of **13**

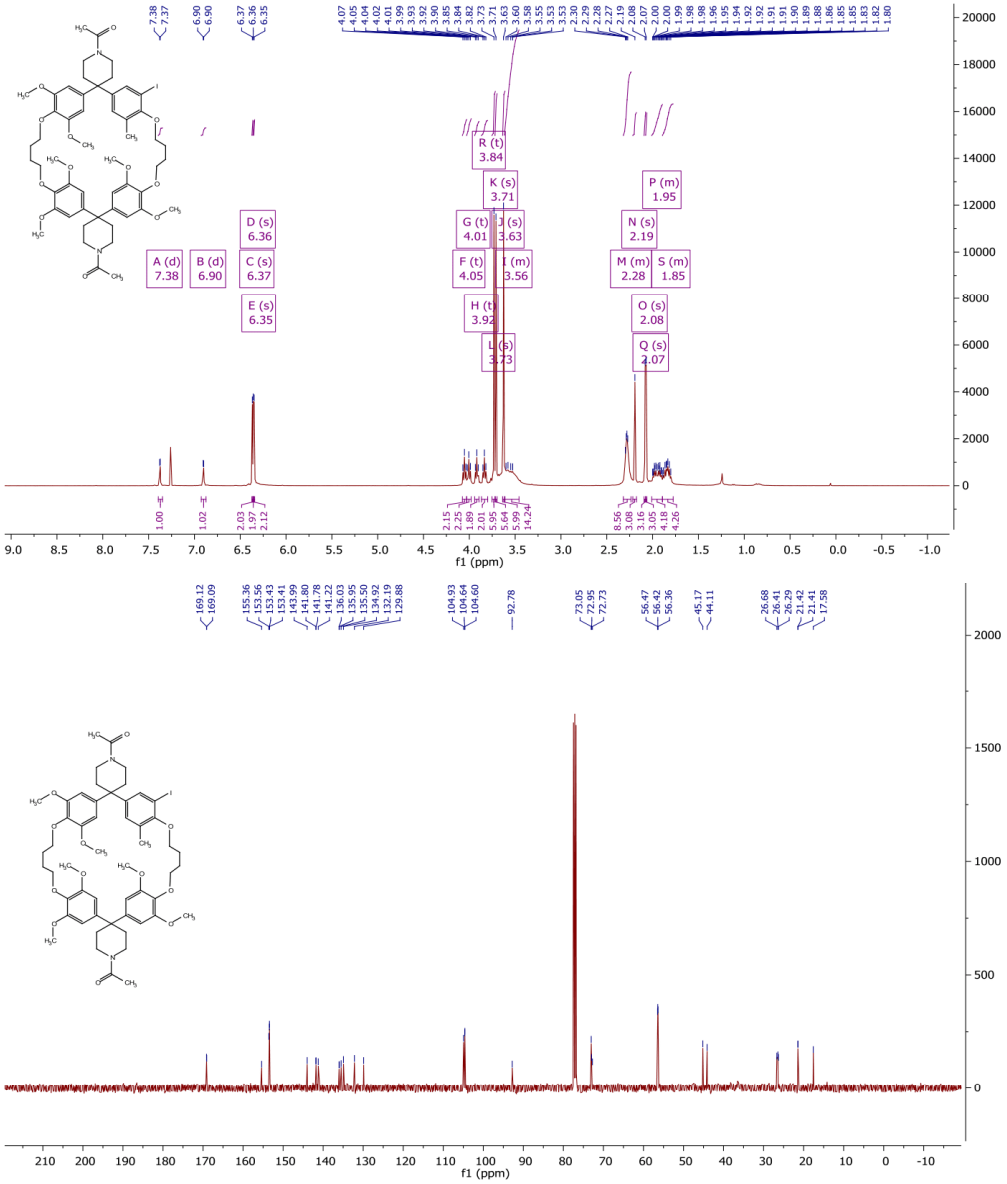

FT12370 Yves Aeschi/Mayor - CyMeO6I - DCM / DCTB

ETH Eidgenössische Technische Hochschule Zürich Swiss Federal Institute of Technology Zurich

Acquisition Parameter

Method:	MALDI_MS_POS_300-2600_2M_16AvScans			Acquisition Date:	20.09.2017 16:22:39
File Name:	D:\ETH\Data\FT123xx\FT12370_0_P8_000001.d			Operator:	Louis Bertschi
Source	Dual (MALDI/ESI)	Polarity	Positive	Nebulizer Gas	1.3 bar
Broadband Low Mass	303.1 m/z	n/a	n/a	Drying Gas Flow Rate	3.7 L/min
Broadband High Mass	2600.0 m/z	Laser Power	30.8 lp	Capillary	4500.0 V
No. of Cell Fills	1	n/a	n/a	Drying Gas	200.0 °C
Apodization	Full-Sine	Time of Flight to Detector	0.001 sec	Temperature	

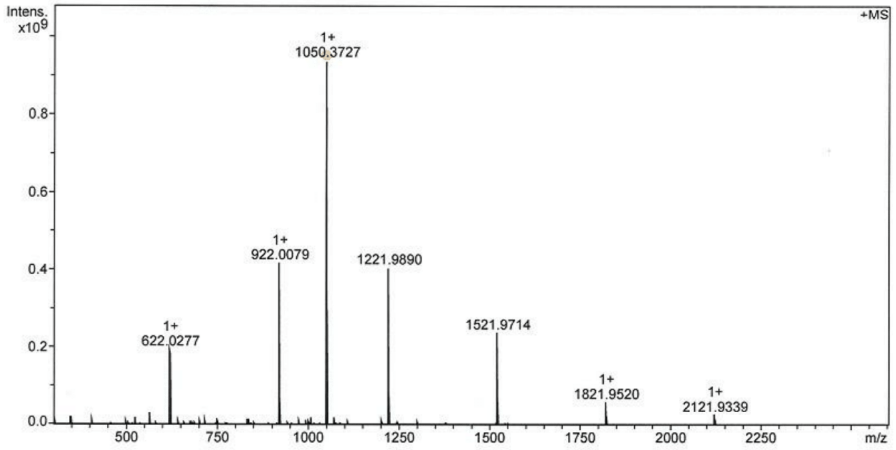

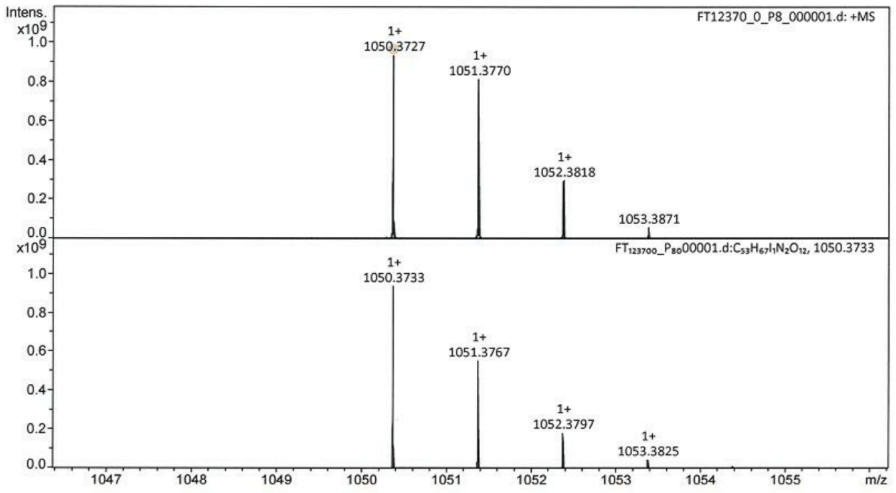

FT12370 Yves Aeschi/Mayor - CyMeO6I - DCM / DCTB

ETH Eidgenössische Technische Hochschule Zürich Swiss Federal Institute of Technology Zurich

Acquisition Parameter

Method:	MALDI_MS_POS_300-2600_2M_16AvScans			Acquisition Date:	20.09.2017 16:22:39
File Name:	D:\ETH\Data\FT123xx\FT12370_0_P8_000001.d			Operator:	Louis Bertschi
Source	Dual (MALDI/ESI)	Polarity	Positive	Nebulizer Gas	1.3 bar
Broadband Low Mass	303.1 m/z	n/a	n/a	Drying Gas Flow Rate	3.7 L/min
Broadband High Mass	2600.0 m/z	Laser Power	30.8 lp	Capillary	4500.0 V
No. of Cell Fills	1	n/a	n/a	Drying Gas	200.0 °C
Apodization	Full-Sine	Time of Flight to Detector	0.001 sec	Temperature	

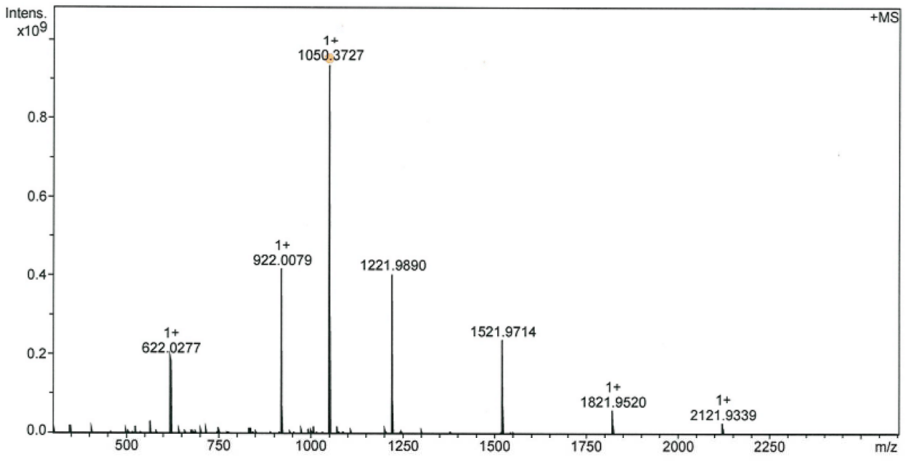

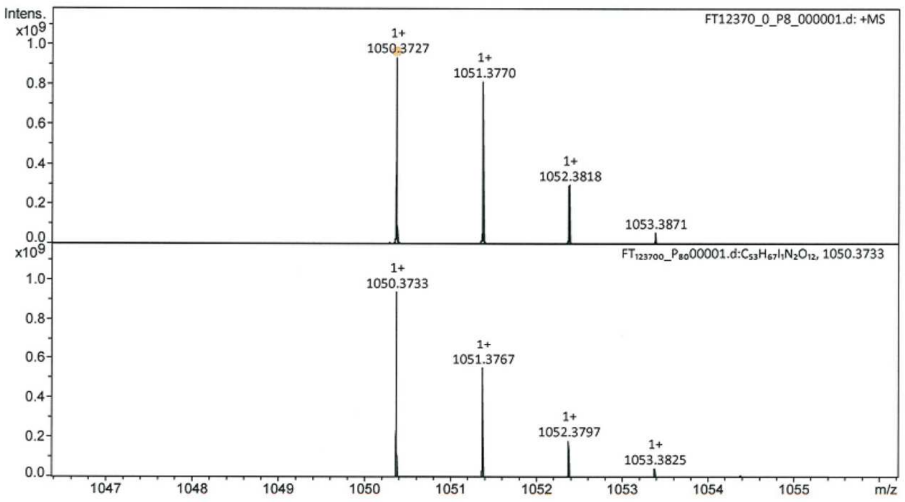

^{1}H-, ^{13}C-NMR spectra and HRMS of **14**

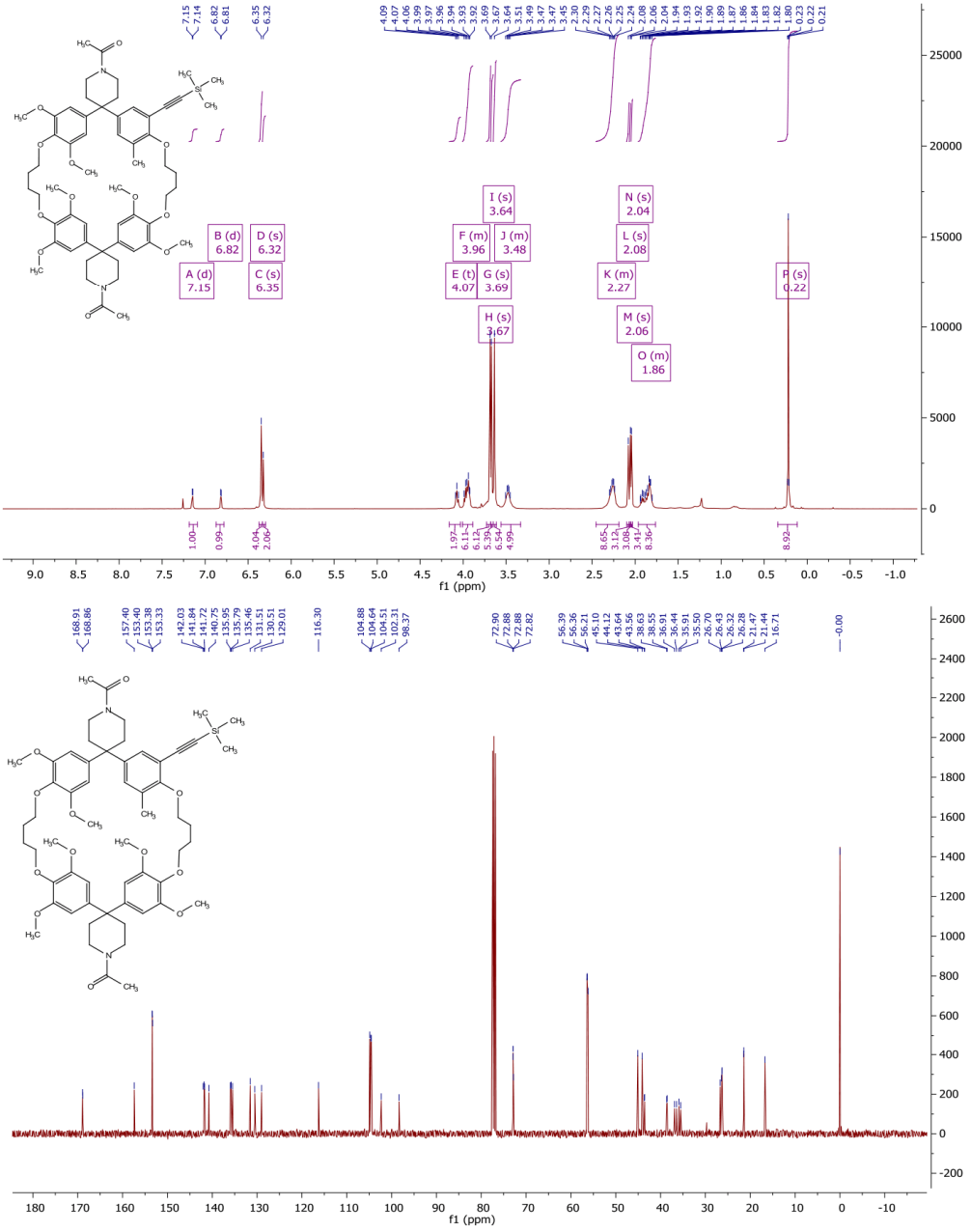

FT12369 Yves Aeschi/Mayor - CyMeO6TMSA - DCM / DCTB

ETH Eidgenössische Technische Hochschule Zürich Swiss Federal Institute of Technology Zurich

Acquisition Parameter

Method:	MALDI_MS_POS_300-2600_2M_16AvScans			Acquisition Date:	20.09.2017 16:20:25
File Name:	D:\ETH\Data\FT123xx\FT12369_0_P7_000001.d			Operator:	Louis Bertschi
Source	Dual (MALDI/ESI)	Polarity	Positive	Nebulizer Gas	1.3 bar
Broadband Low Mass	303.1 m/z	n/a	n/a	Drying Gas Flow Rate	3.7 L/min
Broadband High Mass	2600.0 m/z	Laser Power	30.8 lp	Capillary	4500.0 V
No. of Cell Fills	1	n/a	n/a	Drying Gas	200.0 °C
Apodization	Full-Sine	Time of Flight to Detector	0.001 sec	Temperature	

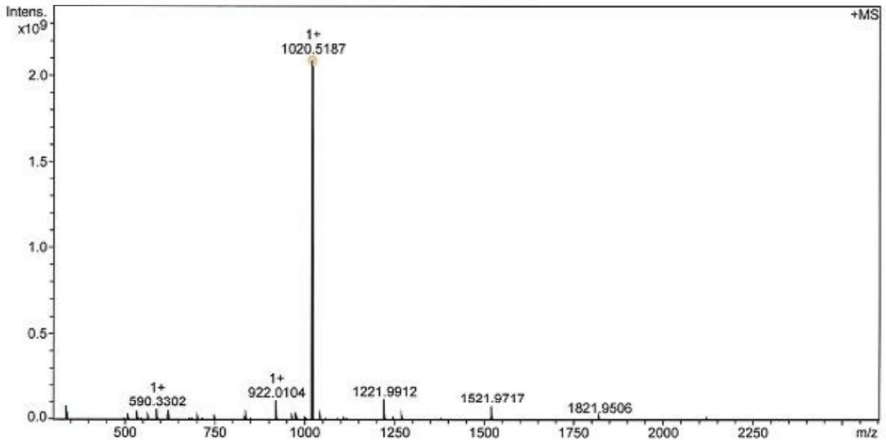

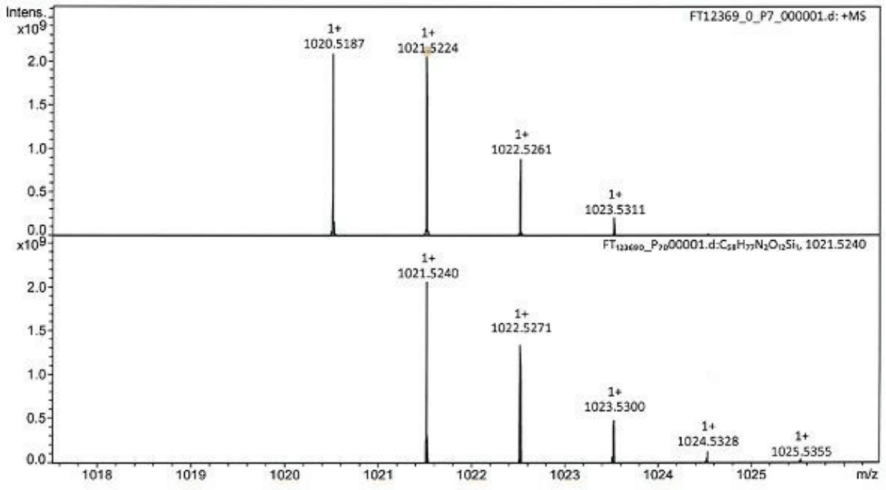

Evaluation Spectra / Validation Formula:

#	Ion Formula	Adduct	m/z	z	Meas. m/z	mSigma	N-Rule	err [mDa]	err [ppm]
1	C58H77N2O12Si	M+H	1021.5240	1+	1021.5224	102.7	ok	1.6	1.6

Calibration Info:

Date:	22.09.2017 11:01:45
Polarity:	Positive
Calibration spectrum:	+MS: Scan
Reference mass list:	MALDI: DCTB Matrix + HP-Mix (pos)
Calibration mode:	Quadratic

Reference m/z	Resulting m/z	Intensity	Error [ppm]
118.0863			
250.1464			
251.1543			
273.1362			
322.0481			
332.2009			
500.2934			
501.3013			
523.2832	523.2834	923493	0.351
622.0290	622.0285	55858628	-0.812
750.4404			
751.4483			
773.4302			
922.0098	922.0104	116782968	0.609
1000.5874			
1001.5953			
1023.5772			
1221.9906	1221.9912	125198688	0.465
1521.9715	1521.9717	83542344	0.163
1821.9523	1821.9506	24191716	-0.937
2121.9332			
2421.9140			
2721.8948			

Standard deviation: 0.915

Mass List:

#	m/z	Res.	S/N	I %	FWHM
1	510.2582	360559	945.8	1.3	0.0014
2	510.7601	387054	1311.9	1.8	0.0013
3	510.7957	398739	478.7	0.7	0.0013
4	511.2619	402999	470.9	0.6	0.0013
5	536.2828	306869	1793.7	2.5	0.0017
6	566.8876	345942	666.8	1.0	0.0016
7	566.8890	349723	588.0	0.8	0.0016
8	590.3302	248690	1921.9	2.8	0.0024
9	591.3338	249118	601.7	0.9	0.0024
10	622.0259	234490	462.5	0.7	0.0027
11	622.0285	378620	1743.7	2.7	0.0016
12	622.0306	404096	1027.0	1.6	0.0015
13	702.8631	326737	707.5	1.2	0.0022
14	702.8655	384052	434.7	0.7	0.0018
15	751.4508	218591	429.6	0.7	0.0034
16	838.8383	283992	750.9	1.4	0.0030
17	838.8419	317286	428.8	0.8	0.0026
18	922.0057	344758	476.9	1.0	0.0027
19	922.0104	243796	2657.0	5.5	0.0038
20	922.0151	300612	1065.9	2.2	0.0031
21	923.0139	230965	484.4	1.1	0.0040
22	965.4654	154322	341.9	0.8	0.0063
23	974.8137	239162	434.7	1.0	0.0041
24	978.4740	149189	481.1	1.1	0.0066
25	1020.5187	187605	45447.2	100.0	0.0054
26	1021.5224	189808	44411.4	97.7	0.0054
27	1022.5261	194550	19340.3	42.6	0.0053
28	1023.5311	197235	4467.5	9.8	0.0052
29	1043.5111	127660	558.5	1.2	0.0082
30	1044.5152	149056	336.8	0.7	0.0070
31	1110.7888	211113	300.4	0.6	0.0053
32	1221.9912	181171	2636.2	5.9	0.0067
33	1222.9952	170739	635.6	1.4	0.0072
34	1270.6690	106993	476.7	1.1	0.0119
35	1271.6731	128154	569.3	1.3	0.0099
36	1521.9585	110550	285.4	0.7	0.0138
37	1521.9717	140108	1670.5	4.0	0.0109
38	1521.9837	242934	666.6	1.6	0.0063
39	1522.9754	139870	527.0	1.3	0.0109
40	1821.9506	110611	437.6	1.1	0.0165

#	m/z	Res.	S/N	I %	FWHM
1	1021.5240	189808		100.0	0.0054
2	1022.5271	94997		69.9	0.0108
3	1023.5209	190179		3.4	0.0054
4	1023.5300	95090		26.4	0.0108
5	1024.5242	190365		2.1	0.0054
6	1024.5328	95184		7.1	0.0108
7	1025.5273	190552		0.7	0.0054
8	1025.5355	95277		1.5	0.0108
9	1026.5303	190738		0.2	0.0054
10	1026.5396	190740		0.2	0.0054

^{1}H-, ^{13}C-NMR spectra and HRMS of **15**

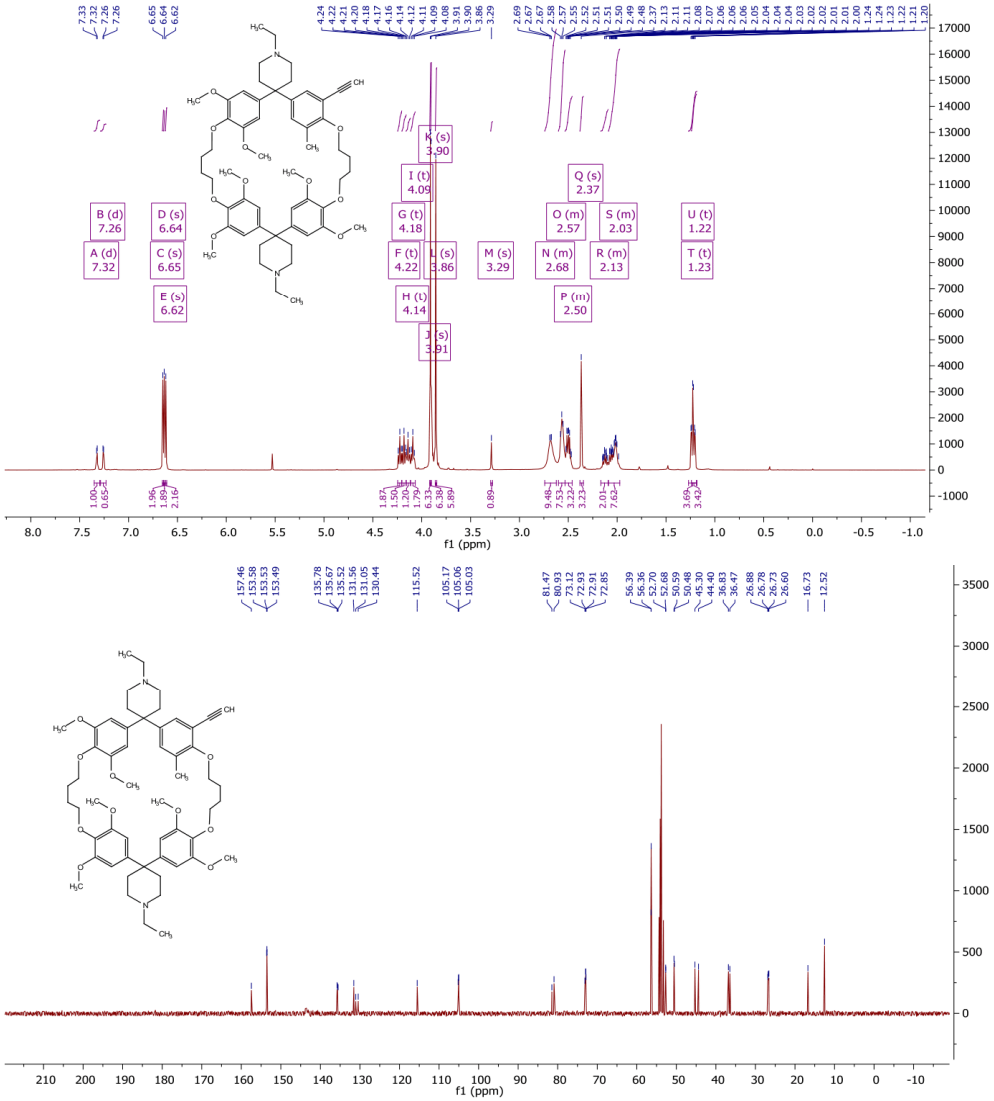

Mass Spectrum SmartFormula Report

Analysis Info

Analysis Name	E:\new acq data for data analysis\Ae 535 001.d	Acquisition Date	12.04.2017 15:31:01
Method	hn Direct_Infusion_pos mode_75-1700 mid 4eV.m	Operator	hn
Sample Name	Yves Aeschi	Instrument / Ser#	maXis 4G 21243
Comment	Ae 535, ca. 10 ug/ml MeOH		

Acquisition Parameter

Source Type	ESI	Ion Polarity	Positive	Set Nebulizer	0.4 Bar
Focus	Not active	Set Capillary	3600 V	Set Dry Heater	180 °C
Scan Begin	75 m/z	Set End Plate Offset	-500 V	Set Dry Gas	4.0 l/min
Scan End	1700 m/z	Collision Energy	8.0 eV	Set Ion Energy (MS only)	4.0 eV

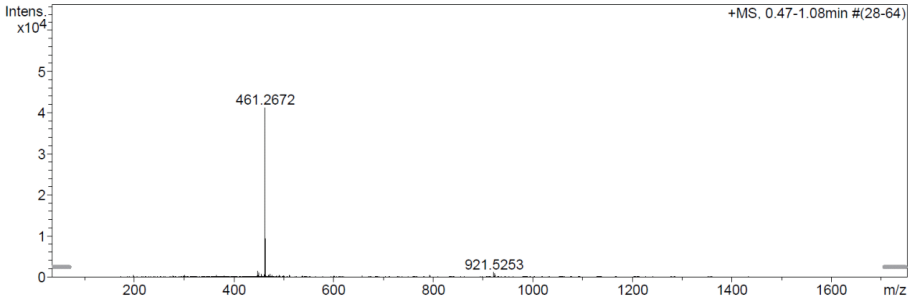

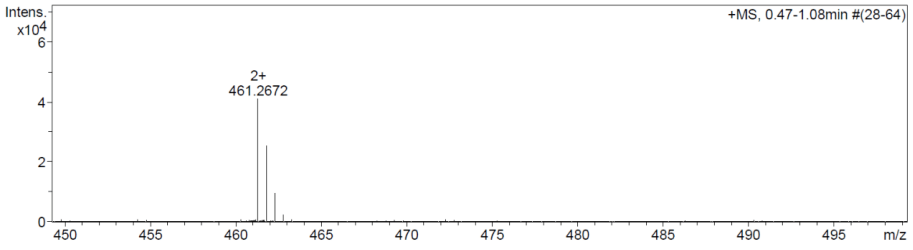

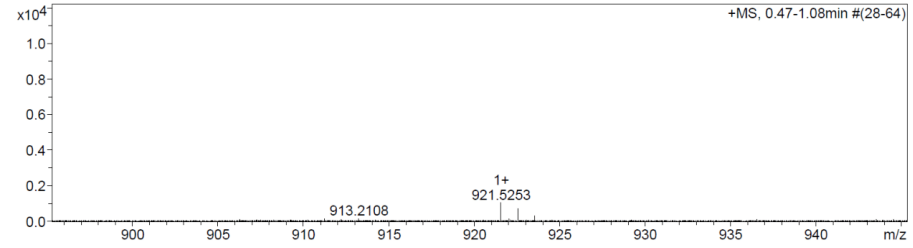

Meas. m/z	#	Formula	Score	m/z	err [mDa]	err [ppm]	mSigma	rdb	e⁻ Conf	z
461.2672	1	C 55 H 74 N 2 O 10	100.00	461.2666	-0.6	-1.3	10.1	20.0	even	2+
921.5253	1	C 55 H 73 N 2 O 10	100.00	921.5260	0.7	0.8	43.1	20.5	even	1+

^{1}H-, ^{13}C-NMR spectra and HRMS of **17**

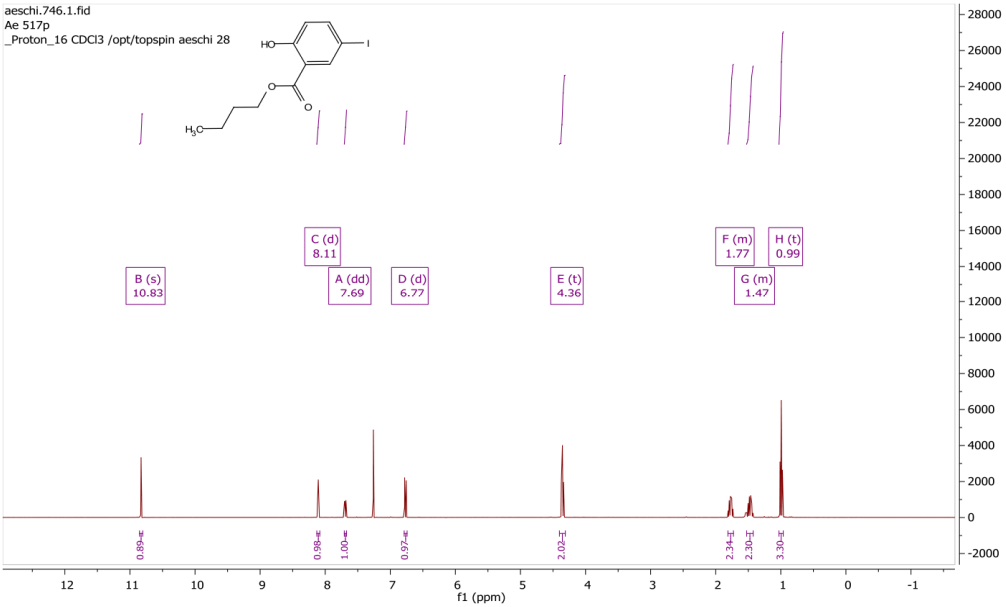

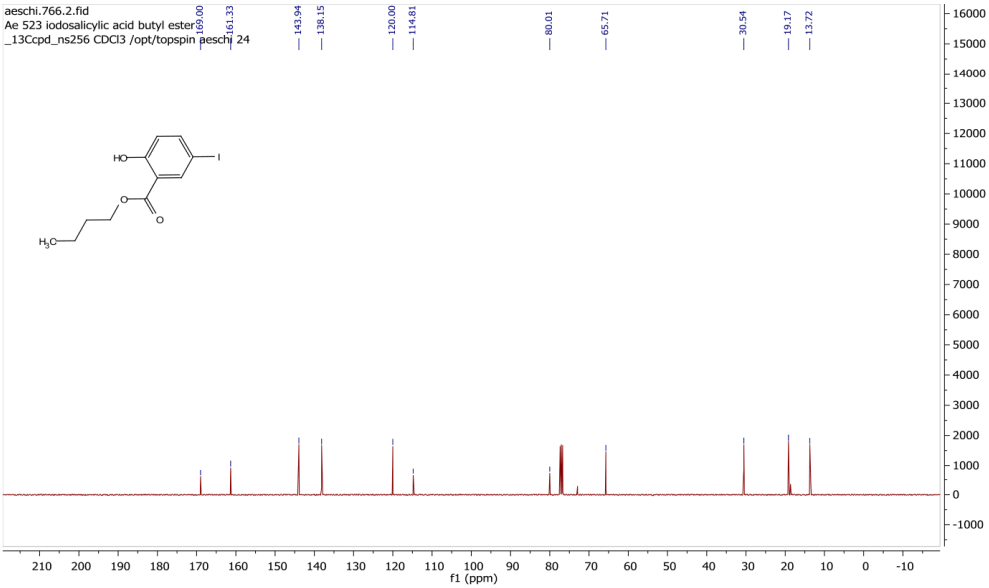

Mass Spectrum SmartFormula Report

Analysis Info

Analysis Name	N:\new acq data\Ae 517 001.d	Acquisition Date	21.04.2016 08:54:46
Method	hn Direct_Infusion_pos mode_75-1700 mid 4eV.m	Operator	hn
Sample Name	Yves Aeschi	Instrument / Ser#	maXis 4G 21243
Comment	Ae 517, ca. 10 ug/ml MeOH		

Acquisition Parameter

Source Type	ESI	Ion Polarity	Positive	Set Nebulizer	0.4 Bar
Focus	Not active	Set Capillary	3600 V	Set Dry Heater	180 °C
Scan Begin	75 m/z	Set End Plate Offset	-500 V	Set Dry Gas	4.0 l/min
Scan End	1700 m/z	Set Collision Cell RF	350.0 Vpp	Set Ion Energy (MS only)	4.0 eV

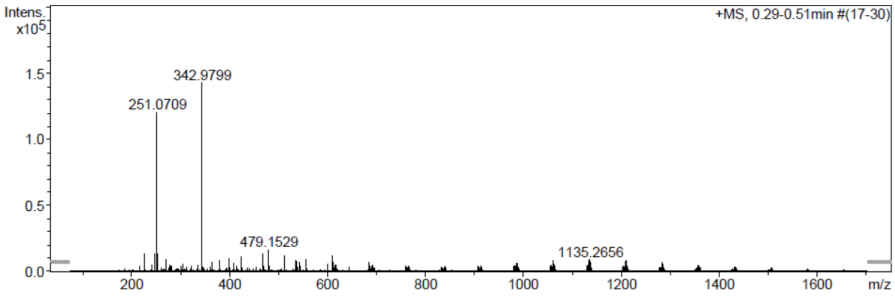

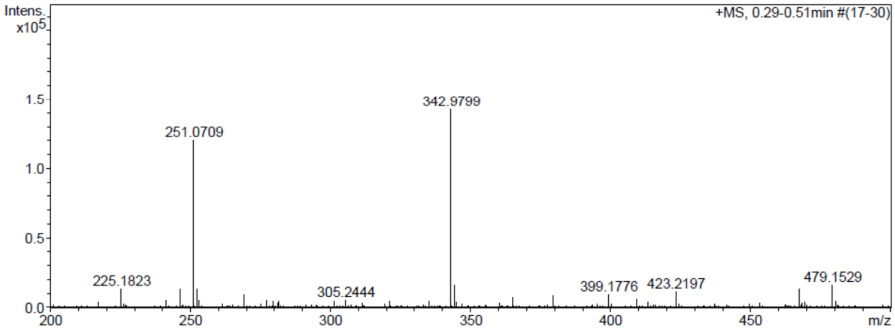

Meas. m/z	#	Formula	Score	m/z	err [mDa]	err [ppm]	mSigma	rdb	e⁻ Conf	N-Rule	z
342.9799	1	C 11 H 13 I Na O 3	100.00	342.9802	0.2	0.6	8.2	4.5	even	ok	1+

^{1}H-, ^{13}C-NMR spectra and HRMS of **18**

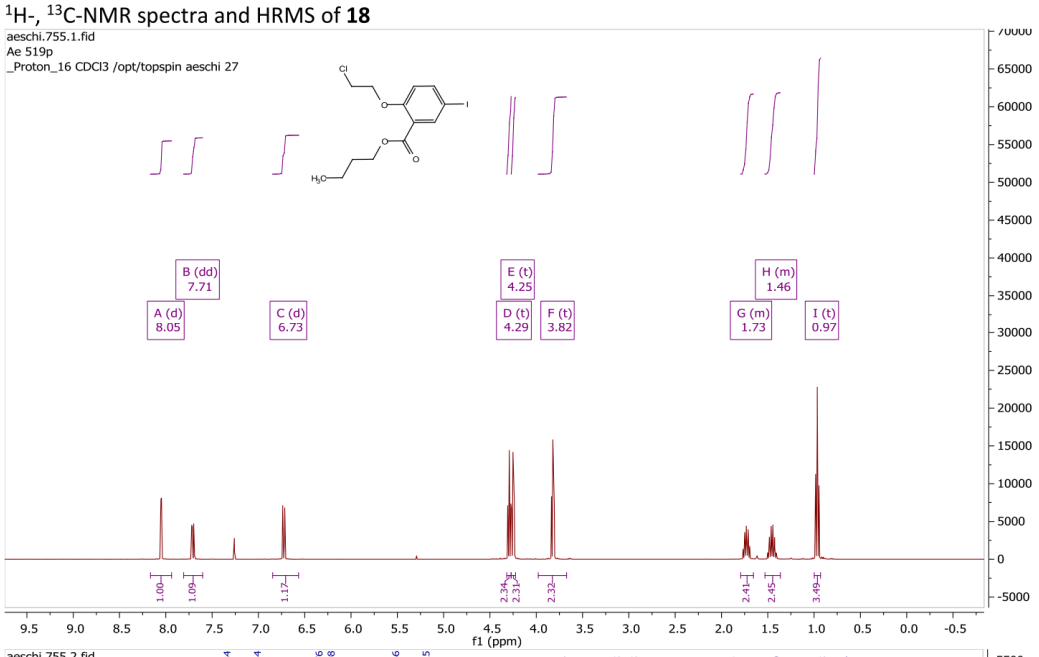

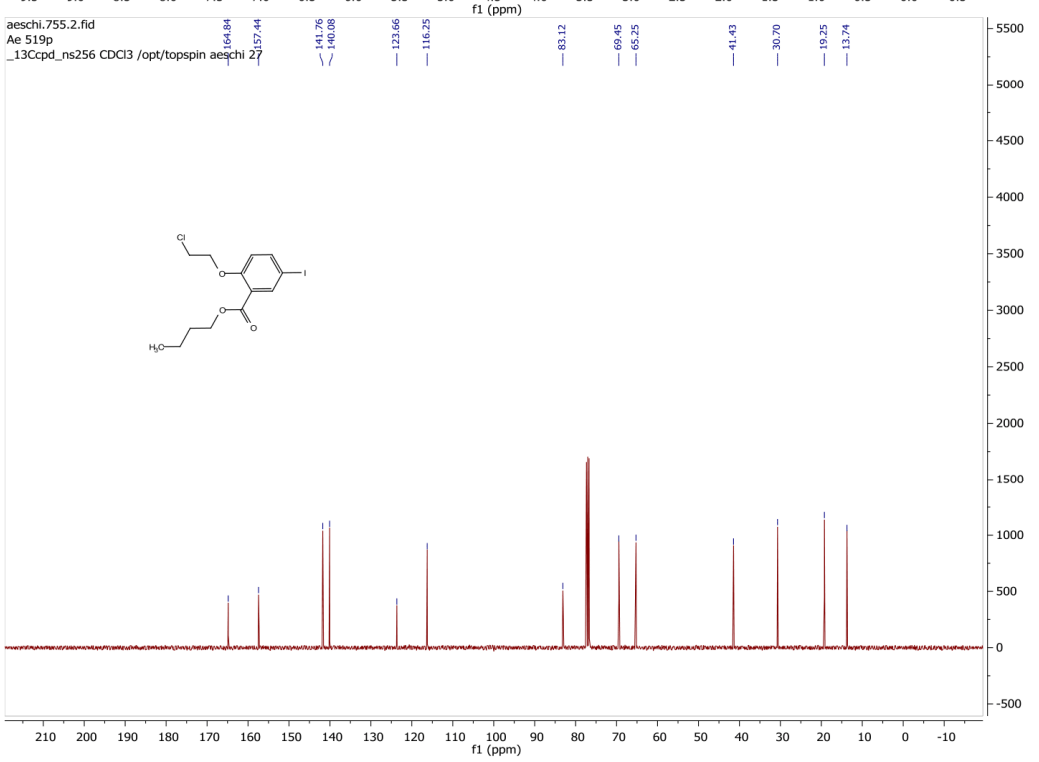

Mass Spectrum SmartFormula Report

Analysis Info

Analysis Name	E:\new acq data for data analysis\Ae 519 001.d	Acquisition Date	27.07.2016 14:48:46
Method	hn Direct_Infusion_pos mode_75-1700 low 4eV.m	Operator	hn
Sample Name	Yves Aeschi	Instrument / Ser#	maXis 4G 21243
Comment	Ae 519, ca. 10 ug/ml MeOH		

Acquisition Parameter

Source Type	ESI	Ion Polarity	Positive	Set Nebulizer	0.4 Bar
Focus	Not active	Set Capillary	3600 V	Set Dry Heater	180 °C
Scan Begin	75 m/z	Set End Plate Offset	-500 V	Set Dry Gas	3.0 l/min
Scan End	1700 m/z	Set Collision Cell RF	350.0 Vpp	Set Ion Energy (MS only)	4.0 eV

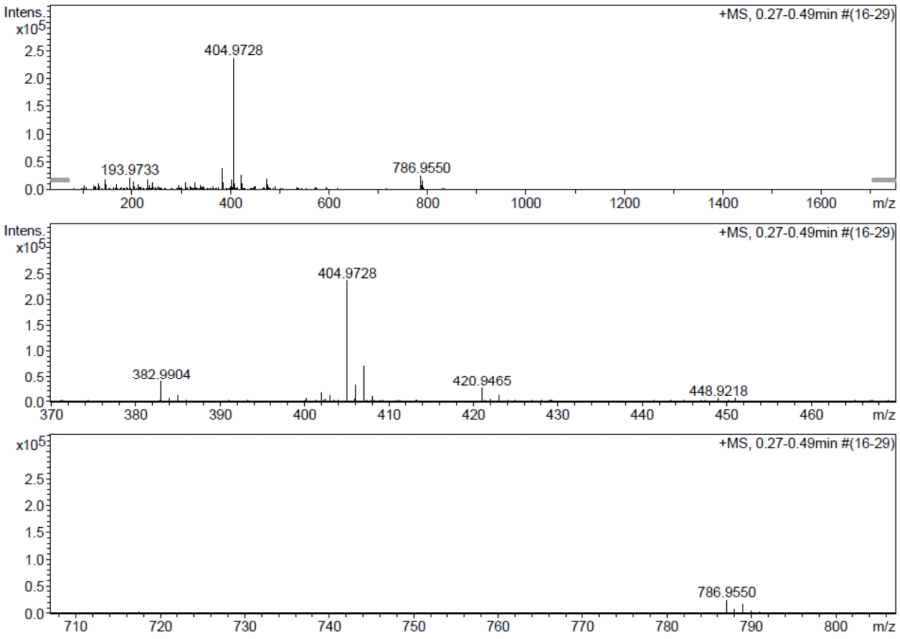

Meas. m/z	#	Formula	Score	m/z	err [mDa]	err [ppm]	mSigma	rdb	e⁻ Conf	N-Rule	z
382.9904	1	C 13 H 17 Cl I O 3	100.00	382.9905	0.1	0.2	6.9	4.5	even	ok	1+
404.9728	1	C 13 H 16 Cl I Na O 3	100.00	404.9725	-0.3	-0.7	15.4	4.5	even	ok	
420.9465	1	C 13 H 16 Cl I K O 3	100.00	420.9464	-0.0	-0.1	33.6	4.5	even	ok	
786.9550	1	C 26 H 32 Cl 2 I 2 Na O 6	100.00	786.9558	0.7	0.9	9.8	8.5	even	ok	

^{1}H-, ^{13}C-NMR spectra and HRMS of **19**

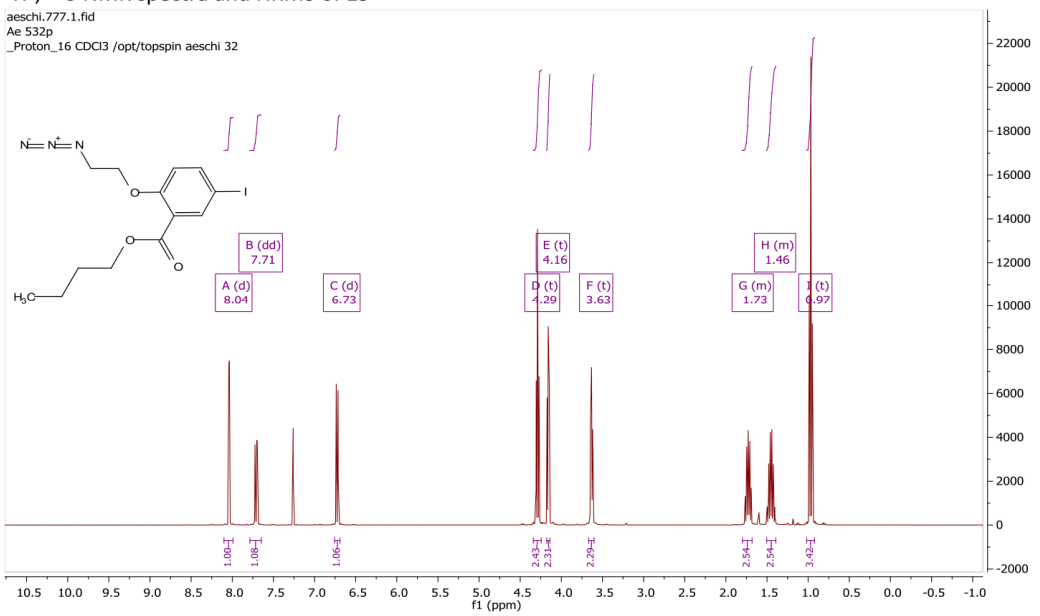

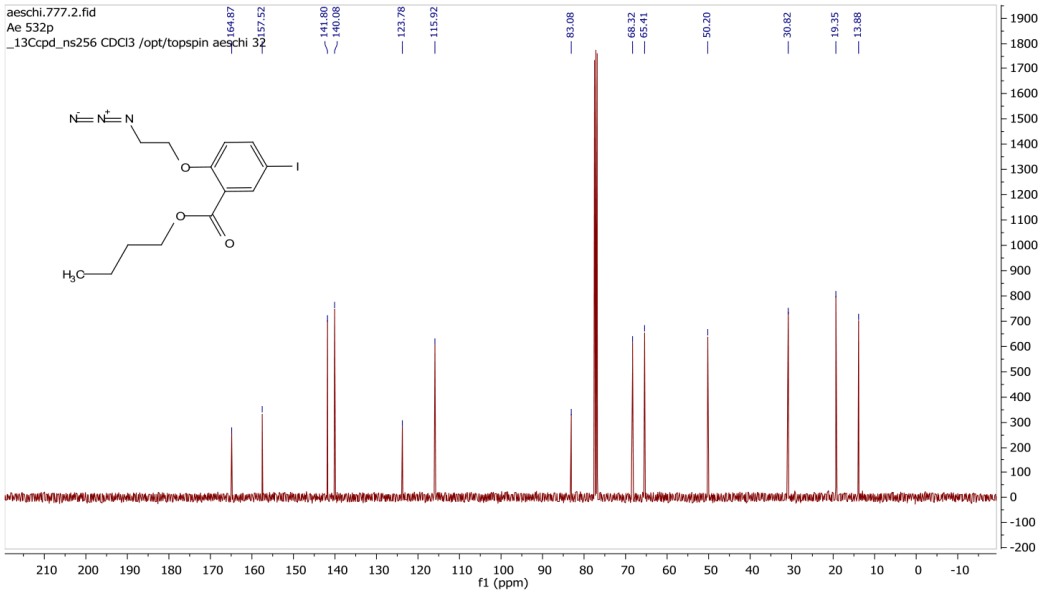

Mass Spectrum SmartFormula Report

Analysis Info

Analysis Name	E:\new acq data for data analysis\Ae 532 001.d	Acquisition Date	12.04.2017 14:01:33
Method	hn Direct_Infusion_pos mode_75-1700 mid 4eV.m	Operator	hn
Sample Name	Yves Aeschi	Instrument / Ser#	maXis 4G 21243
Comment	Ae 532, ca. 10 ug/ml MeOH		

Acquisition Parameter

Source Type	ESI	Ion Polarity	Positive	Set Nebulizer	0.4 Bar
Focus	Not active	Set Capillary	3600 V	Set Dry Heater	180 °C
Scan Begin	75 m/z	Set End Plate Offset	-500 V	Set Dry Gas	4.0 l/min
Scan End	1700 m/z	Collision Energy	8.0 eV	Set Ion Energy (MS only)	4.0 eV

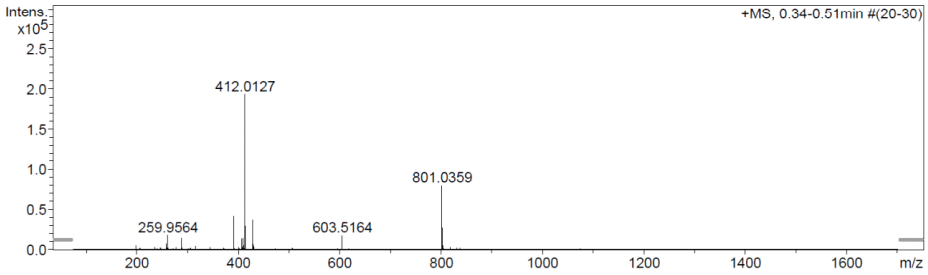

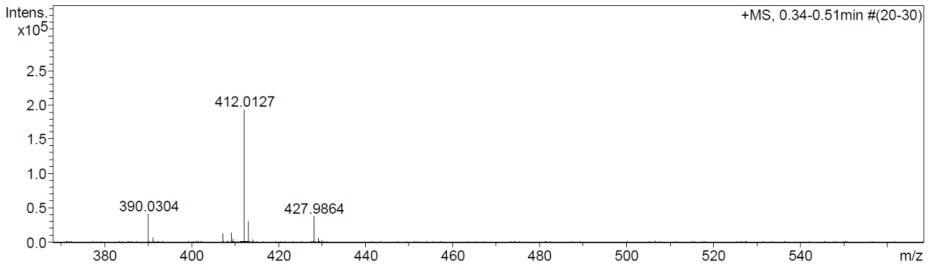

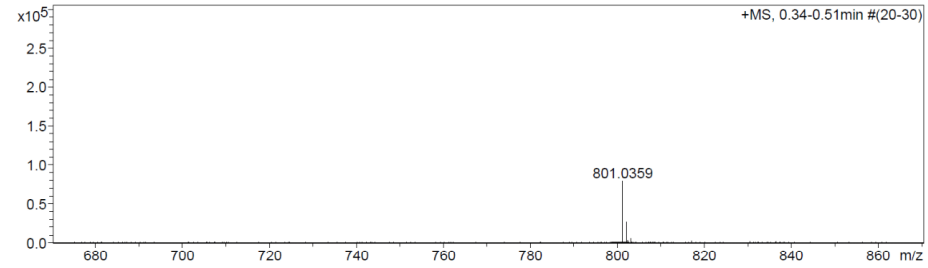

Meas. m/z	#	Formula	Score	m/z	err [mDa]	err [ppm]	mSigma	rdb	e¯ Conf	z
390.0304	1	C 13 H 17 I N 3 O 3	100.00	390.0309	0.5	1.4	4.9	6.5	even	1+
407.0569	1	C 13 H 20 I N 4 O 3	100.00	407.0575	0.6	1.4	13.2	5.5	even	
412.0127	1	C 13 H 16 I N 3 Na O 3	100.00	412.0129	0.2	0.4	1.4	6.5	even	
427.9864	1	C 13 H 16 I K N 3 O 3	100.00	427.9868	0.3	0.8	7.5	6.5	even	
801.0359	1	C 26 H 32 I 2 N 6 Na O 6	100.00	801.0365	0.6	0.8	17.9	12.5	even	
817.0109	1	C 26 H 32 I 2 K N 6 O 6	100.00	817.0104	-0.5	-0.6	53.1	12.5	even	

^{1}H-, ^{13}C-NMR spectra and HRMS of **20**

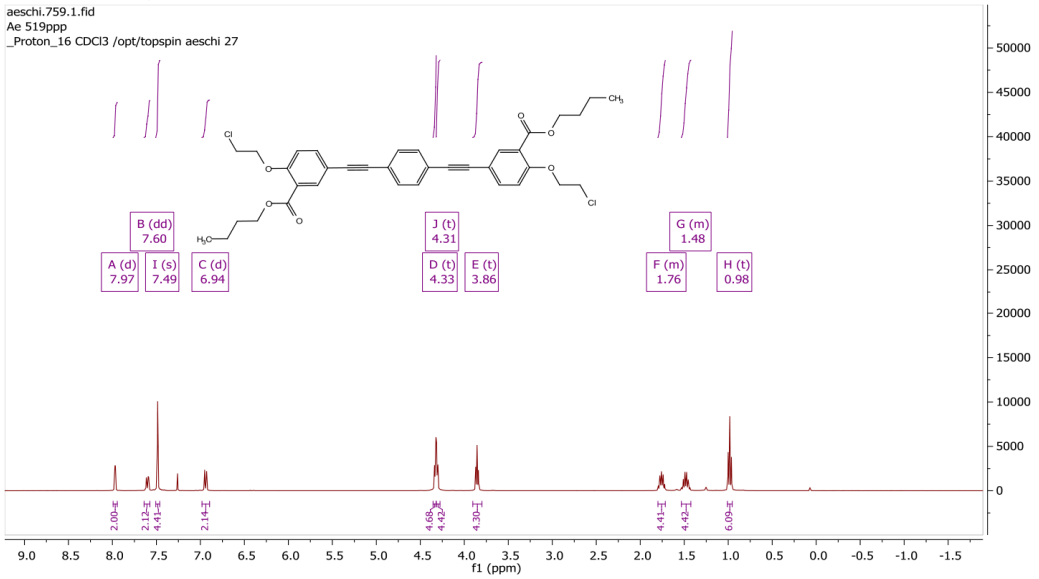

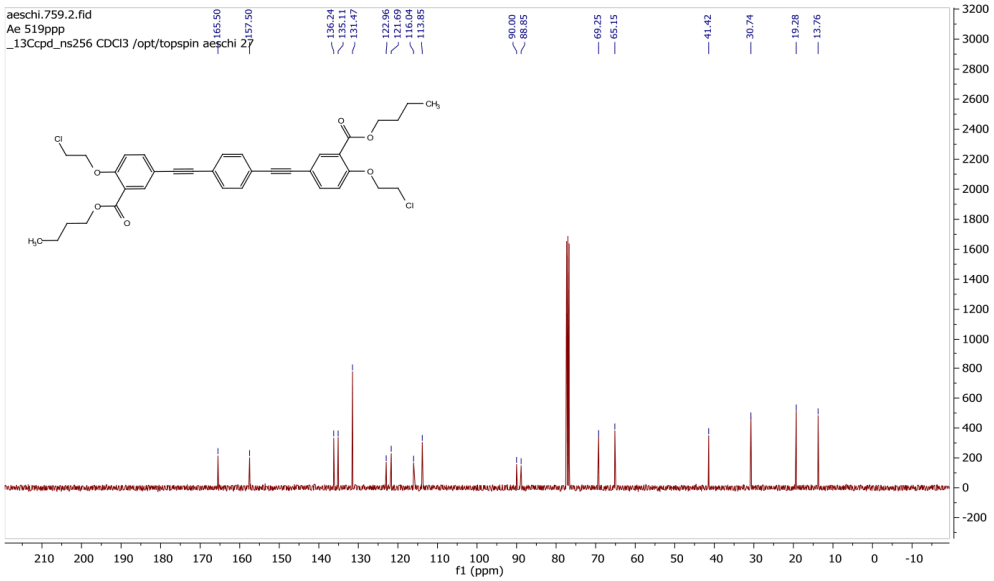

FT12366 Yves Aeschi/Mayor - OPE_SalBuCl - DCM / DCTB

ETH Eidgenössische Technische Hochschule Zürich Swiss Federal Institute of Technology Zurich

Acquisition Parameter

Method:	MALDI_MS_POS_100-1000_2M_16AvScans			Acquisition Date:	20.09.2017 16:08:24
File Name:	D:\ETH\Data\FT123xx\FT12366_0_P4_000001.d			Operator:	Louis Bertschi
Source	Dual (MALDI/ESI)	Polarity	Positive	Nebulizer Gas	1.0 bar
Broadband Low Mass	77.0 m/z	n/a	n/a	Drying Gas Flow Rate	3.7 L/min
Broadband High Mass	1050.0 m/z	Laser Power	23.4 lp	Capillary	4000.0 V
No. of Cell Fills	1	n/a	n/a	Drying Gas	200.0 °C
Apodization	Full-Sine	Time of Flight to Detector	0.001 sec	Temperature	

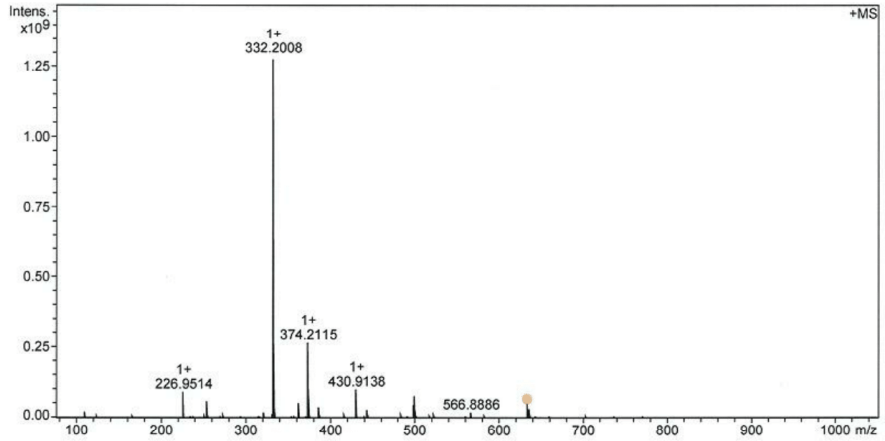

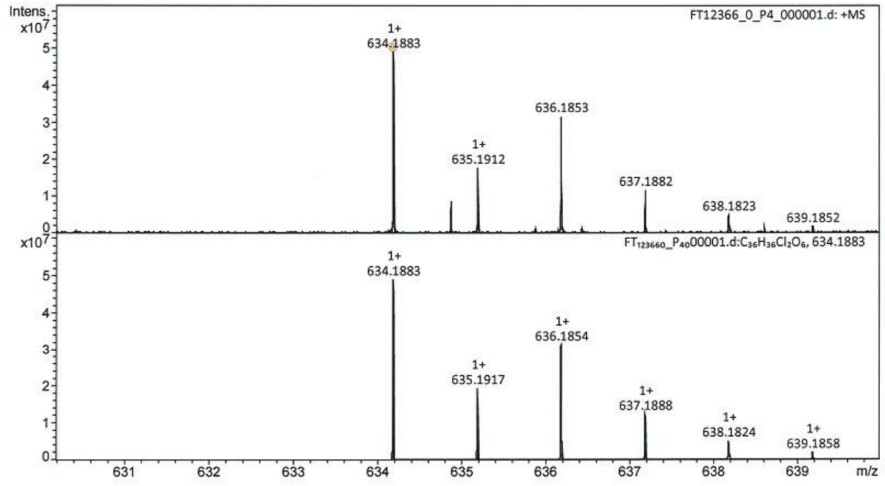

Evaluation Spectra / Validation Formula:

#	Ion Formula	Adduct	m/z	z	Meas. m/z	mSigma	N-Rule	err [mDa]	err [ppm]
1	C36H36Cl2O6	M	634.1883	1+	634.1883	34.4	ok	0.1	0.1

Calibration Info:

Date: 22.09.2017 10:52:49
Polarity: Positive
Calibration spectrum: +MS: Scan
Reference mass list: MALDI: DCTB Matrix + Na-Format Cluster (pos)
Calibration mode: Quadratic

Reference m/z	Resulting m/z	Intensity	Error [ppm]
90.9766	90.9766	233778	-0.016
158.9641	158.9641	2909232	0.205
226.9515	226.9514	91687200	-0.475
250.1464	250.1466	1011957	0.486
251.1543	251.1542	7951669	-0.197
273.1362	273.1361	11169235	-0.308
294.9389	294.9390	5336449	0.210
332.2009	332.2008	1286698752	-0.215
362.9263	362.9264	52854808	0.162
430.9138	430.9138	101135992	0.115
498.9012	498.9012	46036864	0.033
500.2934	500.2935	78137280	0.025
501.3013			
523.2832	523.2831	11719675	-0.132
566.8886	566.8886	18135192	0.015
634.8760	634.8760	8897983	0.018
702.8635	702.8634	6304892	-0.101
750.4404			
751.4483	751.4486	965339	0.459
770.8509	770.8509	3205691	0.011
773.4302			
838.8383	838.8383	2634658	-0.044
906.8257	906.8256	2182009	-0.159
974.8131			
1000.5874			
1001.5953			
1023.5772			
1042.8006			
1110.7880			
1178.7754			
1246.7628			
1314.7503			
1382.7377			
1450.7251			
1518.7125			

Standard deviation: 0.250

Mass List:

#	m/z	Res.	S/N	I %	FWHM
1	110.7337	445281	277.5	0.8	0.0002
2	110.7352	416589	222.9	0.7	0.0003
3	166.1005	293532	212.2	0.7	0.0006
4	226.9514	157900	2087.2	7.1	0.0014
5	251.1542	163274	175.5	0.6	0.0015
6	254.1903	158245	1283.5	4.5	0.0016
7	255.1936	154422	254.1	0.9	0.0017
8	273.1361	153794	241.2	0.9	0.0018
9	321.2765	143516	431.8	1.6	0.0022
10	331.1932	132732	175.1	0.7	0.0025
11	332.2008	137191	26709.6	100.0	0.0024
12	333.2043	130403	5447.8	20.4	0.0026
13	334.2077	126662	552.3	2.1	0.0026
14	362.9264	125030	1052.9	4.1	0.0029
15	374.2115	122548	5303.8	20.7	0.0031
16	374.2339	116961	229.8	0.9	0.0032
17	375.2149	121154	1579.7	6.2	0.0031
18	376.2183	126161	210.8	0.8	0.0030
19	386.2843	115426	758.2	3.0	0.0033
20	387.2876	114798	214.2	0.9	0.0034
21	416.2948	111216	205.9	0.8	0.0037
22	430.9138	109896	1908.7	7.9	0.0039
23	431.9172	109006	128.3	0.5	0.0040
24	444.2898	106431	519.0	2.2	0.0042
25	445.2930	105661	179.4	0.8	0.0042
26	484.3211	100514	184.9	0.8	0.0048
27	498.9012	95025	818.5	3.6	0.0053
28	499.2856	96668	221.8	1.0	0.0052
29	500.2935	96213	1390.6	6.1	0.0052
30	501.2966	88471	447.8	2.0	0.0057
31	501.3018	104401	291.0	1.3	0.0048
32	518.3041	93882	147.4	0.7	0.0055
33	523.2831	90536	201.7	0.9	0.0058
34	566.8886	85205	302.5	1.4	0.0067
35	583.3319	83142	114.3	0.5	0.0070
36	634.1883	75942	808.9	3.8	0.0084
37	634.8760	76194	145.4	0.7	0.0083
38	635.1912	80928	294.4	1.4	0.0078
39	636.1853	73981	523.1	2.5	0.0086
40	637.1882	79267	191.7	0.9	0.0080

#	m/z	Res.	S/N	I %	FWHM
1	634.1883	75942		100.0	0.0084
2	635.1917	76062		39.6	0.0084
3	636.1854	76181		64.0	0.0084
4	636.1948	76182		8.9	0.0084
5	637.1888	76301		25.3	0.0084
6	637.1977	76302		1.4	0.0084
7	638.1824	76420		10.2	0.0084
8	638.1918	76421		5.7	0.0084
9	638.2006	76422		0.2	0.0084
10	639.1858	76540		4.1	0.0084
11	639.1947	76541		0.9	0.0084
12	640.1889	76661		0.9	0.0084
13	640.1977	76662		0.1	0.0084
14	641.1918	76781		0.1	0.0084

^{1}H-, ^{13}C-NMR spectra and HRMS of **21**

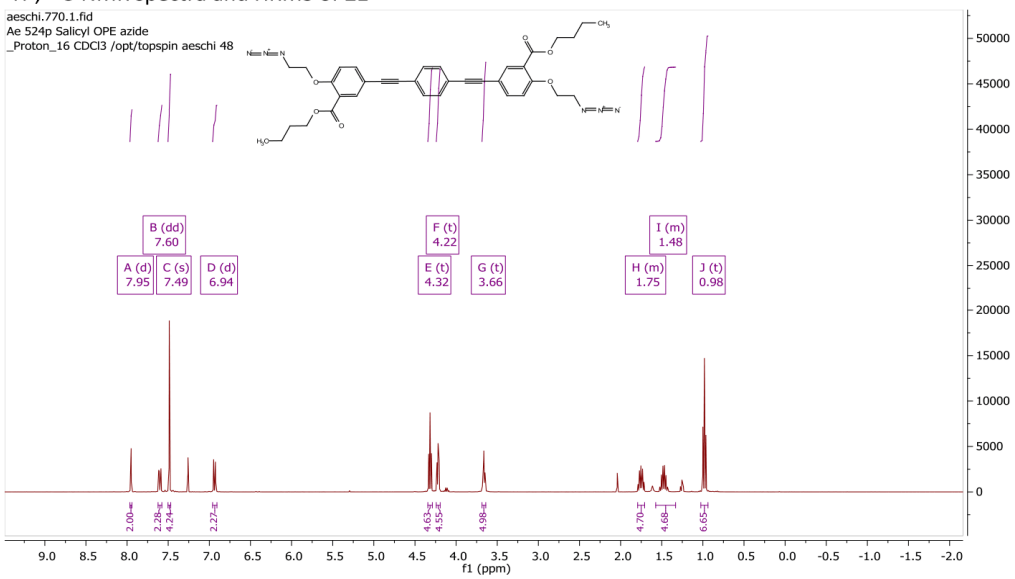

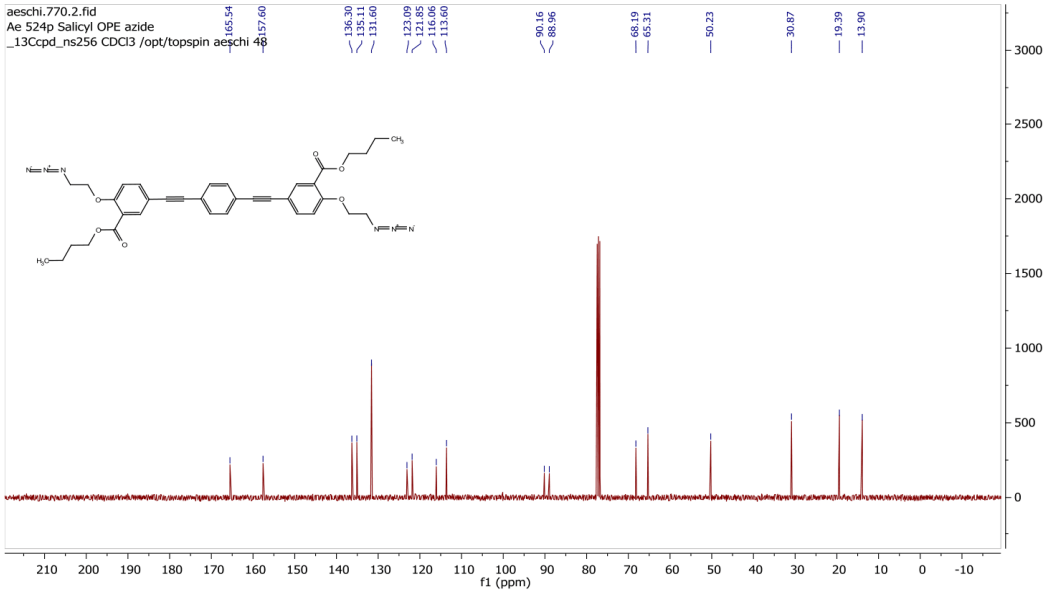

FT12365 Yves Aeschi/Mayor - OPE_SalBuN3 - DCM / DCTB

ETH Eidgenössische Technische Hochschule Zürich Swiss Federal Institute of Technology Zurich

Acquisition Parameter

Method:	MALDI_MS_POS_100-1000_2M_16AvScans			Acquisition Date:	20.09.2017 16:06:59
File Name:	D:\ETH\Data\FT123xx\FT12365_0_P3_000001.d			Operator:	Louis Bertschi
Source	Dual (MALDI/ESI)	Polarity	Positive	Nebulizer Gas	1.0 bar
Broadband Low Mass	77.0 m/z	n/a	n/a	Drying Gas Flow Rate	3.7 L/min
Broadband High Mass	1050.0 m/z	Laser Power	23.4 lp	Capillary	4000.0 V
No. of Cell Fills	1	n/a	n/a	Drying Gas	200.0 °C
Apodization	Full-Sine	Time of Flight to Detector	0.000 sec	Temperature	

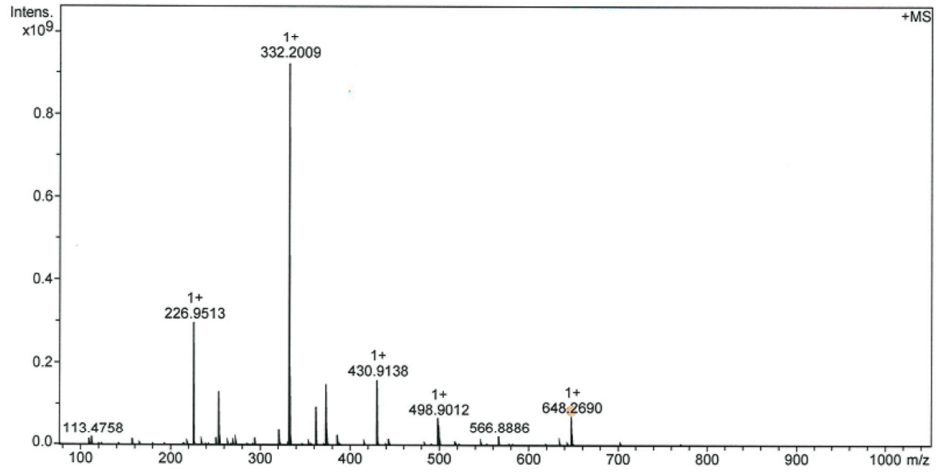

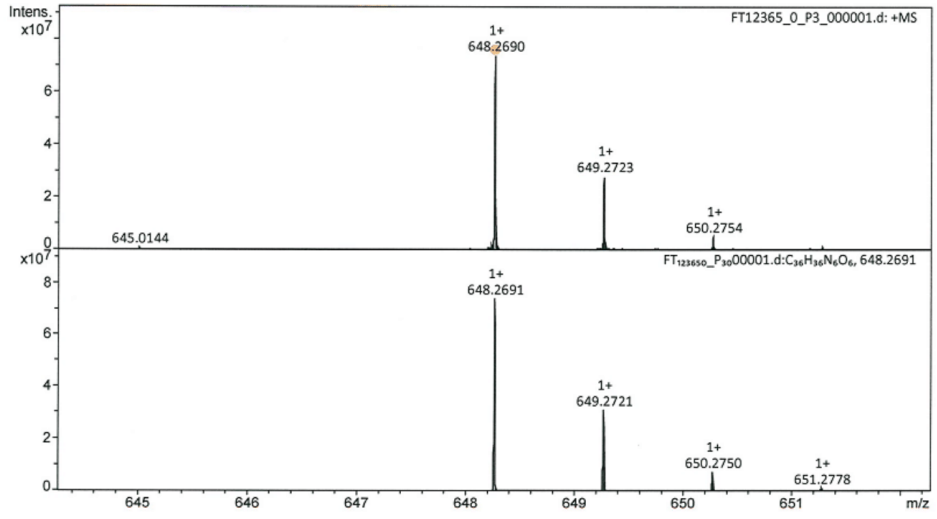

FT12365 Yves Aeschi/Mayor - OPE_SalBuN3 - DCM / DCTB

ETH Eidgenössische Technische Hochschule Zürich Swiss Federal Institute of Technology Zurich

Evaluation Spectra / Validation Formula:

#	Ion Formula	Adduct	m/z	z	Meas. m/z	mSigma	N-Rule	err [mDa]	err [ppm]
1	C36H36N6O6	M	648.2691	1+	648.2690	23.4	ok	0.1	0.1

Calibration Info:

Date: 22.09.2017 10:49:55
Polarity: Positive
Calibration spectrum: +MS: Scan
Reference mass list: MALDI: DCTB Matrix + Na-Format Cluster (pos)
Calibration mode: Quadratic

Reference m/z	Resulting m/z	Intensity	Error [ppm]
90.9766	90.9766	500362	0.004
158.9641	158.9641	17017856	-0.033
226.9515			
250.1464	250.1465	1353135	0.299
251.1543	251.1542	17776622	-0.189
273.1362	273.1362	11311035	-0.248
294.9389	294.9390	19179470	0.128
332.2009	332.2009	928544000	-0.043
362.9263	362.9264	95820960	0.149
430.9138	430.9138	161371008	0.082
498.9012	498.9012	68594288	0.023
500.2934	500.2935	50858704	0.052
501.3013			
523.2832	523.2832	3008286	-0.113
566.8886	566.8886	23081602	0.068
634.8760	634.8761	10308090	0.036
702.8635	702.8634	5523663	-0.009
750.4404			
751.4483			
770.8509	770.8507	2220371	-0.292
773.4302			
838.8383			
906.8257			
974.8131			
1000.5874			
1001.5953			
1023.5772			
1042.8006			
1110.7880			
1178.7754			
1246.7628			
1314.7503			
1382.7377			
1450.7251			
1518.7125			

Standard deviation: 0.165

Mass List:

#	m/z	Res.	S/N	I %	FWHM
1	110.7337	450874	219.1	0.9	0.0002
2	113.4758	429176	532.5	2.2	0.0003
3	158.9641	256200	411.5	1.8	0.0006
4	219.0828	159945	185.1	0.9	0.0014
5	226.9513	150391	6766.0	32.2	0.0015
6	227.9545	145876	220.8	1.1	0.0016
7	235.1228	153706	214.2	1.0	0.0015
8	251.1542	161619	393.4	1.9	0.0016
9	254.1903	158532	2915.4	14.2	0.0016
10	255.1936	151896	548.3	2.7	0.0017
11	265.1046	152729	163.2	0.8	0.0017
12	270.9777	150119	173.2	0.9	0.0018
13	273.1362	153678	244.3	1.2	0.0018
14	294.9390	149756	408.5	2.1	0.0020
15	321.2765	143927	830.8	4.3	0.0022
16	322.2799	144407	171.0	0.9	0.0022
17	332.2009	133693	19348.5	100.0	0.0025
18	333.2044	127844	4007.2	20.7	0.0026
19	334.2077	124580	411.5	2.2	0.0027
20	355.0577	128276	138.8	0.7	0.0028
21	362.9264	125540	1930.9	10.3	0.0029
22	374.2115	122055	3010.1	16.1	0.0031
23	374.2340	119627	254.8	1.4	0.0031
24	375.2149	121184	880.0	4.7	0.0031
25	386.2842	116573	500.3	2.7	0.0033
26	387.2876	116304	136.1	0.8	0.0033
27	416.2948	112494	133.3	0.7	0.0037
28	430.9138	109703	3086.0	17.4	0.0039
29	431.9172	106695	195.9	1.1	0.0040
30	444.2897	105704	311.8	1.8	0.0042
31	498.9012	95774	1234.5	7.4	0.0052
32	499.2856	96349	145.2	0.9	0.0052
33	500.2935	96651	914.7	5.5	0.0052
34	501.2966	97638	316.0	1.9	0.0051
35	501.3018	153736	158.8	1.0	0.0033
36	547.1975	88728	144.4	0.9	0.0062
37	566.8886	85139	389.0	2.5	0.0067
38	634.8761	77048	167.5	1.1	0.0082
39	648.2690	75052	1185.6	8.0	0.0086
40	649.2723	79027	449.6	3.0	0.0082

#	m/z	Res.	S/N	I %	FWHM
1	648.2691	75052		100.0	0.0086
2	649.2721	75168		41.8	0.0086
3	650.2750	75284		9.7	0.0086
4	651.2778	75401		1.6	0.0086
5	652.2808	75517		0.2	0.0086

^{1}H-, ^{13}C-NMR spectra and HRMS of **23**

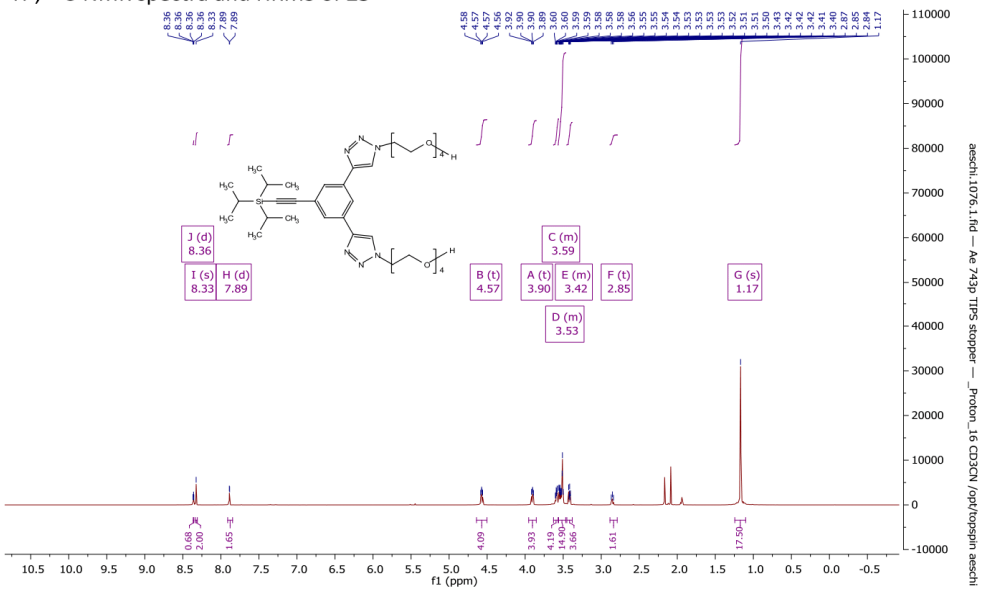

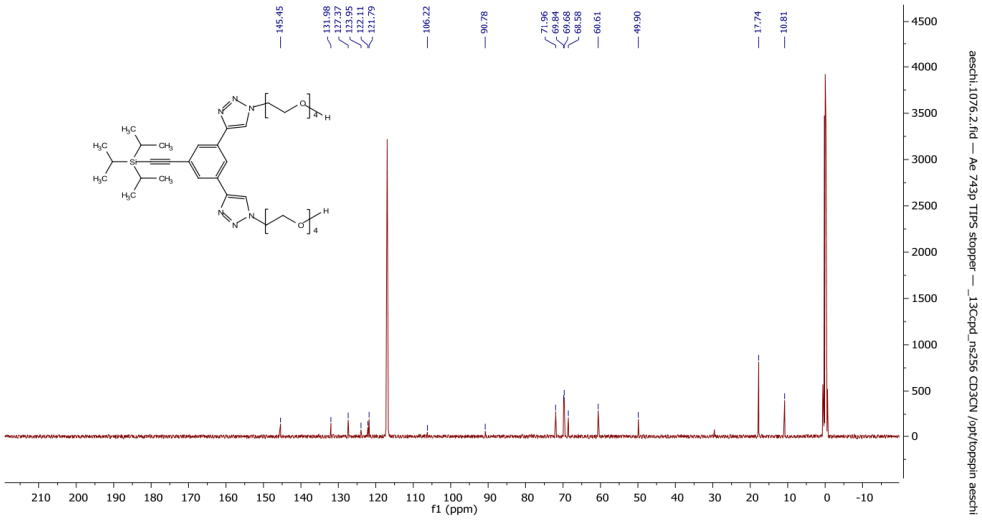

Mass Spectrum SmartFormula Report

Analysis Info

Analysis Name	E:\acq data for data analysis\AE TIPS TEG 01.d	Acquisition Date	25.04.2018 16:24:44
Method	23 Direct_pos_higher.m	Operator	Miff
Sample Name	Yves Aeschi	Instrument / Ser#	maXis 4G 21243
Comment	10 ug/mL in MeOH + HCOOH		

Acquisition Parameter

Source Type	ESI	Ion Polarity	Positive	Set Nebulizer	0.4 Bar
Focus	Not active	Set Capillary	3600 V	Set Dry Heater	180 °C
Scan Begin	75 m/z	Set End Plate Offset	-500 V	Set Dry Gas	4.0 l/min
Scan End	1700 m/z	Collision Energy	8.0 eV	Set Ion Energy (MS only)	4.0 eV

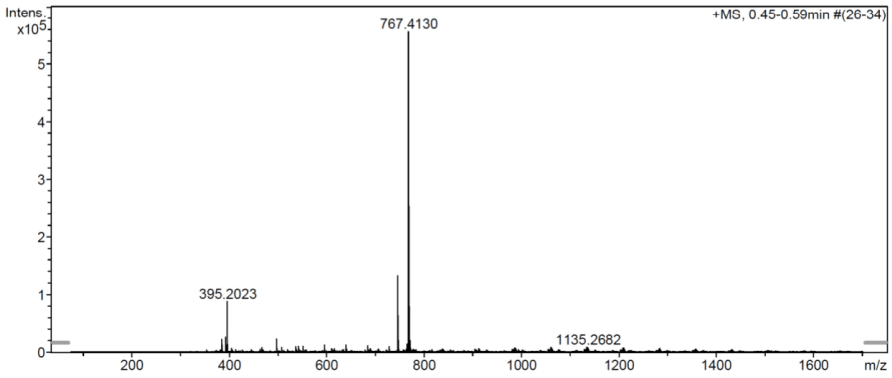

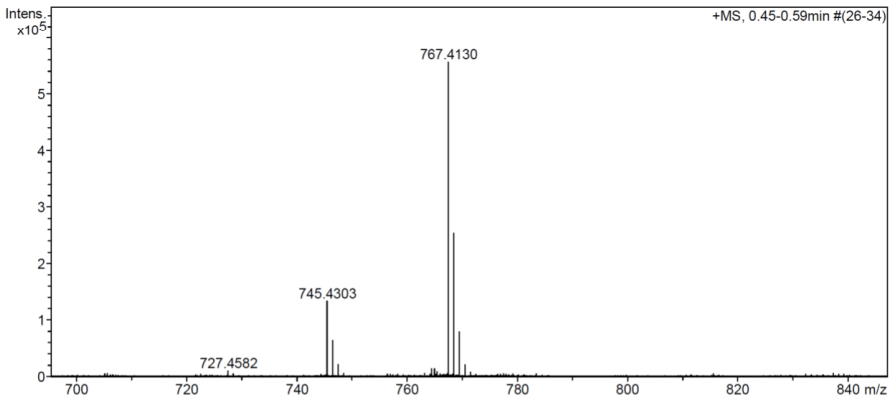

Meas. m/z	#	Formula	Score	m/z	err [mDa]	err [ppm]	mSigma	rdb	e⁻ Conf	z
745.4303	1	C 37 H 61 N 6 O 8 Si	100.00	745.4315	1.2	1.6	1.8	11.5	even	1+
767.4130	1	C 37 H 60 N 6 Na O 8 Si	100.00	767.4134	0.4	0.6	15.5	11.5	even	

Slow Formation of Pseudorotaxanes in Water: Large Influence of the Substitution Pattern

ChemPubSoc Europe

DOI: 10.1002/ejoc.201801864

EurJOC European Journal of Organic Chemistry Communication

Check for updates

Supramolecular Chemistry

SPECIAL ISSUE

Slow Formation of Pseudorotaxanes in Water

Yves Aeschi,[a,b] Laurent Jucker,[a] Daniel Häussinger,[a] and Marcel Mayor*[a,b,c,d]

Dedicated to Professor Gottfried Schill as visionary pioneer and mastermind of mechanically interlocked superstructures

Abstract: The synthesis of two water-soluble oligophenyleneethynylene (OPE)-rods with substituted iso- and terephthalate end groups is presented. Both undergo slow association with a *Diederich*-type cyclophane in aqueous solution. Formation of [2]pseudorotaxanes occurs with reaction half-lives of several hours. Characterization of the supermolecules by ^{1}H-NMR spectroscopy reveals a high thermodynamic stability and kinetic inertness of the pseudorotaxanes. The phthalate precursors are functionalized with peripheral azide groups, which make them modular precursors for construction of mechanically interlocked molecules in water.

Introduction

For the realization of catenane- and (pseudo)rotaxane-based molecular pumps or directional motors, ratchet mechanisms can be employed to achieve directionality.[1–3] Control over kinetics and thermodynamics of host-guest association and/or interconversion of translational isomers is required for this purpose.[4–9] Whereas the choice of a certain recognition motif dictates thermodynamic strength of association in host-guest systems often in an intuitive way, the kinetics of their formation is usually less straight forward to predict. Steric interactions are frequently used for this purpose,[10–14] although electrostatic repulsion[15] or attraction[16] may also be engaged. Incremental variation of steric factors is often required to reveal design rules for rational adjustment of exchange kinetics.[10–14] The factors controlling exchange kinetics are highly specific to the host/guest combination. This was initially observed in the "slipping" assembly of rotaxanes,[10,11,17,18] for which a stopper unit must be tailored such that it is insurmountable at ambient conditions, but can be overcome by applying heat or pressure. It has already been discussed that the identity as rotaxane or pseudorotaxane is not clearly defined and may become a matter of definition,[19] depending on its kinetic inertness at a given set of conditions.

Rigid and extended π-conjugated guests were rarely integrated into (pseudo)rotaxane systems exhibiting slow assembly or slipping processes.[20,21] This is in part certainly due to their low solubility and the resulting necessity of attaching solubilizing groups. These may interfere with the host/guest assembly formation and pose additional synthetic efforts. An elegant way to circumvent these limitations is the intramolecular slipping approach for the synthesis of [1]rotaxanes.[22] This enabled the assembly of oligophenyleneethynylene (OPE)-type insulated wires with remarkable properties.[23–26]

The aim of this work was the synthesis of highly water-soluble OPE rods, which exhibit high association strength towards *Diederich*-type cyclophanes.[27–29] Naphthalene-[30–33] and OPE-based[34–36] guests have shown to bind strongly to **4** (Scheme 1). We recently presented the synthesis of daisy chains based on a salicylate-terminated OPE rod and a cyclophane derived from **4**.[36] Slow exchange on the ^{1}H-NMR timescale (500 MHz) was observed, however both the daisy chains and mixtures of the model compounds **4** and **3** equilibrated within less than a few minutes, such that complex formation could not be observed by time-dependent ^{1}H-NMR spectroscopy. By replacing the salicylate moiety with a sterically more demanding end-group, even lower exchange rates should be achieved. In addition, the resulting OPE rods must be suitable for integration into larger, mechanically bonded assemblies. Copper(I)-catalyzed azide–alkyne cycloaddition click-chemistry (CuAAC)[37] is ideal for this purpose, therefore the guest axles presented herein are terminally functionalized with azide groups similar to **3**. The synthetic challenge was to find a reasonably compact design of the substitution pattern, which integrates a kinetic barrier, solubilizing groups, azide functionality and a leaving group for Pd^0-catalyzed cross-coupling reactions into a single precursor. Substituted iso- and terephthalate derivatives were identified as interesting building blocks for this purpose, providing synthetic accessibility in combination with the desired compact substitution pattern. The synthesis and characteriza-

[a] Department of Chemistry, University of Basel
St. Johanns-Ring 19, 4056 Basel, Switzerland
E-mail: marcel.mayor@unibas.ch
www.chemie.unibas.ch/~mayor
[b] Swiss Nanoscience Institute, University of Basel
Klingelbergstrasse 82, 4056 Basel, Switzerland
[c] Institute for Nanotechnology (INT), Karlsruhe Institute of Technology (KIT)
P. O. Box 3640, 76021 Karlsruhe, Germany
[d] Lehn Institute of Functional Materials (LIFM), School of Chemistry,
Sun Yat-Sen University (SYSU)
Guangzhou 510275, China

Supporting information and ORCID(s) from the author(s) for this article are available on the WWW under https://doi.org/10.1002/ejoc.201801864.

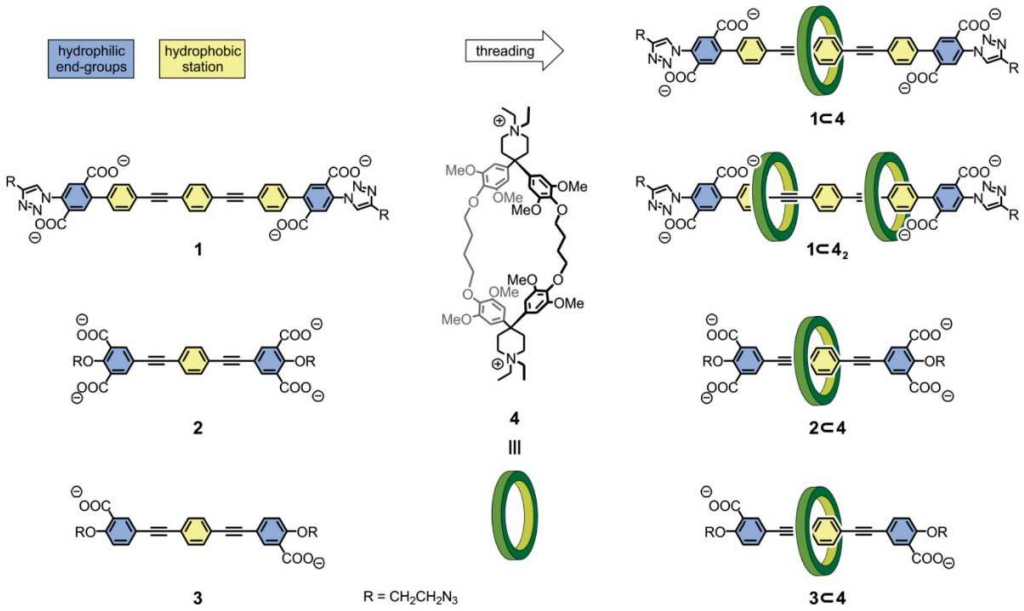

Scheme 1. Conceptual assembly of pseudorotaxanes from OPE rods **1**, **2**, **3**, and cyclophane **4**.

tion of two OPE rods incorporating such a compact phthalate-based moiety is presented herein. The binding strength and association kinetics are evaluated and compared to the previously reported OPE rod **3**.

Results and Discussion

The conceptual design of the OPE rods **1** and **2** resembles the one of the already reported dicarboxylate rod **3**. A central hydrophobic station is squeezed between solubilizing end-groups, which carry an additional azide substituent enabling further functionalization by CuAAC. Aliphatic spacers were introduced between the aromatic unit and the azide groups as π-extended aromatic azides are known for their photosensitivity.[38,39] A central 1,4-substituted phenylene moiety is either linked to the phthalate moiety via ethynylene or 4-phenylethynylene linkers. The additional phenylene moiety in **1** serves to avoid potential stability issues with *o*-carboxy-substituted phenylacetylenes.

Terephthalate-based OPE rod **1** was synthesized starting from commercially available dimethyl-2-aminoterephthalate (see Scheme 2). Iodination with NIS in MeOH/DCM proceeded smoothly to give **5** in a yield of 74 %. In the following step, a diazotization/azidation protocol using *t*BuONO and $TMSN_3$[40] in acetonitrile was employed, which led to a clean transformation to azide **6** in a yield of 97 % after recrystallization. The aromatic azide group was transformed into a triazole moiety by CuAAC with 3-butyn-1-ol, giving **7** in 86 % yield. The classical "click" conditions with sodium ascorbate and $CuSO_4$ in this case led to partial deiodination, probably due to the strong activation of the iodo-substituent *ortho* to the carboxylate. This was prevented by using 2 mol% TBTA and $Cu(CH_3CN)_4PF_6$, avoiding the presence of a reducing agent. The hydroxyl group was transformed to the alkyl bromide by an *Appel*-reaction to give **8** in 93 % yield. Nucleophilic substitution with sodium azide in DMF proceeded smoothly to give **9** in 94 % yield after short chromatographic purification.

The central OPE unit **10** was obtained by *Sonogashira* cross-coupling of 4-iodophenylboronic acid pinacol ester with 1,4-diethynylbenzene, yielding 83 % of the desired compound after crystallization. *Suzuki* cross-coupling of **9** and **10** using $Pd(dppf)Cl_2{\cdot}CH_2Cl_2$ as precatalyst yielded **11** in 57 % yield. After saponification of the methyl esters with NaOH, **1** was obtained in 82 % yield.

The synthesis of the rod **2** is displayed in Scheme 3. The isophthalate moiety was obtained from 2-hydroxyisophthalic acid by a one-pot iodination/*Fischer* esterification procedure in methanol using first NIS, followed by the addition of H_2SO_4. This provided **12** in 54 % yield after crystallization from the reaction mixture. The following alkylation of the phenolic hydroxyl group with 1-bromo-2-chloroethane in DMSO in presence of Cs_2CO_3 proceeded in a clean conversion to give **13** in 96 % yield. Nucleophilic substitution with NaN_3 in DMSO at 60 °C proceeded cleanly as well, only requiring extraction for purification to provide **14** in 96 % yield. *Sonogashira* cross-coupling to 1,4-diethynylbenzene proceeded efficiently at room temperature, to give 82 % of **15** after crystallization. Final saponification of the methyl esters with NaOH in a mixture of

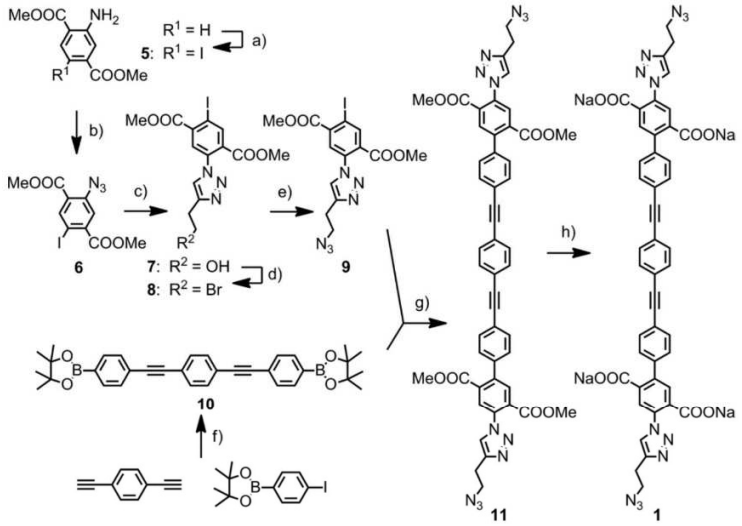

Scheme 2. a) NIS, MeOH/DCM (1:1), reflux, 16 h, 74 %; b) *t*BuONO, $TMSN_3$, CH_3CN, 0 °C, 1 h, 97 %; c) 3-butyn-1-ol, $Cu(CH_3CN)_4PF_6$, TBTA, CH_3CN, r.t., 86 %; d) CBr_4, Ph_3P, THF, –20 °C to r.t., 6 h, 93 %; e) NaN_3, DMF, 50 °C, 18 h, 94 %; f) $Pd(PPh_3)_2Cl_2$, CuI, Et_3N/THF (1:2), r.t., 20 h, 83 %; g) $Pd(dppf)Cl_2{\cdot}CH_2Cl_2$, Na_2CO_3, PhMe/H_2O (5:1), 80 °C, 4 h, 57 %; h) NaOH, THF/MeOH/H_2O (5:5:1), 60 °C, 30 min, 82 %.

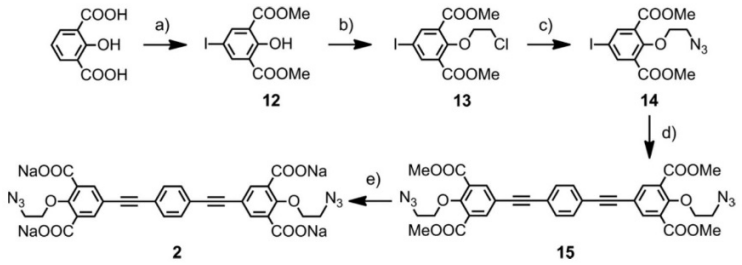

Scheme 3. a) NIS, MeOH, r.t., 16 h, then H_2SO_4, reflux, 10 h, 54 %; b) 1-bromo-2-chloroethane, Cs_2CO_3, DMSO, r.t., 16 h, 96 %; c) NaN_3, DMSO, 60 °C, 20 h, 96 %; d) 1,4-diethynylbenzene, $Pd(PPh_3)_2Cl_2$, CuI, Et_3N/THF (1:6), r.t., 14 h, 82 %; e) NaOH, THF/MeOH/H_2O (4:4:1), 60 °C, 1 h, 78 %.

THF/MeOH/H_2O gave OPE **2** in 78 % yield. Both OPE rods **1** and **2** exposing four carboxylates contain residual solvents and/or traces of salts (sodium bicarbonate in **2**), which we were not able to remove in spite of numerous purification attempts. To maintain reasonable control over the stoichiometry, the samples were dried under vacuum and the content of the desired rod per weight of the sample was determined by ^{1}H-NMR and elemental analysis. The investigation revealed product contents of 88 % for **1** and 91 % for **2**.

Upon complexation of the aromatic moieties of **1** and **2** by the cyclophane **4**, an upfield shift of 2–2.5 ppm was expected for encircled protons.[30,34,35] Indeed, when **4** was added to solutions of **1** and **2** in D_2O, signals between 5.0 and 6.0 ppm slowly started to appear within minutes to a few hours (Figure 1 and Figure 3). This process was considerably accelerated by higher temperatures. Complexation studies to determine the stoichiometry were performed at 0.5 mM host/guest concentration in D_2O. The chosen concentration window was an optimized compromise where no precipitation was observed visually and sharp signals were still observed in the ^{1}H-NMR spectra with an acceptable signal to noise ratio. Higher concentrations tended to precipitate host/guest conglomerates, most likely the neutral combinations of an OPE rod (**1** or **2**) with two molecules cyclophane **4**. Solutions of the OPE rod (**1** or **2**) with either 1, 2 or 5 equivalents of **4** were heated to 90 °C for 16 h and compared to the spectrum in absence of **4** (Figure 1).

For the terephthalate-terminated rod **1**, mainly a 1:1 binding stoichiometry was observed when adding 1 equivalent of **4** with the phenylene resonance being shifted from 7.68 to 5.86 ppm. Upon addition of a 4-fold excess of **4**, almost quantitative precipitation was observed instantaneously. This behavior is most likely due to the extended hydrophobic backbone of **1**, which results in an increased tendency to co-precipitate quickly with the relatively lipophilic dication **4**. Another intriguing con-

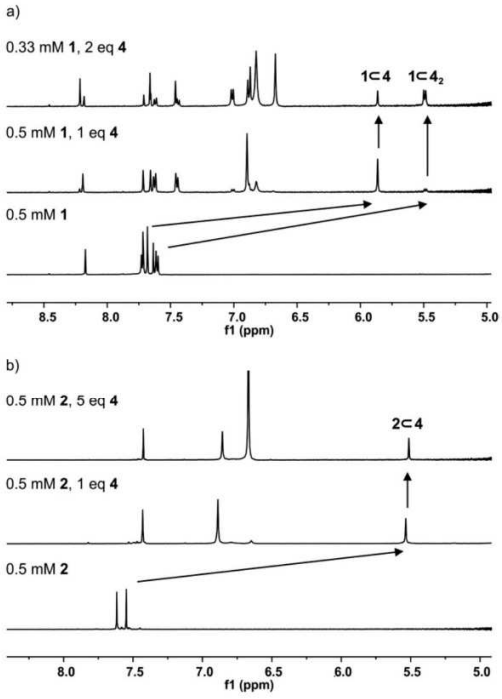

Figure 1. Distinct chemical shifts in the ^{1}H-NMR spectra of a) **1** and b) **2** in the presence of various equivalents of **4** displaying the formation of the [2]/[3]-pseudorotaxanes **1⊂4**, **1⊂4$_2$**, and **2⊂4** respectively after heating. Arrows are guiding the eye to the most strongly shifted resonances.

sequence of the elongated backbone of **1** is its ability to form [3]pseudorotaxanes. Already in the 1:1 mixture of **1** and **4**, a faint doublet at 5.49 ppm points at the presence of the [3]pseudorotaxane **1⊂4$_2$**. The doublet becomes more pronounced with increasing equivalents of **4** and in a spectrum of **1** (0.33 mM) in presence of 2 equivalents **4** (0.66 mM), a ratio of 1:3 between **1⊂4** and **1⊂4$_2$** was determined by integration of ^{1}H-NMR signals. Although very little precipitation was already observed in this sample, a K_a of > 10^4 M^{-1} for the second association process could be estimated from this single point measurement. The doublet coupling pattern reveals that **4** resides on the 1,4-substituted phenylene moiety of the terminal biphenyl unit. This results in a large change of chemical shift from 7.61 to 5.49 ppm, while the central phenylene unit of **1⊂4$_2$** appears at about 6.9 ppm with only moderate shift of about 0.8 ppm compared to the free rod **1**. This observation supports the absence of an encircling cyclophane on the central phenylene subunit in **1⊂4$_2$**, which results from the mutual electrostatic repulsion of the receptors.

The situation becomes simpler for **2**, which is too short to accommodate more than one cyclophane on the axle. And indeed, exclusively a 1:1 binding stoichiometry at 0.5 mM was observed by ^{1}H-NMR regardless of the excess of **4**. Even with 5 equivalents of **4**, precipitation was not observed pointing at the more hydrophilic nature of **2**. The cyclophane as host resides on the central phenylene subunit of the guest axle **2**, which displays a change in chemical shift from 7.55 to 5.53 ppm. Overall, the behavior of **2** resembles the one of **3**,[36] from which **2** differs only by two additional carboxylate groups.

The positions of the cyclophane **4** on the axles **1** and **2** in their superstructures **1⊂4**, **2⊂4**, and **1⊂4$_2$** were corroborated by the corresponding ^{1}H-NOESY spectra. In particular, cross peaks between the protons of the axles' central phenylene unit and the cyclophane's aryl- and methoxy groups were observed for **1⊂4** and **2⊂4**. In the case of **1⊂4$_2$**, cross peaks of the cyclophane protons to the biphenyl protons confirmed the arrangement of both cyclophanes on the terminal biphenyl subunits of the axles.

Limited photostability of the rods **1** and **2** hampered the investigation of the superstructures by optical spectroscopy. The optical characterization was performed exclusively with freshly prepared samples and series of consecutive measurements were avoided. Both rods displayed comparable spectroscopic behavior upon formation of their superstructures (Figure 2). To guarantee the presence of the superstructures **1⊂4** and **2⊂4** respectively, the samples for optical spectroscopy were prepared by dilution of the already equilibrated 0.5 mM NMR samples in D_2O to concentrations of 1 μM. In their UV/Vis spectra, a slight decrease in the extinction coefficient was observed upon complexation with **4** (16 % for **1** and 11 % for **2**). In the case of **2**, an additional bathochromic shift of about 4 nm was observed upon formation of **2⊂4**. In their fluorescence spectra, a more pronounced reduction in intensity was observed upon formation of the superstructures. The fluorescence signal intensities of the superstructures **1⊂4** and **2⊂4** were reduced by 64 % and 90 % compared to the signals of the parent rods **1** and **2**. To assure that the reduced fluorescence is due to the formation of the superstructures, 1 μM mixtures of the rods **1** or **2** and the cyclophane **4** were prepared and their fluorescence spectra were recorded immediately, before the pseudorotaxane could form. And indeed, the emission intensities resembled the ones of the pure samples of the rods **1** and **2** (Figure S14 and Figure S15). After storing for 40 h in the dark, a reduced emission was recorded for both samples, pointing at the partial formation of the pseudorotaxanes **1⊂4** and **2⊂4**. The lower fluorescence intensities upon encirclation with **4** compare well to a structurally related OPE-based rotaxane by Anderson et al.[35] The rather small changes in optical properties upon formation of the pseudorotaxanes point at weak electronic interactions of the mechanically interlinked components. Determination of association constants by either fluorescence- or UV/Vis-titration experiments in water was hampered by both the limited photostability of **1** and **2** and the low exchange rates with **4**. The latter also impeded measurements by isothermal titration calorimetry (ITC).

To get a hand on the association constants (K_a) involved between the rods and the cyclophane, detailed ^{1}H-NMR studies were performed. A dilution series of 1:1 mixtures of the rods (**1** or **2**) and the cyclophane **4** in D_2O displayed still saturation at 10 μM concentration, which is almost at the sensitivity limit

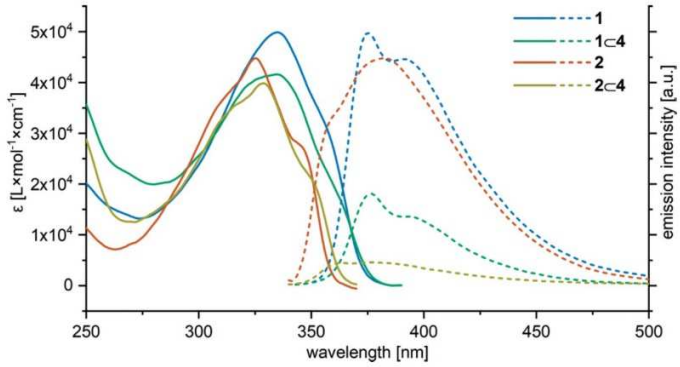

Figure 2. Absorption (left, solid lines) and emission (right, dotted lines) spectra of **1**, **2**, **1⊂4**, and **2⊂4** at 1 μM concentrations in water. Fluorescence intensities of **1** and **2** are normalized to their corresponding absorption maxima; emission intensities of **1⊂4** and **2⊂4** are displayed relative to the emission intensities of **1** and **2** respectively. The emission spectra were corrected for complexation-induced changes in absorption.

of our ^{1}H-NMR spectrometer. The measurements were thus performed with 0.5 mM concentrations in a [D_4]methanol/D_2O (19:1) mixture, which reduces the binding strength considerably due to partial disruption of the hydrophobic effect. As a consequence of the methanol addition, the association constants are in a range observable by ^{1}H-NMR experiments.[41] The K_a values were obtained from single point measurements of aged 1:1 mixtures of the rods **1**–**3** and **4**, as the exchange dynamic was considerably slower than the time resolution of the experiment. Of particular interest was the K_a of $1.6 \times 10^3 \pm 100$ M^{-1} determined for the formation of the pseudorotaxane **3⊂4** in this solvent mixture, as the aggregation constant of this pseudorotaxane was also determined to be 4×10^6 M^{-1} in pure water by ITC.[36] The solvent shift from pure water to the [D_4]methanol/D_2O (19:1) mixture causes a loss of about three orders of magnitude in the association constant between **3** and **4**, and the structural resemblance of **1** and **2** with **3** suggest comparable effects concerning their association with **4**. Similar observations have been reported by Anderson et al. with an anionic OPE based rod structure and **4**.[35] A comparable K_a value of 3.5×10^3 M^{-1} was obtained for the elongated terephthalate terminated rod **1** and the cyclophane **4** in the [D_4]methanol/D_2O (19:1) mixture, while an increased K_a of 9.0×10^3 M^{-1} was recorded for the isophthalate terminated rod **2** with **4** under the same conditions. The stronger binding of the di-cationic host **4** on rod **2** compared to **1** probably reflects the improved electrostatic interactions. The anionic carboxylate groups of **2** are closer to the cationic subunits of the cyclophane than in the case of **1** and the increased association constant reflects the distance dependence of the Coulomb attraction.

In conclusion, the two dicarboxylate terminated rods **1** and **2** display binding strengths towards **4** which are at least comparable (**1**) or even higher (**2**) than **3**. Interestingly, in the limited temperature range of a VT-^{1}H-NMR experiment (25–90 °C), the spectral features of the pseudorotaxane complexes did not display temperature dependence (Figure S6 and Figure S10). This thermal insensitivity might comprise both, thermodynamic and kinetic contributions. While a temperature insensitive equilibrium constant thermodynamically would point at an entropically dominated driving force, the bulkiness of the terminal unit might kinetically disfavor the unthreading. The efficient pseudorotaxane formation at 90 °C favors the kinetic reasoning, and the completeness of the process points at a high thermodynamic binding strength (Figure 1a and Figure 1b). A similar thermal insensitivity was also recorded for **3⊂4**, and the sterically less demanding termini of **3** reduce the weight of the kinetic argument, at least in this case. However, even if the complexation should be purely thermodynamically driven, conclusions concerning its driving force (enthalpic or entropic) cannot be drawn from the thermal insensitivity of the ^{1}H-NMR spectra, due to the minor effect on the association constant in the small experimentally accessible temperature range.

The formation kinetics of the pseudorotaxanes **1⊂4** and **2⊂4** were monitored by time-dependent ^{1}H-NMR spectroscopy (Figure 3). Rate constants and reaction orders were determined by nonlinear least-squares fitting of time dependent concentrations.[42] Initial experiments were conducted with equimolar concentrations (0.5 mM) of the rods (**1** or **2**) and the cyclophane **4** in D_2O. Interestingly, the expected second order formation kinetic was only observed for the isophthalate terminated rod **2**, while for the complexation of **1**, a reasonable fit of the data was only possible for a first order kinetic. Attempts to vary the host/guest ratio of **2**/**4** to a point where a transition to a pseudo first-order reaction occurs was not possible due to signal broadening. With the potential formation of [3]pseudorotaxanes as main difference between **1** and **2**, this was the first hypothesis for the surprising first order kinetics. To suppress the formation of [3]pseudorotaxanes, the experiment was repeated with a **1** (0.5 mM)/**4** (0.25 mM) ratio but still displayed first order kinetics, although no ^{1}H-NMR signal for the formation of a [3]pseudorotaxane was observed. The half-life of cyclophane disappearance was determined to be 2.5 h (2:1 ratio) for **1** and 16 h for **2** with equimolar amounts of **4** at 0.5 mM concentration. Rate constants are given in Table 1.

The unexpected first order kinetics observed for the formation of **1⊂4** most likely arise from a fast pre-equilibrium be-

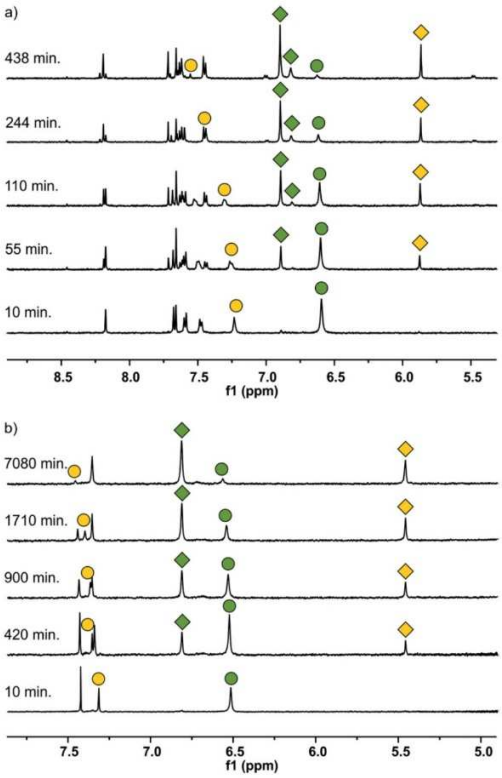

Figure 3. Slow equilibration process of the pseudorotaxane formation of **1** (a) and **2** (b) with **4** as monitored with ^{1}H-NMR (298 K, **1**: 500 MHz; **2**: 400 MHz in D_2O). Yellow circles denote the disappearing phenylene resonances of the free axles (**1** and **2**) and yellow diamonds the appearing signals of the axles in **1**⊂**4** and **2**⊂**4**. Green circles denote the disappearing aryl resonances of the free cyclophane (**4**) and green diamonds the appearing signals of the cyclophane complexed as **1**⊂**4**, **1**⊂**4**$_2$, and **2**⊂**4** respectively.

Table 1. Kinetic data, UV/Vis absorption and emission maxima and binding strength. Rate constants obtained from ^{1}H-NMR spectra in D_2O. *k*-values in the first row were obtained from cyclophane disappearance, in the second row from [2]pseudorotaxane formation. Optical parameters recorded at 1 μM concentrations.

	$T_{1/2}$ h	k^{1st} s^{-1}	k^{2nd} L mol^{-1} s^{-1}	λ_{max}^{abs} nm	K_a[d] M^{-1}
1	2.5[a]	1.4×10^{-4}[a] 1.3×10^{-4}[a]	–	335 (335)[c]	3500 ± 300
2	16[b]	–	2.8×10^{-2}[b] 2.1×10^{-2}[b]	325 (329)[c]	9000 ± 500

[a] 0.5 mM **1** + 0.25 mM **4** in D_2O, determined by ^{1}H-NMR. [b] 1:1 ratio of **2** and **4**, 0.5 mM in D_2O, determined by ^{1}H-NMR. [c] Complex with **4** immediately measured after dilution. [d] Determined in 19:1 [D_4]methanol/D_2O.

tween **1** and **4**. Intuitively, the first hypothesis was a fast pre-equilibrium where the terminal triazole subunits of **1** are threaded in cyclophane **4**. However, the formation of such a supramolecular complex as pre-equilibrium should be detectable in the chemical shift of the triazole proton immediately after the addition of **4**. Inspection of the corresponding spectra revealed a constant value for the chemical shift of the triazole signal disfavoring the hypothesis. But an immediate upfield shift by 0.45 ppm upon addition of equimolar amounts of **4** was monitored for the protons of the central phenylene unit of **1** (Figure S20), pointing at a lateral aggregation of the cyclophane **4** on the rod **1** as a possible fast supramolecular pre-equilibrium. And indeed, the comparable dimensions of the extended hydrophobic backbone of **1** and the hydrophobic macrocycle of **4** might favor such an arrangement with the cationic piperidinium centers of **4** in close proximity of the carboxylate termini of **1**. Interestingly, the electrostatic attraction between both molecules might even be maximized by the ability of rod **1** to adjust the distance between both anionic carboxylate groups by varying the torsion angles between both terminal terephthalate groups. The distance between the carboxylate termini of **2** is significantly smaller, reducing the likelihood of forming a lateral aggregate with **4**. It is noteworthy however, that also for the rod **2** for which the expected second order kinetics were observed, a slight shift (0.15 ppm) of the protons of the central phenylene unit was monitored immediately after the addition of **4**.

The significantly slower pseudorotaxane formation with the cyclophane **4** of the rods **1** and **2** compared with **3** can be explained by the increased steric demand of the additional carboxylate on the terephthalate and isophthalate terminal subunits. In particular in the rod **2** the rigid 1,2,3-substitution pattern of the isophthalate group causes a high steric barrier for complexation. The quicker **1**⊂**4** pseudorotaxane formation compared with **2**⊂**4** suggests that the terephthalate subunit of **1** is sterically less demanding than the isophthalate of **2**. Most likely the two opposed carboxylate groups in *ortho* positions with respect to the rod axis allow the cyclophane to surpass both carboxylate groups in a stepwise manner.

Conclusion

On our quest for the ideal molecular axle for thermodynamically stable and kinetically slow superstructures, we identified tere- and isophthalic subunits as consummate terminal groups for OPE-type molecular axles. Both subunits increase the solubility of the axle in aqueous solution, slow down the kinetics of the supramolecular equilibration and increase the thermodynamic stability of the superstructure. Furthermore, these properties of interest can be fine-tuned by the solvent mixture employed. We are thus striving for integrating these subunits in our future rotaxane and daisy chain designs.

The potential of these units was displayed by the water-soluble model compounds **1** and **2**, which are advancements of the concept of the previously reported OPE **3**. While the central, hydrophobic station and the azide decoration were maintained, the increased number of carboxylate groups improved water solubility and decelerated association kinetics with the cyclophane **4**. The isophthalate-terminated rod **2** shows the slowest association kinetics and the highest stability of the pseudoro-

taxane **2**⊂**4**. The terephthalate-terminated rod **1** displayed faster formation kinetics and due to its extended hydrophobic backbone, it was able to form the [3]pseudorotaxane **1**⊂$\mathbf{4}_2$. While the pseudorotaxane formation kinetics are explained by the bulkiness of the rod's terminal groups, the stability of the superstructure is supported substantially by the electrostatic attraction between its components. An additional promising feature of the superstructures formed in water is their thermal insensitivity, further enlarging the scope of reaction conditions enabling their integration in larger architectures as well defined, mechanically integer subunits.

Experimental Section

Supporting Information (see footnote on the first page of this article): Experimental details and synthetic procedures are given in the electronic supporting information.

Acknowledgments

Generous financial support by the Swiss Nanoscience Institute (SNI grant number P1303), the Swiss National Science Foundation (SNF grant number 200020-178808), and the Volkswagen-Stiftung (Az. 93438) is gratefully acknowledged. M. M. acknowledges support by the 111 project (90002-18011002).

Keywords: Supramolecular chemistry · Pseudorotaxanes · Cyclophanes · Association kinetics · Hydrophobic effect

[1] E. R. Kay, D. A. Leigh, F. Zerbetto, *Angew. Chem. Int. Ed.* **2007**, *46*, 72–191; *Angew. Chem.* **2007**, *119*, 72.
[2] S. Erbas-Cakmak, D. A. Leigh, C. T. McTernan, A. L. Nussbaumer, *Chem. Rev.* **2015**, *115*, 10081–10206.
[3] C. Pezzato, C. Cheng, J. F. Stoddart, R. D. Astumian, *Chem. Soc. Rev.* **2017**, *46*, 5491–5507.
[4] V. Serreli, C.-F. Lee, E. R. Kay, D. A. Leigh, *Nature* **2007**, *445*, 523–527.
[5] J. V. Hernandez, E. R. Kay, D. A. Leigh, *Science* **2004**, *306*, 1532–1537.
[6] C. Cheng, P. R. McGonigal, W.-G. Liu, H. Li, N. A. Vermeulen, C. Ke, M. Frasconi, C. L. Stern, W. A. Goddard III, J. F. Stoddart, *J. Am. Chem. Soc.* **2014**, *136*, 14702–14705.
[7] G. Ragazzon, M. Baroncini, S. Silvi, M. Venturi, A. Credi, *Nat. Nanotechnol.* **2015**, *10*, 70–75.
[8] C. Cheng, P. R. McGonigal, S. T. Schneebeli, H. Li, N. A. Vermeulen, C. Ke, J. F. Stoddart, *Nat. Nanotechnol.* **2015**, *10*, 547–553.
[9] M. R. Wilson, J. Solà, A. Carlone, S. M. Goldup, N. Lebrasseur, D. A. Leigh, *Nature* **2016**, *534*, 235–240.
[10] M. Asakawa, P. R. Ashton, R. Ballardini, V. Balzani, M. Bělohradský, M. T. Gandolfi, O. Kocian, L. Prodi, F. M. Raymo, J. F. Stoddart, M. Venturi, *J. Am. Chem. Soc.* **1997**, *119*, 302–310.
[11] C. Heim, A. Affeld, M. Nieger, F. Vögtle, *Helv. Chim. Acta* **1999**, *82*, 746–759.
[12] P. Linnartz, S. Bitter, C. A. Schalley, *Eur. J. Org. Chem.* **2003**, 4819–4829.
[13] T. Oshikiri, Y. Takashima, H. Yamaguchi, A. Harada, *J. Am. Chem. Soc.* **2005**, *127*, 12186–12187.
[14] P. R. McGonigal, H. Li, C. Cheng, S. T. Schneebeli, M. Frasconi, L. S. Witus, J. F. Stoddart, *Tetrahedron Lett.* **2015**, *56*, 3591–3594.
[15] M. Hmadeh, A. C. Fahrenbach, S. Basu, A. Trabolsi, D. Benítez, H. Li, A.-M. Albrecht-Gary, M. Elhabiri, J. F. Stoddart, *Chem. Eur. J.* **2011**, *17*, 6076–6087.
[16] A. C. Catalán, J. Tiburcio, *Chem. Commun.* **2016**, *52*, 9526–9529.
[17] I. T. Harrison, *J. Chem. Soc., Chem. Commun.* **1972**, 231–232.
[18] P. R. Ashton, M. Bělohradský, D. Philp, N. Spencer, J. F. Stoddart, *J. Chem. Soc., Chem. Commun.* **1993**, 1274–1277.
[19] P. R. Ashton, I. Baxter, M. C. T. Fyfe, F. M. Raymo, N. Spencer, J. F. Stoddart, A. J. P. White, D. J. Williams, *J. Am. Chem. Soc.* **1998**, *120*, 2297–2307.
[20] B. J. Slater, E. S. Davies, S. P. Argent, H. Nowell, W. Lewis, A. J. Blake, N. R. Champness, *Chem. Eur. J.* **2011**, *17*, 14746–14751.
[21] Y. Yu, Y. Li, X. Wang, H. Nian, L. Wang, J. Li, Y. Zhao, X. Yang, S. Liu, L. Cao, *J. Org. Chem.* **2017**, *82*, 5590–5596.
[22] S. Tsuda, J. Terao, N. Kambe, *Chem. Lett.* **2009**, *38*, 76–77.
[23] J. Terao, S. Tsuda, Y. Tanaka, K. Okoshi, T. Fujihara, Y. Tsuji, N. Kambe, *J. Am. Chem. Soc.* **2009**, *131*, 16004–16005.
[24] J. Terao, A. Wadahama, A. Matono, T. Tada, S. Watanabe, S. Seki, T. Fujihara, Y. Tsuji, *Nat. Commun.* **2013**, *4*, 1691.
[25] H. Masai, J. Terao, S. Makuta, Y. Tachibana, T. Fujihara, Y. Tsuji, *J. Am. Chem. Soc.* **2014**, *136*, 14714–14717.
[26] H. Masai, J. Terao, T. Fujihara, Y. Tsuji, *Chem. Eur. J.* **2016**, *22*, 6624–6630.
[27] F. Diederich, K. Dick, D. Griebel, *Chem. Ber.* **1985**, *118*, 3588–3619.
[28] F. Diederich, *Angew. Chem. Int. Ed. Engl.* **1988**, *27*, 362–386; *Angew. Chem.* **1988**, *100*, 372–396.
[29] S. B. Ferguson, E. M. Seward, F. Diederich, E. M. Sanford, A. Chou, P. Inocencio-Szweda, C. B. Knobler, *J. Org. Chem.* **1988**, *53*, 5593–5595.
[30] S. B. Ferguson, E. M. Sanford, E. M. Seward, F. Diederich, *J. Am. Chem. Soc.* **1991**, *113*, 5410–5419.
[31] D. R. Benson, J. Fu, *Tetrahedron Lett.* **1996**, *37*, 4833–4836.
[32] D. R. Benson, J. Fu, C. K. Johnson, S. W. Pauls, D. A. Williamson, *J. Org. Chem.* **1998**, *63*, 9935–9945.
[33] Y. Aeschi, S. Drayss-Orth, M. Valášek, F. Raps, D. Häussinger, M. Mayor, *Eur. J. Org. Chem.* **2017**, *2017*, 4091–4103.
[34] S. Anderson, R. T. Aplin, T. D. W. Claridge, T. Goodson III, A. C. Maciel, G. Rumbles, J. F. Ryan, H. L. Anderson, *J. Chem. Soc., Perkin Trans. 1* **1998**, 2383–2398.
[35] P. N. Taylor, A. J. Hagan, H. L. Anderson, *Org. Biomol. Chem.* **2003**, *1*, 3851–3856.
[36] Y. Aeschi, S. Drayss-Orth, M. Valášek, D. Häussinger, M. Mayor, *Chem. Eur. J.* **2019**, *25*, 285–295.
[37] K. D. Hänni, D. A. Leigh, *Chem. Soc. Rev.* **2010**, *39*, 1240–1251.
[38] P. R. Serwinski, P. M. Lahti, *Org. Lett.* **2003**, *5*, 2099–2102.
[39] M. C. Martos-Maldonado, I. Quesada-Soriano, J. M. Casas-Solvas, L. García-Fuentes, A. Vargas-Berenguel, *Eur. J. Org. Chem.* **2012**, 2560–2571.
[40] K. Barral, A. D. Moorhouse, J. E. Moses, *Org. Lett.* **2007**, *9*, 1809–1811.
[41] P. Thordarson, *Chem. Soc. Rev.* **2011**, *40*, 1305–1323.
[42] C. L. Perrin, *J. Chem. Educ.* **2017**, *94*, 669–672.

Received: December 20, 2018

Supporting Information. Slow Formation of Pseudorotaxanes in Water: Large Influence of the Substitution Pattern

Supporting Information

Slow Formation of Pseudorotaxanes in Water

Yves Aeschi, Laurent Jucker, Daniel Häussinger, and Marcel Mayor*

ejoc201801864-sup-0001-SupMat.pdf

Contents

Syntheses

2-hydroxyisophthalic acid:

2-Nitroisophthalic acid (12.0 g, 56.8 mmol) was suspended in a mixture of *i*-PrOH (100 mL) and MeOH (20 mL). A solution of sodium hydroxide (4.54 g, 114 mmol) in MeOH (40 mL) was added to the suspension. The solvent was partially distilled off at 70 °C under reduced pressure (200 mBar). The precipitated disodium 2-nitroisophthalate was filtered off, washed with *i*-PrOH and TBME and dried at 90 °C/10 mBar. This product was placed in a flask and NaOH (11.0 g, 275 mmol) was added, followed by dry DMSO (40 mL). The mixture was bubbled with Ar for 2 h and then it was heated to 160 °C for 3 h. The reaction mixture was then poured into water (350 mL) and acidified with 10 % aqueous HCl until a pH < 2 was reached. Saturated brine (100 mL) and EtOAc (50 mL) were added. Insoluble matter was removed by filtration over Celite, which was acidified by rinsing with 10 % aqueous HCl prior to filtration. The filter cake was washed with water (50 mL) and EtOAc (50 mL) and the organic phase was separated from the filtrate. The aqueous phase was extracted with EtOAc (5 * 50 mL), until only a faint product spot was observed on TLC (Silica gel, acetone, R_f = 0.7, product exhibits blue fluorescence) when spotting the organic phase. The combined organic phases were washed with 1:1 brine/water (100 mL), dried over Na_2SO_4 and evaporated to give 5.4 g (52 %) of a brown powder, which was pure enough for the next step. Variable yields between 35 and 62 % were obtained from this reaction, the product usually contained traces of DMSO.

^{1}H NMR (250 MHz, CD_3CN) δ 8.13 (d, *J* = 7.8 Hz, 2H), 7.06 (t, *J* = 7.8 Hz, 1H). The spectral data match the values from literature[2]

Compound 1

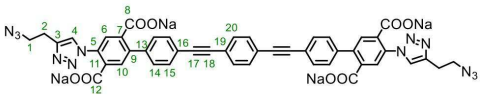

OPE **10** (256 mg, 0.274 mg) was placed in a flask and NaOH (175 mg, 4.38 mmol) was added, followed by a mixture of H_2O (1 mL), MeOH (5 mL) and THF (5 ml). It was stirred at 60 °C for 30 min and a clear solution was obtained. Upon cooling, a white substance precipitated, which was isolated by centrifugation. The pellet was redispersed in THF/MeOH 1:1 (10 mL) and centrifugated. This procedure was repeated with *i*-PrOH to give a first crop of product. The supernatant liquids from centrifugation were combined, neutralized with dry ice and the evaporated. The solid was redissolved in MeOH and centrifuged to remove insoluble salts. The supernatant liquid was subjected to size exclusion chromatography (Sephadex LH-20, MeOH) to give another crop of a white solid. Both fraction were combined and subjected to size exclusion chromatography (Sephadex LH-20, MeOH) to give 248 mg (82 %) of a white powder. The compound could not be prepared without traces of solvents or water. ^{13}C-NMR revealed the presence of bicarbonate, which was found to be difficult to remove by chromatography. A purity of 88 % was determined by ^{1}H-NMR titration with **4**. The elemental analysis matches with this observation, as carbon- and nitrogen contents are approximately 10 % too low: calcd. For $C_{46}H_{26}N_{12}Na_4O_8$ (%) C 57.15; H 2.71; N 17.39, found: C 52.42; H 3.71; N 15.46. The yield was corrected for the actual product content.

^{1}H NMR (500 MHz, MeOD) δ 8.13 (s, 2H, H-4), 7.70 (s, 2H, H-6), 7.67 (s, 2H, H-10), 7.64 (d, *J* = 8.5 Hz, 4H, H-14), 7.58 (d, *J* = 8.5 Hz, 4H, H-15), 7.56 (s, 4H, H-20), 3.68 (t, *J* = 7.1 Hz, 5H, H-2), 3.06 (t, *J* = 7.1, 4H, H-1).

^{13}C NMR (126 MHz, MeOD) δ 176.31 (C-8), 173.75 (C-12), 145.25 (C-3), 143.06 (C-5), 142.27 (C-7), 140.22 (C-11), 136.93 (C-13), 134.00 (C-9), 132.63 (C-20), 132.43 (C-15), 131.31 (C-6), 129.90 (C-14), 125.46 (C-4), 125.28 (C-10), 124.57 (C-19), 123.30 (C-16), 92.17 (C-17), 90.28 (C-18), 51.63 (C-2), 26.39 (C-1).

HRMS (ESI, +): calcd. for $C_{46}H_{30}N_{12}O_8$ 879.2382 $[M-4Na+5H]^+$, found 879.2395.

Compound 2

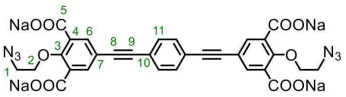

OPE **14** (500 mg, 0.735 mmol) was placed in a flask and THF (8 mL) was added. To this solution was added a solution of NaOH (470 mg, 11.8 mmol) in H_2O (2 mL) and MeOH (8 mL). It was stirred at 60 °C for 1 h, during which a clear solution was obtained. The mixture was then concentrated to approximately one third of its initial volume and redissolved in MeOH (20 mL). Residual NaOH was neutralized with CO^2 (dry ice) and the precipitate was removed by centifugation and decantation. The decanted liquid was subjected to size exclusion chromatography (Sephadex LH-20, MeOH) to obtain 451 mg (78 %) of the desired compound as a white solid. Similar to 1, residual solvent and water could not be completely removed. A purity of 91 % was determined by ^{1}H-NMR titration with **4**. The elemental analysis matches with this observation, as carbon- and nitrogen contents are approximately 10 % too low: calcd. For $C_{46}H_{26}N_{12}Na_4O_8$ C, 50.58; H, 2.26; N, 11.80, found: C 47.05; H 3.24; N 10.41. The yield was corrected for the actual product content.

^{1}H NMR (500 MHz, MeOD) δ 7.56 (s, 4H, H-6), 7.50 (s, 4H, H-11), 4.25 (t, *J* = 5.6 Hz, 4H, H-2), 3.65 (t, *J* = 5.7 Hz, 4H, H-1).
^{13}C NMR (126 MHz, MeOD) δ 174.80 (C-4), 153.74 (C-3), 137.06 (C-5), 132.67 (C-6), 132.53 (C-11), 124.47 (C-10), 119.12 (C-7), 91.53 (C-8), 89.27 (C-9), 73.93 (C-2), 52.10 (C-1).
HRMS (ESI, +): calcd. for $C_{30}H_{20}N_6NaO_{10}$ 647.1133 $[M-3Na+ 3H]^+$, found 647.1132

Dimethyl 2-amino-5-iodoterephthalate (5):

Dimethyl-2-aminoterephthalate (10.0 g, 47.8 mmol) was dissolved in MeOH/DCM 1:1 (150 mL) and N-iodosuccinimide (11.3 g, 50.2 mmol) was added. The mixture was heated to a gentle reflux for 16 h in the absence of light. It was concentrated to a residual volume of approx. 60 mL, which was then allowed to cool to room temperature. A large amount of mustard-yellow crystals formed, which were filtered off and washed with cold MeOH (100 mL) until the filtrate was almost colorless, yield after air-drying was 11.6 g. The filtrate was evaporated, partioned between EtOAc and water and the organic phase was washed with sodium thiosulfate solution (10 %) and dried aver Na_2SO_4. The solvent was removed and the crude was crystallized from Et_2O to give an additional 1.3 g of the desired product. Total yield: 12.9 g (74 %)
^{1}H NMR (400 MHz, $CDCl_3$) δ 8.36 (s, 1H), 7.08 (s, 1H), 5.83 (s, 2H), 3.91 (s, 3H), 3.88 (s, 3H).
The analytical data matched the previously described ones.[1]

Dimethyl 2-azido-5-iodoterephthalate (6):

Dimethyl-2-amino-5-iodoterephthalate (2.0 g, 6.0 mmol) was dissolved in CH_3CN (30 mL) and cooled in an ice bath. *Tert*-butyl nitrite (1.1 mL, 8.4 mmol, 1.4 eq) was added and it was stirred for 30 min in the ice bath. This was followed by the slow addition of trimethylsilyl azide (1.3 mL, 96 mmol, 1.6 eq). The cooling bath was removed and it was stirred for 1 h at room temperature, then evaporated to give a brown solid (2.1 g, 97 %) which was sufficiently pure for the next step. An analytical sample was obtained by recrystallization from cyclohexane.
^{1}H NMR (400 MHz, $CDCl_3$) δ 8.39 (s, 1H), 7.62 (s, 1H), 3.97 (s, 3H), 3.92 (s, 3H).
^{13}C NMR (101 MHz, $CDCl_3$) δ 165.8, 164.1, 144.5, 140.7, 139.4, 126.2, 122.7, 87.5, 53.5, 53.3.
HRMS (ESI, +): calcd. for $C_{10}H_8IN_3NaO_4$ 383.9452 $[M+Na]^+$, found 383.9460.

Compound 7:

Dimethyl-2-azido-5-iodoterephthalate (4.30 g, 11.9 mmol) and 3-Butyn-1-ol (0.98 mL, 13.1 mmol) were dissolved in CH_3CN (30 mL) and it was degassed with Ar for 10 min. $Cu(CH_3CN)_4PF_6$ (90 mg, 0.24 mmol) and tris[(1-benzyl-1*H*-1,2,3-triazol-4-yl)methyl]amine (126 mg, 0.238 mmol) were added. It was stirred for 6 h and then adsorbed on silica gel for dryload column chromatography (Silica gel, EtOAc) to give a clear oil, which was dried at 60 °C, 2 mBar to give 4.40 g (86 %) of a clear oil, which solidified upon standing over night.

^{1}H NMR (500 MHz, $CDCl_3$) δ 8.53 (d, *J* = 0.7 Hz, 1H), 7.91 (s, 1H), 7.73 (d, *J* = 0.7 Hz, 1H), 3.99 (q, *J* = 5.7 Hz, 2H), 3.95 (s, 3H), 3.76 (s, 3H), 3.04 (t, *J* = 5.7 Hz, 2H), 2.67 – 2.59 (m, 1H).
^{13}C NMR (126 MHz, $CDCl_3$) δ 164.8, 163.7, 145.7, 143.7, 138.6, 135.8, 130.1, 128.4, 123.3, 94.7, 61.5, 53.1, 53.1, 28.71.
HRMS (ESI, +): calcd. for $C_{14}H_{15}IN_3O_5$ 432.0051 $[M+H]^+$, found 432.0058.

Compound 8:

Compound **7** (4.40 g, 10.2 mmol) was placed in a flask and THF (30 mL) was added. It was cooled to -20 °C and CBr_4 (3.72 g, 11.2 mmol) was added, followed by Ph_3P (3.48 g, 13.3 mmol). It was stirred and allowed to warm to r.t. during the course of 6 h. A large amount of precipitation was formed, which was filtered off and washed with TBME. The filtrate was evaporated and the crude compound was purified by column chromatography (Silica gel, Petroleum ether → Petroleum ether/EtOAc 3:2). The product fractions were evaporated and recrystallized from cyclohexane/TBME to give 4.70 g (93 %) of a white solid after drying at 2 mBar.
^{1}H NMR (500 MHz, $CDCl_3$) δ 8.56 (s, 1H), 7.92 (s, 1H), 7.77 (s, *J* = 0.7 Hz, 1H), 3.97 (s, *J* = 1.5 Hz, 3H), 3.77 (s, 3H), 3.73 (t, *J* = 6.7 Hz, 2H), 3.40 (t, *J* = 6.7 Hz, 2H).
^{13}C NMR (126 MHz, $CDCl_3$) δ 165.0, 163.8, 145.2, 143.9, 138.8, 135.9, 130.4, 128.7, 123.5, 95.0, 53.3, 53.3, 31.6, 29.43.
HRMS (ESI, +): calcd. for $C_{14}H_{14}BrIN_3O_4$ 493.9207 $[M+H]^+$, found 493.9208.

Compound 9:

Compound **8** (4.60 g, 9.31 mmol) and NaN_3 (0.666 g, 10.2 mmol) were placed in a flask and DMF (15 mL) was added. The mixture was stirred at 50 °C for 18 h. It was then poured into water (600 mL) and it was extracted with TBME twice. The combined organic phases were washed with water, dried over Na_2SO_4 and evaporated. The crude compound was purified by short column chromatography (Silica gel, cyclohexane/EtOAc 2:1 → 3:2) to give the compound as a colorless oil, which solidified upon standing. Yield: 3.97 g (94 %)

^{1}H NMR (500 MHz, $CDCl_3$) δ 8.54 (s, 1H), 7.91 (s, 1H), 7.73 (s, 1H), 3.96 (s, 3H), 3.76 (s, 3H), 3.69 (t, *J* = 6.7 Hz, 2H), 3.08 (t, *J* = 6.7 Hz, 2H).

^{13}C NMR (126 MHz, $CDCl_3$) δ 164.8, 163.7, 144.5, 143.8, 138.6, 135.7, 130.2, 128.5, 123.4, 94.8, 53.1, 53.1, 50.5, 25.6.

HRMS (ESI, +): calcd. for $C_{14}H_{14}IN_6O_4$ 457.0116 $[M+H]^+$, found 457.0122.

Compound 10:

1,4-Diethynylbenzene (355 mg, 2.81 mmol, 1.00 eq) and 4-Iodophenylboronic acid pinacol ester (1.90 g, 5.76 mmol, 2.05 eq) were dissolved in a mixture of THF (8.0 mL) and Et_3N (4.0 mL). The mixture was bubbled with Ar for 5 min, bis(triphenylphosphine)palladium dichloride (39 mg, 56 µmol, 2 mol%) and CuI (5.4 mg, 28 µmol) were added. It was stirred for 20 h and the solvents were then removed. The crude product was suspended in MeOH, the suspension was acidified with AcOH (1 mL) and the solids were filtered off. The filter cake was washed with MeOH (3*10 mL) to give 1.23 g (83 %) of a white powder.

^{1}H NMR (500 MHz, $CDCl_3$) δ 7.79 (d, *J* = 8.3 Hz, 4H), 7.53 (d, *J* = 8.3 Hz, 4H), 7.51 (s, 4H), 1.35 (s, 24H).

^{13}C NMR (126 MHz, $CDCl_3$) δ 134.8, 131.7, 130.9, 129.3 (broad, identified by HMBC), 125.8, 123.3, 91.6, 90.5, 84.1, 25.0.

HRMS (MALDI, +): calcd. for $C_{34}H_{36}B_2O_4$ 530.2794 M^+, found 530.2793.

Compound 11:

Compound **9** (596 mg, 1.31 mmol, 2.1 eq) and **10** (330 mg, 0.622 mmol, 1.0 eq) were placed in a flask, sodium carbonate (344 mg, 2.49 mmol, 4.0 eq), toluene (5,0 mL) and water (1.0 mL) were added. It was bubbled with Ar for 15 min and $Pd(dppf)Cl_2 * CH_2Cl_2$ (45 mg, 0.062 mmol, 0.1 eq.) was added. It was stirred at 80 °C for 4 h, when conversion was found to be complete by LC/MS. The mixture was then partitioned between 2 % aqueous HCl and DCM and the organic phase was separated. It was dried over Na_2SO_4, evaporated, redissolved in DCM and adsorbed on silica gel. Purification by column chromatography (Silica gel, DCM/EtOAc 3:2) gave a yellowish solid 330 mg, (57 %).

^{1}H NMR (400 MHz, $CDCl_3$) δ 7.99 (s, 2H), 7.98 (s, 2H), 7.79 (s, 2H), 7.62 (d, *J* = 8.1 Hz, 4H), 7.55 (s, 4H), 7.36 (d, *J* = 8.0 Hz, 4H), 3.77 (s, 6H), 3.73 (t, *J* = 6.8 Hz, 4H), 3.72 (s, 6H), 3.12 (t, *J* = 6.7 Hz, 4H).

^{13}C NMR (101 MHz, $CDCl_3$) δ 166.6, 164.9, 144.4, 143.2, 138.9, 135.0, 134.2, 133.4, 131.6, 129.6, 128.4, 128.0, 123.5, 123.2, 123.1, 90.9, 90.4, 53.0, 52.7, 50.6, 25.7.

HRMS (ESI, +): calcd. for $C_{50}H_{38}IN_{12}NaO_8$ 957.2828 $[M+H]^+$, found 957.2810.

Dimethyl-2-hydroxy-5-iodoisophthalate (12):

2-hydroxyisophthalic acid (1.2 g, 6.6 mmol) was placed in a flask and MeOH (30 mL) was added, followed by *N*-iodosuccinimide (1.48 g, 6.46 mmol). The mixture was stirred for 16 h in the absence of light and then H_2SO_4 (1 mL) was added. It was heated to reflux for 10 h. After cooling to rt, a precipitate appeared, which was filtered off and washed with cold MeOH to give 1.2 g (54 %) of a white substance.

^{1}H NMR (400 MHz, $CDCl_3$) δ 11.73 (s, 1H), 8.31 (s, 2H), 3.95 (s, 6H).

^{13}C NMR (101 MHz, $CDCl_3$) δ 166.9, 161.2, 144.5, 118.8, 79.1, 52.9.

HRMS (ESI, +): calcd. for $C_{10}H_9INaO_5$ 358.9387 $[M+Na]^+$, found 358.9388

Compound 13:

Dimethyl-2-hydroxy-5-iodoisophthalate (501 mg, 1.49 mmol) and cesium carbonate (2.43 g, 7.46 mmol) were placed in a flask, dry DMSO (4 mL) was added, giving a yellow suspension. 1-Bromo-2-chloroethane (1.8 mL, 22 mmol) was added, the flask was capped with a septum and it was stirred at room temperature for 16 h, giving a colorless suspension. It was partitioned between water and TBME, the organic phase was separated and the aqueous phase was extracted with TBME. The combined organic phases were adsorbed on silica gel (~10 g) and the solvent was removed. The desired compound was obtained by column chromatography (Silica gel, cyclohexane → cyclohexane/EtOAc 3:1) to give 574 mg (96 %) as a white solid.

^{1}H NMR (500 MHz, $CDCl_3$) δ 8.23 (s, 2H), 4.28 (t, *J* = 5.8 Hz, 2H), 3.92 (s, 6H), 3.85 (t, *J* = 5.8 Hz, 2H).

^{13}C NMR (126 MHz, $CDCl_3$) δ 164.7, 157.9, 144.0, 128.9, 87.0, 76.0, 53.1, 42.8.

HRMS (ESI, +): calcd. for $C_{12}H_{13}ClIO_5$ 415.9756 $[M+H]^+$, found 415.9754

Compound 14:

Compound **13** (3.37 g, 8.46 mmol) was placed in a flask and DMSO (20 mL) was added, followed by sodium azide (660 mg, 10.2 mmol). The reaction was stirred at 60 °C for 20 h and then cooled to r.t., then it was poured into water (300 mL) and extracted with TBME (2 * 50 mL). The combined organic phases were washed with 5 % aqueous HCl and water, dried over Na_2SO_4 and then evaporated at reduced pressure, giving 3.30 g (96 %) of a colorless oil, which slowly crystalized.

^{1}H NMR (400 MHz, $CDCl_3$) δ 8.24 (s, 2H), 4.23 (d, *J* = 5.1 Hz, 2H), 3.94 (s, 6H), 3.64 (t, *J* = 5.1 Hz, 2H).

^{13}C NMR (101 MHz, $CDCl_3$) δ 164.3, 157.6, 143.6, 128.6, 86.6, 74.6, 52.7, 52.7, 50.8.

HRMS (ESI, +): calcd. for $C_{12}H_{12}IN_3NaO_5$ 427.9714 $[M+Na]^+$, found 427.9717

Compound 15:

Compound **14** (3.35 g, 8.26 mmol, 2.45 eq) was dissolved in a mixture of THF (30 mL) and Et_3N (5 mL). Copper(I) iodide (25.7 mg, 0.135 mmol, 4 mol%) and bis(triphenylphosphine)palladium dichloride (47.3 mg, 67.4 µmol, 2 mol%) were added and it was bubbled with Ar for 5 min, then 1,4-diethynylbenzene (425 mg, 3.37 mmol) was added, followed by further bubbling with Ar for 5 min. A precipitate started to form after 10 min. It was stirred for 14 h and then the solvents were distilled off at reduced pressure. The crude mixture was stirred in MeOH/acetone 2:1 (60 mL) and then filtered off and washed with a small amount of diethyl ether to give a yellowish powder (1.43 g), which was pure according to ^{1}H-NMR analysis. A second, slightly discolored fraction was obtained by evaporation of the filtrate and suspension in cold MeOH, followed by filtration and washing with cold diethyl ether (0.44g), total yield 1.87 g, (82 %).

^{1}H NMR (400 MHz, $CDCl_3$) δ 8.09 (s, 4H), 7.50 (s, 4H), 4.26 (t, *J* = 5.0 Hz, 4H), 3.95 (s, 12H), 3.65 (d, *J* = 5.0 Hz, 4H).

^{13}C NMR (101 MHz, $CDCl_3$) δ 165.2, 157.6, 138.0, 131.8, 127.3, 123.0, 119.4, 90.4, 89.0, 74.8, 52.7, 51.0.

HRMS (ESI, +): calcd. for $C_{34}H_{28}N_6NaO_{10}$ 703.1559 $[M+Na]^+$, found 703.1566

^{1}H-NMR complexation studies of 1 with 4

NMR samples were prepared from stock solutions of 1 mM concentration in D_2O in the appropriate ratios directly in an NMR tube followed by vigorous shaking. **1** tended to precipitate upon addition of > 1 eq **4**, sometimes even during mixing of the equimolar samples. Directly after mixing, the samples were immersed into a heating bath at 90 °C.

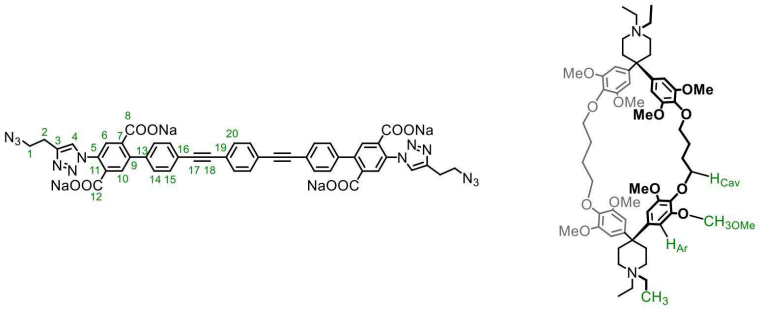

Figure SI 1. Atom numbering of OPE **1** and **4**

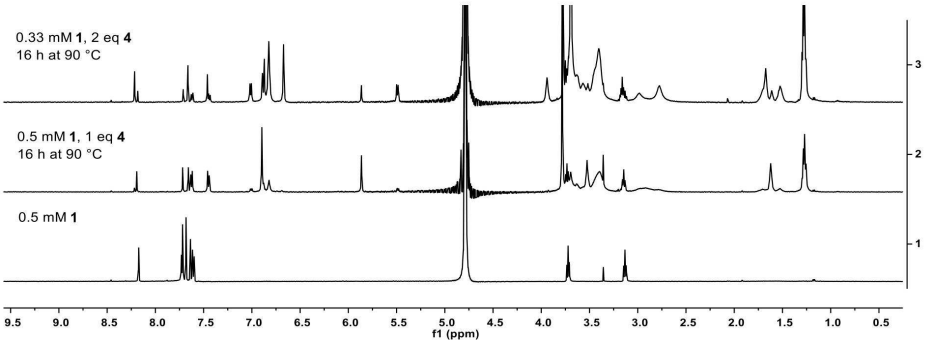

Figure SI 2. Complexation studies: Full range ^{1}H-NMR spectra (500 MHz, D_2O, 298 K) of **1** and complexes thereof after heating to 90 °C for 16 h.

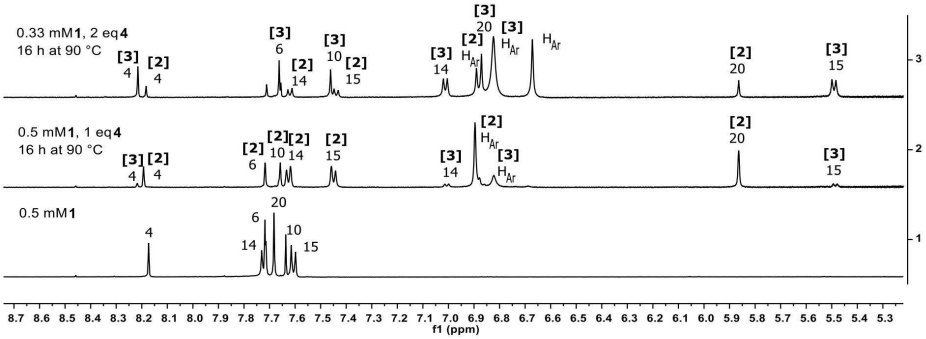

Figure SI 3. Aromatic range of ^{1}H-NMR spectra (500 MHz, D_2O, 298 K) of **1** and complexes thereof. For assignments, numbers in brackets indicate the belonging to either [2]- or [3]pseudorotaxanes or uncomplexed species (no bracket, numbers of structural assignments).

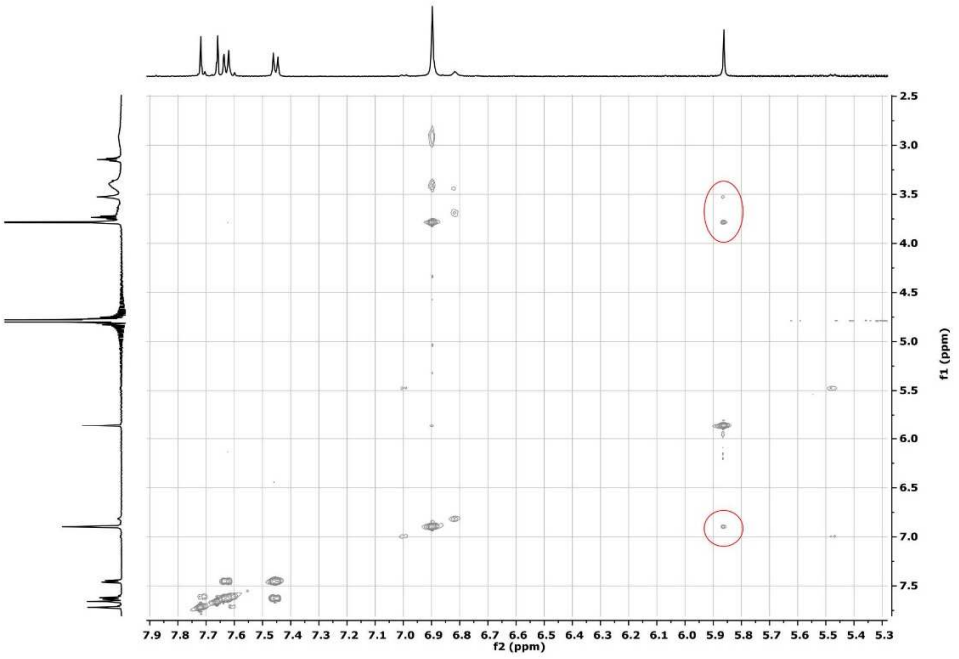

Figure SI 4. Partial ^{1}H NOESY (500 MHz, D_2O, 298 K) of **1** ⊂ **4** (0.5 mM). Red circles: Cross-peaks of **1**-H-20 to **4** H_{Ar}, H_{Cav}, and CH_{3OMe}

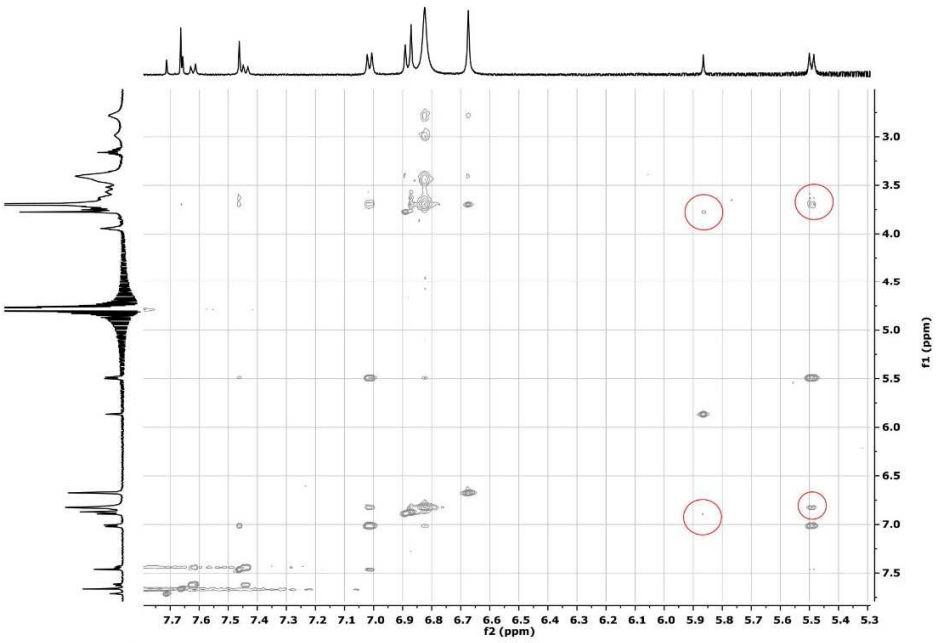

Figure SI 5. Partial ^{1}H NOESY (500 MHz, D_2O, 298 K) of **1** ⊂ $\mathbf{4_2}$ (0.33 mM). Red circles: Cross-peaks of **1**-H-20 to **4** H_{Ar}, and CH_{3OMe}

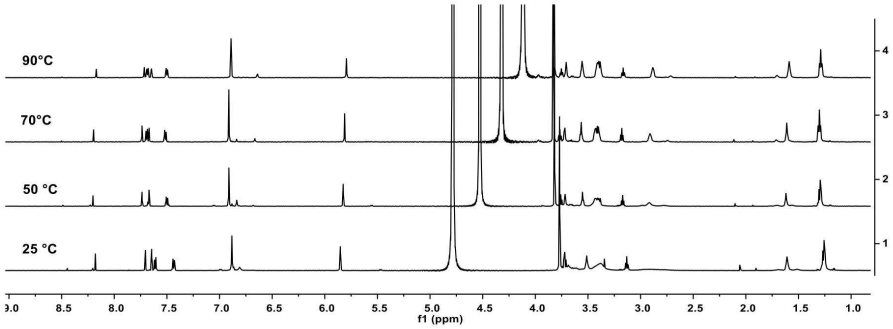

Figure SI 6. VT-^{1}H-NMR of **1**⊂**4** (0.5 mM in D_2O, 600 MHz).

^{1}H-NMR complexation studies of 2 with 4

NMR samples were prepared from stock solutions of 1 or 5 mM concentration in D_2O in the appropriate ratios directly in an NMR tube followed by vigorous shaking. The tendency to precipitate is less pronounced for **2** than for **1**. Therefore, a sample of **2** in presence of 5 eq **4** could be prepared without formation of any visible precipitate. Directly after mixing, the samples were immersed into a heating bath at 90 °C.

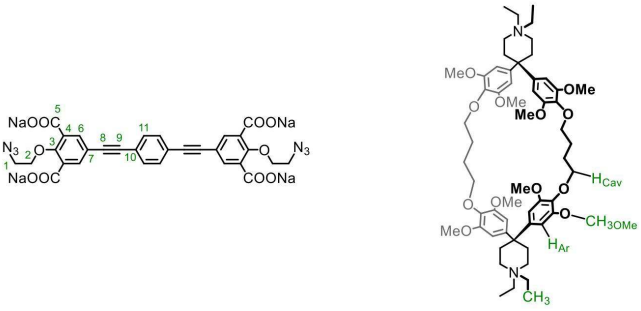

Figure SI 7. Atom numbering of OPE **2** and **4**

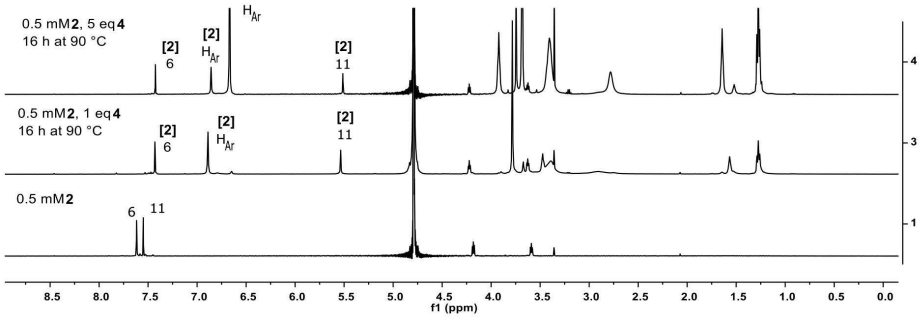

Figure SI 8. Full range ^{1}H-NMR spectra (500 MHz, D_2O, 298 K) of **2** and complexes thereof after heating to 90 °C for 16 h. Assignments of aromatic protons are given according to figure SI 1. Numbers in brackets indicate the belonging to [2]pseudorotaxanes or uncomplexed species (no bracket, numbers of structural assignments).

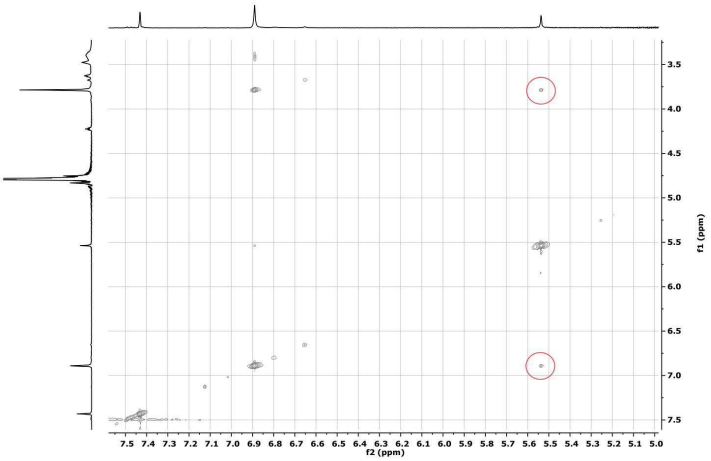

Figure SI 9. Partial ^{1}H NOESY (500 MHz, D_2O, 298 K) of **2**⊂**4** (0.5 mM). Red circles: Cross-peaks of **2**-H-20 to **4** H_{Ar}, and CH_{3OMe}

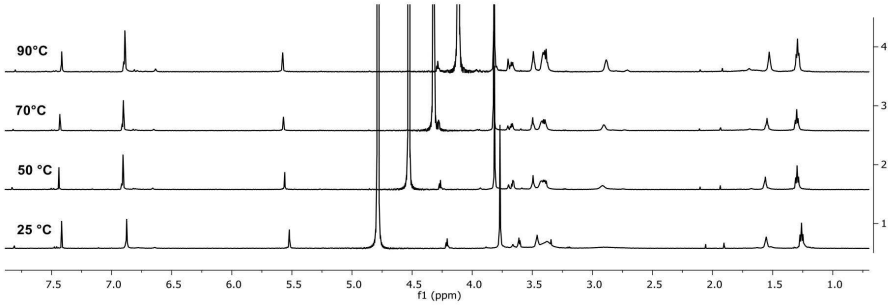

Figure SI 10. VT-^{1}H-NMR of **2**⊂**4** (0.5 mM in D_2O, 600 MHz).

UV Vis and Fluorescence

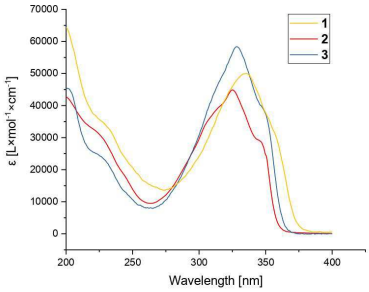

Figure SI 11. UV Vis spectra of **1**, **2** and **3.**

For UV Vis and Fluorescence spectra, all components were measured at 1 µM concentration. **1** or **2**⊂**4** was measured by dilution of an equilibrated NMR sample 0.5 mM in D_2O, the samples were immediately measured after dilution and again after 40 h. **1** or **2** + **4** solutions were prepared by mixing both components from 1 mM stock solutions, followed by immediate measurement and again after 40 h. The spectra of the pseudorotaxanes showed practically no change, whereas the mixtures of the components slowly equilibrate.

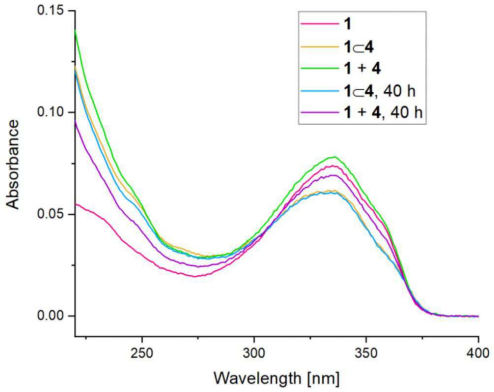

Figure SI 12. UV Vis spectra of **1**, **1**⊂**4** and **1** + **4**.

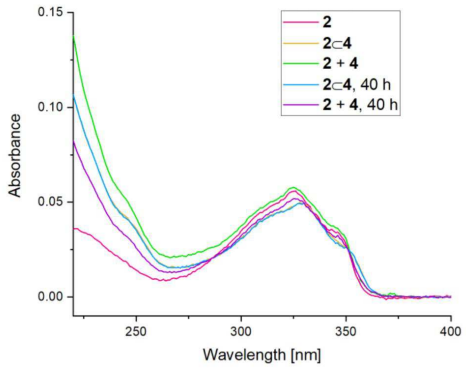

Figure SI 13. UV Vis spectra of **2**, **2**⊂**4** and **2** + **4**.

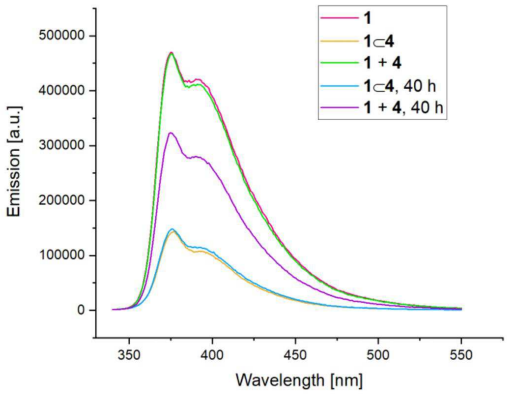

Figure SI 14. Fluorescence spectra of **1**, **1**⊂**4** and **1** + **4**.

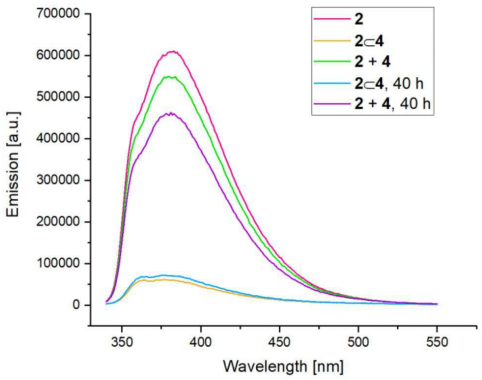

Figure SI 15. Fluorescence spectra of **2**, **2**⊂**4** and **2** + **4**.

Kinetic measurements of 1 and 2

To follow the course of the reaction, 0.5 mM stock solutions of either **1** or **2** in D_2O were diluted with D_2O if necessary and mixed thoroughly with the appropriate amounts of a 0.5 or 5 mM solution of **4** in D_2O. The time delay of the first measurement was assumed to be 10 minutes before the first FID was accumulated. For **1**, 256 scans were accumulated per spectrum (400 MHz, 298 K), and for **2** 128 scans (500 MHz, 298 K). The stacked spectra were then baseline-corrected by the multipoint method provided by MestReNova 11.0.2. Peaks of interest were all integrated in stacked mode to ensure an equal integration width. As a reference integral for concentration determination, the CH_3-resonances belonging to the ethylpiperidinium moiety of **4** were chosen. They are not strongly affected by the complexation process and do not overlap with any other signal. The integral of these protons is slightly overestimated with respect to the cyclophane aryl protons, therefore a correction factor was calculated for each spectrum:

$$C = \frac{I_{CH_3}*2}{I_{H_{Ar}}*3}$$

With I_{CH_3} corresponding to the integral the spiropiperidine methyl groups and $I_{H_{Ar}}$ to the sum of integrals belonging to the cyclophane aryl protons (i.e. those of the complexed and uncomplexed cyclophane). The $\frac{2}{3}$ factor arises from the normalization on the proton count of the corresponding signals. All concentrations of **4** and **1** / **2**⊂**4** were then corrected by this factor.

The following equations[3] were used for fitting:

$$[H] = [H]_0 e^{-kt}$$; First order kinetics disappearance of host.

$$[HG] = [G]_0 - [G]_0 e^{-kt}$$; First order kinetics, formation of host⊂guest

$$[H] = \frac{[H]_0([H]_0-[G]_0)}{[H]_0-[G]_0 e^{-([H]_0-[G]_0)kt}}$$; Second order kinetics disappearance of host.

$$[HG] = [G]_0 - \frac{[G]_0([G]_0-[H]_0)}{[G]_0-[H]_0 e^{-([G]_0-[H]_0)kt}}$$; Second order kinetics formation of host⊂guest.

$[H]$: Time-dependent host concentration.
$[HG]$: Time-dependent concentration of pseudorotaxane
$[H]_0$: Starting concentration of host.
$[G]_0$: Starting concentration of guest
k : First- or second order rate constant
t : Time

The second order equations can in principle be simplified under the assumption that $[H]_0 = [G]_0$. However, exact matching of the stoichiometric 1:1 ratio is difficult at low concentrations, especially when considering that partial precipitation might occur. Even so, when the data were fitted using the simplified version[3] of the above equations, the k values remained almost identical.

Kinetic measurements of 1

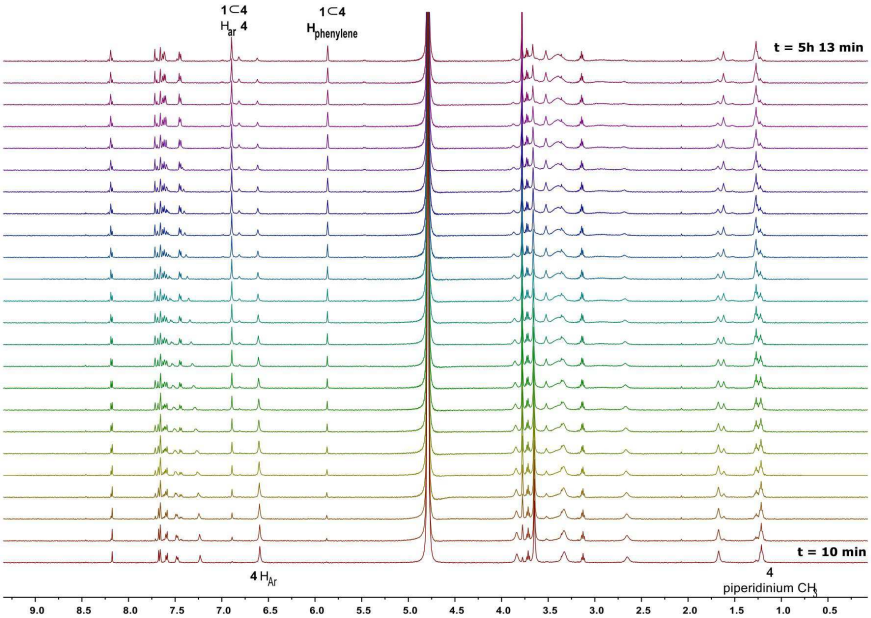

Figure SI 16. Arrayed full range ^{1}H-NMR spectra (500 MHz, D_2O 298 K, 128 scans) of kinetic measurement at 0.5 mM equimolar concentrations of **1** and **4**. Selection of every second spectrum up to 5 h 13 min. The resonances used for determination of *k* are labeled.

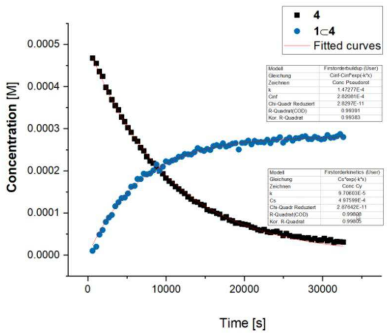

Figure SI 17. Formation of **1** ⊂ **4**, disappearance of **4** and corresponding curve fits. The data points were obtained by integration of the peaks indicated in the above NMR spectra. The concentration of **1** ⊂ **4** is approaching saturation at approx. 0.3 mM concentration. This is due to competitive formation of **1** ⊂ **4**$_2$.

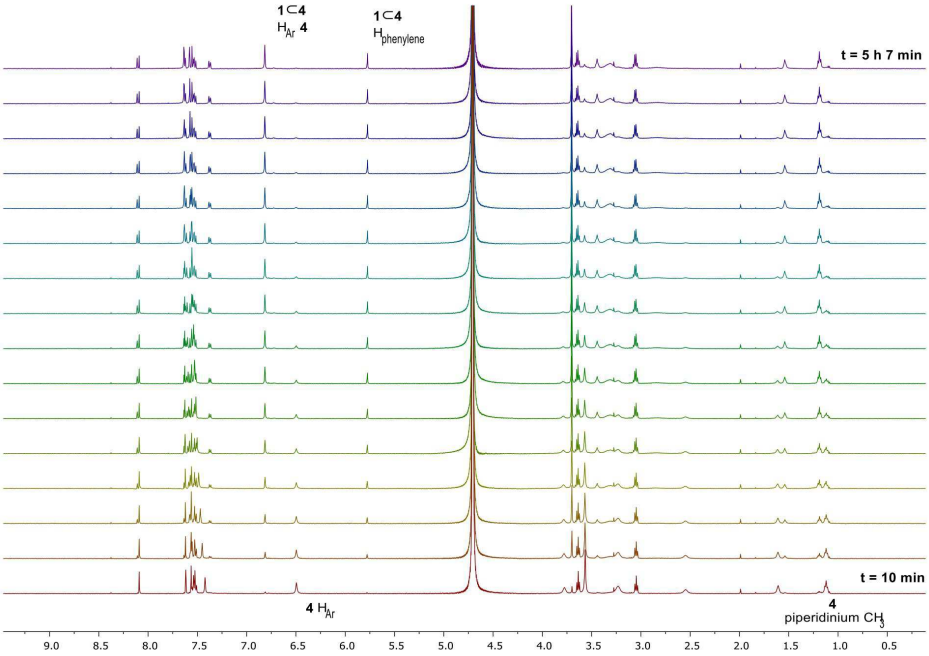

Figure SI 18. Arrayed full range ^{1}H-NMR spectra (500 MHz, D_2O, 298 K, 128 scans) of kinetic measurement with concentrations of 0.5 mM **1** and 0.25 mM **4**. Selection of every second spectrum up to 5 h 7 min. The resonances used for determination of *k* are labeled.

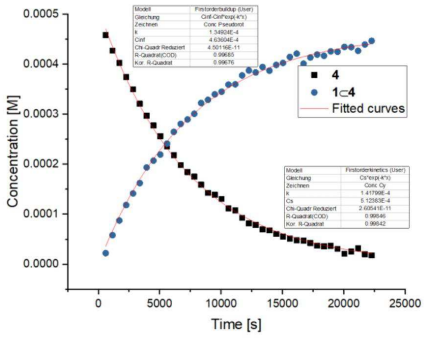

Figure SI 19. Formation of **1**⊂**4** and disappearance of **4** with corresponding curve fits. The data points were obtained by integration of the peaks indicated in the above NMR spectra. Formation of **1**⊂**4**$_2$ was prevented by using an excess of **1**, therefore, the concentration of **1**⊂**4** saturates close to the expected 0.5 mM.

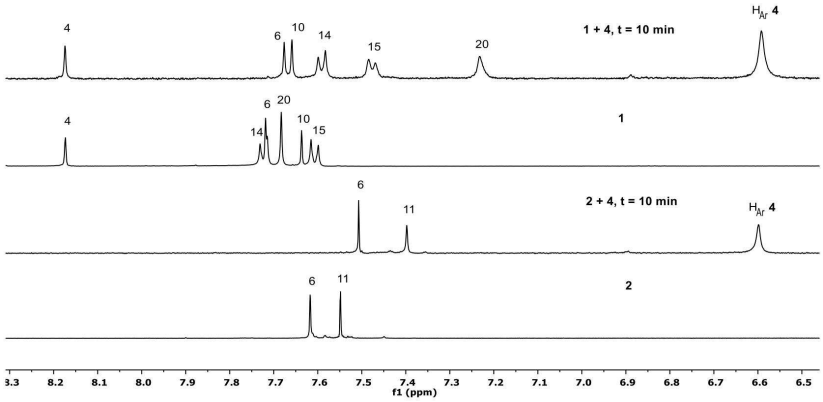

Figure SI 20. Aromatic region of ^{1}H-NMR spectra (500 MHz, D_2O, 298 K) of **1** (0.5 mM) and **2** (0.5 mM) before and 10 min after addition of **4** (0.5 mM). Numbering as in Figure SI 1 and 7.

Kinetic measurements of 2

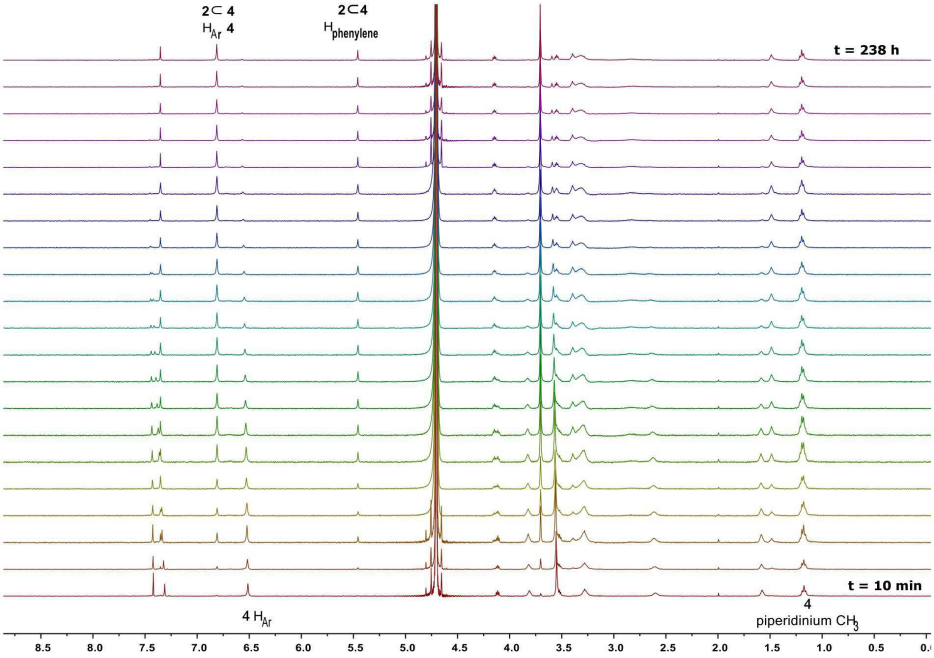

Figure SI 21. Arrayed ^{1}H-NMR spectra (400 MHz, D_2O, 298 K), full range. The resonances used for determination of *k* are labeled.

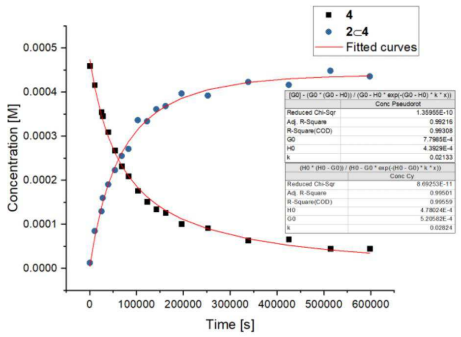

Figure SI 22. Formation of **2⊂4** and disappearance of **4** with corresponding curve fits. The data points were obtained by integration of the peaks indicated in the above NMR spectra.

References

[1] P. Xin, S. Tan, Y. Wang, Y. Sun, Y. Wang, Y. Xu, C.-P. Chen, *Chem. Commun.* **2017**, *53*, 625–628.
[2] M. Kim, J. A. Boissonnault, P. V. Dau, S. M. Cohen, *Angew. Chem. Int. Ed.* **2011**, *50*, 12193–12196.
[3] C. L. Perrin, *J. Chem. Educ.* **2017**, *94*, 669–672.

^{1}H-NMR spectrum of 2-Hydroxyisophthalic acid

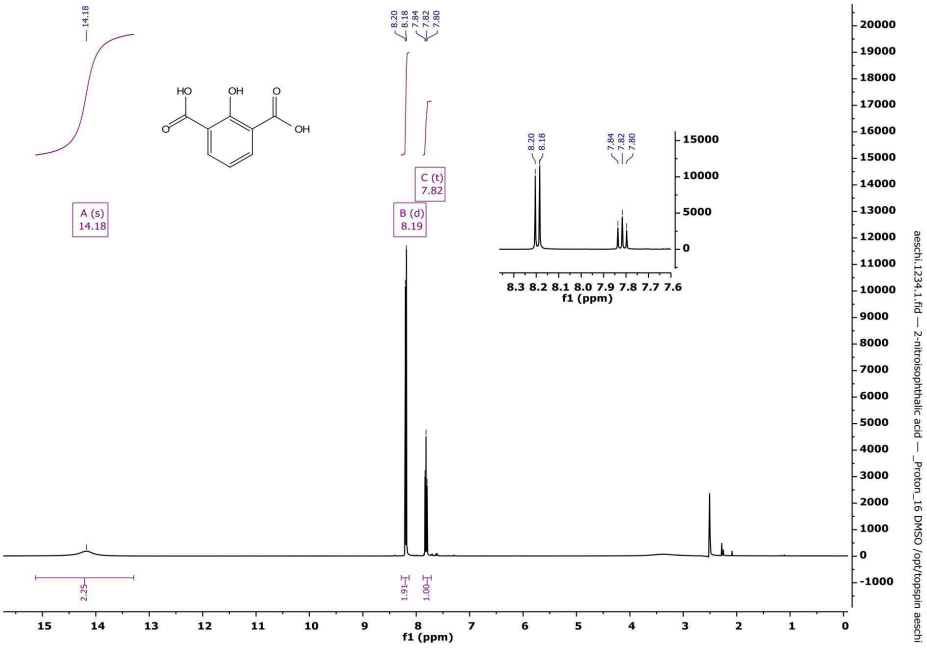

^{1}H-, ^{13}C-NMR 1D-spectra of 1:

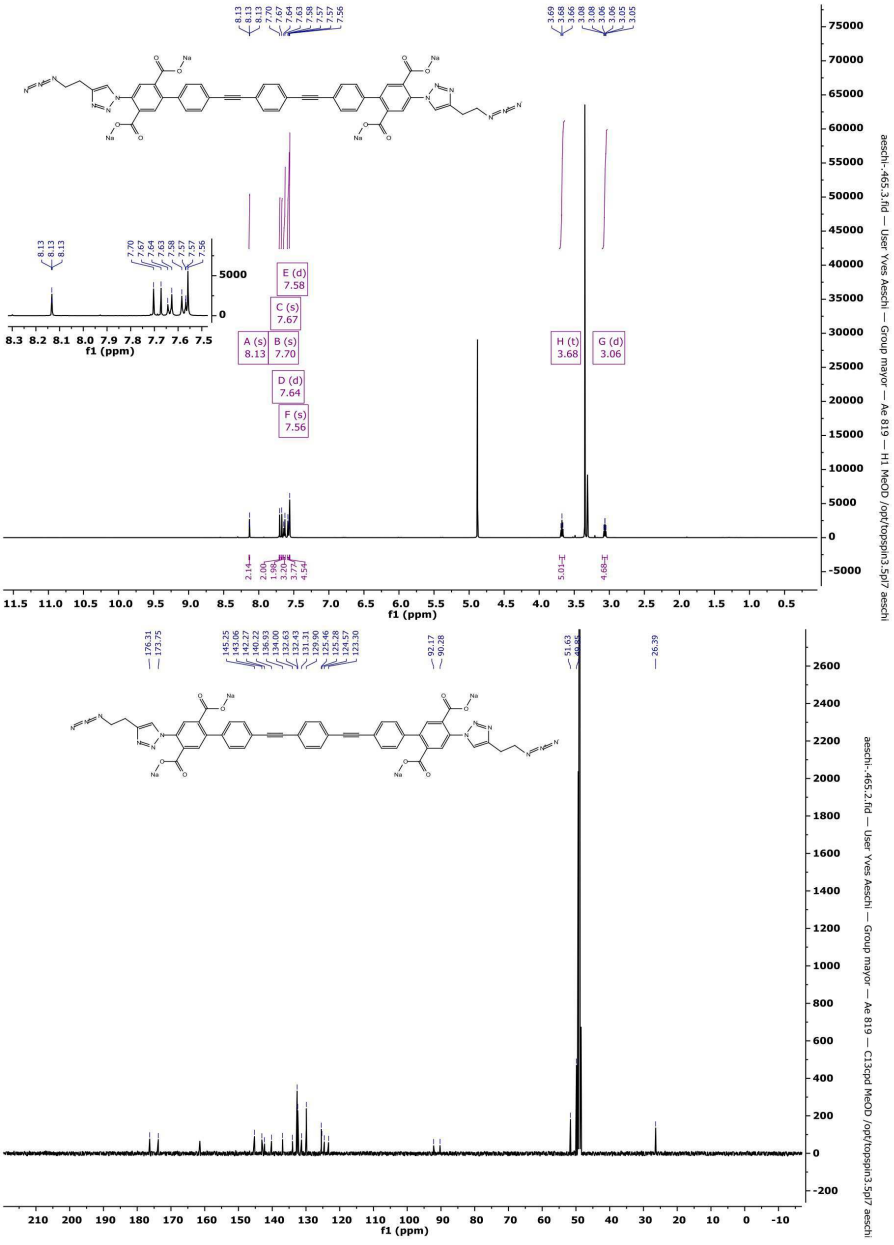

HMBC and HMQC spectra of 1:

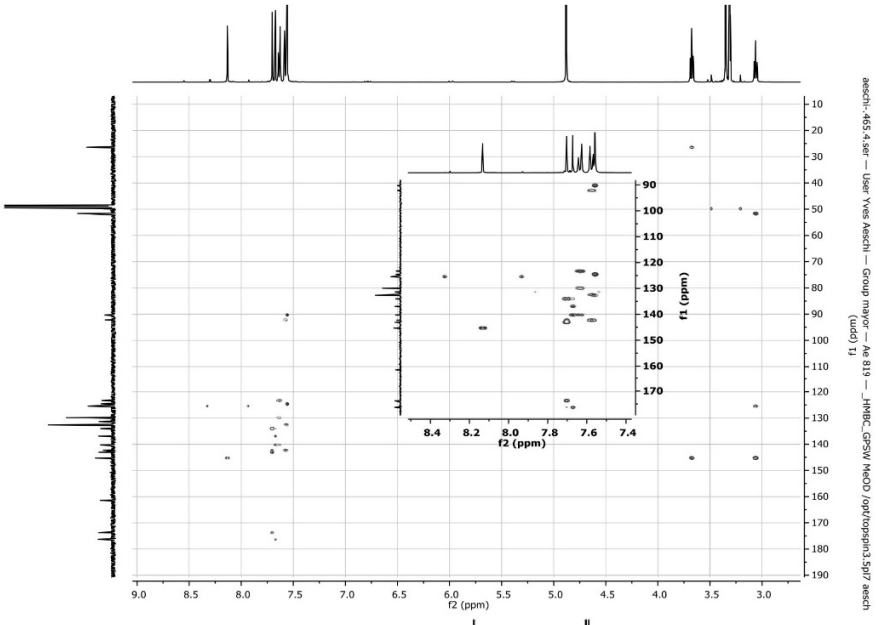

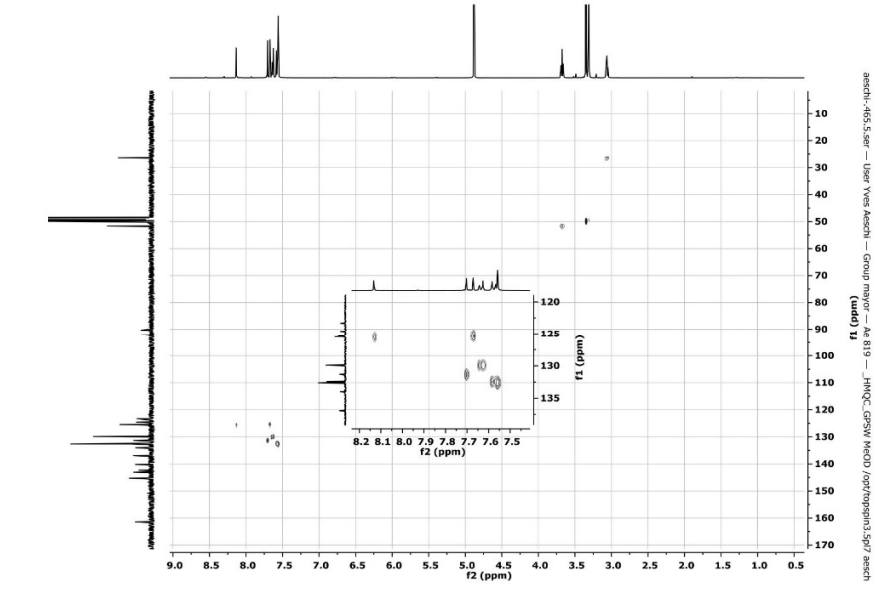

ESI-TOF HRMS of 1:

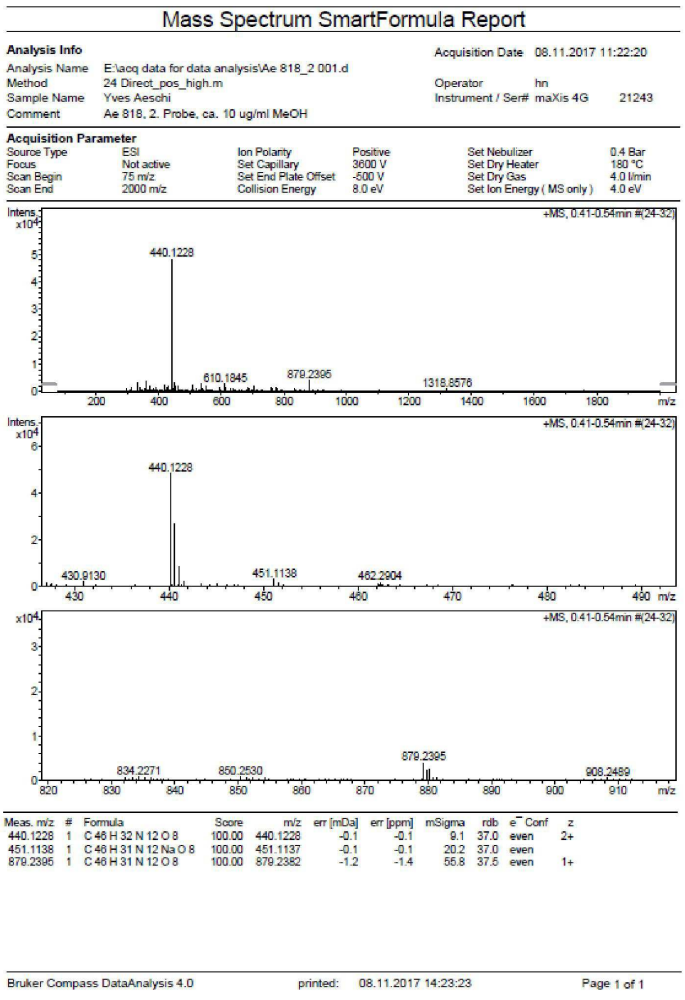

Mass Spectrum SmartFormula Report

Analysis Info

Analysis Name	E:\aoq data for data analysis\Ae 818_2 001.d	Acquisition Date	08.11.2017 11:22:20
Method	24 Direct_pos_high.m	Operator	hn
Sample Name	Yves Aeschi	Instrument / Ser#	maXis 4G 21243
Comment	Ae 818, 2. Probe, ca. 10 ug/ml MeOH		

Acquisition Parameter

Source Type	ESI	Ion Polarity	Positive	Set Nebulizer	0.4 Bar
Focus	Not active	Set Capillary	3600 V	Set Dry Heater	180 °C
Scan Begin	75 m/z	Set End Plate Offset	-500 V	Set Dry Gas	4.0 l/min
Scan End	2000 m/z	Collision Energy	8.0 eV	Set Ion Energy (MS only)	4.0 eV

Meas. m/z	#	Formula	Score	m/z	err [mDa]	err [ppm]	mSigma	rdb	e⁻ Conf	z
440.1228	1	C 46 H 32 N 12 O 8	100.00	440.1228	-0.1	-0.1	9.1	37.0	even	2+
451.1138	1	C 46 H 31 N 12 Na O 8	100.00	451.1137	-0.1	-0.1	20.2	37.0	even	
879.2395	1	C 46 H 31 N 12 O 8	100.00	879.2382	-1.2	-1.4	55.8	37.5	even	1+

Bruker Compass DataAnalysis 4.0 printed: 08.11.2017 14:23:23 Page 1 of 1

^{1}H-, ^{13}C-NMR 1D spectra of 2:

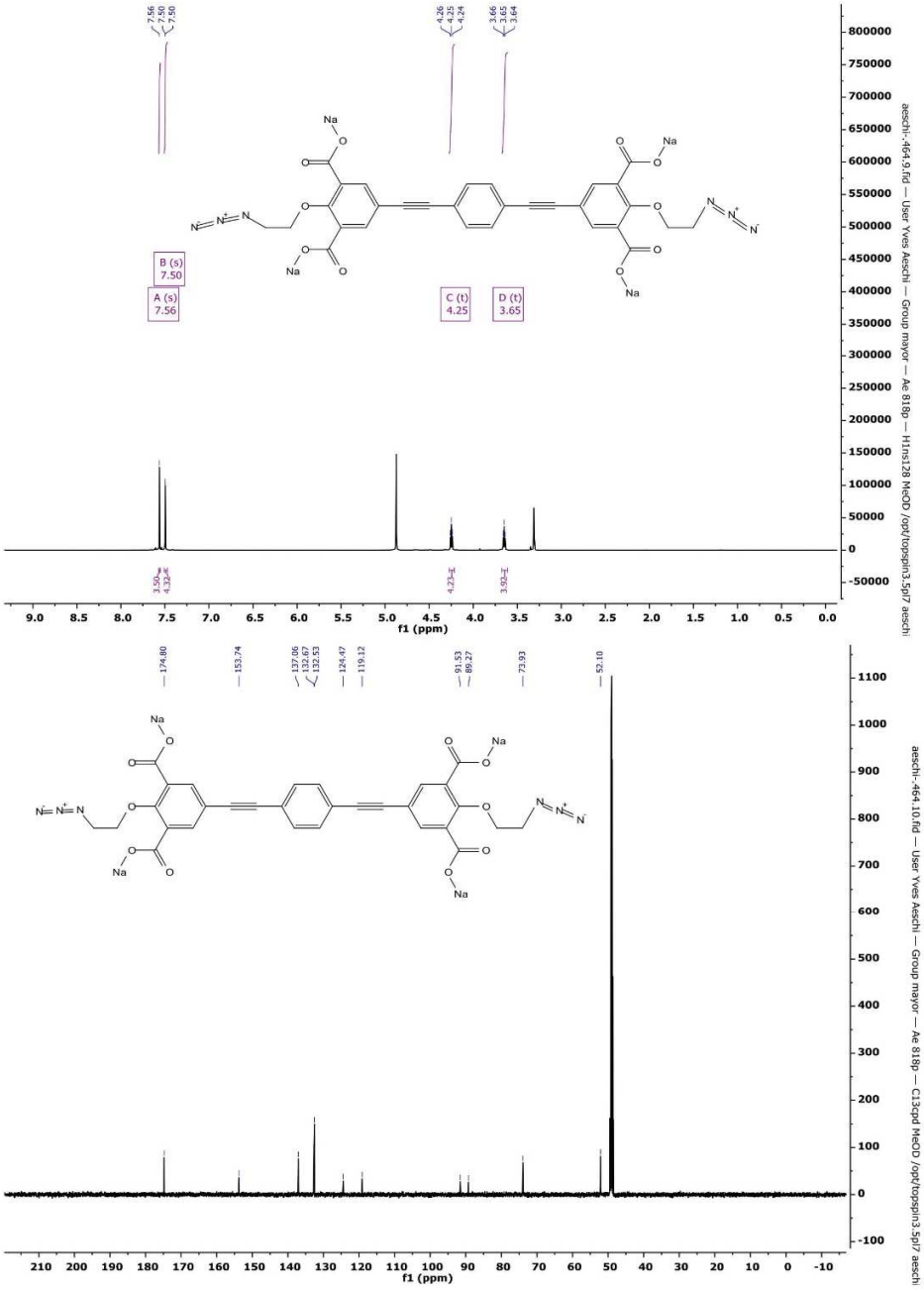

HMBC and HMQC spectra of 2:

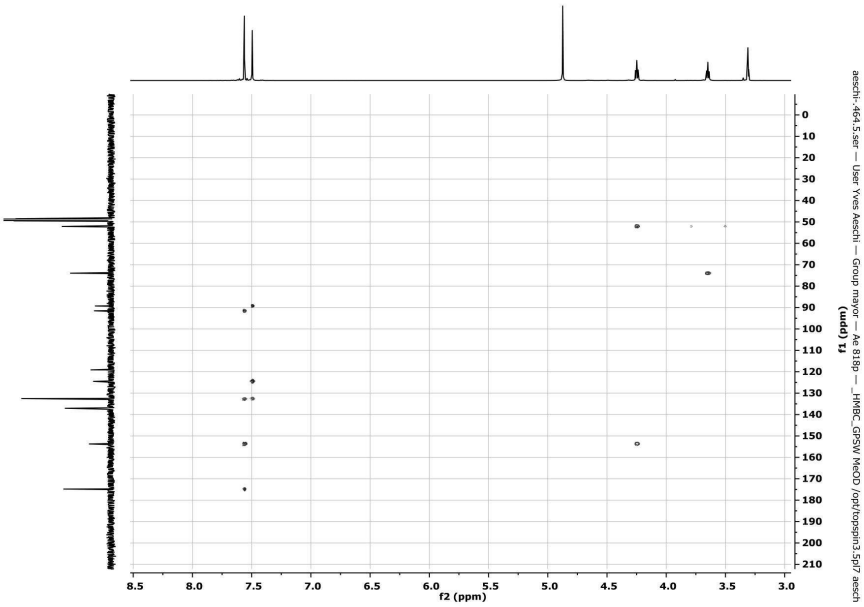

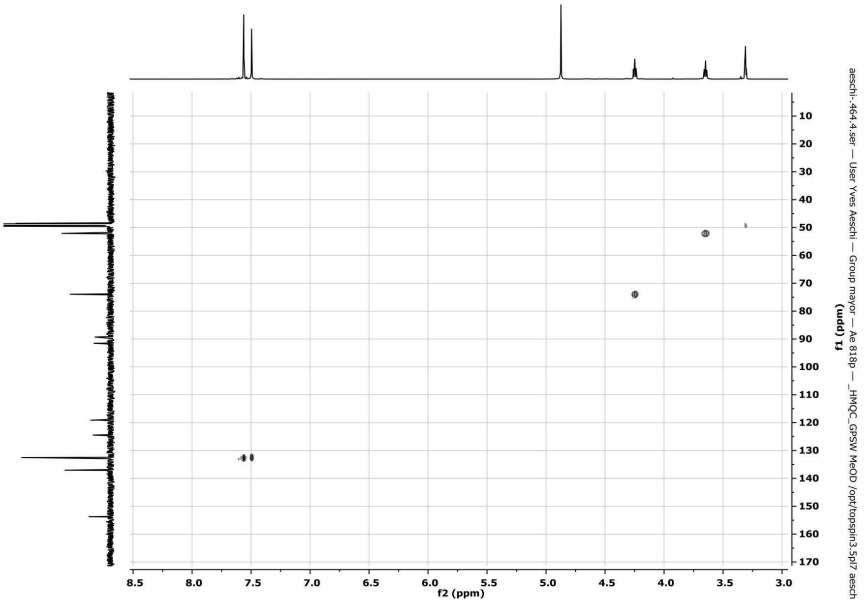

ESI-TOF HRMS of 2:

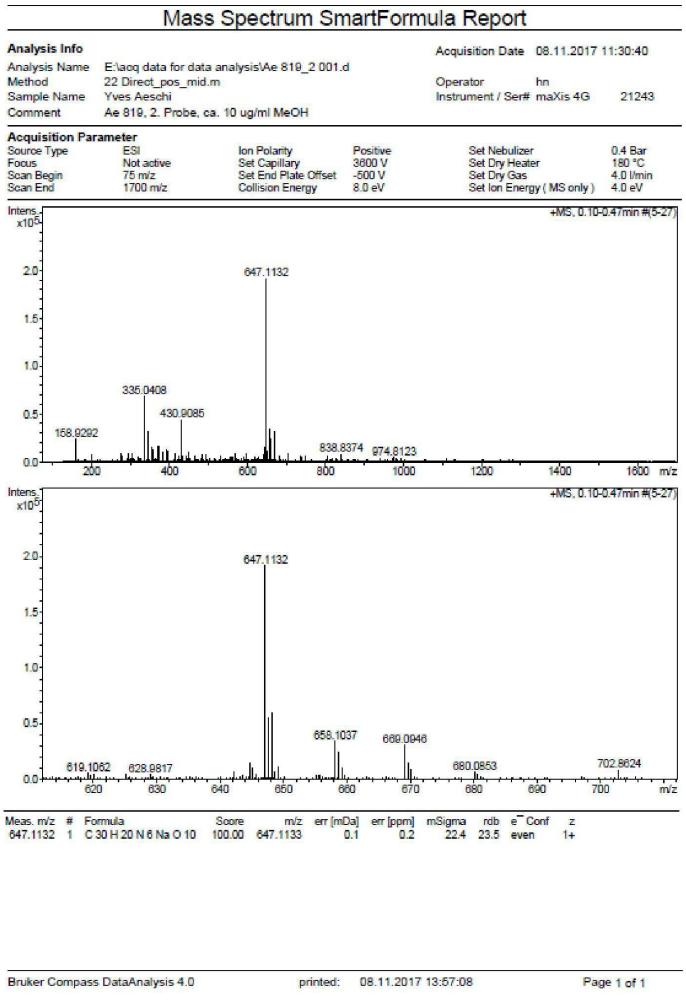

Mass Spectrum SmartFormula Report

Analysis Info

Analysis Name	E:\aoq data for data analysis\Ae 819_2 001.d	Acquisition Date	08.11.2017 11:30:40
Method	22 Direct_pos_mid.m	Operator	hn
Sample Name	Yves Aeschi	Instrument / Ser#	maXis 4G 21243
Comment	Ae 819, 2. Probe, ca. 10 ug/ml MeOH		

Acquisition Parameter

Source Type	ESI	Ion Polarity	Positive	Set Nebulizer	0.4 Bar
Focus	Not active	Set Capillary	3600 V	Set Dry Heater	180 °C
Scan Begin	75 m/z	Set End Plate Offset	-500 V	Set Dry Gas	4.0 l/min
Scan End	1700 m/z	Collision Energy	8.0 eV	Set Ion Energy (MS only)	4.0 eV

Meas. m/z	#	Formula	Score	m/z	err [mDa]	err [ppm]	mSigma	rdb	e⁻ Conf	z
647.1132	1	C 30 H 20 N 6 Na O 10	100.00	647.1133	0.1	0.2	22.4	23.5	even	1+

Bruker Compass DataAnalysis 4.0 printed: 08.11.2017 13:57:08 Page 1 of 1

^{1}H-NMR spectrum of 5:

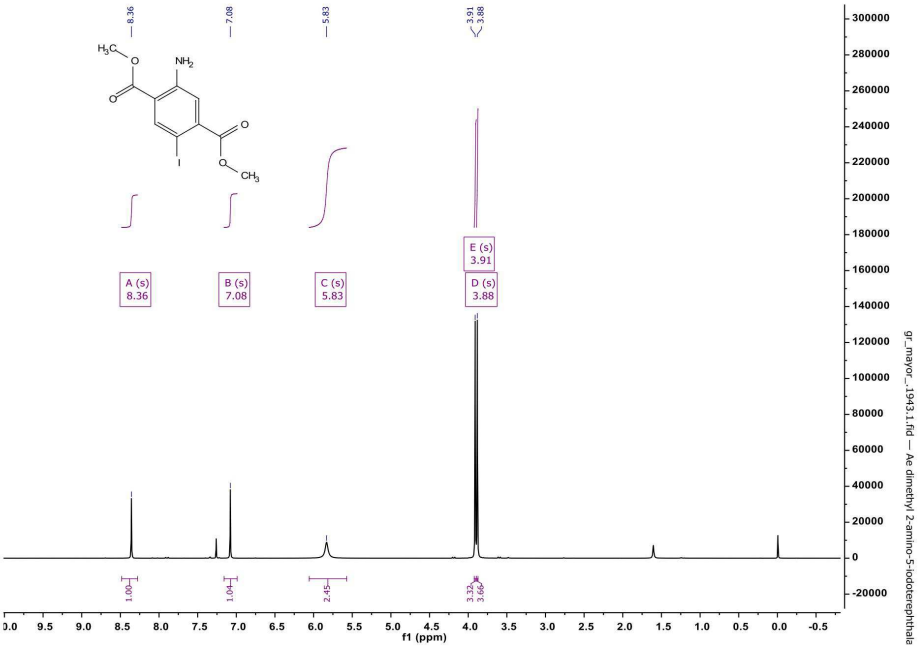

^{1}H-, ^{13}C-NMR spectra of 6:

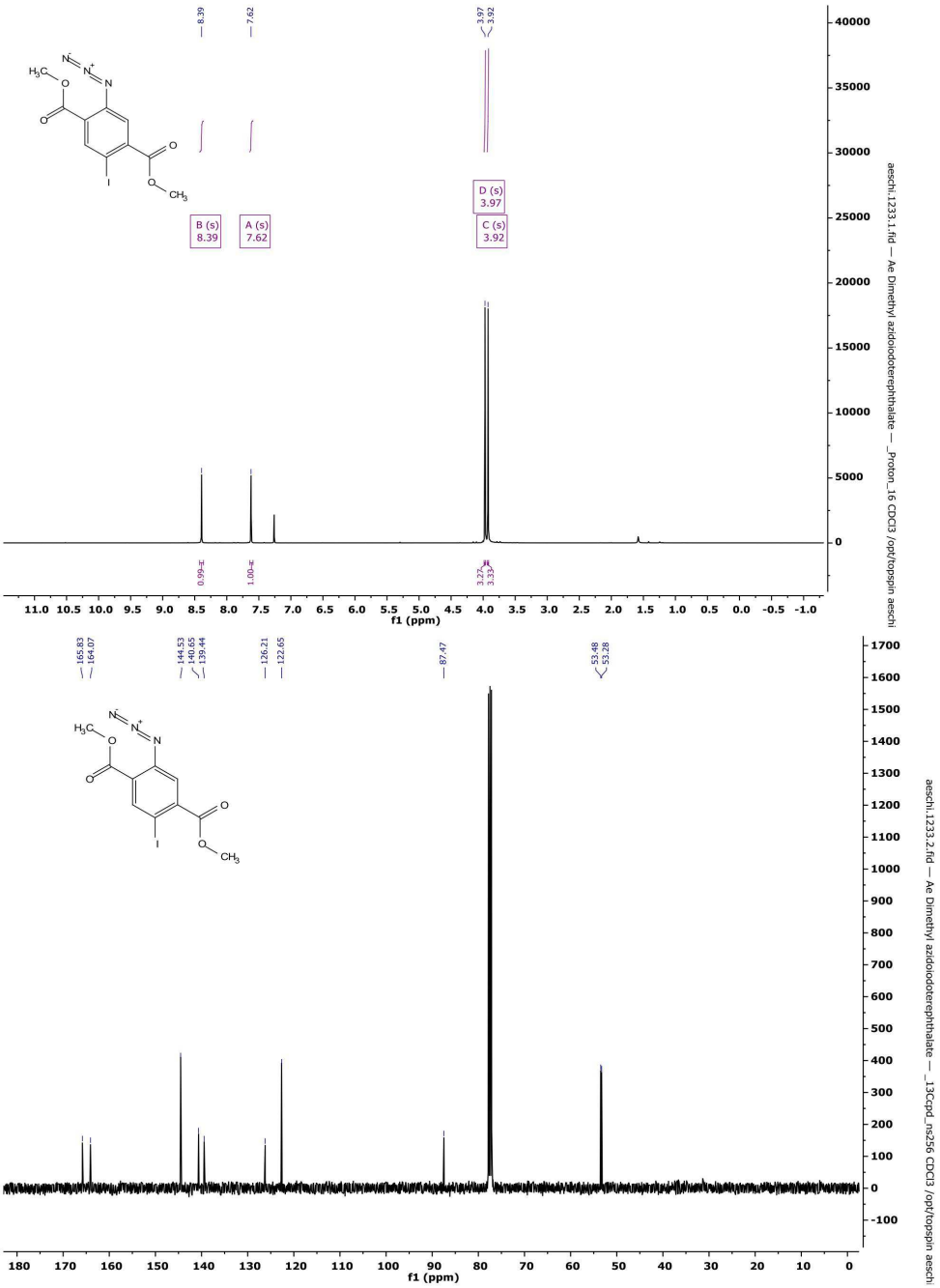

CHEMISTRY
A European Journal

Supporting Information

Aqueous Assembly of Zwitterionic Daisy Chains

Yves Aeschi,[a, b] Sylvie Drayss-Orth,[a] Michal Valášek,[c] Daniel Häussinger,[a] and Marcel Mayor*[a, b, c, d]

chem_201803944_sm_miscellaneous_information.pdf

^{1}H-, ^{13}C-NMR spectra of 7:

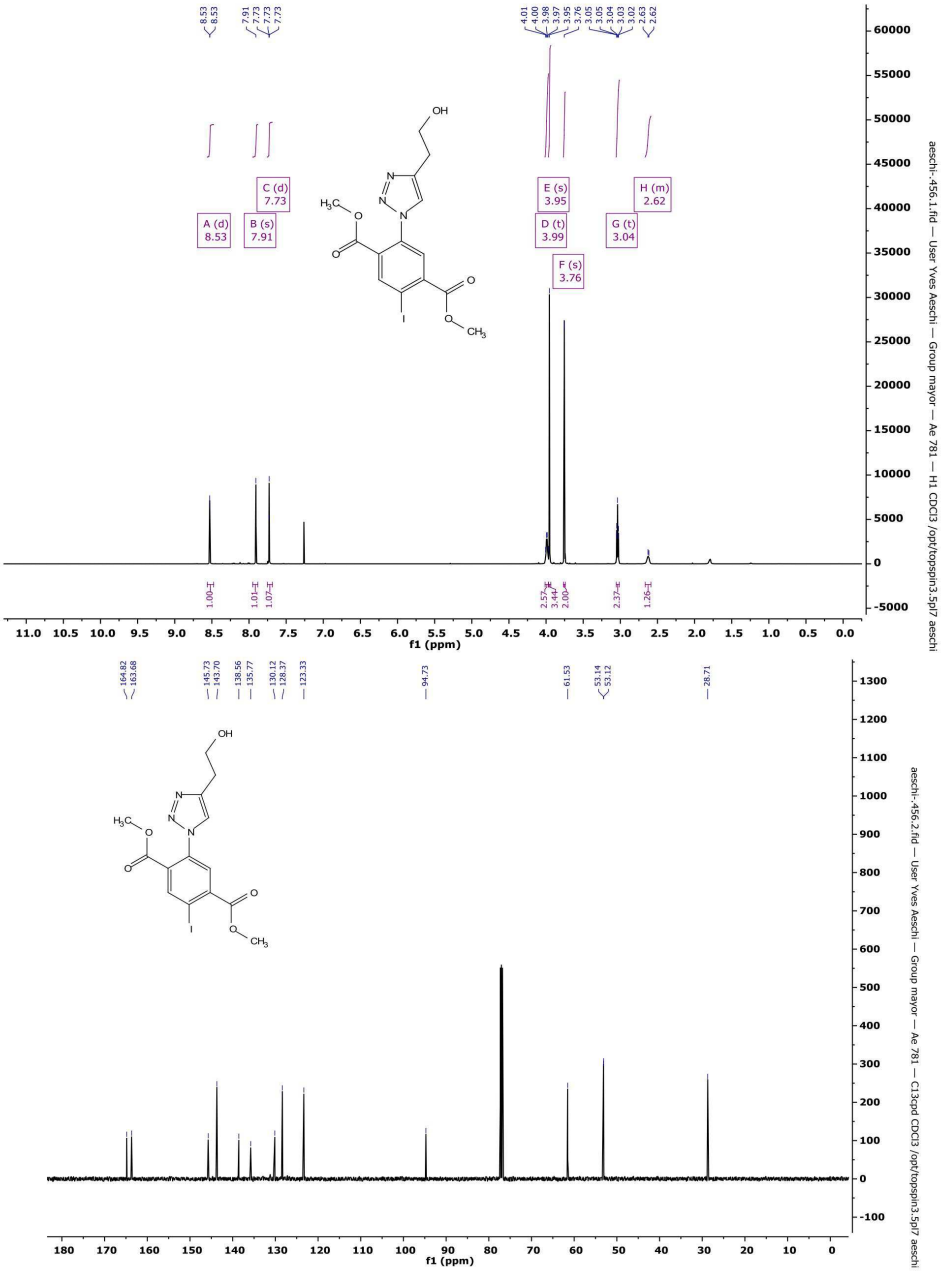

^{1}H-, ^{13}C-NMR spectra of 8:

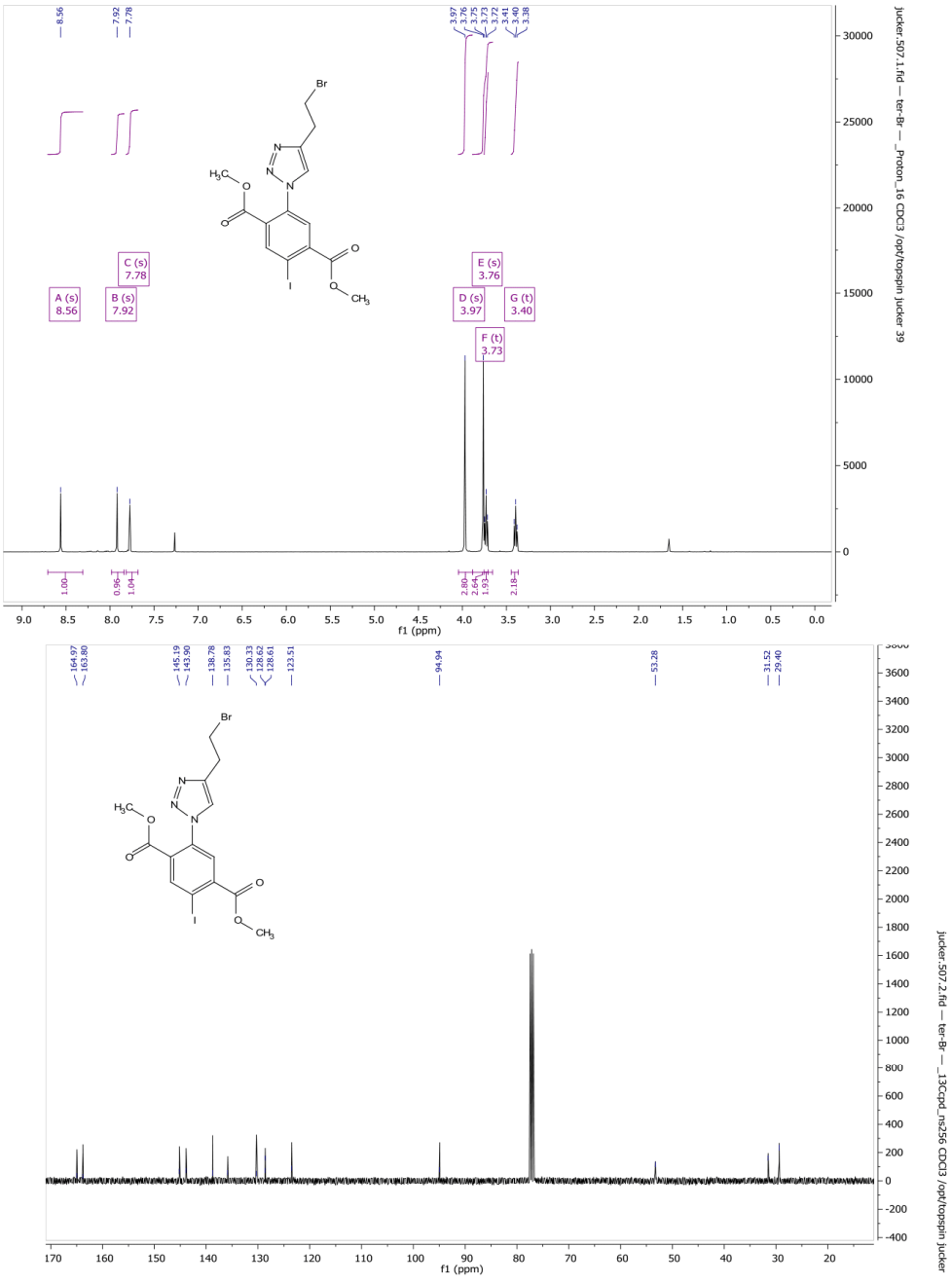

^{1}H-, ^{13}C-NMR spectra of 9:

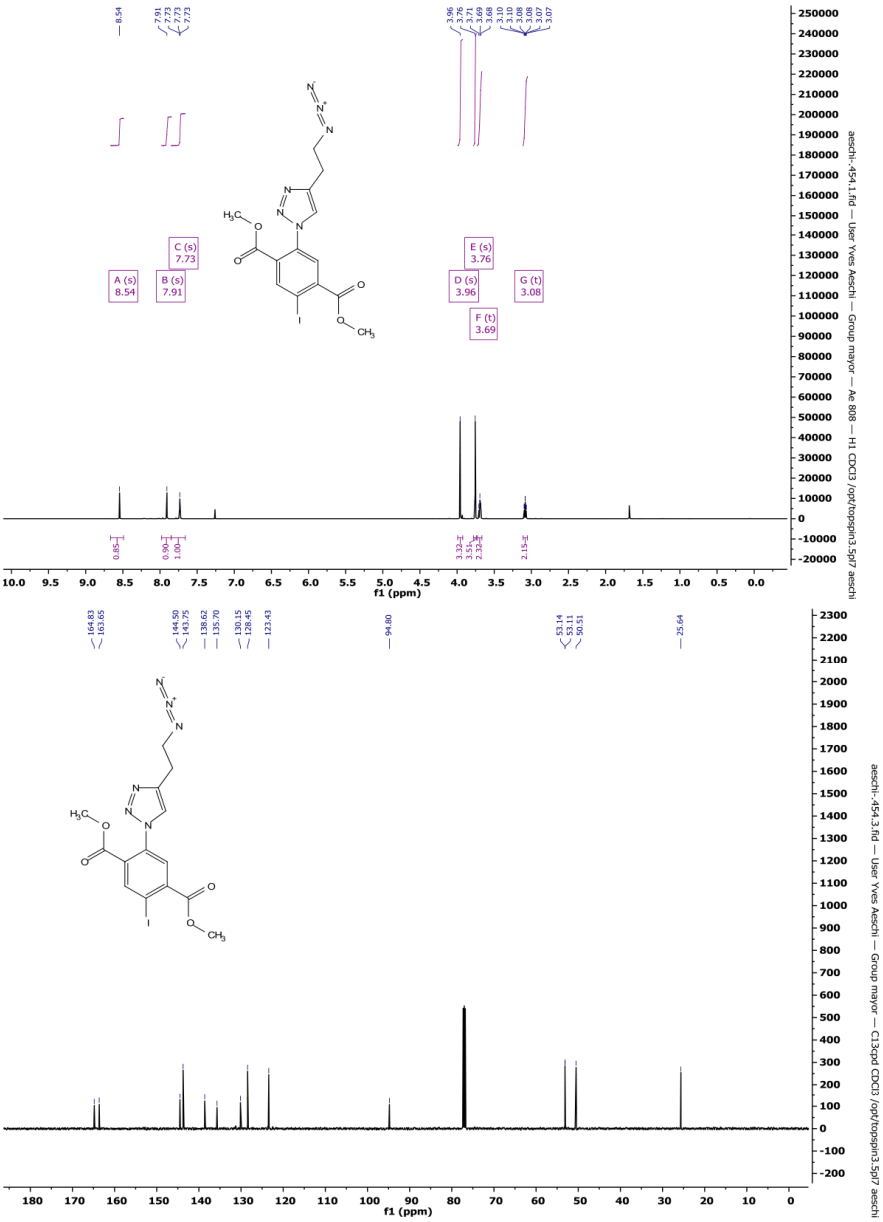

^{1}H-, ^{13}C-NMR spectra of 10:

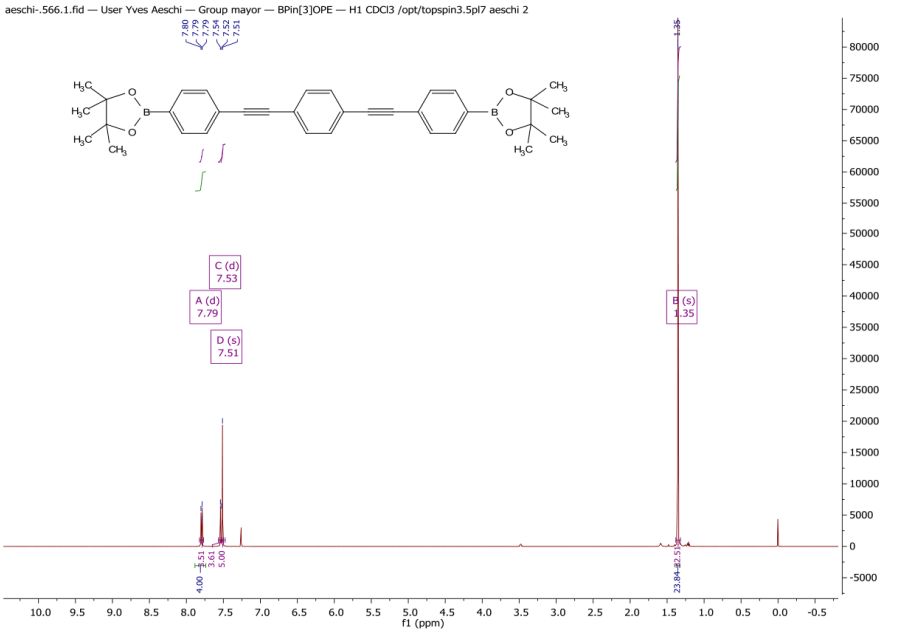

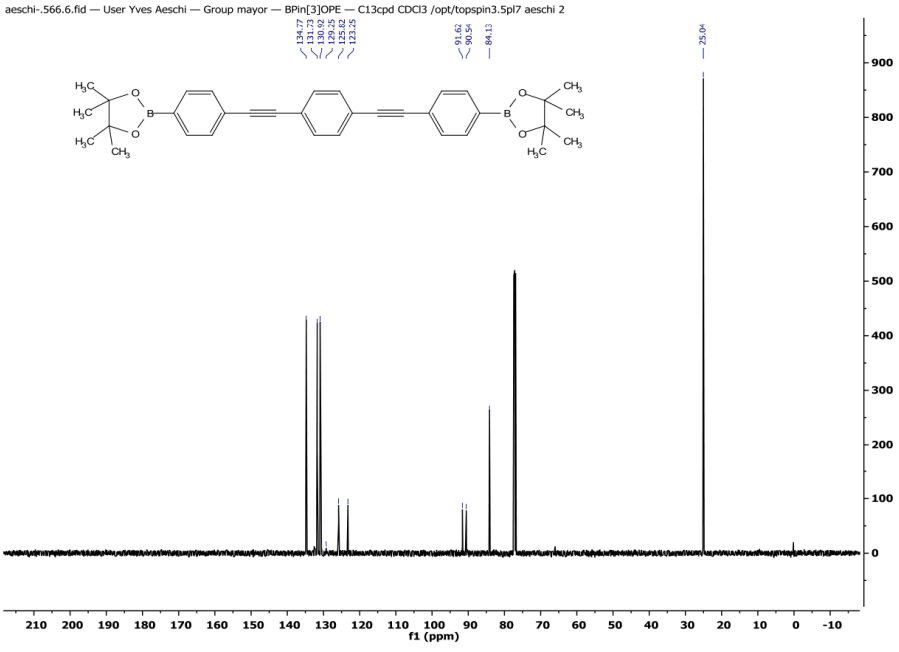

HMBC spectrum of 10:

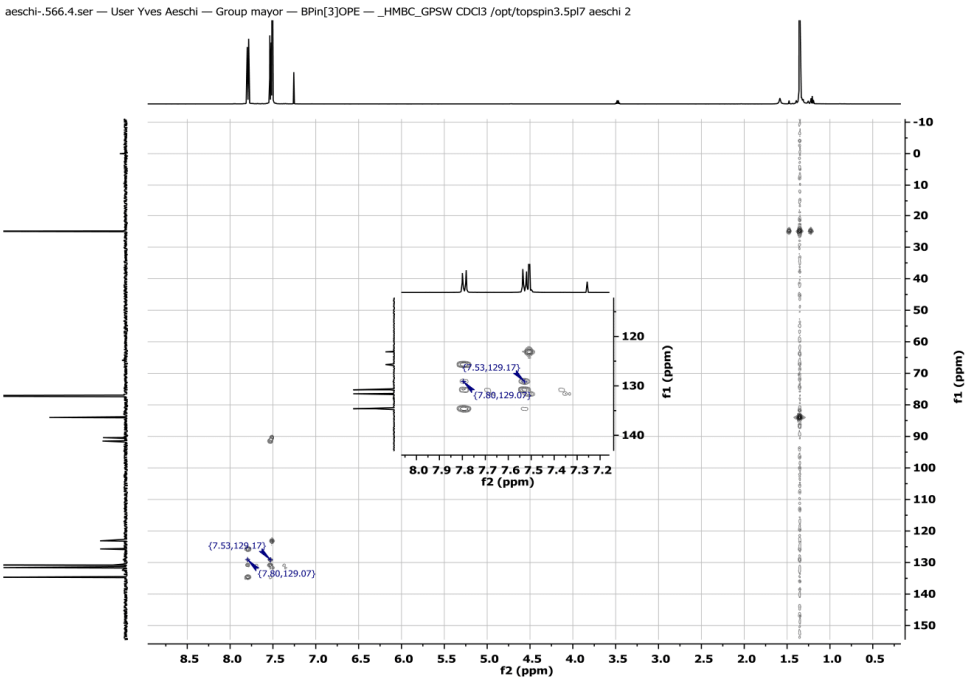

^{1}H-, ^{13}C-NMR spectra of 11:

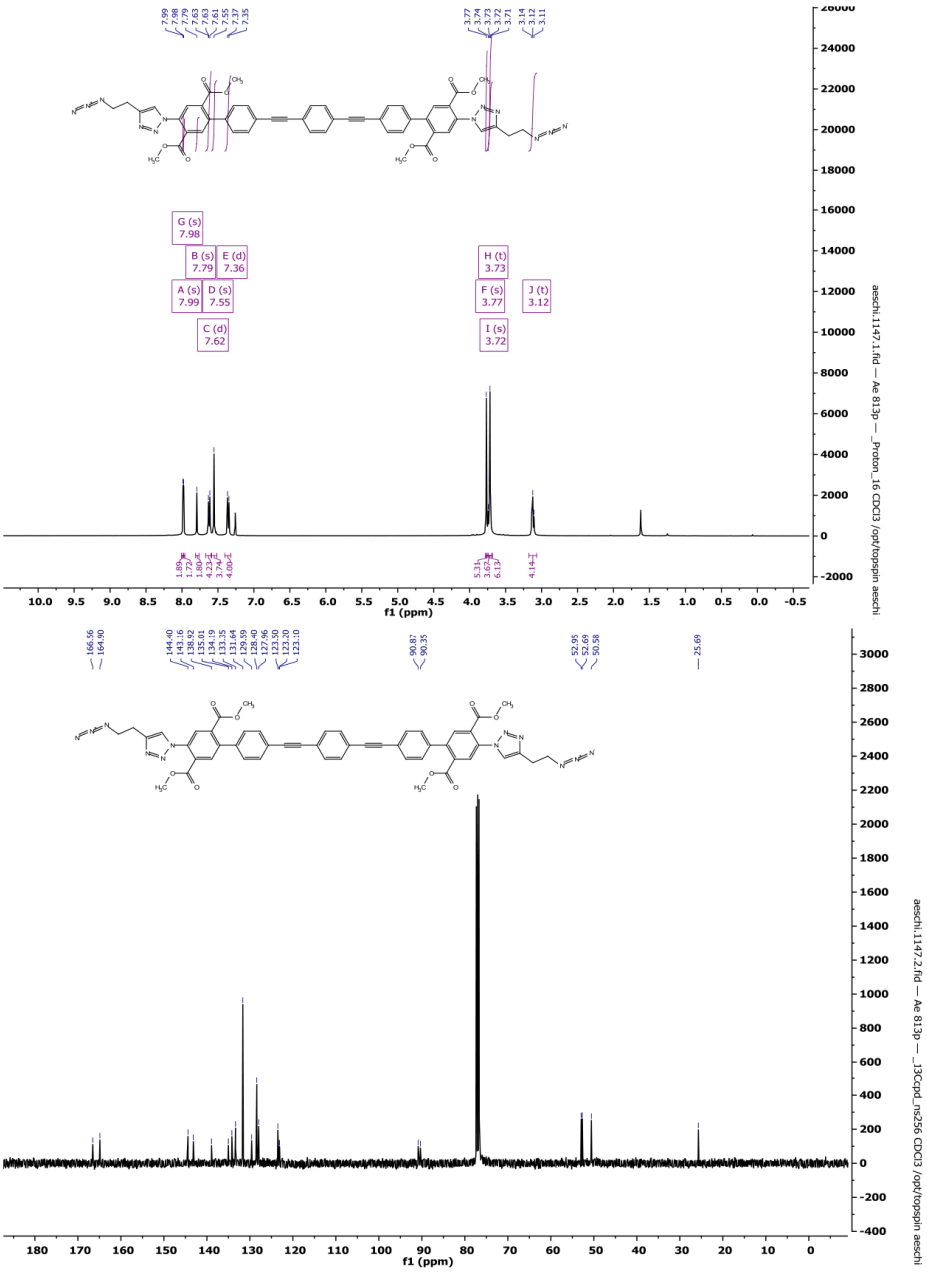

^{1}H-, ^{13}C-NMR spectra of Dimethyl-2-hydroxy-5-iodoisophthalate (12):

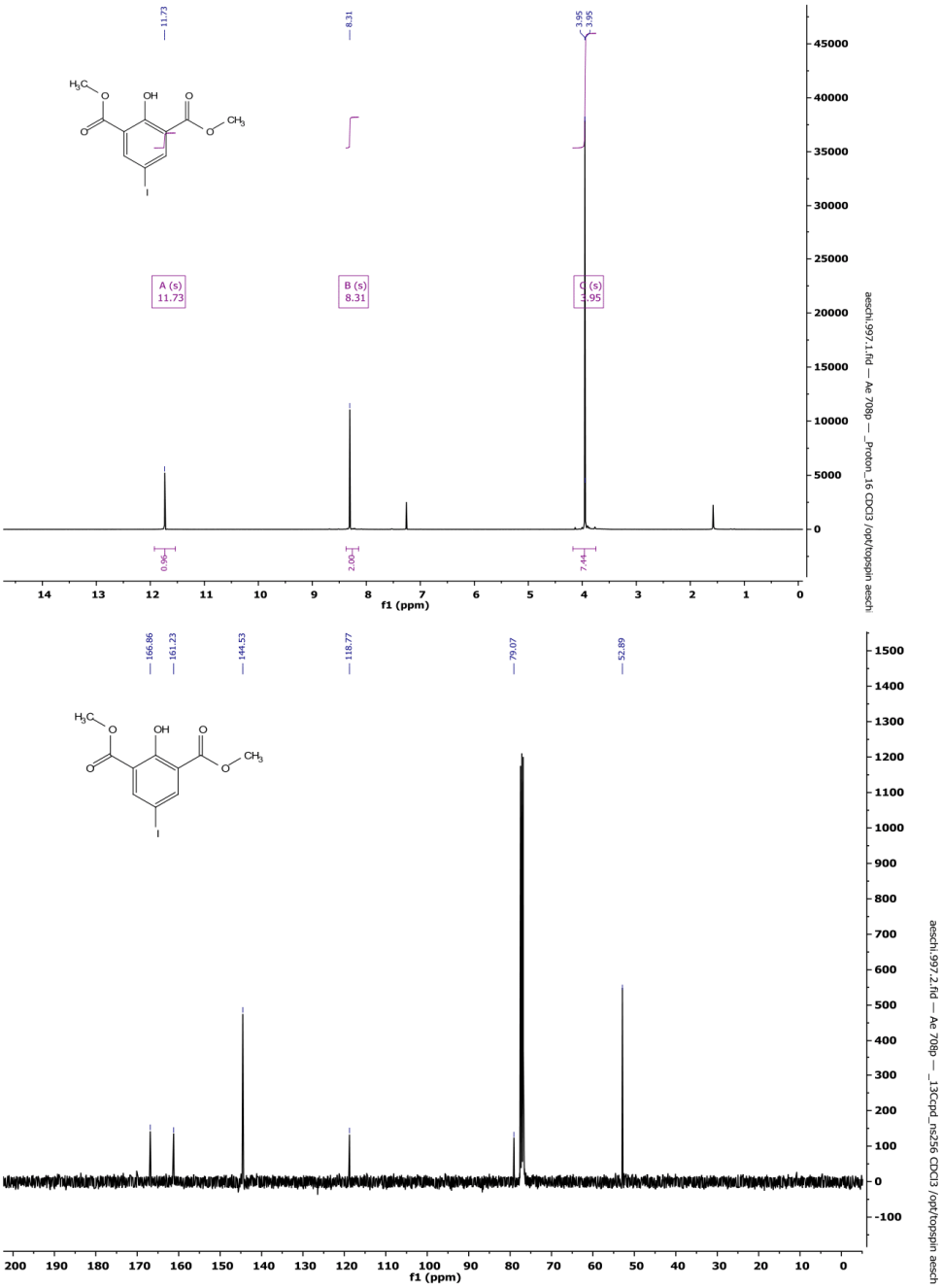

^{1}H-, ^{13}C-NMR spectra of 13:

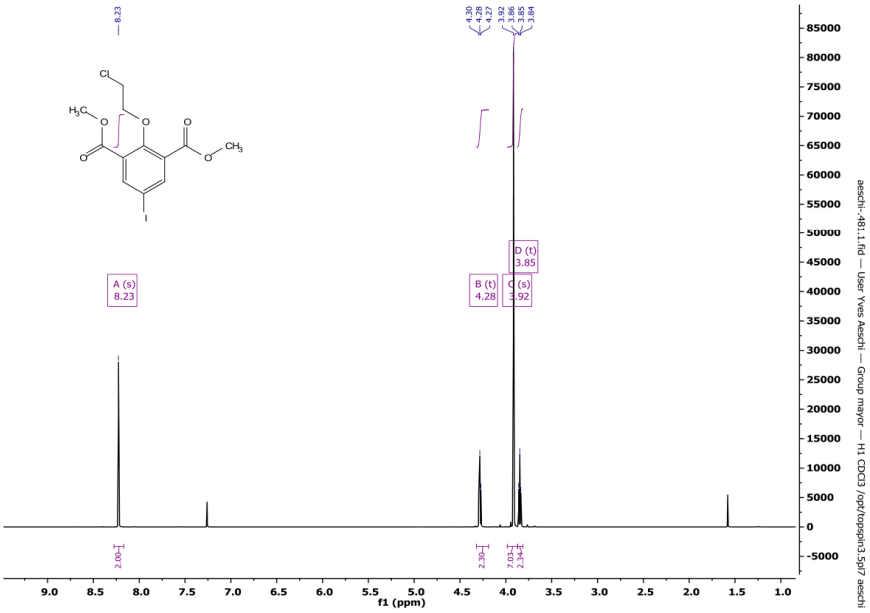

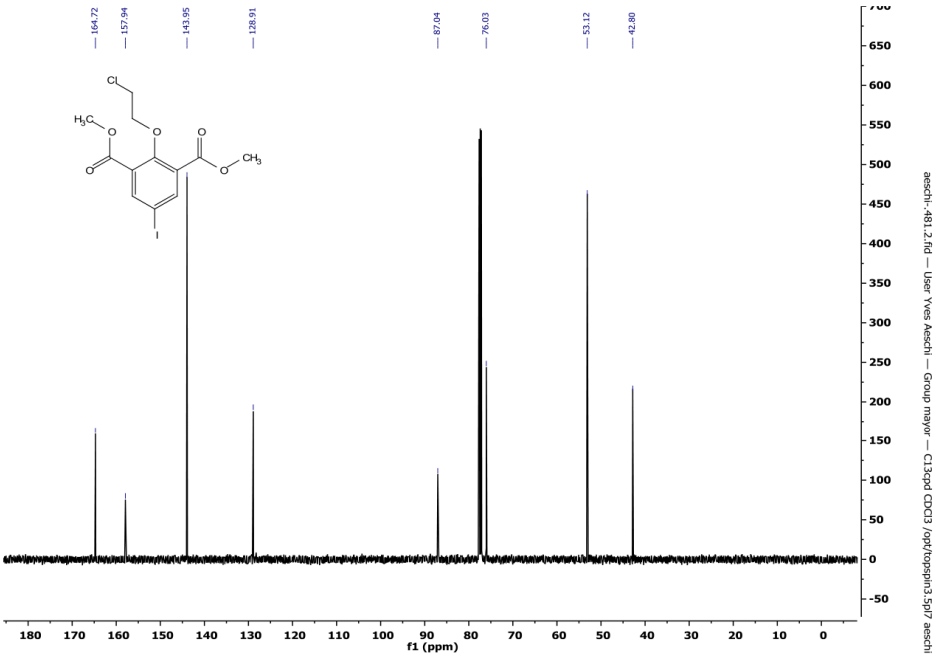

^{1}H-, ^{13}C-NMR spectra of 14:

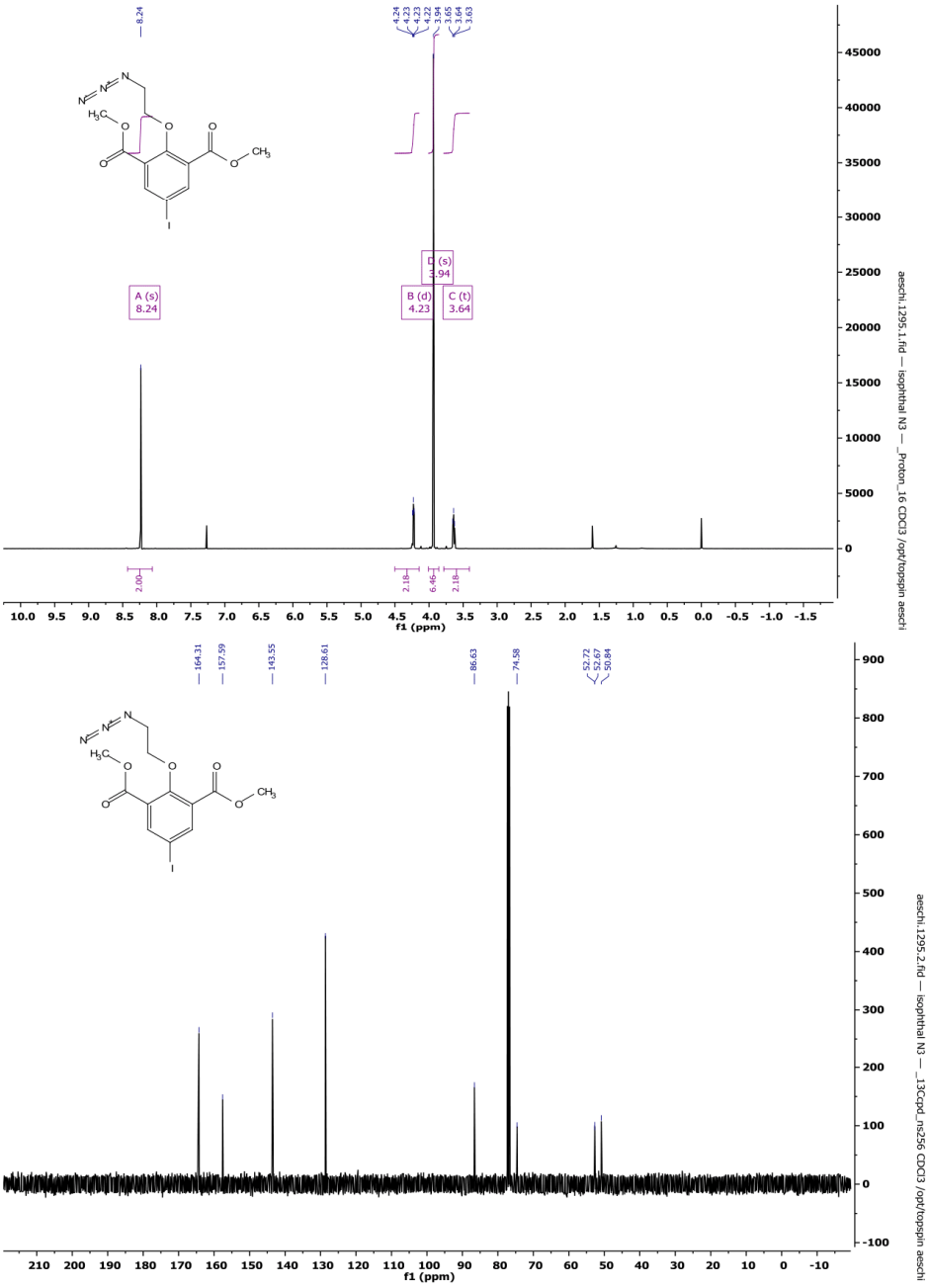

^{1}H-, ^{13}C-NMR spectra of 15:

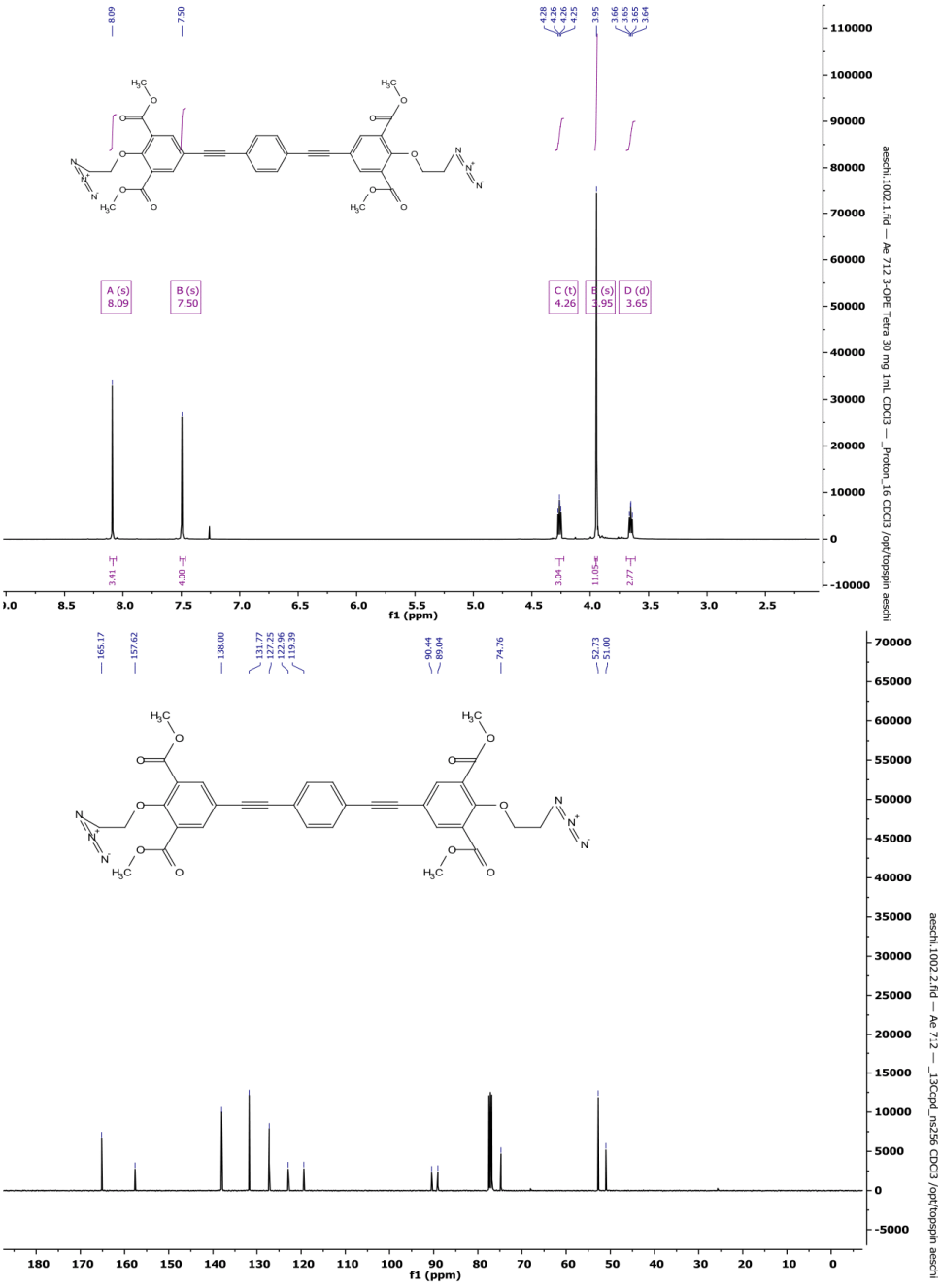

Outlook: Towards Kinetically Controlled Assembly of Molecular Daisy Chains

In the work of the preceding chapters, rotaxanes and daisy chains based on *Diederich*-type cyclophanes and hydrophobic guests have been synthesized and fully characterized. By combining a hydrophobic driving force with ion-pairing effects, pseudorotaxane association constants larger than 10^6 M^{-1} have been achieved in water. Additionally, association proved to be thermally robust. Furthermore, the possibility of controlling the association strength and also association kinetics was shown.

The combination of a kinetic brake for complexation and high association strength could, in principle, be combined in daisy chains with kinetically controllable association modes. In an ideal case, such an idea could translate to a daisy chain monomer, which assembles to polymeric daisy chains at room temperature, but equilibrates to [*c*2]daisy chains within longer reaction times or upon heating (Figure 1). The formation of acyclic daisy chains (or oligomeric cycles with more than two subunits) can occur in a step-wise assembly. Each step can be expected to require a similar amount of activation energy. However, if a daisy chain monomer is designed with axial rigidity, the formation of a cyclic dimer requires a simultaneous threading of two pseudo-stoppers. This results in a higher activation energy requirement for [*c*2]daisy chain formation, which could be overcome by heating. The formation of daisy chains has an inherent entropic penalty due the loss of translational and conformational degrees of freedom. This must be compensated for by strongly binding recognition motifs as otherwise, self-assembly to daisy chains will be thermodynamically disrupted at elevated temperatures. The hydrophobic/ion pair recognition motif developed in this work seems ideal for such a purpose since it is a good basis for thermally robust host-guest complexes.

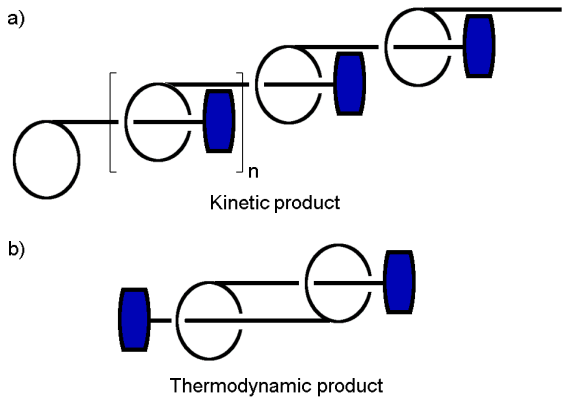

Figure 1. a) Representation of [*a*n]daisy chains which could be obtained in a kinetically controlled reaction b) [*c*2]daisy chains which could be obtained after thermal equilibration. The blue stopper unit represents merely a pseudo-stopper which still allows for slow exchange dynamics.

A possible daisy chain design relying on these findings is presented in Scheme 1. It relies on a spiro-functionalized *Diederich*-type cyclophane with a rigidly attached OPE rod. The target structure is axially rigid as proposed before, although a rotation about the C-C bond of the diphenylmethane-triazole linkage is still possible. The desired precursor **1** could be assembled in a CuAAC reaction from building blocks **2** and **3** followed by three additional synthetic steps: 1) Alkylation of the triazole moiety, 2) Saponification of the methyl esters, 3) Introduction of the azide group. The terminal azide is not essential to probe the functionality of this molecule. However, the introduction of positive/negative charges is required in order to profit from ion pairing effects. Synthetic efforts to yield cyclophane **2** were successful (scheme 2), however further synthetic investigations towards the assembly of **1** are still required.

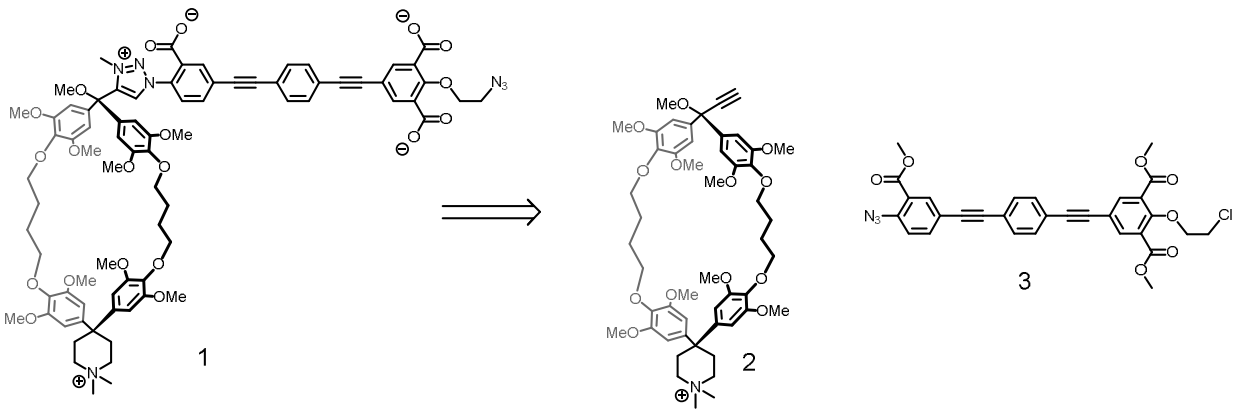

Scheme 1. A possible structure of a heteroditopic monomer **1** which could allow for kinetically controlled daisy chain assembly. Such a structure can be assembled from cyclophane **2** and azide-functionalized OPE rods such as **3**. The synthesis of **2** was established in few steps.

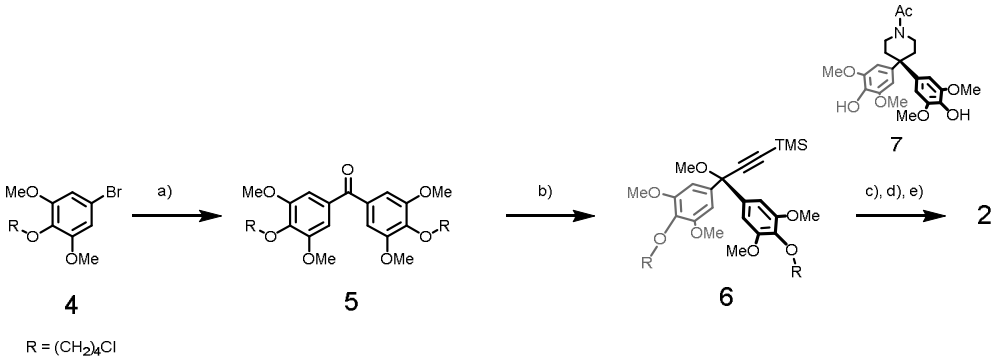

Scheme 2. Synthesis of **2**. a) n-BuLi, THF, -78 °C, then N,N-dimethylcarbamoyl chloride, 64 %; b) Li-TMSA, THF, -78 °C to r.t., MeI; 99%; c) **7**, Cs_2CO_3, DMF, 44 % of **8**; d) NaOH, EtOH, reflux, 84 % of **9**; e) MeI, CH_3CN, K_2CO_3, then KPF_6, H_2O, 98 %.

The synthesis (Scheme 2) starts by lithiation of **4** in THF solution followed by nucleophilic addition of N,N-dimethylcarbamoyl chloride, affording benzophenone **5** in 64 % yield. Trimethylsilyl acetylide was added to the carbonyl group by nucleophilic addition. Subsequent methylation of the tertiary hydroxyl group gave **6** in an excellent yield of 99 %. The methylation was necessary to avoid elimination of the acetylene in the following cyclization step, similar to the deprotection of an acetylenic 2-hydroxypropyl group. Cyclization of **6** and bisphenol **7** afforded the macrocycle **8** in 44 % yield. Deacetylation gave piperdine **9** in 85 % yield. Subsequent alkylation with iodomethane and final ion exchange to the hexafluorophosphate anion afforded the acetylene-functionalized cyclophane **2** in 98 % yield.

Experimental

Compound 5

In a two-necked flask, **3** (16.9 g, 52.2 mmol, 2 eq.) was placed and set under inert atmosphere by flushing with argon for 10 minutes. Then **4** was dissolved in 110 ml dry, previously degassed THF before being cooled to -78 °C in an acetone/dry ice bath. Under vigorous stirring, 33.0 ml of 1.6 M *n*-BuLi in hexanes (52.8 mmol, 2 eq.) was slowly added followed by stirring for 1 h. The reaction was allowed to reach -40 °C in an acetonitrile/dry ice bath before 2.4 ml of N,N-dimethylcarbamoyl chloride (2.81 g, 26.0 mmol, 1 eq.) were slowly added. The cooling bath was removed and the mixture was stirred for 20 minutes. 100 ml of saturated aqueous $NaHCO_3$ solution were added. The organic layer was removed and the aqueous phase was extracted with TBME (100 mL) and the combined organic phases were dried over Na_2SO_4. After removal of the solvents, the crude mixture was purified by column chromatography (silica gel, cyclohexane/TBME 2:1). After evaporation of the organic solvents, **5** was obtained as a white solid (8.60 g, 64 %).

^{1}H NMR (400 MHz, $CDCl_3$) δ 7.06 (s, 4H), 4.10 (t, *J* = 6.1 Hz, 4H), 3.86 (s, 12H), 3.66 (t, *J* = 6.6 Hz, 4H), 2.12 – 1.99 (m, 4H), 1.92 (dq, *J* = 8.9, 6.3 Hz, 4H).

^{13}C NMR (101 MHz, $CDCl_3$) δ 194.9, 153.2, 141.1, 132.9, 107.7, 72.6, 56.4, 45.0, 29.3, 27.6.

MS (ESI +, m/z): found 515.1, calcd. 515.2 $[M + H]^+$

Compound 6

An oven-dried flask was set under inert atmosphere by three vacuum/argon refilling cycles. Then 35 ml of dry THF were added followed by ethynyltrimethylsilane (4.10 ml, 29.0 mmol, 2.1 eq.). It was cooled to -78 °C in an acetone/dry ice bath. 17.0 ml of *n*-BuLi 1.6 M in hexanes (27.2 mmol, 2 eq.) were added and the cooling bath was removed after 30 minutes to allow the mixture to reach room temperature.

In another oven-dried, two-necked flask, **5** (7.00 g, 13.6 mmol, 1 eq.) was placed and set under inert atmosphere by three vacuum/argon refilling cycles. Then the white solid was dissolved in 90 ml of dry THF and cooled to -78 °C in an acetone/dry ice bath. The previously prepared LiTMSA solution was added by cannula transfer which led to a rise of temperature to -50 °C. The cooling bath was removed and the mixture was allowed to warm to room temperature. Iodomethane (2.40 ml, 5.47 g, 38.5 mmol, 2.8 eq.) was added dropwise and the solution was allowed to stir overnight at room temperature. The solvents were then removed and the crude was purified by column chromatography (silica gel, cyclohexane/TBME 2:1). The final removal of the solvents resulted in 8.53 g of product **6** which was obtained as a brown viscous oil in a yield of 99 %.

^{1}H NMR (400 MHz, $CDCl_3$) δ 6.78 (s, 4H), 3.97 (t, *J* = 6.2 Hz, 4H), 3.80 (d, *J* = 1.7 Hz, 12H), 3.64 (t, *J* = 6.7 Hz, 4H), 3.35 (s, 3H), 2.09 – 1.97 (m, 4H), 1.93 – 1.82 (m, 4H), 0.25 (s, 9H).

^{13}C NMR (101 MHz, $CDCl_3$) δ 153.0, 138.2, 136.6, 104.3, 94.9, 81.4, 72.2, 56.1, 56.1, 52.8, 45.0, 29.3, 27.5, 0.0.

MS (ESI +, m/z): found 595.2, calcd. for $[M\text{-}OMe]^+$ 595.2.

Compound 8

7 (4.26 g, 9.88 mmol, 1 eq.) and **6** (6.20 g, 9.88 mmol, 1 eq.) were placed in a flask and dry cesium carbonate (9.66 g, 29.6 mmol, 3 eq) was added, followed by dry DMF (1.2 L). The mixture was vigorously stirred at room temperature for 10 minutes and then immersed into a preheated oil bath at 100 °C. After 6 h, all starting materials were consumed. DMF was evaporated, the residue was partitioned between DCM and Water (500:100 mL) and the organic phase was separated. The aqueous phase was extracted twice with DCM (50 mL) and the combined organic phases were washed with water, 1 % HCl and then dried over Na_2SO_4 and neutralized with solid $NaHCO_3$. The solvents were removed and the crude product was loaded on silica gel. The compound was purified by column chromatography (silica gel, acetone/petroleum ether 1:1 to give the compound as a white foam which was dried at 2 mBar/100 °C (4.0 g, 44 %).

^{1}H NMR (400 MHz, $CDCl_3$) δ 6.70 (s, 4H), 6.36 (s, 4H), 4.04 – 3.90 (m, 8H), 3.69 (s, 12H), 3.67 (s, 12H), 3.49 (dt, *J* = 8.4, 2.9 Hz, 4H), 3.33 (s, 3H), 2.88 (d, *J* = 1.0 Hz, 1H), 2.33 – 2.23 (m, 4H), 2.06 (s, 3H), 1.90 – 1.78 (m, 8H).

^{13}C NMR (101 MHz, $CDCl_3$) δ 168.9, 153.3, 153.1, 141.7, 138.1, 136.6, 135.8, 104.7, 104.0, 82.8, 80.7, 72.8, 72.7, 56.3, 56.1, 52.6, 45.0, 43.6, 38.6, 36.8, 35.8, 26.3, 26.2, 21.4.

Compound 9

8 (3.75 g, 4.10 mmol) and NaOH (2.0 g, 50 mmol) were placed in a flask, EtOH (5.0 mL) was added. The solution was heated to reflux for 3 days. The solvent was removed and a 3:2 mixture of H_2O/MeOH (50 mL) was added. After stirring for 10 minutes, a precipitate was formed and collected by filtration. It was recrystallized from 3:2 H_2O/MeOH and filtered off to give an off-white powder (2.99 g, 84 %).

^{1}H NMR (500 MHz, $CDCl_3$) δ 6.70 (s, 4H), 6.39 (s, 4H), 3.99 (t, *J* = 6.7 Hz, 4H), 3.95 (t, *J* = 6.3 Hz, 4H), 3.70 (s, 12H), 3.68 (s, 12H), 3.34 (s, 3H), 2.90 (t, *J* = 5.2 Hz, 4H), 2.88 (s, 1H), 2.27 (t, *J* = 5.1 Hz, 4H), 1.87 – 1.76 (m, 8H).

^{13}C NMR (126 MHz, $CDCl_3$) δ 153.2, 153.2, 143.3, 138.2, 136.7, 135.5, 105.0, 104.1, 82.9, 80.8, 77.6, 72.9, 72.9, 56.3, 56.2, 52.7, 45.3, 43.4, 37.8, 26.3, 26.3.

MS (ESI +, m/z): found 872.4, calcd.872.6 $[M\text{-}PF_6]^+$

Compound 2

8 (1.55 g, 1.78 mmol) was dissolved in CH_3CN (10 mL), K_2CO_3 (0.49 g, 3.6 mmol) and MeI (0. 55 mL, 8.9 mmol) were added. The mixture was stirred for 4 h and checked by LC/MS which indicated complete conversion to a single species. To the reaction mixture was added a solution of KPF_6 (4 g) dissolved in a mixture of H_2O (50 mL). MeOH (20 mL) was added to give a filterable precipitate. It was filtered off and washed with H_2O (2 * 40 mL), MeOH (10 mL) and Et_2O (40 mL) to give a gray powder (1.83 g, 98 %).

^{1}H NMR (500 MHz, $CDCl_3$) δ 6.71 (s, 4H), 6.38 (s, 4H), 3.96 (d, *J* = 6.5 Hz, 4H), 3.91 (t, *J* = 5.8 Hz, 4H), 3.70 (s, 24H), 3.34 (s, 3H), 3.27 (s, br, 4H), 2.98 – 2.91 (m, 6H), 2.89 (s, 1H), 2.60 (s, br, 4H), 1.86 – 1.74 (m, 8H).

^{13}C NMR (101 MHz, Acetone) δ 154.6, 154.1, 139.4, 137.7, 136.9, 104.9, 83.5, 81.5, 79.5, 72.9, 72.8, 61.0, 56.6, 56.4, 52.7, 44.0, 27.1, 27.0.

MS (ESI +, m/z): found 900.6, calcd.900.5 $[M\text{-}PF_6]^+$

ja, s'isch tiptop, guet
sitzt, passt
ou itz heimer es problem
schief, diese o schief
sitzt nid, passt nid, het ke luft

itz müesst der em chli gäh
müesst em eifach no chli gäh
gäht em no chli, gäht em no chli mit em rüedu, gäht em no chli
dir chöit em guet no chli gäh

sitzt nid, passt nid, het ke luft
dir hättit's sölle la loufe
s geit alles mit em computer, he

Stiller Has – Znüni näh